Imperial College London
Faculty of Natural Sciences

Department of Life Sciences
and
Department of Physics

Changes in productivity across northern terrestrial ecosystems

Rebecca Thursa Thomas

Submitted in fulfilment of the requirements for the degree of
Doctor of Philosophy, May 2018

Abstract

It is well established that the terrestrial biosphere is currently a net carbon sink, driven by increases in productivity, but the mechanisms involved remain uncertain. Observations indicating large-scale increases in productivity across northern terrestrial ecosystems include aircraft data that show an increase in the amplitude of the seasonal cycle of CO_2 (ASC) between 45-90°N of 56$\pm$9.8% over the last 50 years (1958-61 - 2009-11), and satellite observed greening trends of 0.25-0.5%yr^{-1} between 30-90°N since the 1980s. I analyse output from 13 terrestrial biosphere models taking part in the Multi-scale Synthesis and Terrestrial Model Intercomparison Project (MsTMIP) against these observations, which together provide a powerful benchmarks for models. I also validate a simple, data-driven model for photosynthesis, the P-model, which I use to further examine changes in productivity. New approaches are also required for analysing how model output relates to real-world observations. Thus, I additionally use the metric of ecosystem light-use efficiency (eLUE), the ratio of ecosystem productivity to the light absorbed, to distinguish structural (i.e. greening) from physiological (i.e. rate of carbon fixation) vegetation changes in models on ecosystem scales.

The MsTMIP models have good skill at representing observed greening trends and thus capture structural changes in vegetation, but they underestimate the observed increase in ASC, indicating that they underestimate changes in eLUE and productivity. The P-model, which is driven by observed greening, has a similar trend in productivity to the MsTMIP models and eLUE changes contribute only 34% to this trend. Although both the P-model and MsTMIP models show that productivity changes were driven primarily by CO_2 fertilisation, this analysis suggests that models require better representation of CO_2 fertilisation and other processes that can increase eLUE. Overall these results indicate that eLUE trends, larger than current models allow, are driving increases in productivity across high northern latitudes.

Declaration

I declare that the contents of this thesis is my own original work, and all work not done by myself has been fully cited.

The copyright of this thesis rests with the author and is made available under a Creative Commons Attribution Non-Commercial No Derivatives licence. Researchers are free to copy, distribute or transmit the thesis on the condition that they attribute it, that they do not use it for commercial purposes and that they do not alter, transform or build upon it. For any reuse or redistribution, researchers must make clear to others the licence terms of this work.

Research carried out for this thesis has led to the following peer-reviewed publication:

Thomas, R. T., Prentice, I. C., Graven, H., Ciais, P., Fisher, J. B., Hayes, D. J., Huang, M. Y., Huntzinger, D. N., Ito, A., Jain, A., Mao, J. F., Michalak, A. M., Peng, S. S., Poulter, B., Ricciuto, D. M., Shi, X. Y., Schwalm, C., Tian, H. Q. and Zeng, N. Incrased light-use efficiency in northern terrestrial ecosystems indicated by CO_2 and greening observations. *Geophysical Research Letters*, 43(21): 11339-11349, 2016.

Permissions to use the figures and text from the publication in this thesis in Chapter 2 are shown in Appendix A.

Acknowledgements

Firstly, I thank my PhD supervisors, Heather Graven and Colin Prentice, for devising this project and for taking the time to give me the guidance and support I needed to learn how to become a scientific researcher. I would like to thank the Grantham Institute for providing the funding to allow me to complete this research, and also for the opportunities they have given me to expand my boundaries beyond my desk through the DTP. I also want to thank MsTMIP team who provided lots of the data I have used in this research, and useful comments on my first published paper.

Secondly, I want to thank my friends, especially those from the Space and Atmospheric Physics group, my DTP cohort and my wonderful office-mates who have helped me to solve countless problems and made the last few years so enjoyable. In particular Kieran Brophy, who has provided me with much comic relief when it was so often needed.

I want to thank Annabelle, Mary and Nigel Thomas for their endless encouragement and attempts to understand all the finer details of this research. And finally I want to thank Sam Phibbs for his support, patience and continued efforts to make me less stressed.

Whatever it is you're seeking won't
come in the form you're expecting.

Haruki Murakami

Kafka on the shore

Contents

Abstract **2**

Acknowledgements **4**

1 Introduction **14**

1.1 The terrestrial biosphere as a net carbon sink 14

1.2 The terrestrial component of the global carbon cycle 16

1.3 Observed ecosystem changes 18

1.3.1 The increased amplitude of the seasonal cycle of atmospheric CO_2 18

1.3.2 Increases in vegetation greenness 19

1.3.3 Changes in ecosystem light-use efficiency 20

1.4 Photosynthesis and respiration 21

1.4.1 Photosynthesis 21

1.4.2 Respiration 22

1.4.3 Observing photosynthesis and respiration 23

1.5 Modelling the terrestrial biosphere 26

1.5.1 Modelling photosynthesis 26

1.5.2 Modelling respiration 28

1.5.3 Terrestrial biosphere models 30

1.5.4 Model benchmarking 30

1.6 Environmental drivers of photosynthesis and respiration 31

1.6.1 Environmental controls, recent changes and ecosystem responses 32

1.7 Modelled drivers of productivity changes in the terrestrial biosphere 39

1.7.1 Earth system models 39

1.7.2 Terrestrial biosphere models 40

1.8 Outline 42

2 Evaluation of current terrestrial biosphere models 43

2.1 Introduction 43

2.2 Methodology 48

2.2.1 Observed Data 48

2.2.2 Model Output 49

2.3 Results 51

2.3.1 Seasonal CO_2 amplitude change 51

2.3.2 Vegetation greenness 54

2.3.3 Terrestrial carbon fluxes 54

2.3.4 Light Use Efficiency 58

2.4 Discussion 58

2.5 Conclusion 63

3 The P-model: Evaluation of a next generation model for gross primary production 64

3.1 Introduction . . . 64

3.2 Methodology . . . 68

3.2.1 The P-model . . . 68

3.2.2 Driving data . . . 70

3.2.3 Alternative P-model versions . . . 75

3.2.4 Model for respiration . . . 75

3.2.5 Observations . . . 77

3.2.6 Analysis of the model . . . 81

3.3 Results . . . 82

3.3.1 Optimizing φ_0 . . . 82

3.3.2 Gross primary production . . . 83

3.3.3 Ecosystem respiration . . . 96

3.3.4 Net ecosystem exchange . . . 103

3.4 Discussion . . . 108

3.5 Conclusion . . . 111

4 Analysing changes in northern terrestrial productivity using the P-model 113

4.1 Introduction . . . 113

4.2 Methods . . . 117

4.2.1 The P-model . . . 117

4.2.2 Ecosystem Light-use efficiency . . . 120

4.2.3 Analysis . . . 120
4.2.4 MsTMIP models and GPP-FC . . . 121
4.3 Results . . . 122
4.3.1 Environmental change . . . 122
4.3.2 GPP: P-model vs. other estimates . . . 123
4.3.3 Drivers of GPP trends in the P-model . . . 128
4.3.4 Ecosystem light-use efficiency: P-model vs. other estimates . . . 134
4.3.5 Drivers of eLUE trends in the P-model . . . 136
4.3.6 Contribution to GPP trends from eLUE and APAR . . . 138
4.3.7 Seasonal amplitude of CO_2 . . . 141
4.4 Discussion . . . 143
4.5 Conclusion . . . 149

5 Conclusion **151**
5.1 Summary of key findings . . . 151
5.2 Future Work . . . 154

Appendix **156**

A Permissions **157**

Bibliography **164**

List of Tables

2.1 MsTMIP models 50

3.1 Equations, constants and data used in the P-model 71

3.2 Driving data used for P-model experiments 75

3.3 Respiration model experiments 78

3.4 Fluxnet sites used for P-model validation 79

4.1 Set-up for P-model factorial experiments 118

4.2 Equations used to separate individual factors from P-model experiments 119

4.3 Average GPP and trends for the P-model, MsTMIP models and GPP-FC 126

4.4 Drivers of GPP trends in the P-model 131

4.5 Mean annual eLUE and change for the P-model, GPP-FC and MsTMIP models 136

List of Figures

1.1 Example seasonal cycle of GPP, Reco and NEE 15

1.2 Partitioning of carbon cycle components over time, taken from Le Quere et al. (2018) [their Figure 3]. 16

2.1 Observed and modelled ASC by latitude 52

2.2 Example mean seasonal cycle of CO_2 for observations and models 53

2.3 Mean ASC in 2009-10 and ASC percent change for observations and models . . 53

2.4 Annual GS-fAPAR for observations and models form 1982-2010 for land 30°N-90°N. 54

2.5 Correlation between observed and modelled trend in GS-fAPAR for land 30°N-90°N between 1982-2010 55

2.6 Correlation between modelled ASC and NEP, NPP and Rh and ASC change and change in NEP, NPP and Rh 57

2.7 Contribution to changes in ASC, greening, NPP, Rh and eLUE from climate, LUC, CO_2 and N-deposition in MsTMIP models 59

2.8 Mean annual PAR for land 30-90°N and fitted trend-line. 60

2.9 Observed and modelled ASC by latitude for LUC only 62

3.1 Comparison of environmental variables observed at Fluxnet sites and data used to drive the P-model 73

3.2 Map of the 17 Fluxnet sites used for P-model evaluation 80

3.3 Total RMSE of different φ_0 values for P-model experiments 82

3.4 P-model GPP seasonal cycle and mean monthly GPP compared to Fluxnet data 83

3.5 Observed and modelled monthly GPP, GPP amplitude and mean annual GPP . 87

3.6 Modelled GPP residuals 90

3.7 Resonse of P-model and Fluxnet GPP to environmental drivers 91

3.8 Box and whisker plot of monthly modelled fluxes for GPP, Reco and NEE . . . 93

3.9 Box and whisker plot of flux amplitude for GPP, Reco and NEE 94

3.10 Box and whisker plot of mean annual fluxes for GPP and Reco 95

3.11 Selected results for different estimates of Reco partitioning 97

3.12 Comparison between the Lloyd-Taylor and Carey respiration equations, and the relationship between air and soil temperature 98

3.13 Modelled Reco seasonal cycle and mean monthly Reco compared to Fluxnet data 99

3.14 Observed and modelled monthly Reco, Reco amplitude and mean annual Reco . 102

3.15 Modelled NEE seasonal cycle and mean monthly NEE compared to Fluxnet data 105

4.1 Trend in environmental drivers of the P-model between 1982-2010 122

4.2 GPP and trends for the P-model, MsTMIP models and GPP-FC 124

4.3 Change in GPP amplitude 1982-2010 (%) for the P-model and MsTMIP models 127

4.4 Trend in GPP amplitude and mean annual GPP for the P-model and MsTMIP models 128

4.5 Drivers of GPP trends in the P-model 129

4.6 Mean annual eLUE for the P-model, MsTMIP models and GPP-FC over 1982-2010135

4.7 Trends in eLUE 1982-2010 for the P-model and MsTMIP models 137

4.8 Drivers of eLUE trends in the P-model 139

4.9 Contribution to GPP trends from eLUE and APAR for the P-model and MsT-MIP models 140

4.10 Relationship between GPP trends and ASC changes for the MsTMIP models, and estimated for the P-model 142

A.1 Permissions for Thomas et al. (2016). Figures used in Chapter 2. 158

Chapter 1

Introduction

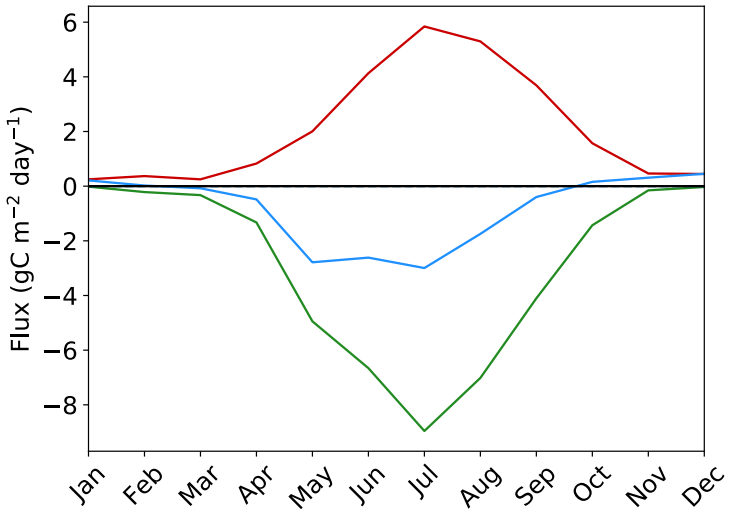
1.1 The terrestrial biosphere as a net carbon sink

Anthropogenic environmental changes since the industrial revolution have fundamentally altered the functioning of the global carbon cycle. The largest annual carbon flux is between the terrestrial biosphere and the atmosphere. This flux has become unbalanced in response to changes in climate and the environment, driven by the emission of carbon dioxide and other trace atmospheric constituents through the burning of fossil fuels, and the human appropriation of land (Le Quere et al., 2018; Ciais et al., 2013). Photosynthetic uptake of carbon dioxide (CO_2) currently exceeds release through respiration and other processes such as fire, and so the terrestrial biosphere currently acts as a net carbon sink, taking up around 32% of anthropogenic CO_2 emitted to the atmosphere each year (Le Quere et al., 2018). Although key drivers of the net carbon sink are well known, the contribution from each factor and the mechanisms driving these historical changes remain uncertain. Thus, the evolution of the terrestrial carbon sink over time remains one of the largest uncertainties in projections of future climate (Friedlingstein et al., 2014).

Northern terrestrial ecosystems (all land 30-90°N) have played a prominent role in the evolution of the net carbon sink (Pan et al., 2011; Gurney et al., 2004; Bonan, 2008; Ciais et al., 2013). These ecosystems have a large seasonal cycle of CO_2 uptake and release due to differences

between the seasonal cycles of carbon fixed by photosynthesis as gross primary production (GPP) and carbon released as ecosystem respiration (Reco) (Figure 1.1). At high northern latitudes, the seasonal cycle of GPP is driven by the seasonal change of incoming light and temperature, peaking in the summer months. Reco continues constantly throughout the year, but also exhibits a seasonal cycle with a peak lagging GPP by up to a few months. In the absence of disturbance (e.g. by fire), the overall balance between GPP and Reco, the net ecosystem exchange (NEE), determines whether the terrestrial biosphere acts as a net source (Reco > GPP) or sink (Reco < GPP) of CO_2 on an annual basis, and thus small changes in the magnitude of either flux can lead to changes in the net CO_2 exchange (McGuire et al., 2001). Since observations indicate that the terrestrial biosphere is currently a net carbon sink, we can infer that GPP is currently increasing faster than Reco. Furthermore observations at these high northern latitudes show greening trends (Murray-Tortarolo et al., 2013; Zhu et al., 2016) and a historical increase in the amplitude of the seasonal cycle of CO_2 (Graven et al., 2013). Together, these observations indicate that productivity has increased across high northern latitudes (Graven et al., 2013; Slayback et al., 2003), but since GPP and Reco cannot be directly measured, there is uncertainty about how much productivity has increased and the role of different mechanisms in driving this change (Wehr et al., 2016; Baldocchi, 2008; Ciais et al., 2013).

Figure 1.1: Example of Seasonal cycle of terrestrial fluxes of GPP (green), Reco (red) and NEE (blue). Positive fluxes are an atmospheric source and negative fluxes are an atmospheric sink. Data taken from FI-Hyy for the year 1998 (Fluxnet, 2017).

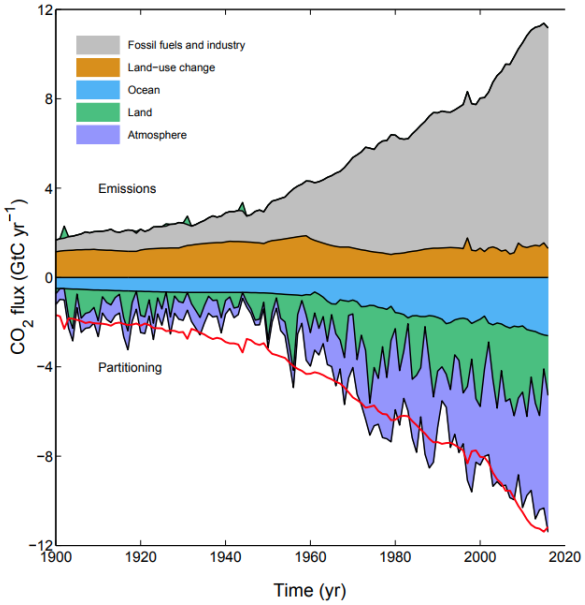


Terrestrial biosphere models are required to further our quantitative understanding of the mechanisms driving changes in terrestrial carbon fluxes. Although models agree with the observation-based estimates and show that increases in productivity in these ecosystems have contributed significantly to the global net carbon sink, there are large differences in the modelled magnitude of this sink over recent decades and the mechanisms driving its evolution (Anav et al., 2013; Stephens et al., 2007; Le Quere et al., 2018). Advancing the understanding of mechanisms that drive changes in productivity in these northern ecosystems can therefore improve model estimates of the historical and future carbon sink.

1.2 The terrestrial component of the global carbon cycle

Measurements of atmospheric CO_2 reflect the net carbon exchange from the terrestrial biosphere, the ocean and anthropogenic emissions (Le Quere et al., 2018). Models and/or additional data are required to partition the CO_2 into the terrestrial, ocean and anthropogenic components (Figure 1.2), and then further to partition the terrestrial flux into its components of photosynthesis, respiration and disturbance.

Figure 1.2: Partitioning of carbon cycle components over time, taken from Le Quere et al. (2018) [their Figure 3].



The carbon emissions from anthropogenic sources are assumed to be well known as these can be calculated from energy and land use data. The emissions from land use change are more uncertain but are smaller and have remained fairly constant, while fossil fuel emissions have increased over time, currently accounting for 82% of the anthropogenic source, which equates to 9.4 ± 0.5PgC yr^{-1} over 2007-2016 (Le Quere et al., 2018). Using these data the percentage of anthropogenic emissions that remain in the atmosphere, known as the airborne fraction, can be calculated. This has remained fairly constant over time at 45%, as the efficiency of uptake by the ocean and terrestrial biosphere sinks have kept up with emissions (Ballantyne et al., 2012; Le Quere et al., 2018).

Separating the ocean and biosphere sink has been made possible with advances in high-precision measurements of atmospheric oxygen concentration (O_2) (Keeling et al., 1996b). Using these measurements of atmospheric O_2 along with CO_2, it is possible to quantify the ocean carbon uptake. Atmosphere-ocean CO_2 exchange does not alter the atmospheric O_2 concentration, but atmosphere-land exchange effects CO_2 and O_2 simultaneously. The carbon sink from the ocean and the terrestrial biosphere can therefore be calculated by using a vector diagram to compare trends of CO_2 and O_2, and taking into account the changes in CO_2 and O_2 due to the burning of fossil fuels and ocean outgassing (Keeling and Manning, 2014). Using this method, the net ocean and net land sink are calculated to be 2.72 ± 0.6 PgC yr^{-1} and 1.05 ± 0.6 PgC yr^{-1}, respectively, for 2000-2010 (Keeling and Manning, 2014) (note that this method estimates the net terrestrial sink which includes the carbon source from land use change. It is therefore smaller than the residual terrestrial carbon sink estimated to be 2.9 ± 0.8 PgC yr^{-1} for 2000-2009 (Keeling and Manning, 2014; Le Quere et al., 2018)).

The terrestrial component can then be further partitioned into GPP (CO_2 uptake through photosynthesis), Reco (CO_2 release through respiration) and disturbances such as fires. The overall balance between GPP and Reco is the net ecosystem exchange (NEE) (Figure 1.1), or if disturbances are also included, the net biome production (NBP) (Chapin et al., 2006).

1.3 Observed ecosystem changes

Large-scale changes in terrestrial ecosystems have been observed using aircraft measurements of atmospheric CO_2 concentration and satellite data of vegetation greenness. We can use long-term records of atmospheric CO_2 concentration to examine the response of vegetation to environmental change because the majority of the seasonal cycle of atmospheric CO_2 in the northern hemisphere can be attributed to the seasonal uptake and release of CO_2 by the terrestrial biosphere (Graven et al., 2013; Keeling et al., 1996a). Recent trends in the seasonal cycle of CO_2 at high northern latitudes have largely been attributed to changes in productivity rather than respiration, and so observed increases in the amplitude of the seasonal cycle can be used to inform us about increases in productivity (Zhao et al., 2016; Graven et al., 2013; Randerson et al., 1997; Forkel et al., 2016). Changes in productivity can also be inferred from satellite derived observations of vegetation greenness, a measure of the amount of light absorbed by vegetation in a particular area. Vegetation greenness can increase if there are more leaves on a particular tree, there is more vegetation in a particular area or if the type of vegetation in an area changes. Changes in vegetation greenness can thus indicate changes in photosynthetic activity in an ecosystem (Myneni et al., 1997; Zhou et al., 2001; Slayback et al., 2003; Zhu et al., 2013).

1.3.1 The increased amplitude of the seasonal cycle of atmospheric CO_2

The observations of atmospheric CO_2 concentration at long-term continuous monitoring stations such as Mauna Loa, Hawaii (MLO), since the 1950's and Point Barrow, Alaska since 1961 show an average increase in the seasonal cycle of CO_2 of $0.32\pm0.07\%yr^{-1}$ and $0.60\pm0.05\%yr^{-1}$, respectively (Graven et al., 2013). These site-scale records have been complemented by aircraft campaigns during the International Geophysical Year (1958-61) and the HIAPPER Pole-to-Pole Observations (HIPPO) (2009-11). These aircraft campaigns measured CO_2 at multiple heights throughout the atmosphere over several seasons and show that the increase in the amplitude of the seasonal cycle of CO_2 (ASC) is a large-scale characteristic of high northern latitudes

over recent decades. Between the two aircraft campaigns, ASC increased by 56±9.8% between 45-90°N at 500 mb (Graven et al., 2013). The increase in ASC has been accompanied by a change in the phasing of the seasonal cycle by up to 7 days at MLO and Point Barrow (Graven et al., 2013). Together, these observations indicate large increases in productivity over the last few decades. This recent analysis of the aircraft data by Graven et al. (2013) has stimulated research on the causes of the increase in ASC, with studies suggesting climate, land use change and CO_2 fertilisation as the key drivers (Forkel et al., 2015; Gray et al., 2014; Zeng et al., 2014; Wenzel et al., 2016). However, none of these studies have used the aircraft measurements as a benchmark for their results, and thus the drivers of the increase in ASC remain uncertain.

1.3.2 Increases in vegetation greenness

Vegetation greenness in the northern hemisphere has increased since satellite records began in the 1980's (Murray-Tortarolo et al., 2013; Zhu et al., 2016). Vegetation greenness is estimated from satellite data by measuring surface reflectance at different spectral bands, usually from the visible and near infra-red wavelengths. Standard formulas are then used to convert these measurements to a vegetation index; either a unitless measure of greenness such as NDVI (normalized difference vegetation index) or fAPAR (fraction of absorbed photosynthetically active radiation), or to LAI (leaf area index), the area of green leaves per area of ground (m^2m^{-2}) (Jiang et al., 2017; Gobron and Verstraete, 2009). Increases in vegetation greenness across high latitudes have been observed since 1982 of 0.25-0.5%yr^{-1} (Myneni et al., 1997; Murray-Tortarolo et al., 2013; Piao et al., 2006; Slayback et al., 2003), although the rate of increase varies over time and between satellite products, and not all products agree with this continued trend (Jiang et al., 2017; Guay et al., 2014). Across high latitudes there is uncertainty in the greening trend of different satellite products as measurements in these regions are often contaminated by clouds and they are seasonally covered in snow or without daylight (Jiang et al., 2017).

An increase in greenness may be caused by an increase in GPP and a subsequent increase in the amount of carbon allocated to leaves, or an increase in greenness may itself increase GPP, as this allows more light to be captured by the vegetation. Suggested causes of this increase

in greenness are an increase in growing season length due to earlier snow melt in a warming climate, CO_2 driven increases in productivity, nitrogen deposition, land use change and shifts in natural vegetation cover (Zhou et al., 2001; Zhu et al., 2016; Mao et al., 2013). Many factors may be driving greening trends in a particular region and models are required to disentangle the contribution from each process (Zhu et al., 2016; Mao et al., 2013; Zhou et al., 2001). An analysis of 10 ecosystems models found that elevated CO_2 has been the primary driver of increased global productivity resulting from greening, but that at high northern latitudes (60-90°N), climate was the most important factor (Zhu et al., 2016). Recent studies have suggested that in some regions, the increases in productivity from greening have be partly offset by a consequent increase in respiration, resulting in a neutral or very small increase in the net carbon sink. Causes for increases in respiration include an increase in available material (Zhu et al., 2016), temperature driven increases in autumn respiration (Welp et al., 2016) and extreme events such as droughts (Sitch et al., 2015).

1.3.3 Changes in ecosystem light-use efficiency

The observed changes in greenness only inform us about structural changes in vegetation, whereby productivity increases as a result of an increase in the amount vegetation that is photosynthesising. However, recent environmental changes may also lead to physiological changes in vegetation i.e. the rate of carbon uptake per unit of vegetation. These physiological changes can be analysed in observations and models using the metric of ecosystem light-use efficiency (eLUE), the productivity per unit of light absorbed calculated over the growing season (Garbulsky et al., 2010). Global estimates of historical eLUE trends do not exist, but site-scale observations from the Free-Air CO_2 Enrichment (FACE) experiments, where CO_2 was artificially increased above ambient levels, show that eLUE was the main driver of increases in productivity at elevated CO_2 in closed-canopy forests with high peak LAI (Norby et al., 2003). Changes in eLUE may also be driven by other environmental changes such as changes in climate, nutrients and land use, but these factors have not been explicitly studied in observations. Structural and physiological changes in vegetation are probably happening simultaneously, and thus there will be a non-linear relationship between vegetation greening and changes in eLUE

to describe trends in productivity.

1.4 Photosynthesis and respiration

1.4.1 Photosynthesis

Photosynthesis is the process by which plants make their energy. Plants use light energy from the sun to take up CO_2 and water to help make carbohydrate (CH_2O) and oxygen, a waste product. Energy is obtained from the CH_2O through mitochondrial respiration and is used for plant growth.

There are two parts to photosynthesis, the light-dependent reactions that transform light energy into chemical energy, and the light-independent reactions which use this chemical energy to reduce CO_2 to carbohydrates. During the light-dependent reactions, photons are absorbed by chlorophyll (leaf pigments). The energy from these photons is used to split water molecules in the leaf into hydrogen, electrons and oxygen. The electrons then excite biochemical compounds within the leaf, creating chemical energy. This chemical energy is used for the Calvin cycle, the light-independent reaction, which uses CO_2 absorbed through leaf stomata to create CH_2O. Stomata are small pores typically found on the underside of a leaf, which simultaneously lose water through evapotranspiration when they open to absorb CO_2. The rate of this exchange is the stomatal conductance, and it is sensitive to ambient CO_2 concentration and atmospheric humidity (Bon; Lam).

Not all plants assimilate CO_2 in the same way. The majority of plants ($\sim$82%), including virtually all trees, follow the C-3 pathway, in which the Rubisco enzyme is used to capture CO_2 from the atmosphere as part of the Calvin Cycle. Rubisco is then regenerated as part of the Calvin Cycle for future CO_2 fixation. Most other plants ($\sim$18%), including tropical grasses and some crops, follow the C-4 pathway in which CO_2 is first captured from the atmosphere by the PEP carboxylase enzyme before entering the Calvin Cycle (Still et al., 2003). This additional step in C-4 plants makes them more efficient at absorbing CO_2 because it results in little to no photorespiration, the process by which Rubisco reacts with oxygen and produces CO_2, as the Rubisco is

not in direct contact with atmospheric oxygen. For C-3 plants however, a significant proportion of the CO_2 taken up (20-40%) is offset by CO_2 released through photorespiration (Cha). The net carbon fixed by vegetation through photosynthesis is the gross primary production (GPP), which in the case of C-3 plants is the total CO_2 taken up through photosynthesis minus CO_2 release through photorespiration. Almost all of the vegetation in the high northern latitudes follows the C-3 pathway (Still et al., 2003), so all future discussion will relate to C-3 plants only.

1.4.2 Respiration

Ecosystem respiration (Reco) is the biogeochemical process that returns carbon stored in plants back to the atmosphere. Reco is composed of autotrophic respiration from plant metabolism and heterotrophic respiration, which is dominated by the metabolism of microbes in the soil (Chapin et al., 2006; Trumbore, 2006). As with all respiratory processes, Reco is sensitive to temperature (Trumbore, 2006; Baldocchi, 2008). Autotrophic respiration (Ra) occurs within the plant over short timescales for growth and maintenance, quickly returning 40-60% of the CO_2 fixed by the plant as GPP back to the atmosphere (Litton et al., 2007). The fraction of GPP used as Ra strongly depends on the ecosystem (Bond-Lamberty et al., 2016; Litton et al., 2007), and increases with stand age (Delucia et al., 2007). The remaining carbon is the net primary production (NPP), defined as GPP - Ra. Most of the NPP is allocated to biomass: foliage, wood and roots, but up to around 10% may be lost to external components such as herbivory, root processes (e.g. nutrient exchange with mycorrhizae and exudation) and emissions of biogenic volatile organic compounds (Luyssaert et al., 2007; Ryan and Law, 2005). The carbon from NPP is delivered to the soil as dead organic matter, where heterotrophic respiration (Rh) takes place and returns CO_2 to the atmosphere over seasonal to decadal timescales (Chapin et al., 2006). Unlike GPP, Reco can take place continuously throughout the year as Rh is mainly controlled by soil temperatures which can be several degrees different from air temperature and may be sufficiently warm for Rh to occur throughout winter particularly if the soil is insulated by snow (Monson et al., 2006; Nobrega and Grogan, 2007; Bon).

Disturbances such as fires, insect outbreaks and disease can also return carbon to the atmo-

sphere (Hayes et al., 2011). These events are sporadic and alter ecosystem functioning by changing the stand age and species distribution in a particular area (Zimov et al., 1999).

1.4.3 Observing photosynthesis and respiration

A global network of CO_2 flux measurement sites (Fluxnet) record local CO_2 concentrations using the eddy covariance technique (Fluxnet, 2017). A site will typically have a measurement footprint of up to 1km (Baldocchi, 2008). The atmospheric CO_2 concentration measured at the Fluxnet site is the net ecosystem exchange (NEE) and must therefore be partitioned into the photosynthetic and respiratory components. Two main methods are used that provide similar estimates of GPP and Reco (Lasslop et al., 2010). In one method, the night-time NEE (i.e. when there is no photosynthesis) is used to quantify Reco, and GPP is then calculated as the difference between NEE and Reco (Reichstein et al., 2005). The other method makes use of the day-time flux of NEE which is fit with a modified light-response curve to include the response of respiration to temperature and photosynthesis to atmospheric moisture (through vapour pressure deficit). Day-time Reco is then taken as the y-intercept of the modified NEE when plotted against light, and GPP is the remaining part of NEE (Lasslop et al., 2010; Suyker and Verma, 2001). Some studies suggest that a key process missing from these methods is the Kok effect, the light inhibition on respiration, which results in lower than expected Reco during the day and thus inaccurate apportionment of NEE between GPP and Reco (Heskel et al., 2013). This has been shown using stable carbon isotope observations, and provides another estimate of the diurnal partitioning between GPP and Reco (Wehr et al., 2016). However, this analysis currently only covers temperate forests, and further isotopic measurements in other ecosystems are needed to develop this method.

Splitting the fluxes of GPP and Reco into NPP, Ra and Rh is difficult as this requires observations of the autotrophic and/or heterotrophic parts of Reco. Observations of these separate parts are generally not possible as some of the Ra takes places below ground by roots in the soil and is therefore difficult to separate from the belowground Rh (Trumbore, 2006; Davidson et al., 2006b). The combination of Rh and below-ground Ra is the soil respiration, the second largest flux from the terrestrial biosphere, estimated to contribute up to 75% of Reco

(Davidson et al., 2006b; Hashimoto et al., 2015) and have a flux that is 35-90% of GPP (Ryan and Law, 2005; Xu and Shang, 2016). Recently, a climate driven model, parametrised using observations, estimated global soil respiration at 91 $\pm$4PgC yr^{-1} (Hashimoto et al., 2015). Soil respiration can be measured using an infra-red gas analyser inside a chamber placed on top of the soil, but difficulties arise when the soil is on a slope and so these areas are under-represented (Xu and Shang, 2016). Despite its importance, soil respiration is still poorly constrained due to the expense and difficulty of making these measurements (Bond-Lamberty and Thomson, 2010). A global database of soil respiration from over 5000 sites around the world has been set-up in order to synthesise current measurements and to compliment Fluxnet measurements (Bond-Lamberty and Thomson, 2010). Improved and more frequent measurements, and novel methods such as the use of carbon isotopes may provide more robust quantification of respiration in the future (Trumbore, 2006; BondLamberty et al., 2004).

Data from the Fluxnet sites have been up-scaled to give global gridded estimates of mean GPP using machine learning algorithms (Beer et al., 2010; Jung et al., 2017). In this method, relationships are constructed between a number of explanatory variables that best explain GPP at Fluxnet sites. Explanatory variables include meteorological data collect at the site such as air temperature and water availability, and global satellite data such as land surface temperature and vegetation greenness (Beer et al., 2010). These relationships are then extrapolated to give global estimates of GPP at 0.5^ox0.5^o resolution using gridded data of plant functional types and climate (Jung et al., 2011; Beer et al., 2010). The estimated global mean GPP for the original dataset using a model tree ensemble approach (GPP-MTE) is 123 $\pm$8 PgC yr^{-1} for 1998-2005 (Anav et al., 2013). This estimate is similar to the GPP estimated by MODIS (Moderate Resolution Imaging Radiospectrometer) of 112 PgC yr^{-1} for 2000-2005 (Anav et al., 2015), which is constructed using the light-use efficiency approach where satellite observations of greening are used to estimate GPP. Both of these estimates do not explicitly account for CO_2 fertilisation, and so they are smaller than other estimates of global GPP which do include rising CO_2 concentrations as a driver. These other approaches include using a model-data hybrid as part of a data assimilation approach in the CARBONES project, which gives a global GPP estimate of 148 PgC yr^{-1} for 1990-2009 (Anav et al., 2015), and a method using oxy-

gen isotopes which gives an estimate of 150-175 PgC yr^{-1} for recent decades (Welp et al., 2011).

Recent advances in satellite technology have provided the opportunity to develop new estimates of global GPP based on sun (or solar) -induced florescence (SIF) (Parazoo et al., 2014). SIF can be used to estimate GPP as it is a measure of light that is re-emitted from leaf pigments when plants photosynthesise, informing us of current photosynthetic activity (Smith et al., 2018; Anav et al., 2015). Current estimates of SIF agree well with GPP-MTE and MODIS GPP estimates, but further analysis of its spatial and temporal variation is still required in order to fully understand how observed SIF relates to GPP across different scales (Anav et al., 2015; Guanter et al., 2012).

Estimating trends in global GPP is challenging. Both the machine learning methods and the MODIS estimate do not use CO_2 as an explanatory variable and thus CO_2 fertilisation is not explicitly accounted for, which is an important driver of GPP trends (De Kauwe et al., 2016; Anav et al., 2015). The oxygen isotope method of Welp et al. (2011) provides only a snapshot of GPP, and is constrained with just a few observations, and the CARBONES estimate is not strictly an observation, as GPP from the ORCHIDEE terrestrial biosphere model is used in places that are not well constrained by data (Anav et al., 2015). Site scale-measurements have now been established for long enough to be able to extract a trend, and recent analysis of forest sites in the USA and Europe suggests that GPP may have increased by 1% yr^{-1} from 1995-2011 (Fernandez-Martinez et al., 2017). This is larger than the trend that was estimated using carbonyl sulfide (COS) samples, which indicate that global GPP may have increased by 30% over the last century (Campbell et al., 2017). The authors note that the GPP trends in their study are appropriate for considering the effect of CO_2 fertilisation on the carbon cycle but not the climate effect (Campbell et al., 2017), which may explain part of the difference between the COS and site-scale GPP trends. Additionally, the site-scale trends are restricted to northern temperate and boreal regions, which have shown significant changes in photosynthetic activity in recent years through vegetation greening and increases in ASC (Graven et al., 2013; Murray-Tortarolo et al., 2013; Zhu et al., 2016), and so GPP trends in these ecosystems are likely to be higher than the global average.

1.5 Modelling the terrestrial biosphere

Models of the terrestrial biosphere are used to help us understand the mechanisms driving changes in photosynthesis and respiration and to make predictions about how these fluxes may respond to continued environmental change. They can be constructed from the top-down, estimating each flux from observed CO_2 concentrations, or bottom-up, modelling individual components and adding-up their contribution to the total CO_2 flux. Top-down models, or inversions, use atmospheric CO_2 data and atmospheric transport models with statistical techniques to find the optimal combinations and distributions for net CO_2 fluxes from land, ocean and fossil fuels. Inverse modelling systems are provided with prior information about these fluxes which are then adjusted to find the best match to an observed distribution, usually achieved by minimising a cost function (Peylin et al., 2013). The inversion technique can be combined with the bottom-up approach by using the same optimisation procedure to constrain fluxes of GPP and Reco in a terrestrial biosphere model (TBM) (Peylin et al., 2016).

In this thesis I focus on bottom-up (or process-based) models. These models start from the individual ecosystem components and build these up to represent all the ecosystem fluxes. For the terrestrial biosphere, this usually involves combining equations for primary production and respiration to calculate net ecosystem exchange. An atmospheric transport model is needed to generate atmospheric CO_2 concentrations that can be compared to observations once additional fluxes from ocean and anthropogenic sources are included (Dargaville et al., 2002). The sensitivity of processes to changes in environmental conditions (such as atmospheric CO_2 and temperature) can be studied as models with different forcings and parameters can be compared.

1.5.1 Modelling photosynthesis

Primary production is typically modelled following either the light-use efficiency approach or the enzyme kinetics equations for C-3 photosynthesis established by Farquhar et al. (1980) (Fisher et al., 2014). For the Farquhar model, instantaneous photosynthetic assimilation is calculated

as either the Rubisco-limited (Ac) or light-limited (Aj) rate of photosynthesis, whichever is smaller (Farquhar et al., 1980):

$$A = (Ac, Aj) \tag{1.1}$$

In this model, Ac and Aj respond to current environmental conditions such as temperature, atmospheric CO_2 concentration and light. The Farquhar et al. (1980) equation or a modified form of it (Collatz et al., 1991) underpins many of the frequently used TBMs including CLM, LPJ and JULES, and over time models have evolved to represent additional limitations and more complex processes such as carbon allocation to different pools, phenology, dynamic vegetation and permafrost (Prentice et al., 2014; Fisher et al., 2014; De Kauwe et al., 2017). These types of models will also commonly estimate their own LAI by allocating a fraction of the assimilated carbon to leaves (Fisher et al., 2014). A drawback of process based models is the possibility that key processes are missing from the model, resulting in an incorrect estimation of GPP. For example the availability of nutrients is known to play an important role in regulating carbon uptake, but many models still do not include a coupled carbon-nitrogen cycle and the equations describing these interactions are still poorly defined (Zaehle et al., 2014). Models which do include carbon-nitrogen or carbon-nitrogen-phosphorus interactions show that limitations in these resources reduce the CO_2 fertilisation effect compared to carbon only simulations (Zhang et al., 2014; Zaehle and Dalmonech, 2011).

An alternative approach is the light-use efficiency (LUE) model (Monteith, 1972; Medlyn, 1998; Fisher et al., 2014). Productivity (GPP or NPP, gC m^{-2}) is estimated to be proportional to the amount of absorbed incoming photosynthetic active radiation (APAR, MJ m^{-2}), a product of the photosynthetic active radiation (PAR, MJ m^{-2}) and the fraction of PAR absorbed by vegetation (fAPAR). The APAR is then scaled by the efficiency with which carbon can be fixed per unit of light absorbed, the light-use efficiency (LUE ,MJ gC^{-1}):

$$GPP = PAR \cdot fAPAR \cdot LUE \tag{1.2}$$

The fAPAR data (unitless) usually comes from satellite products which are often composites from several days of data (Jiang et al., 2017; Zhu et al., 2013), and it is assumed that over these timescales the fAPAR will account for process that are not explicitly modelled, such as water limitation and potential limitations from nutrients (Keenan et al., 2016; Running et al., 2004). In the absence of environmental stresses, LUE is similar across different ecosystems (Cha), but in reality, there are multiple factors altering the maximum LUE and thus although LUE can be a simple constant, in models it is generally a function of additional environmental controls such as temperature and moisture availability (Running et al., 2004; Yuan et al., 2014). The estimate of GPP from MODIS satellite data (Section 1.4.3) is based on the LUE approach, and is sensitive to vapour pressure deficit and temperature (Running et al., 2004). The LUE model can also be coupled to the enzyme kinetic model described in Equation 1.1 (e.g. SiBCASA (Schaefer et al., 2008)). As with the enzyme kinetic models, the choice of limitations included in the model creates large differences between LUE models, particularly when considering the representation of diffuse light and water stress (Yuan et al., 2014).

Further equations for stomatal conductance, the rate of carbon gain or water loss through leaf stomata, are then used to incorporate the relationship between photosynthesis and plant water use. These equations can have many forms (Damour et al., 2010; Medlyn et al., 2011), but typically represent stomatal conductance as a function of atmospheric humidity (e.g. through vapour pressure deficit), the atmospheric CO_2 concentration and photosynthetic assimilation.

1.5.2 Modelling respiration

Unlike GPP, there is not a widely accepted mechanistic equation for Reco (Migliavacca et al., 2011; Davidson et al., 2006a). Respiration is generally modelled as either the Ra and Rh components, or split into above-ground Ra and soil respiration, which is a sum of the below-ground Ra and Rh (Fisher et al., 2014). Ra may be modelled as a function of temperature, available biomass and the carbon to nitrogen ratio, where each function may also be biome dependent (Trumbore, 2006; Schwalm et al., 2010). Ra can also be further split into maintenance and growth respiration, where the growth respiration is typically 20-30% of the GPP minus the

maintenance respiration (Knorr, 2000; Ito and Oikawa, 2002; Tian et al., 1999; Sitch et al., 2003). The remaining carbon (either the NPP when above- and below-ground Ra is modelled, or the litter and soil carbon when only the above-ground Ra is modelled) is then modelled to leave the system as Rh, which is typically a function of soil temperature and moisture (Sitch et al., 2003). The temperature sensitivity in Ra, Rh or soil respiration is often modelled using a Q10 factor, which defines the rate of respiration for a 10^oC increase in temperature and has values ranging from 1-5 (Davidson et al., 2006a), or following the Lloyd-Taylor equation which is a modified Arrhenius equation where respiration increases nearly exponentially with temperature (Sitch et al., 2003; Lloyd and Taylor, 1994). Studies have shown that fixing the Q10 value is not appropriate for representing seasonal or long-term changes in respiration (Davidson et al., 2006a) and so the approach used by Lloyd and Taylor (1994), in which the apparent Q10 varies and declines with temperature, may be more realistic. There is little agreement on how to represent the influence of moisture on respiration in models but typically a model will calculate a scaling factor as some function of soil water content and may include additional thresholds or variations based on soil type (Chen et al., 2015; Suseela et al., 2011). Studies suggest that soil moisture and temperature interact dynamically to alter Rh, but models do not currently include this response (Suseela et al., 2011).

Models use plant functional types (PFTs) to represent differences between ecosystems and plant strategies by fixing parameters such as maximum greenness, temperature limits or turnover time for each PFT (e.g. (Sitch et al., 2003)). Models have a varying number of PFTs, but at minimum tend to differentiate between grassland, evergreen forests and deciduous forests (Wei et al., 2014). PFTs may be unique to a particular pixel, or a pixel may be made up of several PFTs, all contributing a defined fraction to the carbon flux. Some models have dynamic vegetation (DGVMs), allowing the PFT in a pixel to change over time in response to environmental conditions and competition (e.g. LPJ (Sitch et al., 2003)).

1.5.3 Terrestrial biosphere models

The equations for photosynthesis and respiration are combined within a terrestrial biosphere model (TBM) to estimate historical and future carbon fluxes. TBMs can either be used offline, where models are forced by pre-defined environmental data, or as part of a coupled carbon-climate system in Earth System models (ESMs). Offline TBMs primarily consider the fluxes within the terrestrial carbon cycle, although they may also include equations to describe interactions from non-carbon fluxes such as water and nutrients (Fisher et al., 2014). ESMs attempt to model all aspects of the earth system including climate dynamics, oceans and feedbacks between the land, atmosphere and ocean (Ciais et al., 2013). They are typically driven by CO_2 concentrations and other radiative forcings and are used to understand feedbacks within the earth system and to make projections about changes in climate and their resulting effects on the land and ocean (Ciais et al., 2013).

1.5.4 Model benchmarking

As models are becoming increasingly complex and more processes are included, it is important to keep track of whether models are improving, understand the limitations of a model and to know why output from models differs. Models can be compared to observations to inform us about model skill, or compared to each other to inform us about differences in output arising from model structure. Quantifying differences due to model structure are important because variations in the TBM underlying each ESM are more significant that differences in modelled historical climate (Anav et al., 2015) or future emission scenarios (Lovenduski and Bonan, 2017).

Model intercomparison projects (MIPs) isolate structural differences by driving models with identical input. MIPs may also run semi-factorial experiments, where some inputs are held constant in order to evaluate the model sensitivity to each driver. Several ESMs take part in the Coupled Model Intercomparsion Project (CMIP) every five years, where models are provided with different CO_2 concentration pathways (Anav et al., 2015) or emissions scenarios (Friedlingstein et al., 2014). Terrestrial biosphere models have been evaluated in projects

such as TRENDY (Trends in net land-atmosphere carbon exchange over the period 1980-2010) and MsTMIP (Multi-scale Synthesis and Terrestrial MIP) which drive models with identical environmental conditions (Taylor et al., 2012; Sitch et al., 2015; Huntzinger et al., 2013). Experiments were run for the TRENDY models where time-varying CO_2, climate and then land-use history were added to a control run (Zhao et al., 2016), and with MsTMIP where time-varying climate, land-use change, CO_2 and then N-deposition (for models with a coupled C-N cycle) were added to a control run (Huntzinger et al., 2013). The sensitivity to each driver is calculated by subtracting the previous simulation and assuming a linear response between simulations.

1.6 Environmental drivers of photosynthesis and respiration

The balance between photosynthesis and respiration on a seasonal timescale is defined by their responses to environmental conditions including light, ambient CO_2 concentration, temperature, moisture and nutrient availability (Baldocchi et al., 2018). Productivity in a particular region is generally limited by one or more of these resources (Nemani et al., 2003; Anav et al., 2015). Respiration responds to temperature and moisture, and indirectly to all controls as a result of changes in the availability of material. Vegetation may also respond to these controls differently over time as particular conditions become saturating, through acclimation, land use change and as the stand ages (Baldocchi, 2008; Delucia et al., 2007; Reich et al., 2016). Below, I describe how photosynthesis and respiration respond to each control, how these environmental controls have changed over recent years, and how ecosystems have responded to these changes. Although each control is singled out below, it is important to note that variations in environmental conditions occur together (e.g. an increase in atmospheric CO_2 is accompanied by increases in temperature), and that vegetation may respond in a non-linear way such that the overall response from vegetation may be reduced or increased when all factors are considered together.

1.6.1 Environmental controls, recent changes and ecosystem responses

Light

Photosynthesis is dependent on light and so the diurnal and seasonal cycle of GPP reflects that of the sun angle and day-length. Photosynthetically active radiation (PAR) is the part of the spectrum that can be absorbed by leaves (between 400-700nm), accounting for approximately 48% of the incoming shortwave radiation (Frouin and Pinker, 1995). The rate of gross photosynthesis increases with light but net photosynthesis only increases above zero after the light compensation point has been reached. The light compensation point is defined as the amount of incoming light at the point at which gross photosynthesis is equal to photorespiration and mitochondrial respiration. Net photosynthesis increases up to the point at which photosynthetic assimilation becomes limited by the availability of CO_2 and Rubisco and net photosynthesis flattens out at this carboxylation limited region.

The biggest influence on the amount of PAR received in a particular location, and thus the capacity for vegetation to photosynthesise, depends on the seasonal change of incoming light due to the Earth's orbit. At high northern latitudes, this results in a large seasonal cycle in photosynthesis, with a minimum in the winter when little to no PAR is received by vegetation and a maximum in the summer when PAR becomes abundant. On the northern summer solstice, total daily PAR increases with latitude up to a maximum at the Arctic circle. In addition to this large annual cycle, variations in atmospheric composition can alter the quantity of PAR reaching the land surface and the fraction of this PAR that is received as direct or diffuse radiation. Direct radiation travels straight down from the top of the atmosphere to the land surface and is only received by the upper canopy, while diffuse radiation is scattered by clouds and aerosols as it travels towards the land surface, and therefore travels deeper within the canopy and reduces within canopy shading (Baldocchi, 2008). The overall result is that more leaves receive some PAR and fewer leaves are light-saturated, thus increasing photosynthesis. The quantity and type of PAR reaching the land surface is affected by clouds and human-made aerosols, such as sulphate and black carbon. Clouds reduce the overall PAR and can increase diffuse PAR as they scatter radiation. In clear-sky conditions, PAR is altered by aerosols which

change how incoming radiation is scattered or absorbed (Wild, 2016). Indirectly, aerosols also effect clouds, encouraging their formation and altering cloud lifetime and reflectivity (Wild, 2016). The net effect of these changes on photosynthesis depends on the trade-off between decreases in direct radiation and having a sufficient amount of PAR for photosynthesis (Gu et al., 2002; Mercado et al., 2009).

Increases in the emissions of aerosols and changes in cloudiness in the 1950's-1980's resulted in reductions in the amount of PAR, a phenomena known as global dimming. This trend has mostly reversed since the 1980's (brightening) across the northern hemisphere owing to air quality improvements and changes in clouds (Wild, 2016). A modelling study separating diffuse and direct PAR found that the increase in diffuse light between 1960-1999 enhanced the net land sink by around 25% , but that the contribution from diffuse PAR decreased after 1980 (Mercado et al., 2009).

CO_2

Once the rate of CO_2 fixation exceeds the rate of CO_2 production from photorespiration and mitochondrial respiration, the photorespiratory compensation point, the rate of net photosynthesis increases almost linearly with CO_2 until Rubisco becomes limiting (Bon). At this point, the rate of assimilation is limited by the regeneration of Rubisco as part of the Calvin Cycle, which in turn is limited by the transport of electrons from the light-dependent reactions.

Atmospheric CO_2 concentrations have been increasing since the Industrial Revolution in the mid 1700's as a result of fossil fuel burning and land-use change (Ciais et al., 2013). The observation site at Mauna Loa, Hawaii, has documented the increase in atmospheric CO_2 since 1958 (NOAA, 2016) and now forms part of the Global Greenhouse Gas Reference Network. This network consists of over 50 sites around the world that collect a mixture of in-situ and flask samples and measure the dry air mole fraction of CO_2 using an infra-red absorption analyser. Weekly observations are made to look at long term global trends of atmospheric gasses and these show that global mean CO_2 has increased by 64ppm between 1980-2016 (Dlugokencky and Tans, 2018). Studies suggest that this increase in CO_2 concentration has been one of the

main drivers of increases in terrestrial carbon uptake over recent years through the process of CO_2 fertilisation. Increases in atmospheric CO_2 increase the difference between leaf internal and ambient CO_2, driving more CO_2 into the plant and increasing the biochemical rate of photosynthesis with CO_2. CO_2 fertilisation is accompanied by increases in water use efficiency (WUE), as stomata do not have to open as wide to absorb the same amount of CO_2, and therefore lose less water per carbon gained (Field et al., 1995). This may be of more importance in dry and arid ecosystems which are water limited (Franks et al., 2013).

Observations from Fluxnet sites show increases in forest WUE, due to increases in CO_2 (Keenan et al., 2013; Saurer et al., 2014; Frank et al., 2015). However the precise increase in WUE, the mechanisms driving the increase, and the overall consequences on vegetation remain unclear due to difficulties in interpreting measurements and comparing observations across different scales (Knauer et al., 2017, 2018; Penuelas et al., 2011; Keenan et al., 2013).

The magnitude of the CO_2 fertilisation effect and its long term influence is debated (Friedlingstein et al., 2006; Piao et al., 2013; Wenzel et al., 2016), and has resulted in the establishment of the FACE (Free-Air CO_2 Enrichment) Experiments (Norby and Zak, 2011). At a FACE site, the concentration of atmospheric CO_2 over several experimental plots is elevated to around 550-600ppm for many years, and compared to nearby control plots (Long et al., 2004). These studies have found mixed results owing to variations in vegetation type, nitrogen availability and soil communities (Ainsworth and Long, 2005; Terrer et al., 2016), but they have generally shown that increases in atmospheric CO_2 can lead to large and sustained increases in photosynthetic assimilation (Ainsworth and Long, 2005) and increases in plant biomass (Norby and Zak, 2011).

Temperature

Photosynthesis and respiration are both sensitive to temperature. Under light saturated conditions, GPP increases with increasing temperature up to an optimal assimilation rate, then decreases at higher temperatures (Farquhar et al., 1980). However, when light conditions are not saturating, GPP decreases with temperature due to the increase in photorespiration

with temperature (Haxeltine and Prentice, 1996; Peterhansel et al., 2010). Reco is observed to increase with temperature (Bond-Lamberty and Thomson, 2010; Lloyd and Taylor, 1994; Davidson et al., 2006a), but this overall response is composed of several components which have different temperature sensitivities (Trumbore, 2006; Luyssaert et al., 2007) and may also experience different ambient temperatures. Above-ground Ra will respond to air temperature, while below-ground Ra and Rh will respond to soil temperature, which can be very different to the ambient air temperature, particularly under snow (Bon; Monson et al., 2006; Nobrega and Grogan, 2007). The increase in Rh with temperature partly results from an increase in soil microbial respiration and partly because soil organic matter decomposes faster under higher temperatures (Suseela et al., 2011). Although observations have generally shown that soil respiration increases nearly exponentially with soil temperature (Lloyd and Taylor, 1994), recent studies suggest that soil respiration may decrease after $\sim 25^{o}$C due to moisture limitation and reduced microbial enzyme activity at high temperatures (Carey et al., 2016). Temperature also effects Reco indirectly through the supply of material from GPP (Davidson et al., 2006b), further complicating the relationship between observed Reco and temperature.

Global temperatures have increased by around 0.72 ^{o}C (0.49 - 0.88 ^{o}C) from 1951-2012, due primarily to an increase in radiative forcing from the increase in atmospheric CO_2 (Ciais et al., 2013). This global temperature increase has not been homogeneous, particularly in Arctic regions where temperatures have risen around two times faster than the northern hemisphere average. Increasing temperatures at high northern latitudes have generally led to a net increase in carbon uptake, as observations show increases in productivity due to a warming-driven lengthening of the growing season (Miller and Smith, 2012; Zhou et al., 2001; Barichivich et al., 2013). Warming is also driving a northward shift of the tree-line (Harsch et al., 2009; Elmendorf et al., 2012), which may have contributed to the observed increase in ASC at these high northern latitudes (Forkel et al., 2016).

Future warming may continue to increase productivity as studies in boreal and temperate regions suggest that Ra acclimates to increases in temperature faster than photosynthesis (Ryan and Law, 2005; Way and Oren, 2010; Reich et al., 2016). Thus, the fraction of carbon allo-

cated to net primary productivity (NPP = GPP-Ra) may increase as temperatures increase. Additionally, ecosystem warming experiments show that net photosynthesis can significantly increase under elevated temperatures due to increases in nitrogen mineralisation and an increase in the rate of photosynthesis (Lu et al., 2013; Yuan et al., 2018). Although respiration was also observed to increase in these experiments, the net flux tended to result in a continued net sink (Lu et al., 2013). However, most experiments are currently performed on seedlings and so the recorded responses may not be applicable to mature forests (Lu et al., 2013). Furthermore, observations in Arctic ecosystems show that the relationship between productivity trends and temperature has weakened in recent years (Piao et al., 2014, 2017).

Water

Water is essential for plants and soil microbes to function, and it plays a complex role in photosynthesis and respiration. Within the plant, water is needed for the transport of essential substances such as sugars and nutrients, it keeps them turgid to allow them to function correctly and it contributes to most of the biomass of leaves and roots (Lam). Plants take up water from the soil through their roots and lose it through transpiration when their stomata open to absorb CO_2. When plants are water stressed they close their stomata to prevent further water loss through transpiration, decreasing CO_2 uptake and photosynthesis (Osakabe et al., 2014). Thus, both soil and atmospheric moisture play a key role in regulating photosynthesis. Soil moisture is also important for respiration, as microbial activity is reduced if conditions are too wet or too dry (Trumbore, 2006; Houghton et al., 1998). Soil moisture also mediates the rate of increase in Rh with temperature and the magnitude of its influence varies throughout the year as the relationship with temperature is complex (Suseela et al., 2011). Studies have shown that GPP is $\sim 50\%$ more sensitive to drought than respiration (Schwalm et al., 2010), but that two thirds of the decrease in GPP during drought years is offset by the simultaneous reduction in Reco (Jung et al., 2017).

There are many ways to measure atmospheric moisture content, but for vegetation, vapour pressure deficit (VPD) is of key importance (Medlyn et al., 2011). VPD is a measure of the

dryness of the air, calculated as the difference in vapour pressure between the actual and potential moisture the air could hold at saturation (Damour et al., 2010; Medlyn et al., 2011), and is sensitive to temperature as warmer air is able to hold more moisture. At low VPD (i.e. when the difference between the actual and potential vapour pressure is low), the air is near saturation and cannot accept any more moisture, so transpiration from the leaf is low. As VPD increases, atmospheric moisture decreases, resulting in an increase in transpiration and decrease in photosynthesis (Bon). Studies show that VPD has increased globally since the 1980's due to increased warming, and it has been suggested that this has played a significant role in the observed increase in drought areas over this time (Dai and Zhao, 2017).

Soil moisture is difficult to measure as remote sensing techniques only represent the top few centimetres of the soil, and site measurements are not directly representative of larger scales (Entin et al., 2000). Using drought indices calculated since 1950 as a proxy for changes in soil moisture, Dai and Zhao (2017) found drying trends in some regions of the northern hemisphere such as Europe, China and central Canada, and drying in the USA since 1990's. Increases in drought through VPD increases or reductions in soil moisture may be slowing the greening trend in temperate ecosystems (Piao et al., 2014). Drought stress has decreased around 60-90°N, perhaps driven by warming, but since productivity in these regions is not currently limited by moisture (Piao et al., 2014), this change in moisture availability may have little effect on productivity in these ecosystems.

Models indicate that droughts may increase in the future as precipitation patterns change and as the atmosphere continues to warm, driving an increase in evapotranspiration (Dai and Zhao, 2017). However, by considering the effect of ecocological processes (e.g. GPP) as well as hydrological fluxes, Greve et al. (2017) showed that in many regions, the projected drought from reductions in soil moisture and relative humidity may be partly offset by increases in GPP and precipitation. Furthermore, as discussed in Section 1.6.1, several studies conclude that WUE increases with increases in atmospheric CO_2 (Keenan et al., 2013; Saurer et al., 2014; Frank et al., 2015), and recent modelling studies suggest that the increase in WUE due to future increases in CO_2 may counteract negative effects from reduced water availability (Swann et al.,

2016; Mankin et al., 2017). Thus, understanding future water availability will require further understanding of the complex interaction between changes in WUE driven by increasing CO_2, GPP and changes in precipitation (Keenan et al., 2013; Norby and Zak, 2011; Swann et al., 2016).

Nutrients

Nitrogen and other nutrients such as phosphorus are essential for plant functioning (Evans, 1989; Bon). Nitrogen is argued to be the most important nutrient as it limits primary production; adding nitrogen to ecosystems will generally increase growth (Ciais et al., 2013; Bon; Terrer et al., 2018). Nitrogen availability has significantly increased over the last century because of the anthropogenic addition of reactive nitrogen to ecosystems through the use of fertilisers, and this has alleviated limitations to growth in some nitrogen poor ecosystems (Ciais et al., 2013). This increase in nitrogen availability enhances the increase in primary production from elevated CO_2, although the strength of this effect varies between ecosystems (Terrer et al., 2018). Warming can also increase nitrogen availability as it speeds up decomposition, but as warming increases respiration too, the net effect on carbon exchange remains uncertain (Ciais et al., 2013). As ecosystem growth is likely to increase in the future, the demand for nitrogen is projected to increase. Thus nitrogen limitations are expected to limit the future effect of elevated CO_2 and warming (Ciais et al., 2013; Zaehle et al., 2014).

Land use change

The conversion of forested areas to crops, grazing land and urban areas altered around 40% of the total land area between 1750-2000 (Pielke et al., 2011). This conversion to cropland may have a particularly large influence on the seasonal cycle of CO_2, as the growing season of crops is much shorter and more focused than the natural vegetation that has been replaced (Zeng et al., 2014). The change in land use has been particularly significant across northern high latitudes, leading some studies to conclude that the increase in cropland has contributed between 17-25% (Gray et al., 2014) or up to 45% (Zeng et al., 2014) to the increase in ASC observed at these latitudes. The estimate from Gray et al. (2014) was based on observations of changes in crop yield and crop area and may therefore be more robust than the high estimate

from Zeng et al. (2014) which is based on a single model. Other modelling studies suggest that the contribution of cropland to the seasonal cycle amplitude has been small (Forkel et al., 2016; Zhao et al., 2016), but this may result from poor representation of the complexities of croplands (Zhao et al., 2016). Nevertheless, since much of the increase in cropland has occurred between 20-45°N and the increase in seasonal amplitude has been observed at 45-90°N, the lower estimate of Gray et al. (2014) may be more realistic.

Forest management, such as wood harvesting, abandonment and afforestation, also influences terrestrial carbon fluxes as this changes the structure and composition of the vegetation in a particular region (Arneth et al., 2017). These processes are not usually included in TBMs, and instead calculated using bookkeeping models that simulate changes in carbon stocks using local and satellite data (Le Quere et al., 2018). Since these methods do not allow for transient responses to the environment, the contribution to the global carbon budget from land-use change has remained a fairly constant carbon source of around 1.3 PgC yr $^{-1}$ for the last few decades (Le Quere et al., 2018). However, a recent study using several TBMs that included wood harvesting and detailed crop management suggests that the contribution to the global carbon budget from forest management has been underestimated (Arneth et al., 2017). This would require a larger residual terrestrial sink in order to balance the carbon budget.

1.7 Modelled drivers of productivity changes in the terrestrial biosphere

1.7.1 Earth system models

Historical and future carbon fluxes have been analysed in ESMs through a series of CMIPs, most recently CMIP5. Models were evaluated on their response to a variety of CO_2 concentration pathways, including reconstructed historical CO_2 emissions, representative concentration pathways of future emissions projections and a simulation where CO_2 increases at 1% yr^{-1} for 140 years from the pre-industrial concentration of 285ppm to ∼1150ppm (Arora et al., 2013; Friedlingstein et al., 2014). Additional experiments were run in which these changes were re-

stricted to just the radiative or biogeochemical part of the model to give an estimate of the effects of increasing CO_2 on climate and biogeochemical processes (i.e. photosynthesis and respiration) respectively (Arora et al., 2013). There is a large range between modelled estimates of the historical land carbon flux, and not all models show a land carbon sink by 2005 or in the future (Friedlingstein et al., 2014). Further experiments show that all models have an increase in the net land carbon sink driven by CO_2 fertilisation, but that the net carbon uptake was reduced over time due to the saturation of the CO_2 fertilisation effect, climate driven increases in respiration and changes in biomass cycling driven by both CO_2 and climate (Arora et al., 2013). The magnitude of the CO_2 fertilisation effect was also the largest uncertainty between models (Arora et al., 2013).

Recently, Wenzel et al. (2016) used the emergent constraint methodology (Cox et al., 2013) on CMIP5 estimates of GPP amplitude change to suggest that the uncertainty in the CO_2 fertilisation effect in CMIP5 models could be reduced from 20-60% for a doubling of atmospheric CO_2, to 37±9% for ecosystems 60-90°N and 32±9% for ecosystems 30-90°N. However, since the modelled GPP amplitude was only constrained using two sites, rather than the more representative aircraft measurements of CO_2 amplitude change across high northern latitudes from Graven et al. (2013), this result may not be robust. When compared to the aircraft measurements, CMIP5 models all underestimated the increase in the seasonal cycle amplitude observed from 1958/61 - 2009/10 (Graven et al., 2013), suggesting that the CO_2 fertilisation effect across these ecosystems may be larger than estimated by Wenzel et al. (2016).

1.7.2 Terrestrial biosphere models

Terrestrial biosphere models (TBMs) have also been evaluated on their ability to reproduce the change in the CO_2 seasonal cycle amplitude and the net carbon sink. The TRENDY models underestimate the increase in the seasonal cycle amplitude compared to inversions across boreal and temperate (23.5-90°N) ecosystems (Zhao et al., 2016), but show mixed results when transported surface fluxes were compared to 26 surface sampling stations in this region (Piao et al., 2017). The LPJ-mL model was able to capture the increase in the ASC latitudinal

gradient when compared to 19 surface sampling stations between 40-90°N, but underestimated the increase in ASC compared to the aircraft measurements (Forkel et al., 2016). While models agree that carbon uptake is the primary driver of the increase in ASC, they disagree on the main drivers of this change (Zhao et al., 2016; Forkel et al., 2016). Recent analysis showed that the MsTMIP models disagree on the primary driver of the net carbon sink for 85% of land, particularly in temperate biomes (Huntzinger et al., 2017). The increased amplitude in the LPJ-mL model resulted from climate driven changes in vegetation, (Forkel et al., 2016), but overall, CO_2 fertilisation is the main mechanism driving the increase in amplitude for MsTMIP and TRENDY models. The contribution of CO_2 fertilisation to the trend in ASC has a large inter-model range (Zhao et al., 2016; Piao et al., 2017; Ito et al., 2016) which can partly be explained by the inclusion of nutrients, as MsTMIP models with a coupled carbon-nitrogen cycle had a 50% smaller contribution to the net carbon sink from CO_2 fertilisation compared to models without (Huntzinger et al., 2017).

For TBMs, model differences result from differences in model structure, and uncertainties associated with modelled climate are eliminated (Friedlingstein et al., 2014; Graven et al., 2013). The range in outputs given by the literature above support previous analyses showing that the main factor driving uncertainty between models is their representation of the terrestrial biosphere rather than differences in modelled climate of ESMs (Lovenduski and Bonan, 2017; Anav et al., 2015).

Despite increases in model complexity and the number of processes modelled, uncertainties about the mechanisms driving changes in productivity and the seasonal cycle of CO_2 persist (Bonan and Doney, 2018; Zhao et al., 2016; Piao et al., 2017; Ito et al., 2016; Forkel et al., 2016; Prentice et al., 2015). Efforts to improve models are currently focussed on a continued increase in the number of processes modelled and increased coupling between different parts of the model (Eyring et al., 2016; Prentice et al., 2015). Rather than improving our understanding of the mechanisms driving changes in the models, this may simply increase model differences and uncertainty (Prentice et al., 2015). Furthermore, previous studies to understand the mechanisms driving the change in the seasonal cycle amplitude only compared models to a handful

of site observations rather than the more representative aircraft measurements presented in Graven et al. (2013) (Forkel et al., 2016; Wenzel et al., 2016; Piao et al., 2017).

1.8 Outline

The primary focus of this thesis is to further understand the mechanisms driving the changes in productivity at high northern latitudes over recent decades. I do this by combining observational constraints in new ways to analyse current TBMs, and using a new model for GPP, the P-model, which is based on optimal plant behaviour to analyse recent trends in GPP. I analyse factorial experiments run by the current TBMs and the P-model to evaluate the role that different drivers have on the recent changes in productivity. Additionally, I use the concept of ecosystem light-use efficiency (eLUE) as a metric to compare the role of structural and physiological changes in productivity in the P-model and the TBMs.

First, in Chapter 2, I analyse existing terrestrial biosphere models taking part in MsTMIP. I compare them to observed trends in greening from the fAPAR3g data product (Zhu et al., 2013) and aircraft observations of the increasing amplitude of the seasonal cycle of CO_2 (Graven et al., 2013). I consider changes in modelled productivity by calculating modelled changes in eLUE, and analysing experiments performed by the MsTMIP models to quantify the role of CO_2, climate, land-use change and nitrogen deposition. In Chapter 3, I present a simple model of gross primary production, the P-model, and validate it against measurements from selected Fluxnet sites. I use P-model estimated GPP to drive simple models for ecosystem respiration and then calculate NEE fluxes, which are also compared to Fluxnet site observations. Finally, in Chapter 4, I run fully factorial experiments using the P-model to quantify the role of changes in CO_2, climate, fAPAR and PAR on changes in productivity. I again make use of the concept of eLUE to compare the structural and physiological changes in vegetation between the P-model and the MsTMIP models and show how this metric can improve our understanding of recent changes in productivity.

Chapter 2

Evaluation of current terrestrial biosphere models

2.1 Introduction

Observations show that the terrestrial biosphere is responding to anthropogenic environmental change (Friedlingstein et al., 2014; Ciais et al., 2013). Photosynthetic CO_2 uptake currently exceeds release through respiration and other processes, and the terrestrial biosphere removes around a quarter of anthropogenic CO_2 emissions each year (Ciais et al., 2013). Net uptake of CO_2 can be partly attributed to CO_2 fertilisation, since increases in the ambient CO_2 concentration can increase the biochemical rate of photosynthesis and increase water use efficiency (Franks et al., 2013; Penuelas et al., 2011; Keenan et al., 2013). Net uptake of CO_2 may also result in part from changes in climate, land management, ecosystem composition and N deposition, among other factors (Ciais et al., 2013; Sitch et al., 2015; Huntzinger et al., 2013). Better understanding of how the terrestrial biosphere has responded to changes in climate, CO_2 concentration and other drivers over recent years is needed to understand how it might change in the future, and whether it will continue to serve as a net sink (Le Quere et al., 2018; Friedlingstein et al., 2006; Schimel et al., 2015). In this chapter I compare long-term observations of atmospheric CO_2 and greenness to terrestrial biosphere model output.

The seasonal cycle of atmospheric CO_2 concentration in the Northern Hemisphere can be almost entirely attributed to terrestrial biosphere exchange (Randerson et al., 1997; Graven et al., 2013), so changes in the seasonal cycle of atmospheric CO_2 indicate large-scale changes in northern terrestrial ecosystem exchange. Increases in the amplitude of the seasonal cycle of CO_2 (ASC) have been observed at the measurement stations Mauna Loa, Hawaii (MLO), and Point Barrow, Alaska (BRW) of 0.32±0.07 %yr^{-1} and 0.60±0.05 %yr^{-1} respectively, since the early 1960's (Keeling et al., 1996a; Graven et al., 2013). Recently, Graven et al. (2013) measured long-term changes in ASC throughout the higher latitudes of the Northern Hemisphere. Comparisons between two aircraft campaigns in 1958-61 and 2009-11 showed an increase in ASC of 5.0±0.8 ppm (56±9.8%) between 45-90°N at 500 mb, indicating that the seasonal uptake and release of CO_2 in terrestrial ecosystems between 30-90°N increased by 32-59% over this time (Graven et al., 2013). These aircraft measurements have similar relative increases in ASC compared to the surface stations, showing for the first time that the increase in ASC is a large scale feature across high northern latitudes. The largest contribution to the ASC was in the main growing season (Graven et al., 2013). Increases in ASC may therefore be related to the extratropical net carbon sink as studies suggest that increases in net terrestrial carbon uptake during the growing season drive the northern extratropical net carbon sink (Rayner et al., 2015; Gurney and Eckels, 2011).

The change in ASC can result from a change in the phase and/or magnitude of seasonal carbon uptake through photosynthesis and release through respiration, defined as net primary production (NPP) and heterotrophic respiration (Rh) respectively. NPP is the net amount of carbon fixed by vegetation after a fraction of the gross carbon that is assimilated has been used for vegetation growth and maintenance as autotrophic respiration. Most of the carbon fixed by NPP is then returned to the atmosphere each year through heterotrophic respiration as bacteria and other organisms in the soil consume the plant biomass. The difference between NPP and Rh is the net ecosystem production (NEP, NEP = NPP-Rh) (Chapin et al., 2006), the amplitude of which is well correlated to ASC (Graven et al., 2013). At high northern latitudes, NPP and Rh follow a distinct seasonal cycle as each flux responds to changing environmental conditions throughout the year, and the mismatch between these two cycles creates the seasonal cycle

in NEP (Similar to that shown in Figure 1.1). The seasonal cycle of NPP is defined by the seasonal cycle of incoming light and temperature, with a minimum during dark and cold winter months and a peak in the summer months (Falge et al., 2002). Ambient CO_2 concentrations and the availability of nitrogen and water also play an important role in regulating the rate at which carbon is fixed through NPP (Lam). Rh occurs continuously throughout the year, but is strongly dependent on soil temperature so peaks in late summer (Falge et al., 2002). Soil moisture is also an important factor as microbial activity is reduced if conditions are too wet or too dry (Houghton et al., 1998). By considering how environmental drivers influence seasonal NPP and Rh and their change over recent decades, it is clear that the increase in ASC could be driven by multiple mechanisms.

Trends in vegetation greenness, defined here as the fraction of photosynthetically active radiation that is absorbed by green vegetation on land (fAPAR), imply that photosynthetic activity in northern latitudes has increased over the last three decades (Slayback et al., 2003; Zhu et al., 2013). Vegetation greenness has been measured by satellites since mid-1981 (Murray-Tortarolo et al., 2013), and an increase of vegetation greenness has been observed between 30-90°N of 8.7% for all types of vegetation from 1982-2010 (Figures 2.4, 2.7b). Many studies attribute this greening primarily to rising temperatures which have led to a reduction in snow cover, an earlier start to the growing season (Piao et al., 2008; Myneni et al., 1997; Notaro et al., 2005; Xu et al., 2013) and increased peak greenness (Buitenwerf et al., 2015; Myneni et al., 1997).

Observations of the CO_2 seasonal cycle and vegetation greenness, and their changes over time, present opportunities to evaluate terrestrial biosphere models. Reproducing the mean CO_2 seasonal cycle requires that modelled photosynthesis and respiration have the correct phase and magnitude. Reproducing the changes in ASC additionally requires that interactions between the terrestrial biosphere and the environmental drivers, including climate, CO_2, land use and disturbance (e.g. fire, insects) are well represented in models (McGuire et al., 2001). Previous comparisons have shown that the long-term increase in ASC observed in the aircraft data was underestimated by the coupled carbon-climate CMIP5 Earth System Models, but the reasons for this underestimation remain unclear (Graven et al., 2013). The smaller trend observed in

ASC at ground-based NOAA stations over 1982-2011 was captured by one offline dynamic vegetation model (LPJml) (Forkel et al., 2016) while the trend was over- and underestimated by eight dynamic vegetation models from the TRENDY dynamic vegetation model intercomparison project (Piao et al., 2018). In LPJml, the ASC increase was primarily driven by increases in vegetation cover and plant productivity resulting from increasing temperatures at high latitudes (Forkel et al., 2016), whereas the TRENDY models suggested that CO_2 fertilisation was the main driver of the increase in amplitude (Piao et al., 2018). Other studies have examined the drivers of large scale seasonal biosphere fluxes in models. For the offline terrestrial biosphere models taking part in the Multi-scale Synthesis Terrestrial Model Intercomparison Project (MsTMIP) and the TRENDY models, changes in seasonal fluxes were predominately driven by increase in atmospheric CO_2, while climate change was the primary driver in only a minority of models (Ito et al., 2016; Zhao et al., 2016). In comparisons of observed and modelled greening trends, the TRENDY models suggest that greening has been primarily driven by climate change at higher northern latitudes (60-90°N) and by CO_2 at lower northern latitudes (30-60°N) (Zhu et al., 2016).

There is a clear need to identify mechanisms that reconcile observed and modelled changes in ASC and greening, and to clarify the role of CO_2, climate change and other factors driving ecosystem changes. A key distinction can be made between changes in the structure (leaf area) and the physiology (intrinsic rate of carbon uptake) of vegetation by using the concept of light-use efficiency (LUE), the net primary productivity (NPP) per unit of light absorbed (APAR) (Norby et al., 2003; Medlyn, 1998). If increases in NPP for a given ecosystem were driven solely by increased leaf area, and therefore increased APAR, NPP would relate to APAR by a constant factor corresponding to the LUE of the ecosystem. However, increases in NPP may also arise from increases in LUE, even in the absence of APAR increases. A decade of plot-scale observations from four temperate sites in the Free Air CO_2 Enrichment (FACE) experiments show that in medium- to high-density canopies, increases in NPP were driven by LUE increases, while there was no significant change in APAR (Norby et al., 2003; Mccarthy et al., 2006; Long et al., 2004). Analysis of LUE trends in models can therefore help to elucidate mechanisms of ecosystem change and to inform model-data comparisons of fAPAR and CO_2 exchange (Norby

et al., 2005).

In this chapter, I compare observed changes in ASC and greening trends to output from 13 biosphere models in MsTMIP, applying the concept of LUE to interpret the model-data comparison. In MsTMIP, the process-based terrestrial biosphere models ran semi-factorial experiments and were driven by a standard set of observed changes in climate, land use, CO_2, and in some cases N deposition (Huntzinger et al., 2013; Wei et al., 2014). I compare modelled output of greenness to the longest available record of satellite fAPAR data - fAPAR3g (Zhu et al., 2013). I use the TM3 atmospheric transport model with net ecosystem production from MsTMIP to evaluate the modelled seasonal cycle amplitude of atmospheric CO_2 against aircraft measurements in 1958-61 and 2009-10. The aircraft data are more representative of large-scale behaviour than surface measurement stations (Sweeney et al., 2015; Keppel-Aleks et al., 2012; Sawa et al., 2012), showing a clearer and more consistent signal. Thus aircraft data are a stronger constraint on large-scale ecosystem changes than the long-term records at surface stations such as MLO and BRW, but they have previously been compared only with CMIP5 models (Graven et al., 2013).

I show that most MsTMIP models simulate overall greening trends well, but underestimate the observed ASC change. Increases in modelled NPP in northern ecosystems are a combination of CO_2-driven increases in LUE and climate-driven greening. Since models capture greening trends but underestimate the change in ASC, this suggests that models underestimate increases in ecosystem LUE over the past several decades, possible causes of which are discussed.

2.2 Methodology

2.2.1 Observed Data

Seasonal amplitude of atmospheric CO_2

The aircraft campaigns 'International Geophysical Year' in 1958-61 and 'HIAPER Pole-to-Pole Observations' in 2009-11 observed atmospheric CO_2 in the mid to lower troposphere (Graven et al., 2013; Wofsy et al., 2011; Keeling et al.). I focus on the change in the amplitude of the seasonal cycle of CO_2 (ASC) at 500 mb in the 45-90°N region, where the largest increase in ASC was observed: 5.0±0.8 ppm (56±9.8%). I do not consider phase shifts in the CO_2 seasonal cycle, since they are not clearly resolved either by aircraft observations (Graven et al., 2013) or monthly model output.

Vegetation greenness

Vegetation greenness was analysed using the remotely sensed third-generation fAPAR data product, fAPAR3g, at 1/12° resolution (Zhu et al., 2013). The data were averaged to the 0.5° x 0.5° grid of the MsTMIP models over 1982-2011 (Zhu et al., 2013). To account for differences in incoming radiation throughout the year and changes in growing season length, monthly fAPAR was calculated as the mean of 15-day cloud-free composites, weighted by average monthly PAR (Kelley et al., 2013) using WATCH data (Weedon et al., 2011) and then summed for each gridcell and month between 30°N-90°N in which the temperature was above 0° C to get annual growing season fAPAR (GS-fAPAR). The weighting, W, was calculated for each grid cell (i,j) and month (m) as;

$$W_i, j, m = \frac{PAR_{i,j,m}}{\Sigma_{m=1}^{m=12} PAR_{i,j,m}} \tag{2.1}$$

Higher weightings were given to months with more PAR. Total northern hemisphere GS-fAPAR was calculated as the mean of all land grid cells north of 30°N .

2.2.2 Model Output

MsTMIP models

I analyse the CO_2 fluxes from 13 terrestrial biosphere models that generated output for the the MsTMIP V1.0 experiments (Table 2.1) (Huntzinger et al., 2014). The model output used is freely available to download via the MsTMIP website (https://nacp.ornl.gov/). Global monthly model output is at 0.5° x 0.5° resolution. A standard protocol and environmental driver dataset were used to spin up models to steady-state, and control simulations were run for each model with environmental drivers held at pre-industrial levels. Experiments were run in which historical climate, land-use change (LUC) and CO_2 were sequentially included as model drivers, and then N-deposition for: BIOME-BGC, CLM4, CLM4VIC, DLEM, ISAM and TEM6 (Huntzinger et al., 2013). The historical drivers consist of observed and reanalysis data. A land cover map was reinterpreted by each modelling team, for use as the LUC driver (Wei et al., 2014). Since the models are driven by the same data, inter-model differences reflect how terrestrial biosphere processes have been represented in each model (Dalmonech and Zaehle, 2013; Le Quere et al., 2015; Huntzinger et al., 2013; Sitch et al., 2015). Unless otherwise stated, the simulation including all time-varying historical drivers is used in the results. I also analyse individual contributions to fluxes from climate, LUC, CO_2 or N-deposition, which were calculated as the difference between the first simulation in which that type of historical data was used and the previous simulation. One model, BIOME-BGC, only ran the 'climate-only' and 'all-on' experiments, with fixed LUC and N-deposition.

Analysis was carried out on years overlapping with the aircraft and satellite observation periods: 1958-61 and 2009-10, and 1982-2010 respectively. Monthly net ecosystem productivity (NEP) was calculated from model outputs as the difference between net primary production and heterotrophic respiration (NPP-Rh) (Chapin et al., 2006). This neglects fire and other disturbances but these are often absent or poorly represented in models (Graven et al., 2013; Randerson et al., 1997), and poorly constrained by observations (Huntzinger et al., 2013). The CO_2 concentration resulting from the NEP fluxes was calculated for each model and simula-

Table 2.1: About models in MsTMIP. N = Nitrogen (Yes/No = Y/-), DGVM = Dynamic Global Vegetation Model (Yes/No = Y/-), LAI = Leaf Area Index (Calculated by the model/Prescribed = Dynamic/Remote Sensing), Crops (Yes/No = Y/-).a: Generic C3 crops only

Model	N	DGVM	LAI	Crops	Reference
Biome-BGC	Y	-	Dynamic	-	(Thornton et al., 2002)
CLM4	Y	-	Dynamic	Y[a]	(Shi et al., 2011; Mao et al., 2012)
CLM4VIC	Y	-	Dynamic	Y[a]	(Li et al., 2011)
DLEM	Y	-	Dynamic	Y	(Tian et al., 2011, 2012)
GTEC	-	-	Dynamic	-	(Ricciuto et al., 2011)
ISAM	Y	-	Remote sensing	-	(Jain and Yang, 2005)
LPJ-wsl	-	Y	Dynamic	-	(Sitch et al., 2003)
ORCHIDEE-LSCE	-	-	Dynamic	-	(Krinner et al., 2005)
SiB3-JPL	-	-	Remote sensing	-	(Baker et al., 2008)
SiBCASA	-	-	Dynamic	-	(Schaefer et al., 2008)
TEM6	Y	-	Dynamic	-	(Hayes et al., 2011)
VEGAS 2.1	-	Y	Dynamic	-	(Zeng et al., 2005)
VISIT	-	-	Dynamic	-	(Ito and Inatomi, 2012)

tion using the TM3 atmospheric transport model at 5° x 3.83° resolution, forced by NCEP reanalysis data specific for each year (Heimann and Korner, 2003). This captures any changes in atmospheric transport, even though transport effects were shown to have little impact on long-term ASC trends (Graven et al., 2013). Compared to other atmospheric transport models, TM3 does not show large biases in seasonal CO_2 amplitude or vertical exchange (Gurney et al., 2004; Stephens et al., 2007). The simulated CO_2 concentration from NEP was added to simulated CO_2 concentrations from monthly ocean (Patra et al., 2011; Roedenbeck et al., 2003) and fossil fuel (Andres et al., 2011) fluxes for the same years. The total CO_2 concentration for each model was then detrended for each latitude band using a polynomial fit and the mean CO_2 concentration was subtracted, and interpolated to the time and location of individual aircraft observations at 500mb.

Monthly modelled fluxes of NPP, Rh and NEP were each summed over 30-90°N for 1958-61 and 2009-10, and the seasonal amplitude and mean annual flux was calculated for each flux and time period. The flux and CO_2 concentration amplitudes were calculated as the difference between the maximum and minimum of the mean seasonal cycle.

Modelled Leaf Area Index (LAI, the projected area of leaves over an area of ground (Murray-

Tortarolo et al., 2013)) was converted to fAPAR using the Beer's Law approximation:

$$fAPAR = 1 - e^{-0.5LAI}. \tag{2.2}$$

Modelled GS-fAPAR was calculated in the same way as observed GS-fAPAR (Section 2.2.1). Modelled growing-season LUE was calculated for land 30-90°N in 1958-61 and 2009-10 as:

$$GS\text{-}LUE = \frac{GS\text{-}NPP}{GS\text{-}APAR} \tag{2.3}$$

where

$$GS\text{-}APAR = GS\text{-}fAPAR * PAR. \tag{2.4}$$

2.3 Results

2.3.1 Seasonal CO_2 amplitude change

Some of the MsTMIP models are able to reproduce the amplitude of the CO_2 seasonal cycle and its latitudinal gradient at 500mb in 1958-61, but none do in 2009-10 (Figure 2.1). Models simulate a wide range of ASC change north of 45°N, -0.5 to 2.4 ppm, all substantially lower than observed (Figures 2.1, 2.7a). The models generally capture the phase of the CO_2 seasonal cycle in each time period (an example is shown in Figure 2.2).

The primary driver of the modelled increase in ASC is the increase in CO_2 concentration since the largest increase in ASC was found for simulations which included rising CO_2 concentrations (Figure 2.7), similar to Piao et al. (2018) and Zhao et al. (2016). Coupled carbon-nitrogen cycle (C-N) models (BIOME-BGC, CLM4, CLM4VIC, DLEM, ISAM and TEM6) have amongst the smallest changes in ASC, and the weakest CO_2-driven increases. The small CO_2-driven ASC increase in C-N models is likely due to N limitation, as ASC further increases in simulations when time-varying N-deposition is included. LPJwsl is the only model that has a fractional increase in ASC within the observational uncertainty (47%) (Figure 2.3), but its absolute ASC

Figure 2.1: Observed and modelled ASC by latitude for (a) 1958-61, (b) 2009-10 and (c) difference between 2009-10 and 1958-61. Model type depicted by markers: no nitrogen cycle, no dynamic vegetation (circles), no nitrogen cycle, dynamic vegetation (triangles), and nitrogen cycle, no dynamic vegetation (crosses). Observations ('Obs') are the results from (Graven et al., 2013), shown as the dashed black line with grey shading showing the observational uncertainty.

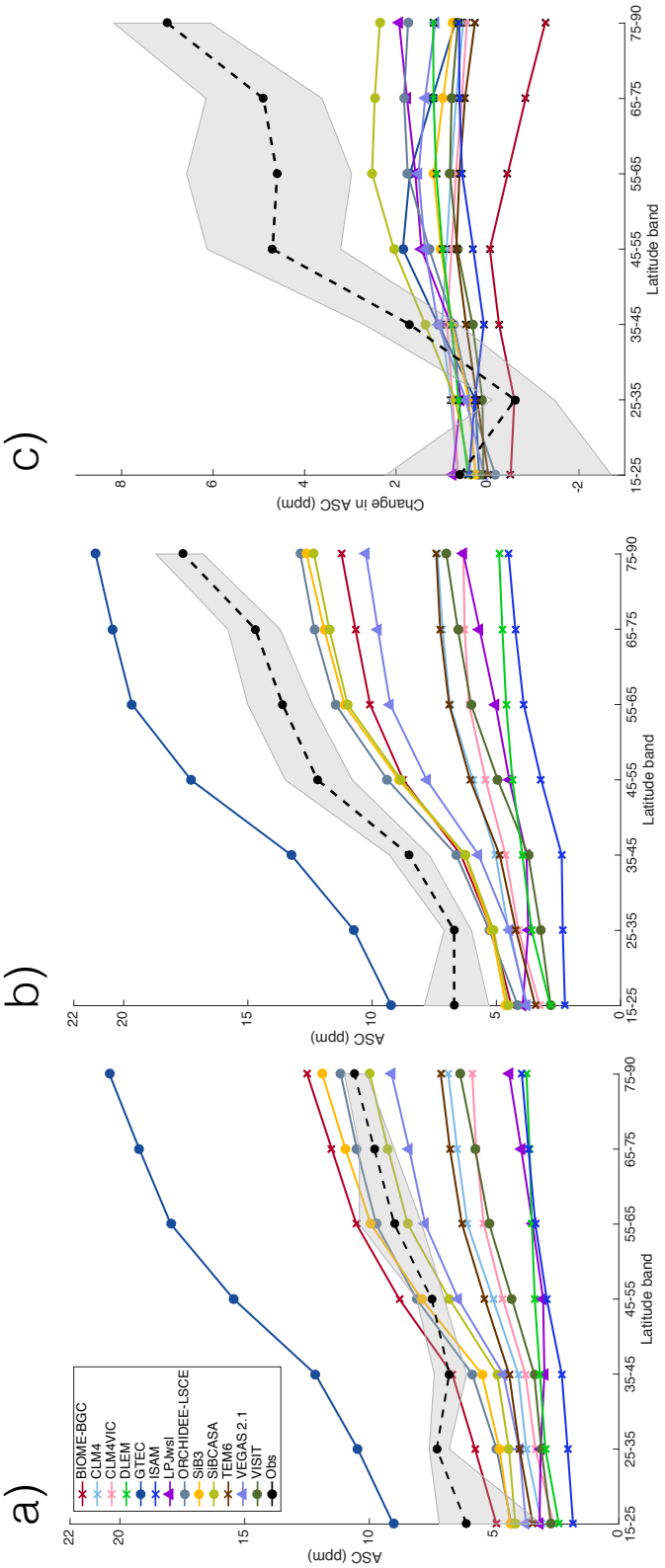


Figure 2.2: Mean seasonal cycle of CO_2 for observations (black line) and models in 2009-10 at 65°N-75°N. Observations are from the 'HIAPER Pole-to-Pole Observations' aircraft campaign. Uncertainty is grey shaded region. Overall, models capture the phase of the seasonal cycle, with trough and peak locations close to observations.

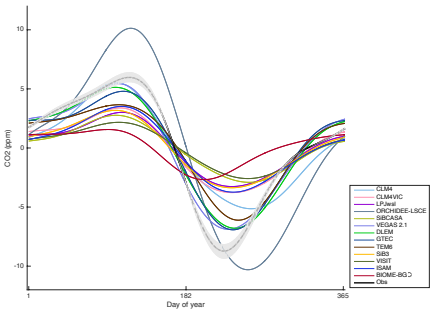
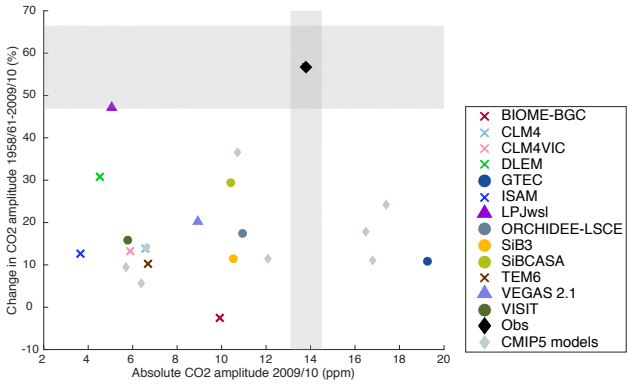


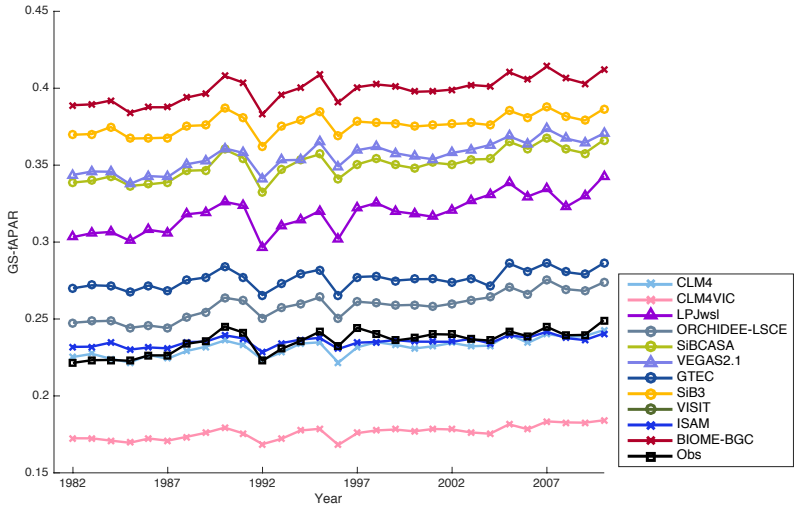
Figure 2.3: ASC in 2009-10 compared to percentage change in ASC from 1958-61 to 2009-10 for aircraft observations (black square), MsTMIP models (coloured markers) and CMIP5 models for TM3 only (grey markers) (revised from (Graven et al., 2013)). Grey shading is observational uncertainty (Graven et al., 2013).



and ASC change are much too small (Figure 2.1). The ASC change in the MsTMIP models is similar to the CMIP5 models (Figure 2.3, (Graven et al., 2013)), although MsTMIP models tend to have smaller 2009-10 amplitudes.

2.3.2 Vegetation greenness

Figure 2.4: Annual GS-fAPAR for observations and models form 1982-2010 for land 30°N-90°N.



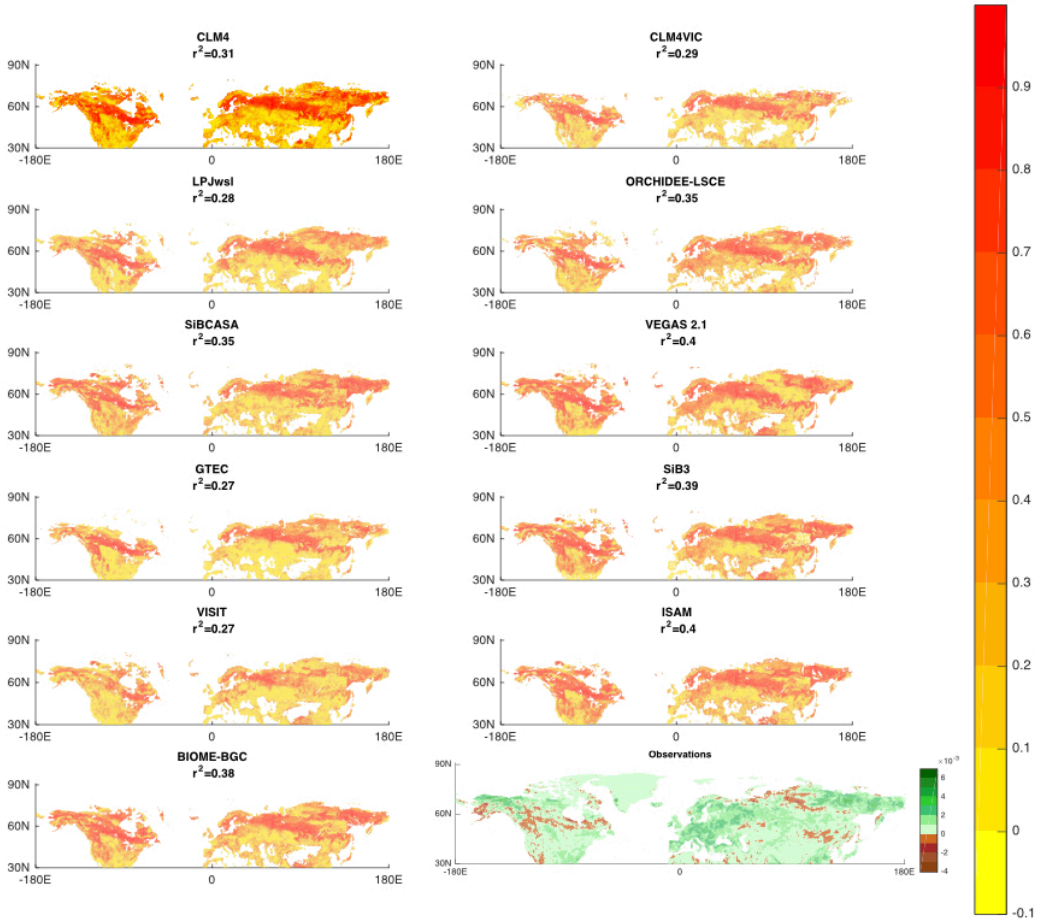
Models are generally able to reproduce the observed inter-annual variability in GS-fAPAR and its increase of 0.02 (8.7%) between 30-90°N from 1982-2010 (Figures 2.4, 2.7b). Observed and modelled greening was due to an increase in greenness per unit area, and only ISAM showed an increase in vegetated area. All models show greening is driven by climate (Figure 2.7b), and models perform best in arctic and boreal regions where greening trends have been driven by increasing temperatures (Piao et al., 2006), (Figure 2.5). There is little influence on the overall greening trend from LUC, CO_2 and N-deposition. These drivers may be of more importance at lower latitudes where models do not match observed trends well (Figure 2.5) and where greening trends depend more on how vegetation is represented in models (Eastman et al., 2013; Murray-Tortarolo et al., 2013; Zhu et al., 2016).

2.3.3 Terrestrial carbon fluxes

NEP

The amplitude of NEP varies from less than 1 $PgCyr^{-1}$ to more than 5 $PgCyr^{-1}$for 2009-10, integrated over areas north of 30°N. This is consistent with previous studies showing MsTMIP models have high inter-model variability in NEP, as well as in its constituent fluxes, gross primary production and ecosystem respiration (Huntzinger et al., 2013; Zscheischler et al., 2014;

Figure 2.5: Correlation between observed and modelled trend in GS-fAPAR for land 30°N-90°N between 1982-2010, and observed trend in GS-fAPAR (bottom right panel). Shading shows the r^2 value for each grid box corresponding to the red/yellow primary colour bar, and the r^2 given above each plot is the mean of these. Shading for observed trend corresponds to the second colour bar (green and brown).



Schwalm et al., 2015). NEP amplitude generally increased (Figure 2.6b), as shown previously for MsTMIP (Ito et al., 2016) and TRENDY (Zhao et al., 2016). NEP amplitude is well correlated to the simulated ASC across the models; r^2=0.95 (Figure 2.6a). There is also a good correlation between NEP amplitude change and ASC change (Figure 2.6b), though somewhat weaker (r^2 =0.70), which may be due to additional influences on ASC change from fluxes south of 30°N.

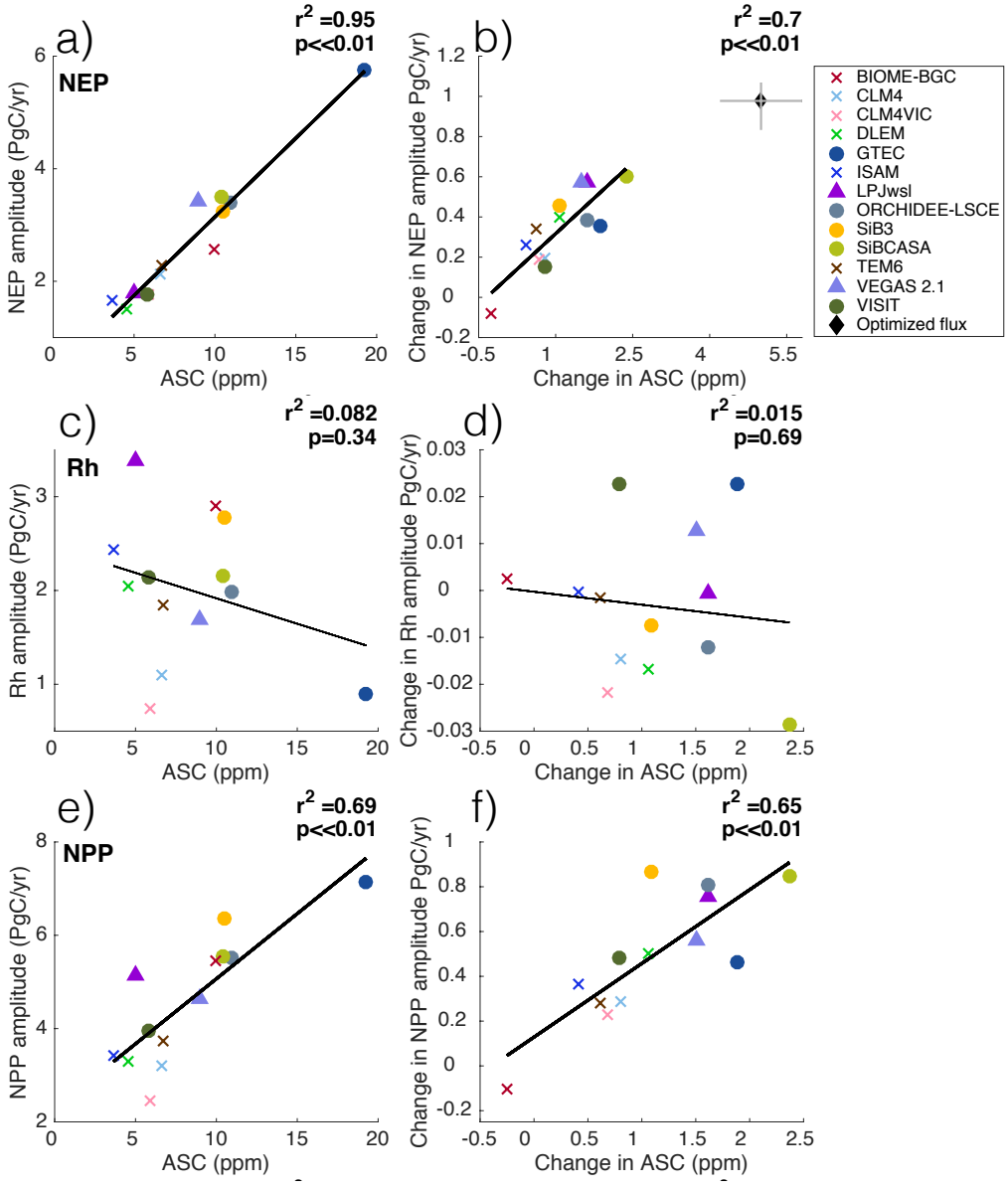
Figure 2.6b also shows the optimized flux of NEP, from Graven et al. (2013), where NEP amplitude in Arctic, boreal and temperate regions was adjusted to best match the pattern of observed ASC change in aircraft and surface data. The optimized increase in NEP amplitude from Graven et al. 2013 is larger than any modelled increase, but it lies within the uncertainty of the model regression line, indicating that the relationship between ASC and NEP amplitude change is similar.

Rh

There is no significant correlation between modelled Rh amplitude and ASC, or between Rh amplitude change and ASC change ($r^2 \approx 0$) (Figure 2.6e, f). Thus changes in Rh cannot be driving the change in modelled NEP amplitude and ASC. Mean annual Rh increased, but changes in Rh amplitude were small because Rh increased throughout the year rather than in the month of maximum Rh (Figure 2.6f, 2.7c). The small changes in MsTMIP Rh amplitude are inconsistent with CMIP5 models, which show much larger Rh amplitude changes (Figure S9 in Graven et al. (2013)), perhaps due to climate feedbacks in CMIP5 models that are not present in the offline MsTMIP models .

The largest increase in modelled mean annual Rh is generally from increases in CO_2, although changes in climate have the largest effect on Rh in VEGAS, LPJwsl, and N-deposition is dominant in CLM4VIC and CLM4 (Figure 2.7c).

Figure 2.6: Left: Modelled ASC and amplitude of (a) NEP, (c), NPP and (e) Rh for 2009-10. This relationship is similar in 1959-61. Right: Modelled ASC change and change in amplitude of (b) NEP, (d) NPP and (f) Rh. All panels except (b) show fluxes for land 30-90°N and ASC for 45°N-90°N at 500mb and regression lines are plotted, with markers as in Figure 2.1. In (b), NEP is for arctic, boreal and temperate regions only, defined by the biome mask in (Graven et al., 2013). The black diamond is observed ASC change and optimised flux of NEP from Graven et al. 2013.



NPP

The modelled seasonal amplitude of NPP and change in NPP amplitude are significantly correlated to modelled ASC and change in ASC across the models; r^2=0.69 and r^2=0.65 respectively (Figure 2.6c, d). Mean annual NPP and seasonal NPP amplitude increased for all models between the two periods (except NPP amplitude in BIOME-BGC) (Figure 2.7c). Hence changes in modelled NPP, not Rh, are driving the change in modelled NEP amplitude and ASC.

CO_2 is the primary driver of NPP increase for most models, while climate and LUC generally result in smaller changes in NPP (Figure 2.7c). Change in NPP and NPP amplitude are smallest in C-N models, resulting in small NEP and ASC change (Figures 2.6b, 2.7a).

2.3.4 Light Use Efficiency

Models show mixed results for the overall change in GS-LUE (-7.8 to 6.9%, Figure 2.7d), but the sign of the LUE response to climate change is consistent across models. Climate-change decreases GS-LUE in all models, while increasing CO_2 increases GS-LUE in all models. Increases in LUE result from N deposition in CLM4 and CLM4VIC, and from LUC in VEGAS2.1 and ORCHIDEE-LSCE, while LUC has little influence on LUE in the other models.

Figure 2.7 shows that increases in CO_2 have driven increases in modelled NPP, which results in increases in GS-LUE and ASC. On the other hand, although climate change drives increases in NPP and greening, this does not translate to increased GS-LUE or ASC.

2.4 Discussion

Current terrestrial biosphere models simulate greening trends reasonably well, but the large increase in observed ASC at high latitudes remains unexplained. There is little difference in simulated ASC or ASC change between models driven with prescribed climate and CO_2 [This study, (Zhao et al., 2016)], or with modelled climate as in CMIP5 (Graven et al., 2013) (Figure

Figure 2.7: Contributions from climate, LUC, CO_2 and N-deposition to modelled changes in: (a) ASC, (b) GS-fAPAR, (c) mean annual NPP and Rh and (d) GS-LUE. ASC is for 45°N-90N at 500mb between 1958-61 and 2009-10 (a). Fluxes are for 30N-90N between 1982-2010 (b) and 1958-61 to 2009-10 (c), (d). Fluxes are positive into the atmosphere. In (a), observations and uncertainty (grey shading) are from (Graven et al., 2013). In (b), the 95% confidence interval in the observed trend is shown (grey shading). LAI was not available for DLEM and TEM6, and LAI was assimilated from remote sensing for SiB3, so no output is shown in (b) or (d) for these models.

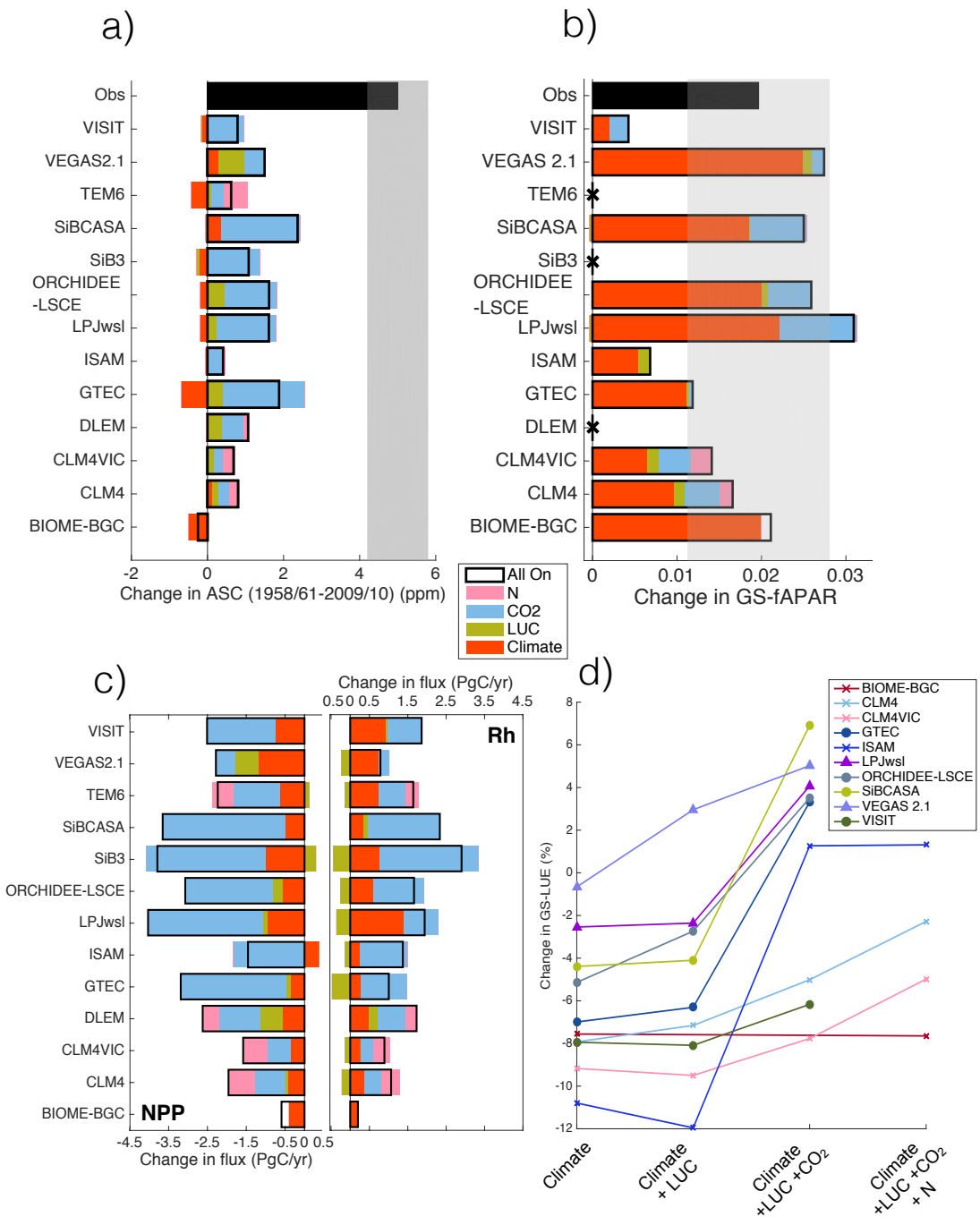
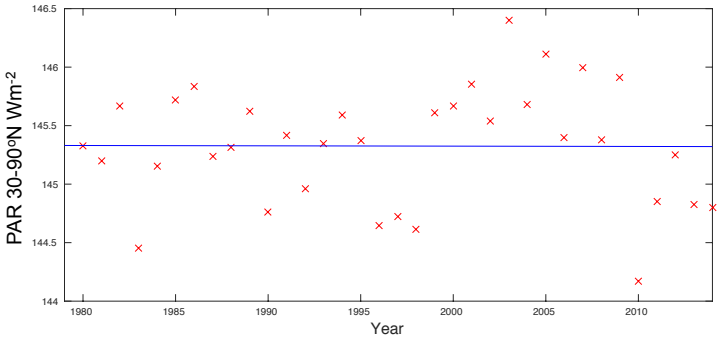


Figure 2.8: Mean annual PAR for land 30-90°N and fitted trend-line.



2.3), indicating that the disagreement between observations and models lies in the modelling of terrestrial biosphere processes rather than in the climatic forcing. Consistent with previous studies, (Graven et al., 2013; Randerson et al., 1997), Figure 2.6 implies that modelled increases in NEP amplitude lead to increases in modelled ASC. Furthermore, our model-based results suggest NPP as the main driver of NEP amplitude change, also consistent with previous studies (Randerson et al., 1997; Forkel et al., 2016; Zhao et al., 2016). NEP changes may also be influenced by respiration or disturbance (Zimov et al., 1999), but these effects must be secondary to NPP (Houghton, 1987; Randerson et al., 1997; Graven et al., 2013; Forkel et al., 2016). Since the MsTMIP models underestimate ASC changes, they are likely also to have underestimated increases in the seasonal amplitude of NPP.

Since NPP can increase through vegetation greening (increased APAR) and/or through an increase in ecosystem LUE (Equation 2.3), the models' ability to capture the greening trends, and the absence of a trend in PAR (Figure 2.8), suggests that discrepancies with observed ASC result primarily from errors in the models' representation of LUE. In particular, we suggest that models are capturing the increase in NPP in the early growing season through climate-driven greening, but underestimating the GS-LUE driven increase in NPP in the peak of the growing season when canopies are more dense. Our model-data comparison thus provide strong evidence for an increase in GS-LUE across ecosystem in high northern latitudes that is larger than simulated by MsTMIP models.

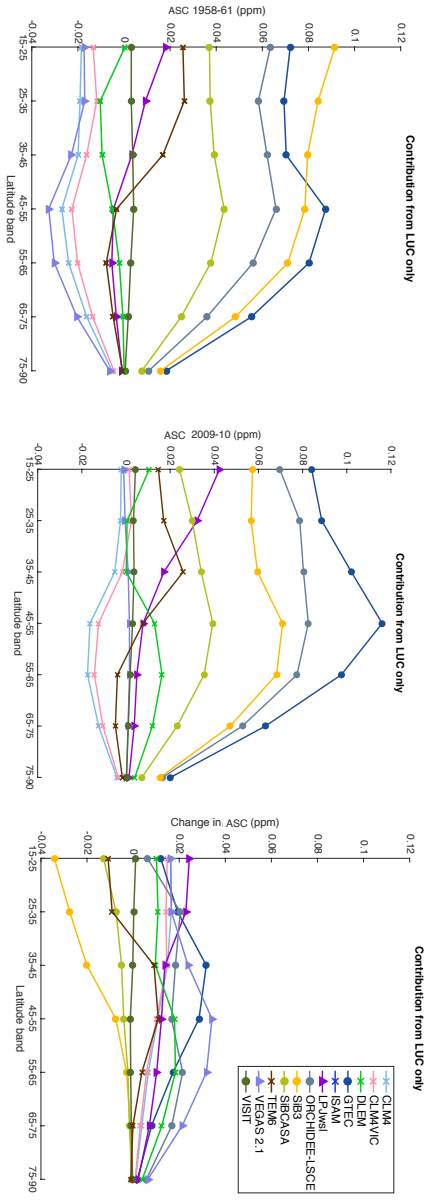
Increased LUE relates to physiological changes that enhance NPP in addition to, or in the ab-

sence of, structural changes through increased leaf area. NPP can increase through CO_2 fertilisation, as elevated CO_2 increases photosynthesis and water use efficiency (Ainsworth and Long, 2005; Norby et al., 2003). CO_2 fertilisation is included in the MsTMIP models (Huntzinger et al., 2013) and it is the primary driver of simulated NPP increases (Figure 2.7c). In models, CO_2 fertilisation plays a key role during the peak growing season when canopies are more dense, as seen in Figure 2.7 in which CO_2-driven NPP increases correspond to GS-LUE and ASC increases. Large uncertainties remain regarding the magnitude of the CO_2 fertilisation effect (Smith et al., 2016; De Kauwe et al., 2016; Schimel et al., 2015), but studies agree that N dynamics are a key, and often missing, component of this effect (Terrer et al., 2016; Wieder et al., 2015).

Climate change may affect photosynthesis and respiration in ways that are not well-represented in MsTMIP models, particularly through temperature acclimation of photosynthesis and autotrophic respiration (Ra), and through carbon allocation and nutrient availability. Ra acclimates to sustained higher temperatures faster than photosynthesis (Ryan and Law, 2005; Way and Oren, 2010; Reich et al., 2016), potentially increasing the fraction of photosynthesis that results in NPP. The only two MsTMIP models that allow for Ra temperature acclimation, LPJwsl and VISIT, have among the largest climate driven increases in absolute NPP (Figure 2.7c). Ra acclimation was also included in the LPJml model, which was shown to reproduce the increase in ASC at ground-based stations (Sitch et al., 2003; Forkel et al., 2016). Warming has also been shown to increase above-ground allocation of carbon (Poorter et al., 2012; Way and Oren, 2010; Melillo et al., 2011), potentially due to accelerated cycling of N through the soil that reduces the requirement for below-ground carbon allocation (Melillo et al., 2011; Wieder et al., 2015). Most MsTMIP models do not include N cycling, and C-N models may underestimate this effect. Above-ground carbon allocation could also drive structural changes that increase leaf area and contribute to greening, depending on the species and on ecosystem conditions (Ainsworth and Long, 2005; Way and Oren, 2010; Melillo et al., 2011; Mccarthy et al., 2006). Models can produce similar annual carbon fluxes from different carbon allocation schemes, but this will lead to different long-term functioning of terrestrial ecosystems (Montane et al., 2017). Thus furthering our understanding of mechanisms that alter carbon allocation is

essential.

Figure 2.9: As for Figure 2.1 but for LUC only simulations.



Recent studies have suggested that land use change (LUC) could be responsible for a substantial portion of the ASC increase (Gray et al., 2014; Zeng et al., 2014). Specifically, the transition from forest to intensive high-yielding crops could increase ASC because such crops can have more concentrated growing seasons and higher NPP than forests (Gray et al., 2014). In MsTMIP models, LUC is not a large contribution to ASC change (Figure 2.9), accounting for -8 to 47% of the increase in modelled ASC (Figure 2.7a). MsTMIP models may not be adequately representing LUC since most models do not explicitly represent crops or land management

(Table 2.1). However, the LPJml model used by Forkel et al. 2016, does explicitly include crops and also finds a small contribution to ASC change from LUC (7%) (Forkel et al., 2016). LUC is unlikely to explain much of the large differences between models and observations in any case, particularly because most LUC has been at 30-45°N (Gray et al., 2014), south of the boreal forest region that contributes the most to observed ASC changes (Graven et al., 2013). Other vegetation changes, such as the observed northward shift of the treeline (Harsch et al., 2009; Elmendorf et al., 2012), may have increased NPP at higher latitudes. This shift is an important driver of the increased ASC in LPJml (Forkel et al., 2016), but may not be captured by MsTMIP models.

2.5 Conclusion

Several factors may be contributing to the observed increase in ASC over the last 50 years. A key factor is an increase in LUE that is larger than simulated by current models. Warming and increases in atmospheric CO_2 may have caused stronger increases in LUE than in the MsTMIP models through a combination of CO_2 fertilisation, respiration acclimation, increases in the rate of N cycling, a shift to aboveground carbon allocation, or other processes. Improving the modelled LUE response to CO_2 and climate change is important not only for process-based models such as those participating in MsTMIP, but also for diagnostic models that use satellite-derived fAPAR to estimate NPP. In the next chapter, I will present a next-generation model (the P-model) for photosynthesis that is driven by observed fAPAR. In the following chapter, I will use the P-model to further analyse the drivers of recent changes in carbon uptake by running fully-factorial experiments.

This chapter has also shown that combining atmospheric CO_2 measurements and observed greening trends provides a powerful constraint on terrestrial biosphere models. The aircraft measurements of ASC change have proved challenging to match, highlighting that our understanding of recent ecosystem changes is still incomplete. The analysis of model output through the metric of LUE is found to be particularly useful, as it can inform us about whether modelled productivity changes are from structural or physiological ecosystem changes.

Chapter 3

The P-model: Evaluation of a next generation model for gross primary production

3.1 Introduction

Observations show that the terrestrial biosphere is changing in response to anthropogenic environmental change. Increases in the amplitude of the seasonal cycle of CO_2 (ASC) (Graven et al., 2013) at high northern latitudes and, simultaneously, greening of vegetation across northern ecosystems (Zhu et al., 2016) indicates that photosynthetic activity has increased over recent decades. While it is agreed that this increase in photosynthetic activity is influenced by increases in atmospheric CO_2, climate change, changes in land use and increases in nitrogen deposition, the role of each driver remains uncertain (Ciais et al., 2013; Le Quere et al., 2018). Terrestrial biosphere models (TBMs) have been used to analyse the influence of historical environmental change on terrestrial carbon fluxes, but our understanding of the mechanisms driving these changes has been hindered by the large differences in model output (Prentice et al., 2014). Models fail to capture the observed increase in ASC (Graven et al., 2013), (Chapter 2) suggesting that our current understanding of the terrestrial biosphere is incomplete.

A key assumption underpinning the majority of current models is a division of the terrestrial biosphere into plant functional types (PFTs). Vegetation is grouped into types such as grasses or evergreen forests according to common features, and each PFT will be assigned some fixed parameters such as maximum rate of carboxylation and vegetation phenology (Rogers et al., 2017; Fisher et al., 2014). While this approach has been useful, it may not be the most appropriate way to represent ecosystems (Wright et al., 2004; Reichstein et al., 2014) and it requires detailed knowledge of the distribution and characteristics of each PFT which is often lacking (Wullschleger et al., 2014). Furthermore fixing of key parameters in space and time may prevent models from being able to evolve freely to environmental changes and does not reflect the ability for vegetation to change in response to the environment (Wullschleger et al., 2014). Recent observations show that vegetation is able to acclimate to changes in growth temperature and elevated CO_2 (Rogers et al., 2017; Kattge and Knorr, 2007; Leakey et al., 2009), but this ability to acclimate is not represented in most current models (Rogers et al., 2017).

A next generation Photosynthesis model, the P-model, has been developed to alleviate some of the issues faced by current models. Current models either use the Farquhar equations for photosynthetic assimilation (Farquhar et al., 1980) or follow the light use efficiency (LUE) approach (Monteith, 1972; Medlyn, 1998). The Farquhar equations assume that instantaneous photosynthetic assimilation is the minimum of either the Rubisco- or light-limited assimilation rate, while the LUE equations assume that photosynthetic assimilation is proportional to the absorbed photosynthetically active radiation (APAR). The P-model uniquely combines the Farquhar and LUE models by assuming that on the order of days, plants acclimate to the amount of incoming light and optimise their carbon usage such that water loss is minimised and carbon gain is maximised (Wang et al., 2014, 2017). The model is driven by observed temperature, PAR, vegetation greenness, vapour pressure and CO_2. Only a few fixed parameters are used, which have been derived from extensive empirical studies (Wang et al., 2017), and the gross primary production (GPP) predicted by the P-model is independent of PFTs. It is assumed that processes which are not explicitly modelled, such as carbon-nitrogen interactions and changes carbon allocation, are accounted for through changes in vegetation greenness (Keenan et al., 2016).

The P-model has already been shown to perform well when driven by CRU climatology data (Wang et al., 2017), giving a mean annual GPP value of 120PgC yr^{-1} which is close to the currently accepted estimate of 123 ± 8 PgC^{-1} from GPP-MTE (Beer et al., 2010). Additionally, when the P-model has been driven by historical data and modelled PAR, the latitudinal distribution of GPP was similar to that of GPP-MTE, but the P-model had less spatial variation with less tropical GPP and more extratropical GPP (Keenan et al., 2016). When coupled to a simple respiration model, Keenan et al. (2016) also showed that the P-model was as skilful at reproducing annual net ecosystem production (NEP) as more complex terrestrial biosphere models, and was able to capture the seasonal cycle of CO_2 at surface stations when TM2 was used to transport the surface fluxes. These previous studies show that annual GPP estimated from the P-model agrees well with Fluxnet data and models. The seasonal cycle of GPP produced by the P-model has not yet been fully validated, and is now presented in this chapter.

I also perform an analysis of P-model based NEE by estimating ecosystem respiration (Reco) using two simple equations. The body of theory for estimating Reco is not as extensive as that for photosynthesis, and a complete understanding of Reco and its components of autotrophic and heterotrophic respiration (Ra and Rh respectively) is lacking (Trumbore, 2006; Davidson et al., 2006a; BondLamberty et al., 2004). This may in part be due to the difficulty in measuring all parts of respiration, and the complications that arise when trying to separate soil respiration into its heterotrophic and autotrophic parts which are needed to verify model estimates against observations. Current models generally use equations based on the Q-10 function, the rate of respiration for a temperature change of 10^oC, or equations based on the model developed by Lloyd and Taylor (1994) that estimate respiration as a nearly exponential function of temperature (Fisher et al., 2014; Davidson et al., 2006a; Ai et al., 2018). A widely debated issue with the Q-10 function is that it is fixed in models, while observations show that it can vary (Davidson et al., 2006a). The Lloyd-Taylor equation essentially has a varying Q-10 function, which is more in line with these observations. The model used by Keenan et al. (2016) was based on the Lloyd-Taylor model, but also included empirical PFT specific parameters (Migliavacca et al., 2011). The derivation of these parameters is under-constrained and so I will not use

this approach. Recently, Ai et al. (2018) showed that it may be possible to estimate global Reco using remote sensing data, such as land surface temperature and the enhanced vegetation index, without the need for PFT specific parameters, but the data required for this approach is only available from 2001.

To make my simple estimate of Reco, I first use the Lloyd-Taylor model with a number of assumptions about the partitioning of Reco between Ra and Rh, and secondly I use an equation developed by Carey et al. (2016) based on a recent analysis of ecosystem experiments that found a reduction in soil respiration at high temperatures. The P-model does not include terms to allocate carbon to different pools (e.g. leaves, roots, wood), but carbon pools are important for estimating respiration in more complex models as the respiration rate in different pools can vary by several orders of magnitude (Ryan and Law, 2005). Multiple carbon pools are currently not used in the P-model as extensive data on allocation patterns is lacking, and current data shows that allocation patterns are highly variable (Poorter et al., 2012).

Model output for GPP and Reco will be compared to observations from 17 fluxnet sites that have been chosen for their homogeneity and long records. The primary focus is to analyse the skill of the P-model in reproducing monthly GPP, seasonal GPP amplitude and mean annual GPP. A secondary focus of this chapter is to evaluate the ability of the P-model + Reco model to estimate seasonal NEE fluxes and so the simple Reco formulations are also analysed on their ability to represent monthly Reco and seasonal Reco amplitude. The model will be driven by global gridded datasets that can be used for global scale estimate of GPP and Reco. Several model versions will be analysed using different input data for the estimate of GPP, and using different formulations for estimating Reco.

3.2 Methodology

3.2.1 The P-model

The P-model is based on the principle that photosynthetic parameters respond optimally to changing environmental conditions over the timescale of days to weeks. GPP in the P-model is predicted for average daily conditions, rather than as an instantaneous response as in the Farquhar model. Currently, the P-model is only used to estimate GPP from plants following the C-3 pathway, which is appropriate for the majority of vegetation in northern terrestrial ecosystems (Still et al., 2003).

The P-model combines elements of the Farquhar and LUE models through the co-limitation hypothesis (Haxeltine and Prentice, 1996; Dewar, 1996; Maire et al., 2012), which assumes that under typical daytime conditions all available light is fully utilised and that GPP, i.e. the rate of photosynthetic assimilation (A), is equal to the Rubisco limited assimilation rate (Ac) and electron transport limited assimilation rate (Aj); A = Ac = Aj. This assumption means that A is a negative function of temperature because Aj decreases with temperature due to increased photorespiration at higher temperatures (Peterhansel et al., 2010). This is different to the temperature function for most current terrestrial biosphere models which assume that GPP increases with temperature up to an optimal point before decreasing (e.g. (Luo, 2007)). Additionally, this assumes that the maximum electron transport (Jmax) and the maximum rate of carboxylation (Vcmax) adjust to typical conditions and that for a particular average light condition, there is an optimal Jmax that maximises assimilation while minimising the cost of maintaining a particular value of Jmax (Wang et al., 2017). Together these assumptions allow a prediction of GPP that is proportional to the mean daily incoming light (Wang et al., 2017).

The second principle of optimality that underlies the P-model is the least-cost hypothesis, which is used to define the ratio of intercellular and ambient CO_2 (ci/ca) and water-use efficiency. It states that plants minimise the combined costs of maintaining capacity for carboxylation and transpiration per unit of assimilation (Prentice et al., 2014; Wright et al., 2003). This is

different to other models as it is generally assumed that the marginal cost of water to carbon gain is constant (Cowan and Farquhar, 1977). However, this assumption is problematic because the constant is not specified by this approach and the cost of maintaining the capacity of carboxylation is not explicitly considered. Wang et al. (2017) use the least-cost hypothesis to derive an exact equation for ci, which is used to define the light-use efficiency term, m, that defines the response of photosynthesis to temperature, CO_2 and vapour pressure deficit (VPD, D in Equation 3.2).

The final equation for GPP is given by:

$$GPP = \varphi_0 \cdot I_{abs} \cdot m\sqrt{1 - (\frac{c^*}{m})^{\frac{2}{3}}}, \tag{3.1}$$

where,

$$m = \frac{C_a - \Gamma^*}{C_a + 2\Gamma^* + 3\Gamma^*\sqrt{1.6 \cdot \eta^* \cdot D \cdot \beta^{-1}(K + \Gamma^*)^{-1})}}, \tag{3.2}$$

and φ_0 is the intrinsic quantum efficiency (mol mol $^{-1}$), I_{abs} is the absorbed light which is a product of the incoming PAR (mol $m^{-2}month^{-1}$) and fAPAR (unitless), C_a is the partial pressure of atmospheric CO_2 (Pa), Γ^* is the photorespiratory compensation point (Pa), η^* is the viscosity of water relative to its value at 25°C, D is the vapour pressure deficit (Pa) and K is the effective Michaelas-Menton coefficient of Rubisco (Pa). There are two constants: $c^* = 0.41$ is the unit cost for the maintenance of electron transport capacity and $\beta = 146$ is the ratio of carboxylation and transpiration costs at 25°C. A full description of all variables and constants is given in table 3.1. All parameter values are fixed across all sites except for φ_0, which is optimised from its default value of 0.084 mol mol $^{-1}$(Wang et al., 2017) to best fit the Fluxnet GPP. This optimisation takes place because the value of φ_0 shows variability (Skillman, 2008), and to scale the estimated GPP to take into account any incomplete utilisation of absorbed light by the vegetation e.g. by non-photosynthesising material or the incomplete utilisation of the solar spectrum by chlorophyll.

GPP is set to zero when air temperature is negative to take into account times when the soil is frozen and vegetation may be green even when it is not photosynthesising (e.g. evergreen needleleaf trees) (Murray-Tortarolo et al., 2013). This is an important limitation at high northern latitudes as up to 50% of the northern hemisphere land area may be frozen on a seasonal basis (Zhang et al., 2003). However, this does not take into account the times when temperatures are positive but the soil remains frozen, and may thus allow GPP to increase too quickly at the start of the growing season (Barichivich et al., 2013; Zhang et al., 2003; Murray-Tortarolo et al., 2013).

It is assumed that the fAPAR data used to drive the model takes into account a number of processes that are not explicitly modelled such as nutrient dynamics, carbon allocation, moisture limitation and disturbances (Keenan et al., 2016; Wang et al., 2014). Work is already under way to include some of these processes in the P-model (e.g. moisture limitations (Stocker et al., 2018)) but these amendments will not be considered in this thesis.

I coded the P-model using Python 2.7, and work is currently under way to publish the code as a git repository.

3.2.2 Driving data

The P-model is driven by global datasets at a monthly timestep for all available years for each site. I choose to drive the P-model with global gridded data rather than the site-scale data measured at each Fluxnet site to ensure that the P-model is consistent with the following chapter in which global runs are performed. For the gridded datasets of PAR, climate and fAPAR, the closest land pixel to each site was chosen using the latitude and longitude given in Table 3.4.

Incoming light

The monthly incoming light was first estimated using the Simple Process Led Algorithms for Simulation Habitats (SPLASH) model (Davis et al., 2016). The SPLASH model calculates

Table 3.1: Equations, constants and data used in the P-model. T_k refers to temperature in Kelvin and T refers to temperature in Celsius. The standard conversion of T_k = T + 273.15 is performed where appropriate.

	Value/Data source	Unit	Definition	Reference
φ_0	0.084	mol mol^{-1}	Photosynthetic quantum yield. Default value	(Wang et al., 2017)
I_{abs}	PPFD · fAPAR	mol $m^{-2}month^{-1}$	Total absorbed photosynthetically active radiation	(Wang et al., 2017)
PPFD	Calculated by SPLASH	mol $m^{-2}month^{-1}$	Absorbed photosynthetic photon flux density. Hourly values are summed to give daily and monthly total values	(Davis et al., 2016)
PAR	0.48 · Watch-WFDEI shortwave radiation	W m^{-2}	Shortwave radiation is reduced to PAR by multiplying by 0.48, and then converted to mol m^{-2} $month^{-1}$ following (Wang et al., 2017; Davis et al., 2016; Frouin and Pinker, 1995)	(Weedon et al., 2011, 2014)
fAPAR	fAPAR3g	n/a	The fraction of photosynthetically active radiation that is absorbed by green vegetation on land	(Zhu et al., 2013)
C_a	SIO MLO	Pa	Ambient CO_2 partial pressure. One global value is used for each month.	(Keeling et al., 2001)
Γ^*	$\Gamma^*_{25} \cdot exp\frac{\Delta Ha \cdot (T_k - 298)}{R \cdot T_k \cdot 298}$	Pa	Photorespiratory compensation point	(Wang et al., 2017)
Γ^*_{25}	4.220	Pa	Photorespiratory compensation point at 25°	(Bernacchi et al., 2001)
ΔHa	37830	J mol^{-1}	Activation energy for Γ^*	(Bernacchi et al., 2001)
T	CRU	C	Monthly air temperature	(Harris et al., 2014)
R	8.3145	J $mol^{-1}K^{-1}$	Universal gas constant	
η^*	$\frac{\eta_T}{\eta_{25}}$	n/a	Viscosity of water at the current temperature relative to it's value at 25°C	(Wang et al., 2017)
D	$0.611 \cdot exp\frac{8.635 \cdot (t_{max} + t_{min})}{0.5 \cdot (t_{max} + t_{min}) + 237.3} - 0.10 \cdot vap$	kPa	Vapour pressure deficit	(Abtew and Melesse, 2013)
t_{max}	CRU	C	Monthly maximum of daily temperature	(Harris et al., 2014)
t_{min}	CRU	C	Monthly minimum of daily temperature	(Harris et al., 2014)
vap	CRU	hPa	Monthly vapour pressure	(Harris et al., 2014)
β	146	n/a	Ratio of carboxylation and transpiration costs at 25°C	(Wang et al., 2017)
K	$K_c \cdot (1 + \frac{P_0}{K_0})$	Pa	Effective Michealis-Menton coefficient of Rubisco	(Wang et al., 2017)
K_c	$39.97 \cdot exp \cdot (\frac{(T_k - 298) \cdot 79430}{R \cdot T_k \cdot 298})$	Pa	Michealis-Menton coefficient for carboxylation	(Wang et al., 2017)
K_0	$27480 \cdot exp \cdot (\frac{(T_k - 298) \cdot 36380}{R \cdot T_k \cdot 298})$	Pa	Michealis-Menton coefficient for carboxylation	(Wang et al., 2017)
P_0	$2.09476E5\dot{1}E - 6\dot{\rho}$	Pa	Partial pressure of oxygen	(Wang et al., 2017)
z	CRU	m	Elevation	(Harris et al., 2014)
c^*	0.41	n/a	Unit carbon cost for the maintenance of electron transport capacity. Allows optimal values of Jmax and Jmax:Vcmax	(Wang et al., 2017)

global incoming radiation based on earth's annual orbit and adjusts the top-of-atmosphere radiation by taking into account average atmospheric transitivity, sunshine fraction, albedo and the fraction of shortwave radiation that can be used for photosynthesis (0.5 - note that this is different to the value used in Equation 3.3) to get the photosynthetic photon flux density (PPFD) (mol m^{-2} day^{-1}) (Davis et al., 2016). The equations give a constant seasonal cycle of radiation at each location each year. Interannual variation comes the sunshine fraction which uses cloud fraction from CRU TS 4.01 (Table 3.1) and is calculated as 1 - cloud fraction. The PPFD is calculated at the resolution of the cloud fraction data and summed for each month to give a total moles of photons received for each month (mol $m^{-2}month^{-1}$).

The SPLASH model was found to underestimate high levels of PPFD, which may reduce peak GPP during the summer when radiation is high (Figure 3.1). Hence, an alternative simulation was run using PPFD calculated from the the reanalysis dataset from Watch-WFDEI shortwave radiation (Weedon et al., 2014, 2011).

The Watch-WFDEI dataset is a reanalysis product that uses the methodology of the Watch forcing data with meterological forcing data from ERA-Interim reanalysis. Importantly, this WFDEI dataset uses aerosol corrections which are not included in the more simplistic SPLASH model. Daily shortwave radiation (SWrad) was converted to monthly PPFD using the following formula:

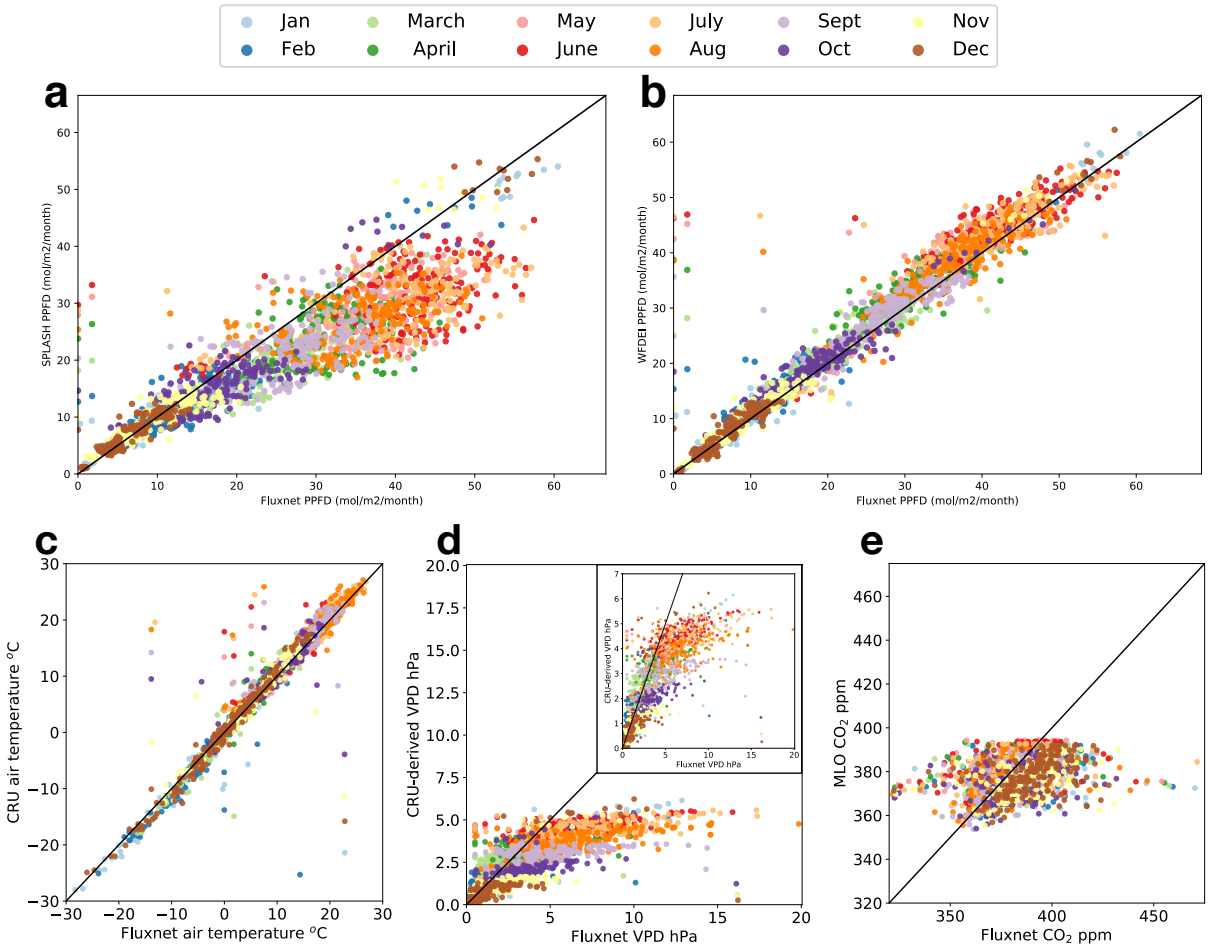
$$PPFD = SWrad \cdot 0.48 \cdot \frac{1}{0.22} \cdot 1 \times 10^{-6} \cdot 86400 \cdot days\_in\_month, \tag{3.3}$$

where the factor 0.48 reduces SWrad to PAR, and the other factors convert the radiation from units of W m^{-2} to mol m^{-2} $month^{-1}$ (Wang et al., 2017).

CO_2

Monthly in-situ CO_2 concentration was downloaded from the Scripps Institution of Oceanography record for MLO (Mauna Loa), Hawaii (Keeling et al., 2001). The 'CO_2 filled' set is used, which is the monthly CO_2 with gap-filling from a fitted curve. The same monthly value was

Figure 3.1: Comparison of environmental variables observed at the 17 Fluxnet sites and data used to drive the P-model. Top panel: Observed photosynthetic photon flux density (PPFD) compared to (a) PPFD calculated from the SPLASH model and (b) from the reanalaysis data product Watch-WDFEI. Bottom panel: (c) Observed temperature compared to CRU temperature, (d) observed VPD compared to VPD calculated from CRU vapour pressure and temperature (Table 3.1) with a magnified inset, and (e) observed CO_2 compared to CO_2 from MLO. Scatter points are coloured by month. RMSE (Root Mean Squared Error) and Bias is shown in the top corner for each panel, and a 1:1 line is plotted.



used for all stations as the MLO record is representative of the global background CO_2 concentration. Although this largely differs from the local CO_2 concentration observed at each site each month (Figure 3.1e), it is the long-term trend in CO2 that is most important for representing GPP, which will be fairly uniform across sites and well represented by the MLO dataset.

Climate

Monthly vapour pressure (vap, hPa) and mean monthly, monthly minimum and monthly maximum temperature (T, tmn, tmx, respectively, ^{o}C) were downloaded from the CRU TS 4.01 dataset (Harris et al., 2014) in which monthly output is provided at 0.5^ox0.5^o. Monthly mean vapour pressure deficit (VPD, kPa) was calculated as described in Table 3.1. Site-scale temperature is well represented by the CRU dataset (Figure 3.1c), but VPD is generally underestimated (Figure 3.1d). The largest underestimation is during summer months as observed VPD typically ranges from 5-10 hPa, while CRU derived VPD is generally between 4-5 hPa. An additional comparison between VPD calculated from daily and monthly data (not shown) indicates that a key reason for this underestimation in the CRU-derived VPD is the different way in which monthly site-scale and CRU-derived VPD was estimated. The site-scale VPD was calculated hourly from relative humidity and air temperature, and then averaged to the monthly estimate, while CRU-derived VPD was calculated from average monthly vapour pressure and minimum and maximum temperature. Thus, the CRU-derived VPD does not capture larger extremes in VPD.

fAPAR

The fAPAR3g dataset was used to drive the model at a monthly timestep (Zhu et al., 2013). Monthly fAPAR was calculated as the average of 15-day cloud-free composites and used at it's original resolution of $\frac{1}{12}$ ^{o} for a high resolution run, and the upscaled 0.5^o version was used for the original and WFDEI runs. The high resolution run is used to check if errors in the GPP estimate were coming from differences in the fAPAR measured at a site and the fAPAR averaged over a larger region. This is only used to identify this error source in the site-scale run, and the high resolution run fAPAR would not be used for the global implementation of the model. The higher resolution fAPAR may be important for cropland sites which have a different

Table 3.2: Driving data used for all P-model versions. Differences from the original set-up are in bold.

	fAPAR	**PAR**	**Climate**	**CO_2**
Original	$0.5^o \times 0.5^o$ fAPAR3g	SPLASH	CRU	MLO
High resolution	$\frac{1}{12}^o \times \frac{1}{12}^o$ **fAPAR3g**	SPLASH	CRU	MLO
WFDEI	$0.5^o \times 0.5^o$ fAPAR3g	**WFDEI**	CRU	MLO

seasonality to surrounding forests, and thus this may improve the representation of GPP at the start and end of the growing season when small changes in fAPAR will play a large role in GPP.

3.2.3 Alternative P-model versions

As mentioned above, three versions of the P-model will but run with slightly different driving data to identify the best choice of driving data (Table 3.2).

3.2.4 Model for respiration

I make the simple and commonly used assumption that at each site the biosphere is net neutral on an annual timescale (Lloyd and Taylor, 1994; Knorr and Heimann, 1995) as annual imbalances between GPP and Reco on the short timescales of the Fluxnet measurements are assumed to be small (Equation 3.4). Reco is split into an autotrophic component (Ra) and a heterotrophic component (Rh) (Equation 3.5). The fraction of GPP allocated to Ra is defined using a constant fraction, ra_{frac}, and monthly Ra (Ra_m) is simply this fraction of monthly GPP (GPP_m) (Equation 3.6). Monthly Rh is calculated as a function of monthly temperature and scaled by the total Rh for each year (Equation 3.7) such that annual Rh is equal to annual GPP - Ra.

$$\sum_{m=1}^{12} GPP = \sum_{m=1}^{12} Reco \tag{3.4}$$

$$Reco = Ra + Rh \tag{3.5}$$

$$Ra_m = ra_{frac} \cdot GPP_m \tag{3.6}$$

$$Rh_m = \frac{Rh_m}{\sum_{m=1}^{12} Rh} \tag{3.7}$$

The default set-up is an Ra fraction (ra_{frac}) of 50%, which assumes that half the respiration follows the shape of GPP and the rest follows the equation for Rh. A range of possible Ra:Rh ratios is considered (Table 3.3), varying between 40-60% (Litton et al., 2007). The fraction of carbon allocated to Ra and Rh has been observed to vary over time (Bradford and Crowther, 2013; Davidson et al., 2006b), but for simplicity it is assumed to be constant throughout the year.

Two equations for Rh were used (Figure 3.12a), both of which are PFT independent and do not used a fixed Q-10 value. First, the Lloyd-Taylor equation for soil respiration (Lloyd and Taylor, 1994) which gives an exponential increase in respiration with temperature;

$$Rh_{LT} = R_0 \times e^{308.56(\frac{1}{56.02} - \frac{1}{T-227.13})} \tag{3.8}$$

The base respiration rate, R_0, is set to 1.0 and temperature, T, is in Kelvin.

Second, the equation developed by Carey et al. (2016) which also has an exponential increase in soil respiration with temperature but has a decrease in respiration at higher temperatures;

$$Rh_C = e^{y1+y2T-y3T^2} \tag{3.9}$$

Where y1 = -1.292, y2 = 0.204 and y3 = 0.0042, given in units of μmol C m^{-2} s, and converted to gC m^{-2} day to use with the GPP output.

All Ra:Rh variations are calculated using the Lloyd-Taylor equation, and estimates are provided

using air and soil temperature for each month (T_m and T_{soil}(m) respectively). The Carey equation is only calculated for Ra:Rh = 50:50, and uses soil temperature for the Rh function (Table 3.3). Monthly soil temperature (T_{soil}) for month m is estimated using the equations from the LPJ model (Sitch et al., 2003) as:

$$T_{soil}(m) = T_{mean} + A \cdot (T_{lag} - T_{mean}), \tag{3.10}$$

where A is a dampening term for the amplitude of the temperature at the soil surface and at a depth of 0.25m, T_{mean} is the mean temperature over the previous 12 months, and the temperature lag, T_{lag}, accounts for the temperature from the previous month and is a function of the phase lag, m_{lag}, for the soil at depth compared to the surface;

$$\begin{aligned} A &= e^{-alag}, \\ T_{lag} &= (T_m - T_{m-1}) \cdot (1 - m_{lag}) + T_{m-1}, \\ m_{lag} &= alag \cdot \frac{6}{\pi}, \\ alag &= \frac{0.25}{\sqrt{12 * \frac{k_{dif}}{\pi}}}. \end{aligned} \tag{3.11}$$

It is assumed that the thermal diffusivity of the soil, k_{dif}, is constant and that all soil is silt such that $k_{dif} = 0.946$ m^2 month^{-1} (Cam). This simplification thus ignores any differences in soil texture and does not require the calculation of monthly soil water (Sitch et al., 2003).

3.2.5 Observations

Model output is compared to GPP, Reco and NEE for 17 Fluxnet sites (Figure 3.2, Table 3.4) chosen for their open access data, homogeneity and because they represent a range of different biomes (Prentice and Thomas, 2017). Uncertainties in validating model output arise because measured NEE requires gap-filling and must be partitioned into its component fluxes of GPP and Reco, the methodologies for which are uncertain (Barr et al., 2013). The main uncertainty

Table 3.3: The version name and set-up for the respiration model. Ra and Rh fractions are the fraction of annual GPP assigned to each flux, the temperature refers to the temperature used in the respiration function and all versions use Equation 3.8 for Rh except the 'Carey' version with uses Equation 3.9.

Version	**Ra fraction**	**Rh fraction**	**Temperature**	**Notes**
LT	0 .	1	Air	All Reco assigned to Rh
RaRh	0.5	0.5	Air	Lloyd-Taylor equation
RaRh_5743	0.57	0.43	Air	Litton 2007 average CUE
RaRh_6436	0.64	0.36	Air	Litton 2007 foliage
RaRh_4060	0.40	0.60	Air	Litton 2007 wood
SoilT	0.5	0.5	Soil	Lloyd-Taylor equation
Carey	0.5	0.5	Soil	Carey equation

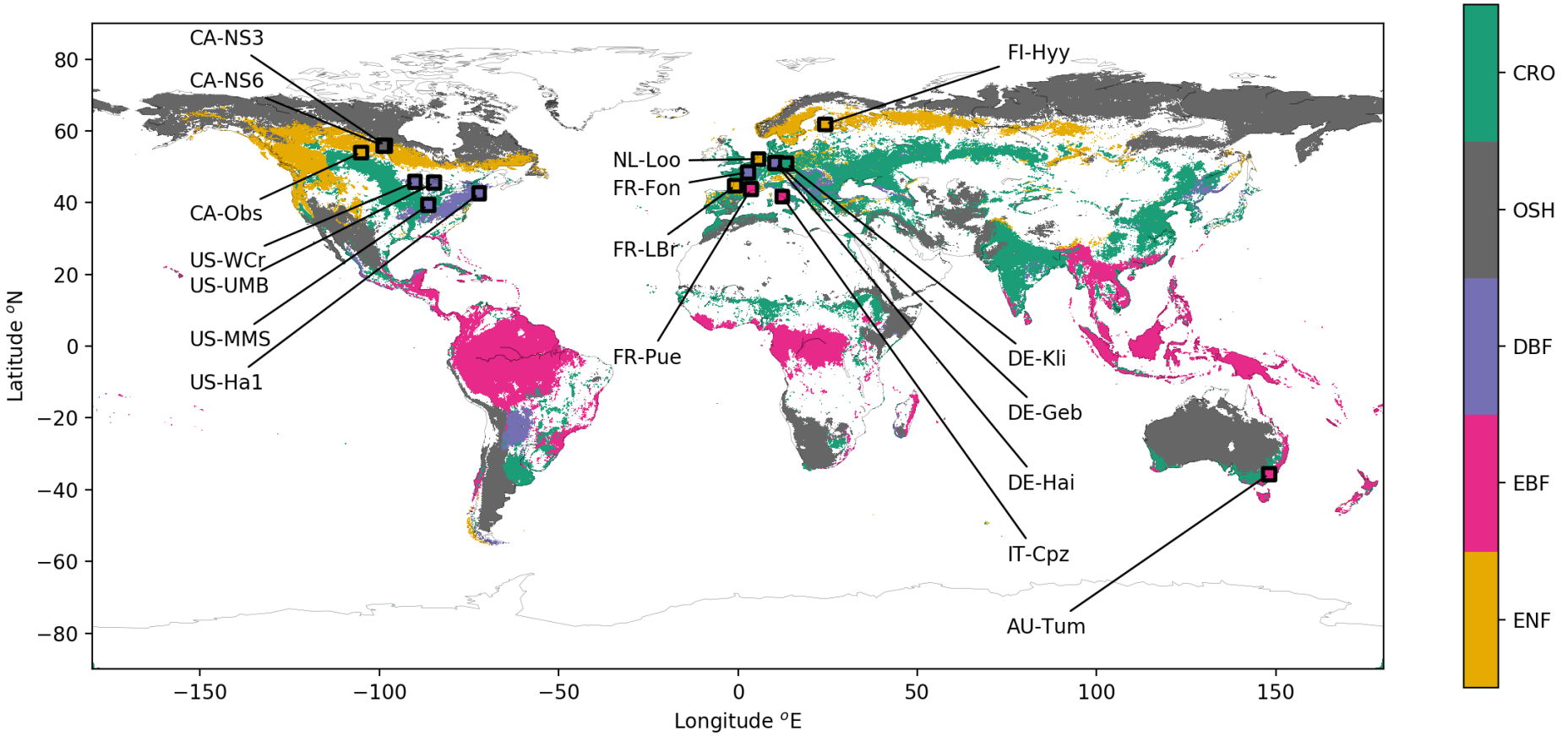
comes from the value chosen for the threshold below which fluxes are removed during stable atmospheric conditions at night, the U* threshold (Fluxnet, 2017). During these periods, fluxes may not be well resolved by the eddy-covariance technique and therefore may not be correct. Since there is still much debate about what value to use for this cut-off, I use multiple estimates of GPP, Reco and NEE to calculate the mean and uncertainty for each flux which includes estimates using a range of U* values. For NEE, I use the mean of the CUT_REF, VUT_REF, CUT_MEAN and VUT_MEAN outputs, which are calculated using constant (CUT) and variable (VUT) U* thresholds for each year for the reference 'best-guess' output (_REF) or the mean of 40 versions using different values of U* (_MEAN) (Fluxnet, 2017). I use all estimates for GPP and Reco, which includes the 40 different U* threshold values and the estimation of fluxes using both the Lasslop and Reischtein flux partitioning methods (Reichstein et al., 2005; Lasslop et al., 2010) (Chapter 1). I remove outliers that have differences from the mean GPP or Reco of more than 1 standard deviation. Uncertainty for NEE is the mean of the joint uncertainty given for the reference case for the CUT and VUT estimates (CUT_REF_JOINTUNC and VUT_REF_JOINTUNC). Uncertainty for GPP and Reco is given as the range of all the values used to calculate the mean flux.

I use the monthly observations for each site provided by Fluxnet, given in gC m^{-2} day^{-1}. All available years for each site are used except for US-Ha1 where I exclude the first year of data (1991) as it was disturbed by site set-up, and 2010 for US-WCr as no data was recorded in this year.

Table 3.4: Fluxnet sites used for model validation. IGBP biome classes: CRO - Cropland, DBF - Deciduous broadleaf forest, EBF - Evergreen broadleaf forest, ENF - Evergreen needleleaf forest, OSH - Open shurbland

Site ID	**Site name**	**Start year**	**End year**	**Latitude ^{o}N**	**Longitude ^{o}E**	**Elevation**	**IGBP biome class**
AU-Tum	Tumbarumba	2001	2014	-35.67	148.2	0	EBF
CA-NS3	UCI-1964 burn site	2001	2005	55.9	-98.4	260	ENF
CA-NS6	UCI-1989 burn site	2001	2005	55.9	-99.0	244	OSH
CA-Obs	Saskatchewan - Western Boreal, Mature Black Spruce	1997	2010	54.0	-105.1	628.94	ENF
DE-Geb	Gebesee	2001	2014	51.1	10.9	161.5	CRO
DE-Hai	Hainich	2000	2012	51.1	10.5	430	DBF
DE-Kli	Klingenberg	2004	2014	50.9	13.5	478	CRO
FI-Hyy	Hyytiala	1996	2014	61.8	24.3	181	ENF
FR-Fon	Fontainebleau-Barbeau	2005	2014	48.5	2.8	103	DBF
FR-LBr	Le Bray (after 6/28/1998)	1996	2008	44.7	-0.8	61	ENF
FR-Pue	Puechabon	2000	2014	43.7	3.6	270	EBF
IT-Cpz	Castelporziano	1997	2009	41.7	12.4	68	EBF
NL-Loo	Loobos	1996	2013	52.2	5.7	25	ENF
US-Ha1	Harvard Forest EMS Tower (HFR1)	1991	2012	42.5	-72.2	340	DBF
US-MMS	Morgan Monroe State Forest	1999	2014	39.3	-86.4	275	DBF
US-UMB	Univ. of Mich. Biological Station	2000	2014	45.6	-84.7	234	DBF
US-WCr	Willow Creek	1999	2014	45.8	-90.1	520	DBF

Figure 3.2: The 17 Fluxnet sites used for P-model evaluation and their vegetation class. The global distribution of the vegetation classes represented by the 17 sites is also shown, generated from the classifications of the land cover type climate modelling grid product from NASA (**?**): CRO - Cropland, OSH - Open shurbland, DBF - Deciduous Broadleaf forest, EBF - Evergreen broadleaf forest, ENF - Evergreen needleleaf forest. Any unshaded regions are vegetation classes that are not represented by these sites. The vegetation class assigned to the Fluxnet site is shown in the scatter point at the site location according to the classification in Table 3.4, and does not always match the underlying vegetation class from the NASA product.



3.2.6 Analysis of the model

I compare modelled GPP, Reco and NEE to Fluxnet site data at a monthly timestep. The root mean squared error (RMSE) and bias are used to analyse the monthly output, annual mean and seasonal amplitude of the fluxes. Bias is calculated as the model estimate - observed value, so an overestimation in a modelled flux results in a positive bias. To assess the best version of the model I also consider the spread of model residuals by calculating their interquartile range (IQR). Standard deviation and variance are not used in case of a non-normal distribution of residuals.

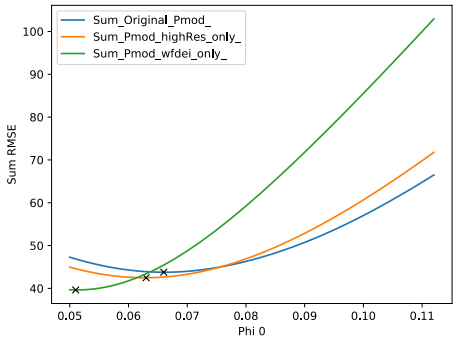
I pose the following questions for the subsequent analysis:

1. Is the model able to capture the seasonal cycle of GPP, Reco and NEE observed at Fluxnet sites in a range of different biomes?
2. Is the skill of modelled GPP linked to the resolution of the fAPAR data driving it?
3. How much does modelled Reco change under different assumptions about Ra:Rh?
4. Is the skill of modelled Reco improved by using estimated soil temperature rather than air temperature?

3.3 Results

3.3.1 Optimizing φ_0

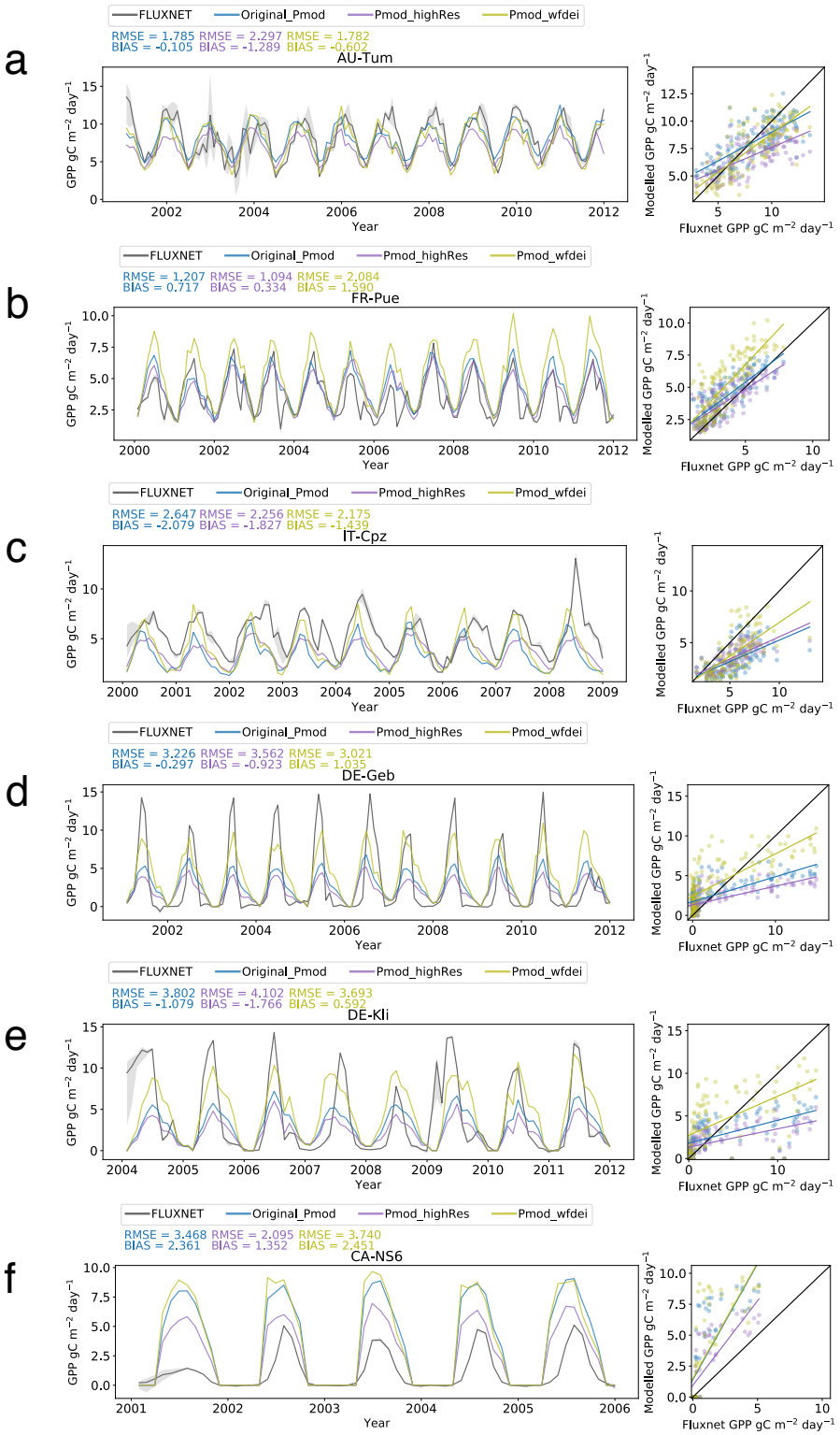
Figure 3.3: The total RMSE summed for all 17 Fluxnet sites for different values of φ_0. The optimal value of φ_0, where RMSE is smallest, is shown with a cross for each P-model version.

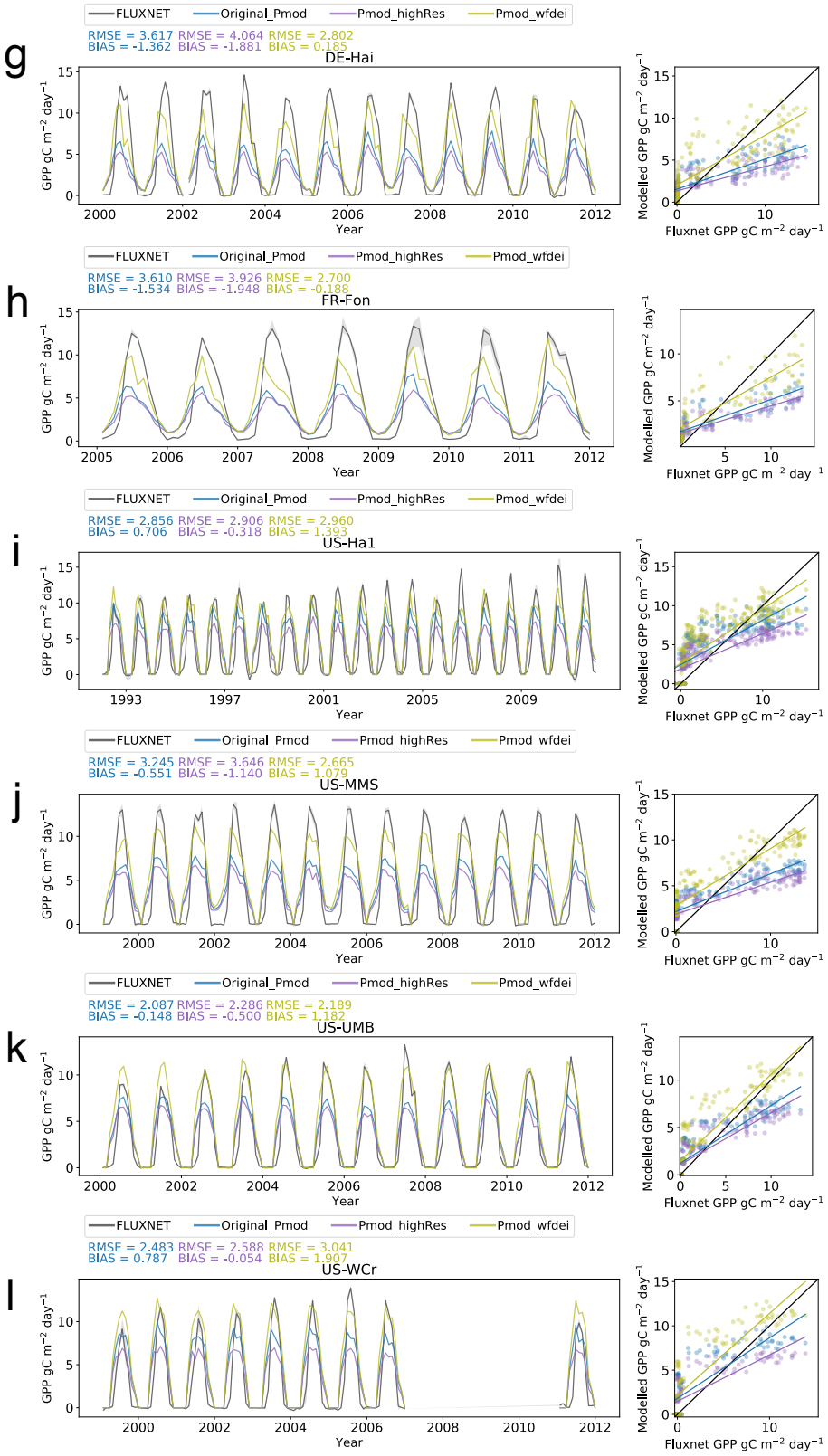


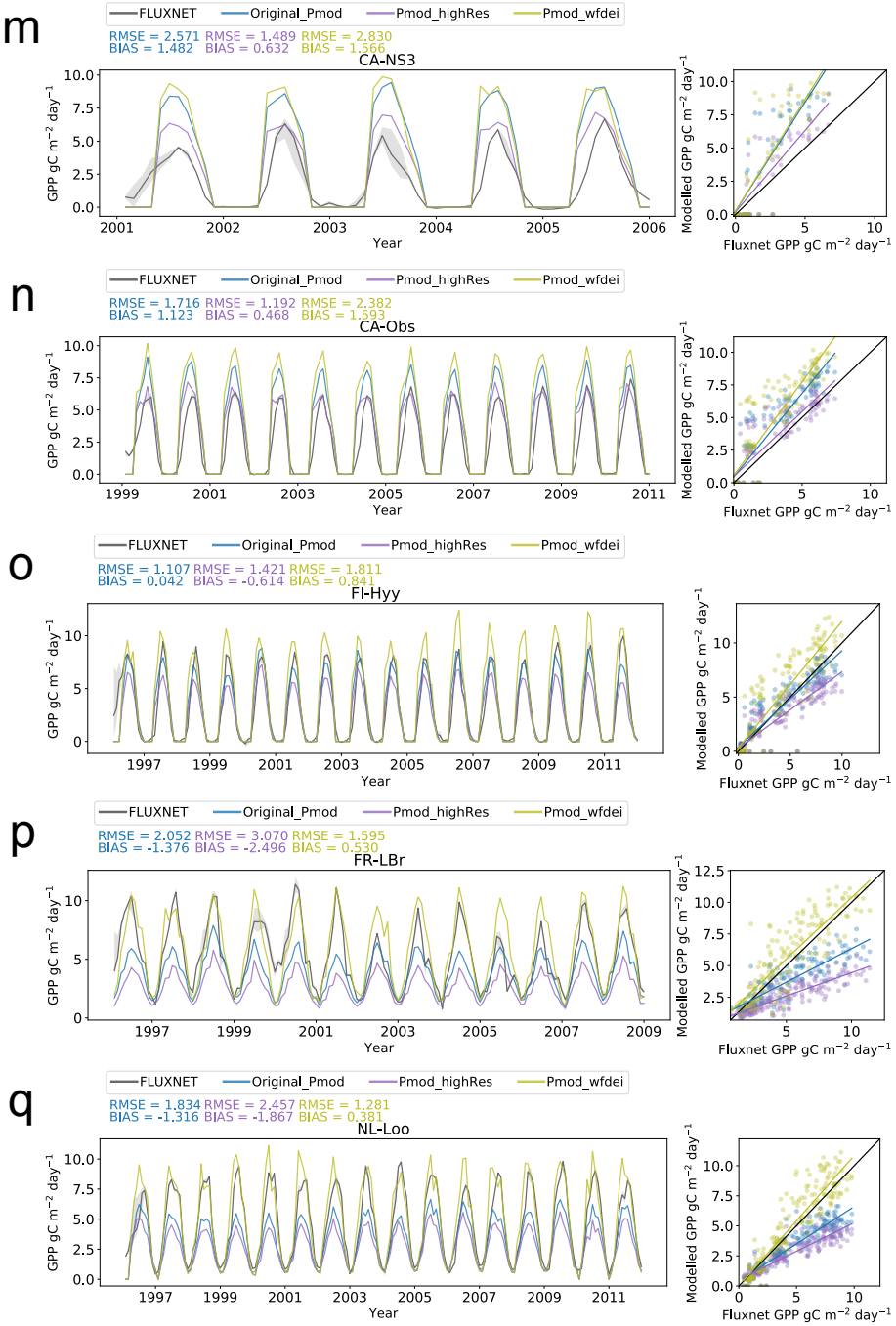
The intrinsic quantum efficiency (φ_0) was optimised to best match GPP observed at the 17 Fluxnet sites. The three implementations of the P-model (Table 3.2) were first run using $\varphi_0 = 0.084$ as the default (Wang et al., 2017) and then φ_0 was optimised for each version using values of φ_0 between 0.05 - 0.112 (Skillman, 2008). The optimal value was found by dividing GPP by the default value (to normalise the GPP) and then calculating the RMSE at all 17 Fluxnet sites for each 0.01 increment in φ_0. The optimal value for φ_0 was then chosen as the minimum of the sum of RMSE across all 17 sites for each P-model implementation. The optimal values of 0.066, 0.063 and 0.051 for the original, high resolution and WFDEI versions respectively are all lower than the default value (Figure 3.3). This systematic decrease in φ_0 compared to the default value may be because the default value already accounted for the incomplete utilisation of the solar spectrum (e.g. through the use of the enhanced vegetation index rather than fAPAR3g for the fAPAR (Wang et al., 2017)). The best result is for the WFDEI version which has the smallest RMSE at its optimal value, although this is not much smaller than for the other two model versions. The original and high resolution versions have very similar RMSE curves and optimal φ_0, indicating that the resolution of the fAPAR driving data may not be important for estimating GPP at the site scale. The values of φ_0 calculated here are used to adjust the GPP output for the results presented below.

3.3.2 Gross primary production

Figure 3.4: GPP seasonal cycle (left) and monthly mean (right) at the 17 Fluxnet sites in gC m^{-2} day $^{-1}$. Panels are grouped by vegetation type: a-c - EBF, d, e - CRO, f - OSH, g-l - DBF, m-q - ENF (Table 3.4). Observations (grey lines) are shown with errors (grey shading) and model output is shown for the original set up (blue - Original_Pmod), using high resolution fAPAR3g (purple - Pmod_highRes) and using WFDEI PAR (green - Pmod_wfdei), with RMSE and bias in the respective colour. In the right panel the regression line is plotted for each simulation and a 1:1 line is shown. Note that each site has a different scale.



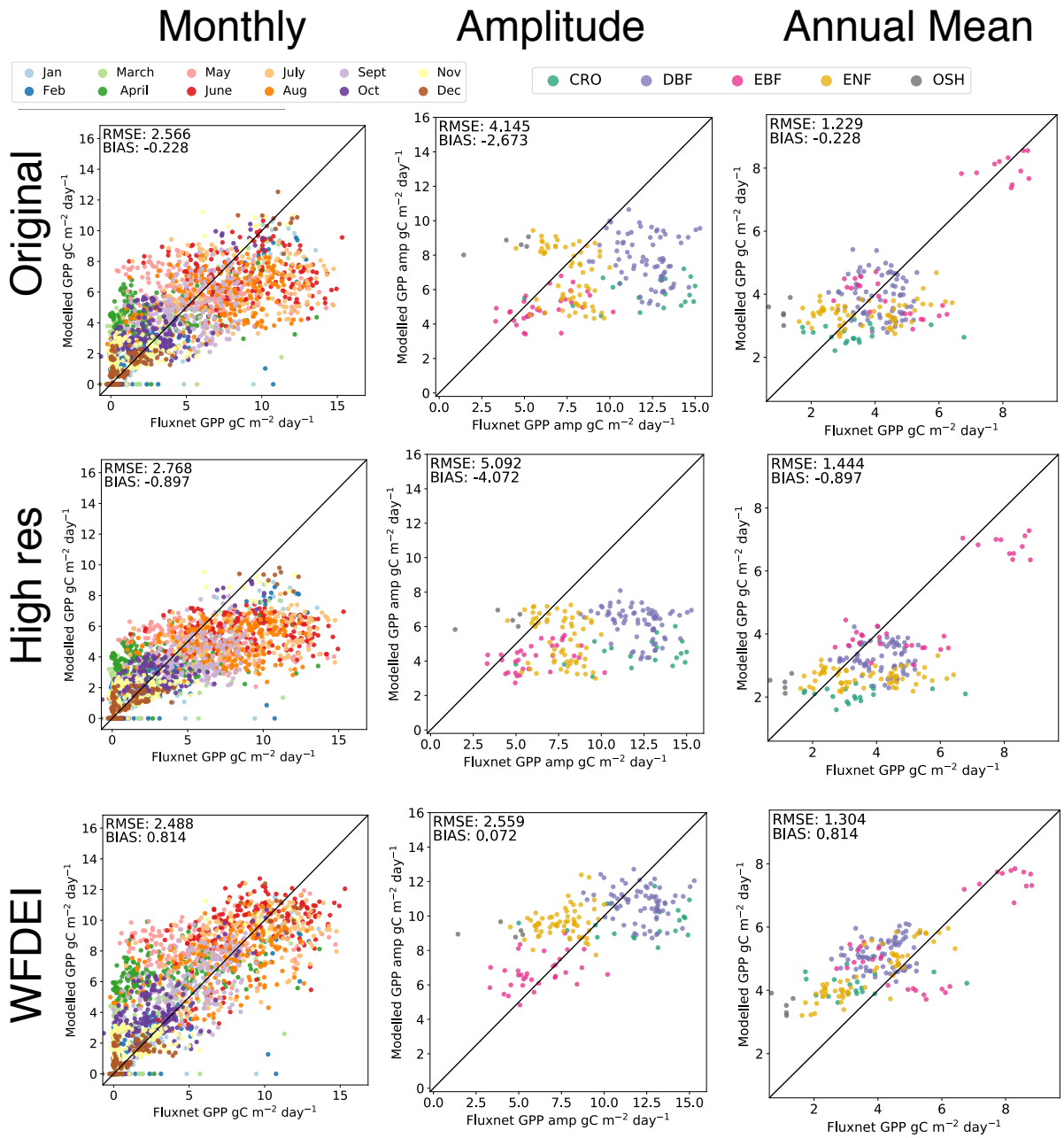

g
FLUXNET Original_Pmod Pmod_highRes Pmod_wfdei
RMSE = 3.617 RMSE = 4.064 RMSE = 2.802
BIAS = -1.362 BIAS = -1.881 BIAS = 0.185
DE-Hai
GPP gC m−2 day−1
Year
Modelled GPP gC m−2 day−1
Fluxnet GPP gC m−2 day−1
h
FLUXNET Original_Pmod Pmod_highRes Pmod_wfdei
RMSE = 3.610 RMSE = 3.926 RMSE = 2.700
BIAS = -1.534 BIAS = -1.948 BIAS = -0.188
FR-Fon
i
FLUXNET Original_Pmod Pmod_highRes Pmod_wfdei
RMSE = 2.856 RMSE = 2.906 RMSE = 2.960
BIAS = 0.706 BIAS = -0.318 BIAS = 1.393
US-Ha1
j
FLUXNET Original_Pmod Pmod_highRes Pmod_wfdei
RMSE = 3.245 RMSE = 3.646 RMSE = 2.665
BIAS = -0.551 BIAS = -1.140 BIAS = 1.079
US-MMS
k
FLUXNET Original_Pmod Pmod_highRes Pmod_wfdei
RMSE = 2.087 RMSE = 2.286 RMSE = 2.189
BIAS = -0.148 BIAS = -0.500 BIAS = 1.182
US-UMB
l
FLUXNET Original_Pmod Pmod_highRes Pmod_wfdei
RMSE = 2.483 RMSE = 2.588 RMSE = 3.041
BIAS = 0.787 BIAS = -0.054 BIAS = 1.907
US-WCr


m
FLUXNET
Original_Pmod
Pmod_highRes
Pmod_wfdei
RMSE = 2.571 RMSE = 1.489 RMSE = 2.830
BIAS = 1.482 BIAS = 0.632 BIAS = 1.566
CA-NS3
GPP gC m−2 day−1
Year
Modelled GPP gC m−2 day−1
Fluxnet GPP gC m−2 day−1
n
RMSE = 1.716 RMSE = 1.192 RMSE = 2.382
BIAS = 1.123 BIAS = 0.468 BIAS = 1.593
CA-Obs
o
RMSE = 1.107 RMSE = 1.421 RMSE = 1.811
BIAS = 0.042 BIAS = -0.614 BIAS = 0.841
FI-Hyy
p
RMSE = 2.052 RMSE = 3.070 RMSE = 1.595
BIAS = -1.376 BIAS = -2.496 BIAS = 0.530
FR-LBr
q
RMSE = 1.834 RMSE = 2.457 RMSE = 1.281
BIAS = -1.316 BIAS = -1.867 BIAS = 0.381
NL-Loo

The monthly mean daily GPP is shown in Figure 3.4 for the original model (blue line), high resolution model (purple line) and WFDEI model (green line). Focusing first on the original implementation, we can see that the magnitude of the peaks is generally not well captured. Most often the summer peaks are underestimated (e.g. US-MMS, US-UMB, Figure 3.4j, k respectively), and only the 3 Canadian sites (Ca-NS3, -NS6 and -Obs, Figure 3.4m, f, n respectively) have an overestimated peak, resulting in a small negative bias in GPP amplitude of -0.228 gC m^{-2} day^{-1} across all sites (Figure 3.5). The imposed assumption that GPP=0 when T<0°C is usually appropriate, but may not be a sufficient limit at all sites (e.g. FR-Fon), where GPP = 0 at T>0°C (Figure 3.4 h). Additionally, GPP phasing is not well captured and GPP at the start of the growing season (April and May) is often overestimated (Figures 3.4, 3.5). This behaviour is common across different vegetation types, while the missing of peak GPP (both over- or under-estimated) is generally just at deciduous broadleaf forest sites (Figure 3.4 g-l). Annual mean GPP is fairly well captured for all biomes as the overestimated spring GPP cancels out the underestimated summer GPP (Figure 3.5).

The high resolution model (purple line) reduces the amplitude of the seasonal cycle of GPP at all sites, while the WFDEI version (green line) increases the amplitude (Figure 3.4, 3.5). The WFDEI version therefore shows an improvement in the modelled seasonal cycle for the majority of sites because the original model generally underestimated peak GPP (e.g. DE-Hai, US-MMS, Figure 3.4g, j respectively), while the high resolution version improves the seasonal cycle where peak GPP was overestimated e.g. the Canadian sites, particularly CA-Obs (Figure 3.4n). Overall, monthly and mean annual GPP in the WFDEI version of the model is more positively biased than the original or high resolution variant at site level, and so the GPP bias switches from a small negative to a small positive (0.814 gC m^{-2} day^{-1}) (Figure 3.5) but there is a significant improvement in GPP amplitude bias from -2.673 gC m^{-2} day^{-1} to 0.072 gC m^{-2} day^{-1} for the original and WFDEI version respectively. Capturing GPP amplitude requires that both the minimum and maximum GPP are well represented. Since all model versions imposed the assumption that GPP = 0 gC m^{-2} day^{-1} when temperatures are below freezing (which is generally true across sites and years (Figure 3.4)), differences in modelled GPP amplitude come from the ability for each model version to capture peak GPP. Thus, the

Figure 3.5: Observed and modelled GPP fluxes at the 17 Fluxnet sites. Monthly GPP, the amplitude of GPP and annual mean GPP is shown for the original setup, high resolution fAPAR3g version and using WFDEI PAR. In the left-hand-side panels, mean monthly GPP scatter points are coloured by month. In the middle and right-hand-side panels, annual GPP amplitude and annual mean scatter points are coloured by vegetation type according to the IGBP class of the site (See Table 3.4 for further information). The RMSE and bias (in gC m^{-2} day $^{-1}$) is shown in the top corner of each panel and a 1:1 line is plotted.



better skill in the WFDEI version comes almost entirely from the improvement in the estimation of summer (June, July, August) GPP (Figure 3.5), and confirms the earlier suggestion that missing peak PAR in the driving data would reduce the ability for the model to capture peak GPP. However, this increased skill at capturing peak GPP results in a slightly worse annual mean GPP estimates and increases RMSE from 1.2 gC m^{-2} day $^{-1}$ to 1.3 gC m^{-2} day $^{-1}$. This is mostly due to an overestimation of GPP for evergreen needleleaf forests and crops (Figure 3.5).

The high resolution version has the highest RMSE and bias for monthly, peak and annual mean GPP. It performs more poorly than the original version as peak GPP is reduced in the summer, particularly for deciduous broadleaf and evergreen needleleaf forests and thus annual mean GPP is too small. However, the reason for this underestimation is not clear. It is possible that at a monthly timescale and high resolution, very few retrievals were made per pixel and that these were not particularly representative of the vegetation over the whole month. This effect would be averaged out when considering a larger number of pixels at the 0.5^o resolution. Additionally, the vegetation around the Fluxnet site is more dense and therefore less accessible than the site, resulting in a generally lower fAPAR at the site location. Surrounding vegetation may also be less managed than the vegetation at the site, which could also influence the mean fAPAR. This is perhaps more important at the two cropland sites (d, e in Figure 3.4) in which the high resolution model tends to show a faster GPP reduction at the end of summer compared to the Original version.

The phasing of the seasonal cycle in the two model variants is poorly captured (Figure 3.4) as the monthly GPP estimated for April, May, October and November are similarly overestimated by all model versions (Figure 3.5). This is somewhat surprising since I expected that the higher resolution fAPAR would improve the ability of the model to capture the start and end of the growing season at site-level. However these results indicate that even with the high resolution fAPAR there is still not enough information in monthly vegetation greenness to accurately represent the start and end of the growing season. Thus, monthly fAPAR data, regardless of resolution, may not be suitable for estimating monthly GPP in the P-model. Data products

for fAPAR exist at higher temporal resolutions (8 to 10 day), and these show better skill at representing GPP at the start and end of the growing season in the P-model (Prentice and Thomas, 2017).

The residuals for all model versions become larger with increasing values of predicted monthly GPP (Figure 3.6) indicating that none of the model versions are skilful at estimating GPP on a monthly timescale. The skew cancels out on average such that the median monthly GPP residual is close to zero for all model versions, although the IQR for the high resolution and WFDEI versions are skewed negative and positive respectively (Figure 3.8a). Biomes which are particularly biased are deciduous broadleaf forests and evergreen needleleaf forests, which represents 11 of the 17 sites (Table 3.4). I expect that the skew in monthly residuals is a result of the poor model performance at the start and end of the growing season, a weakness that was common across the model versions. On the other hand, the residuals for GPP amplitude and annual mean are randomly distributed for all model versions (Figure 3.6, 3.9a, 3.10a), although more so for the WFDEI version for amplitude and the original version for annual mean GPP. Annual GPP is better represented by the original model which has a median closer to zero and less skew (based on mean and median), but the WFDEI version has the smallest IQR (1.3 gC m^{-2} day^{-1} compared to 1.97 gC m^{-2} day^{-1} and 1.88 gC m^{-2} day^{-1} for the original and high resolution versions, respectively).

I now use the WFDEI model version to compare the modelled and observed response to environmental drivers. I use the lm package in R to fit a linear model to GPP using the temperature, VPD and PPFD observed at the Fluxnet sites, and the fAPAR at 0.5o resolution. I omit CO_2 from the model to prevent over-fitting. This is a reasonable omission because CO_2 has a large range (Figure 3.1e), but will mostly contribute to the long-term trend rather than the short-term fluctuations in GPP. Through this analysis I find that the most appropriate model takes the form of a log-transformed GPP, VPD, PPFD and fAPAR and with a quadratic temperature function, excluding negative temperatures. The model takes the form GPP = temperature^2 * PPFD * fAPAR * VPD 1 (where * means that the variable and all interactions are included and -1 forces the regression through the origin). The results, shown in Figure 3.7, suggest that

Figure 3.6: Modelled GPP residuals. Modelled GPP is plotted against GPP residuals (modelled - observed GPP) for monthly GPP, the amplitude of GPP and annual mean GPP for the original setup, high resolution fAPAR3g version and using WFDEI PAR. All scatter points are coloured according to the IGBP class of the fluxnet site.

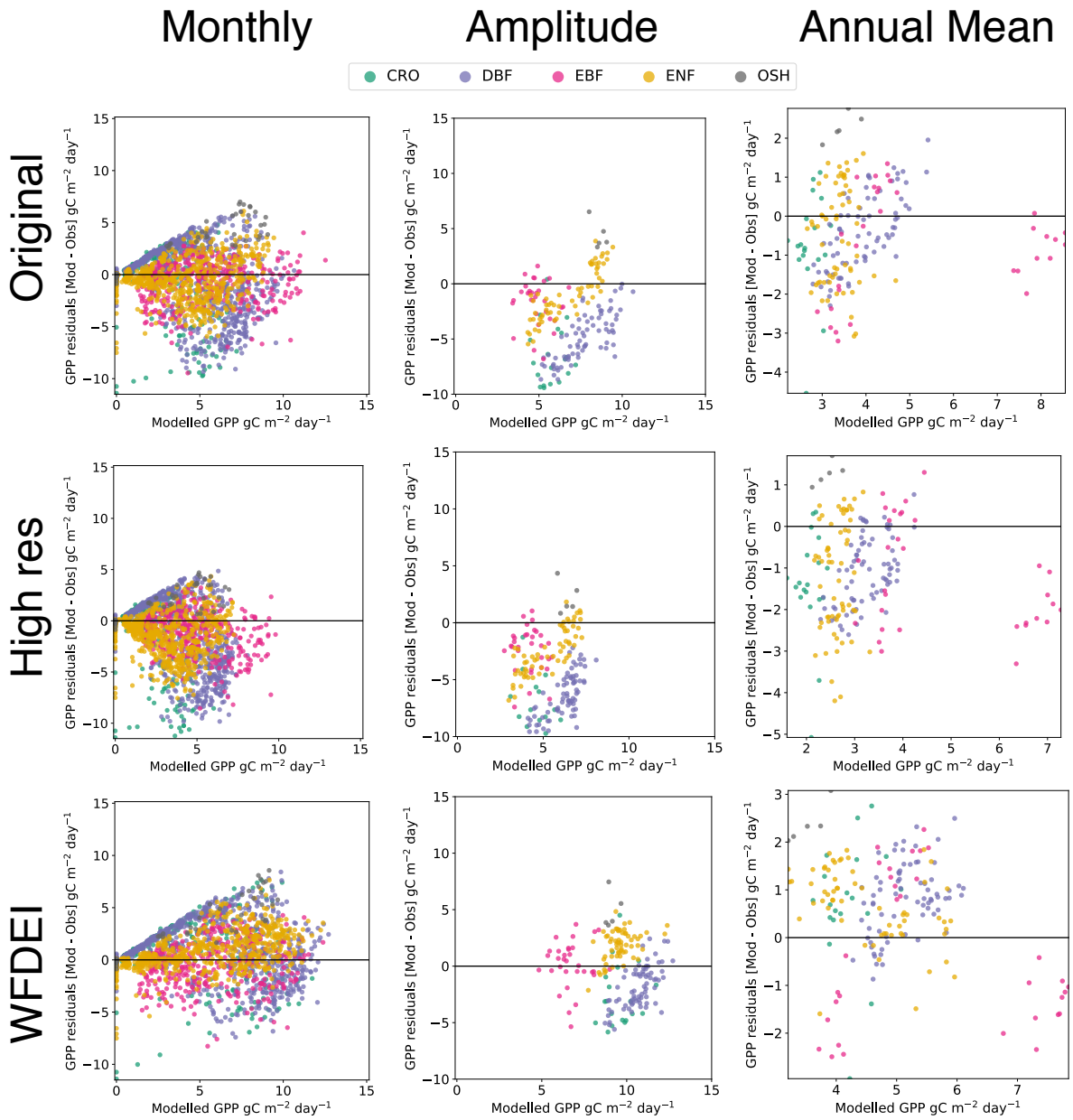
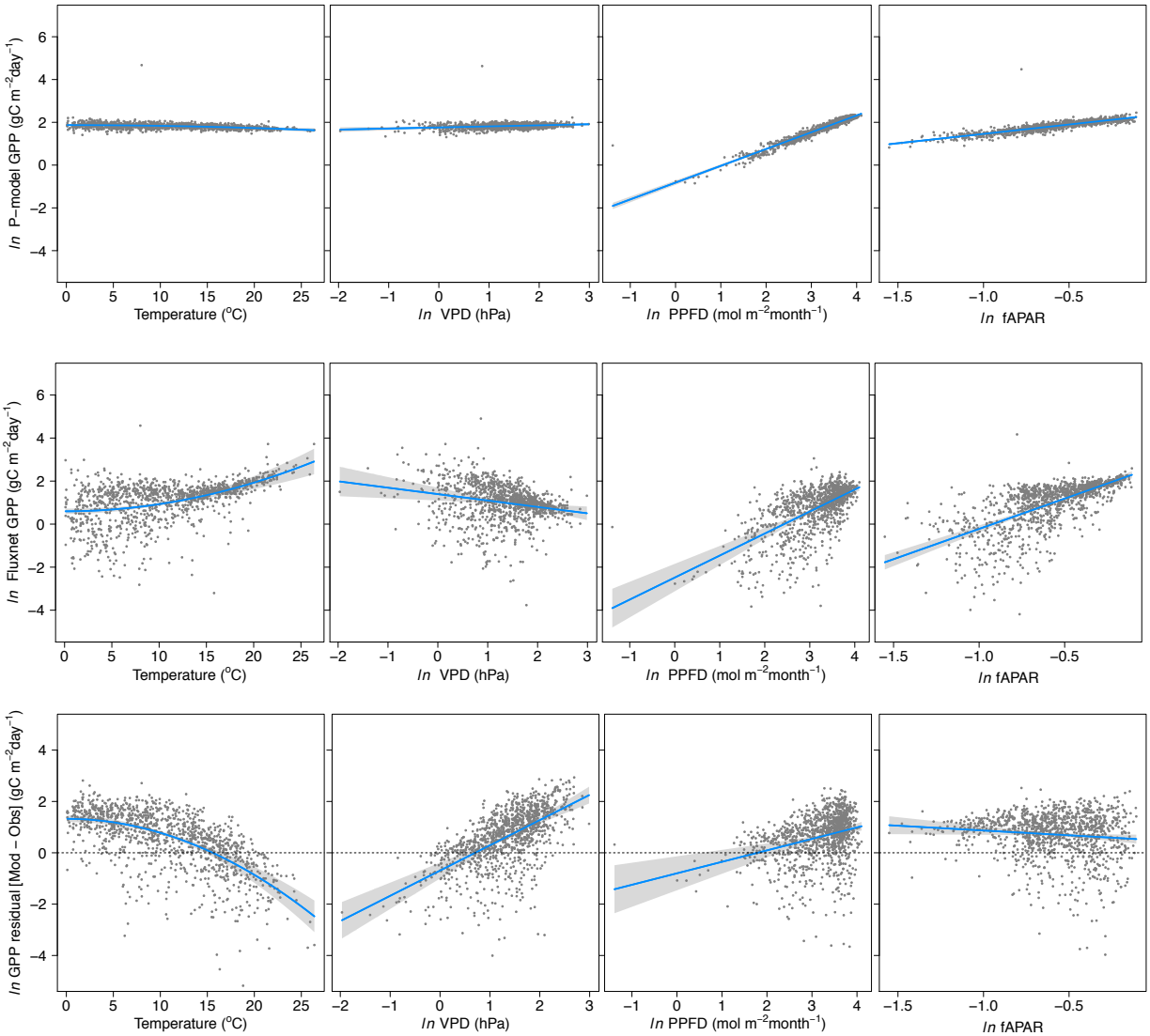


Figure 3.7: Partial residual plots of P-model (top panel) and Fluxnet (middle panel) GPP fitted to a model with temperature, PPFD, VPD and fAPAR as drivers. The model was fitted using the 'lm' function in R, and the plots were created using the visreg package in R. The residuals are also shown (bottom panel).



the P-model generally shows the correct relationship between GPP and PPFD and fAPAR, but not for temperature or VPD. The temperature response for Fluxnet GPP increases with temperature, while the P-model temperature response is flat with a slight decrease. Thus the negative temperature response in the P-model may not be correct. The difference between the temperature response is largest at low temperatures, where the P-model shows a large positive bias. These low temperatures will generally occur during the start and end of the growing season, where the P-model overestimated GPP, and so this may also explain why the P-model performed poorly on a monthly timescale. The VPD response in the Fluxnet sites is negative, while the P-model shows a much flatter response with a slight increase, leading to an overestimation of GPP when VPD is high. The range of VPD values used to drive the P-model is much smaller than the observed range (Figure 3.1), which could partly explain the different response in the P-model compared to Fluxnet GPP. At high VPD and high temperature, the P-model over- and under-estimates GPP. These effects may offset each other as the P-model was able to capture summer GPP well (when temperature and VPD would likely be high). The lack of a soil moisture constraint also contribute to the differing performance of the P-model at low temperatures and high VPD.

Overall, these results give me confidence that the model can be used to analyse GPP amplitude and annual GPP, and that the version driven by WFDEI PAR performs best. The WFDEI version is chosen as the final model for two reasons. First, the driving data for incoming light is not biased, as is the case for the Original model driven by output from the SPLASH model (Figure 3.1). The inclusion of high values of PPFD led to improvements in the capturing of peak GPP at several sites, particularly those in deciduous broadleaf forests. Secondly, the smaller bias in the other model versions is likely due to cancelling out of over- and underestimated values of GPP. Since the overestimation of annual GPP at low values is common across model versions (Figure 3.5), the key difference in model versions is at the high end of GPP, where the WFDEI version performs much better.

Figure 3.8: Box and whisker plots of the residuals between modelled and observed fluxes at all 17 Fluxnet sites for monthly GPP (a), Reco (b) and NEE (c). Shown on the box plot is the IQR (blue box), 1.5xIQR (the blue whiskers), the median (green line), the mean (green triangle) and the outliers (open back circles). Models versions are ordered by median.

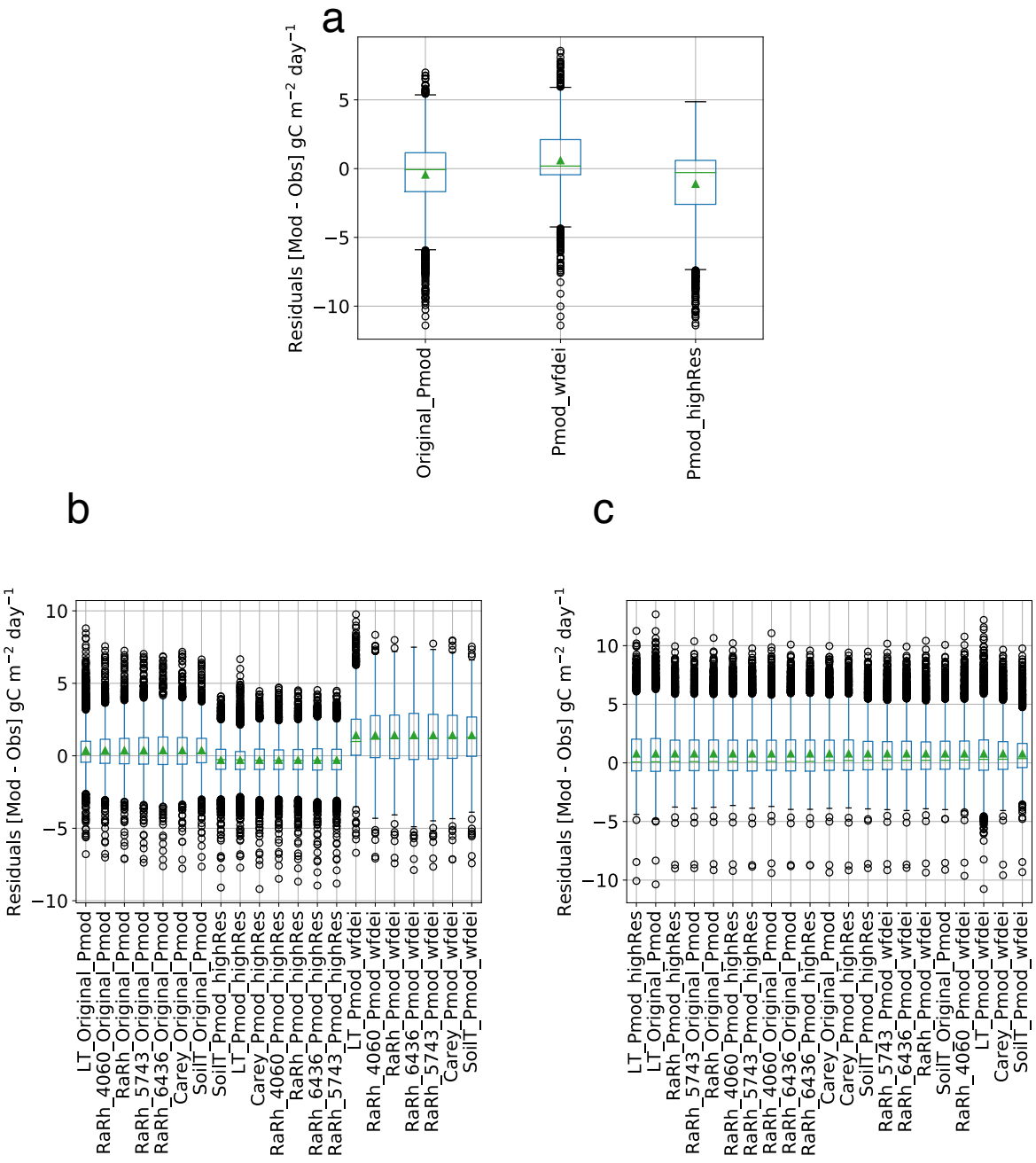


Figure 3.9: Box and whisker plots of the residuals between modelled and observed fluxes at all 17 Fluxnet sites for the seasonal amplitude of GPP (a), Reco (b) and NEE (c). Shown on the box plot is the IQR (blue box), 1.5xIQR (the blue whiskers), the median (green line), the mean (green triangle) and the outliers (open back circles). Models versions are ordered by median.

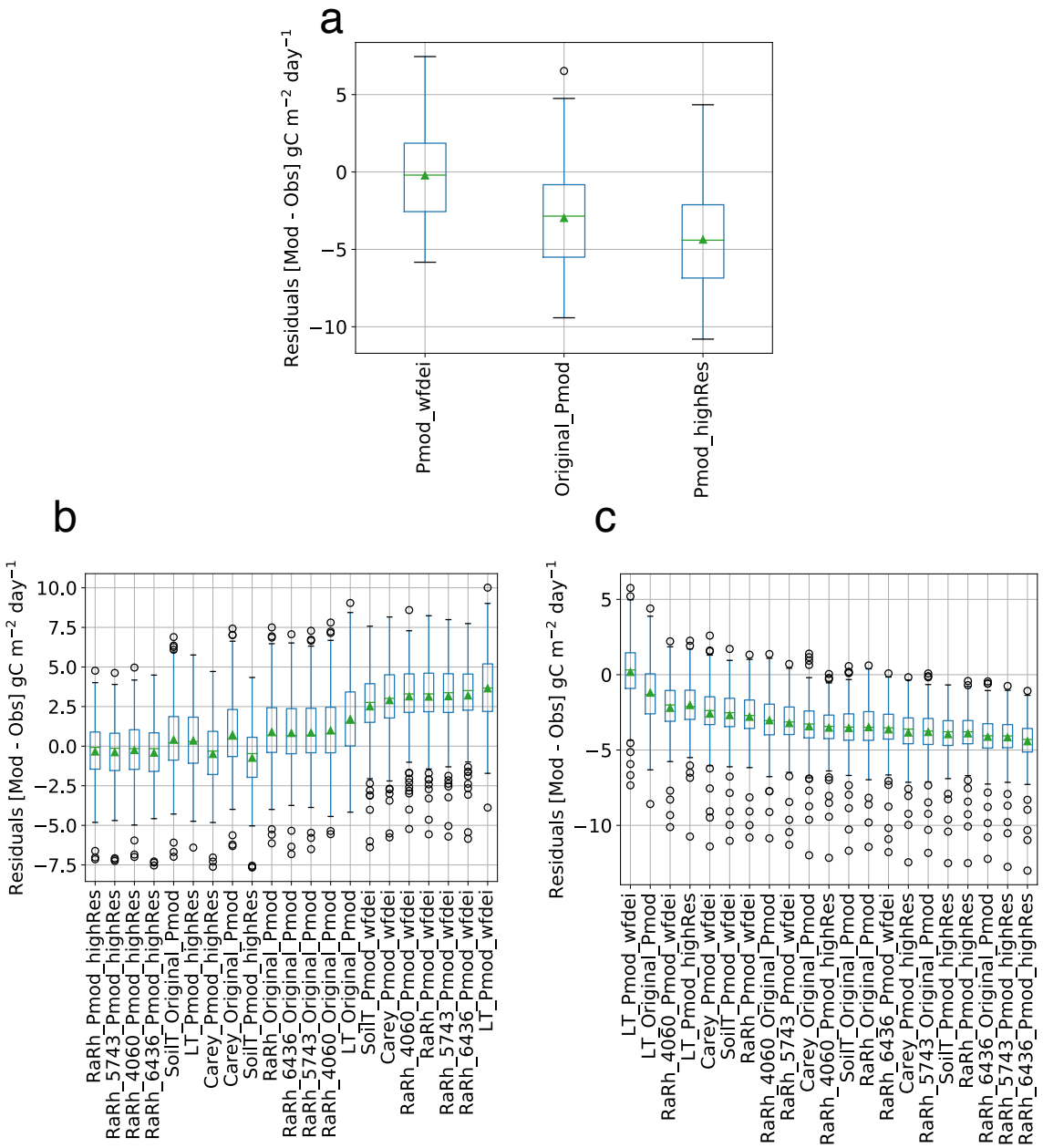
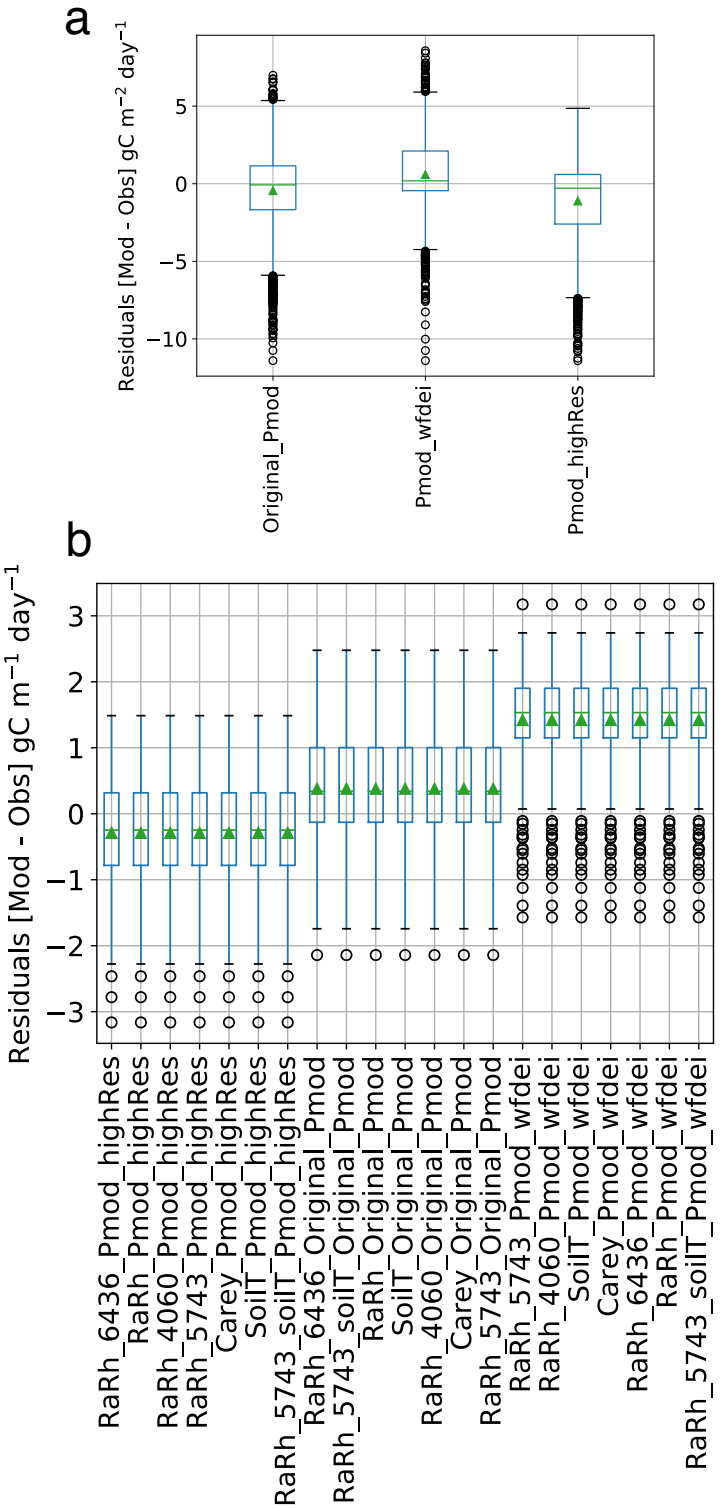


Figure 3.10: Box and whisker plots of the residuals between modelled and observed fluxes at all 17 Fluxnet sites for mean annual GPP (a), Reco (b) and NEE (c). Shown on the box plot is the IQR (blue box), 1.5xIQR (the blue whiskers), the median (green line), the mean (green triangle) and the outliers (open back circles). Models versions are ordered by median.



3.3.3 Ecosystem respiration

Reco was calculated using only the WFDEI P-model version following all the partitioning methods described in Table 3.3. Calculating Reco using only the Lloyd-Taylor equation (Equation 3.8) without any partitioning overestimates peak Reco, particularly in late summer leading to a bias in Reco amplitude and RMSE that is larger than the other partitioning methods (Figure 3.11). However, even the two most different partitioning methods, (40:60 and 64:36) do not show significantly different Reco results for their bias or RMSE in monthly Reco or its amplitude. Therefore, I use the 50:50 partitioning for the rest of the Reco analysis.

The estimates for Rh driven by air or soil temperature using the Lloyd-Taylor equation, or when using the Carey equation show slightly more variation (Figure 3.13), but the overall relationship between Rh and temperature is similar for all estimates (Figure 3.12). In general, Reco is overestimated, particularity in the summer and autumn months, leading to a positive bias in monthly Reco and amplitude (Figures 3.13, 3.14). The amplitude is overestimated mostly for deciduous braodleaf and evergreen needleleaf forests, which also have poor GPP estimations from the P-model. Thus, annual mean Reco, which is the same for all Reco estimates (Equation 3.4), also has a positive bias. The best estimate for monthly Reco and Reco amplitude is found for the Lloyd-Taylor equation with soil temperature because of the slight reduction of Reco amplitude in deciduous broadleaf forests.

Figure 3.11: Selected results for the different estimates of Reco partitioning. a) the seasonal cycle of Reco for DE-Kli which shows the typical range in estimates for the different partitioning fractions, b) scatter plots of monthly and amplitude of Reco for LT only (no partitioning) and the two extreme Ra:Rh partitioning methods, 40:60 and 64:36.

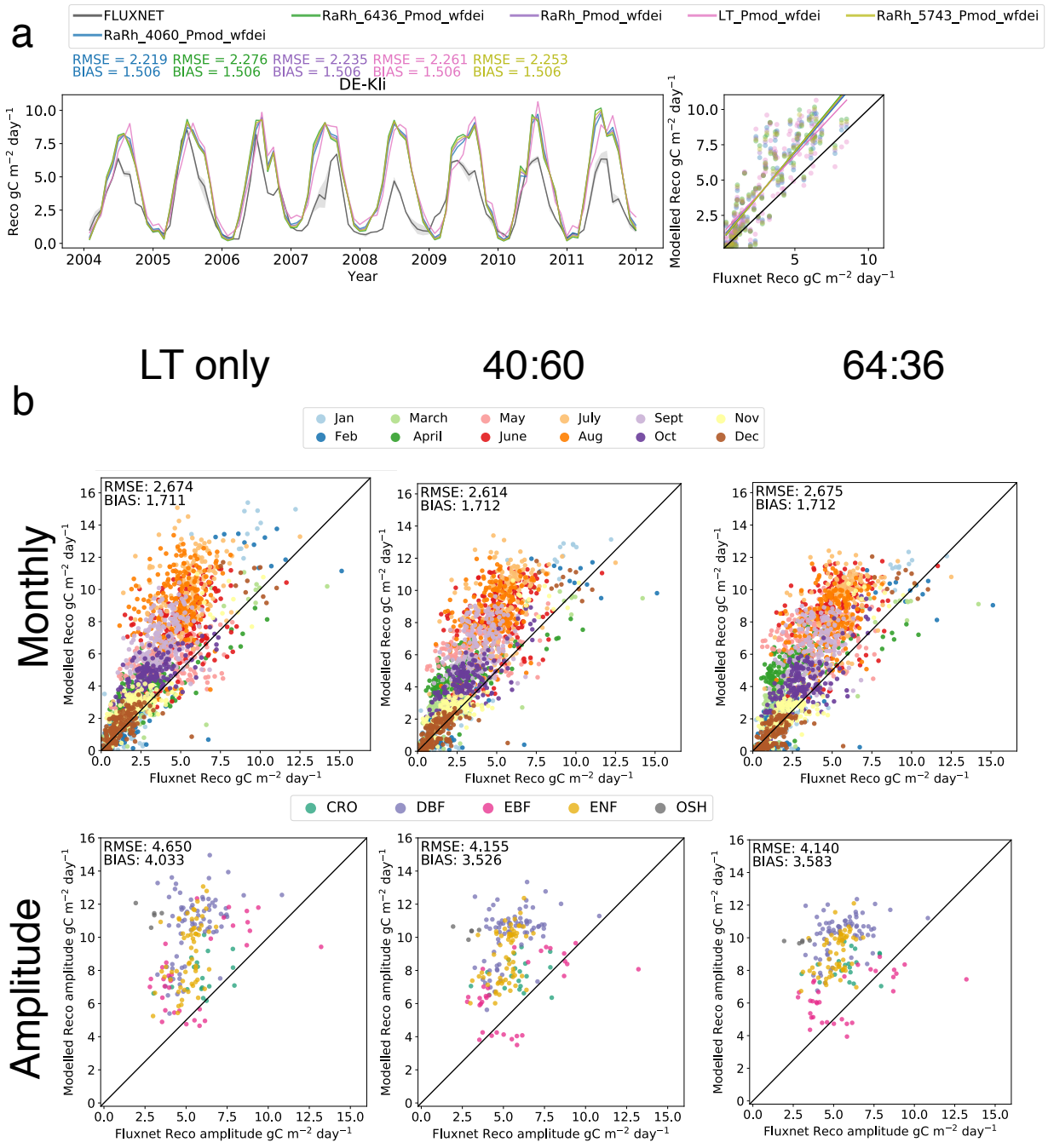


Figure 3.12: Comparison between the Lloyd Taylor (LT) and Carey respiration equations as a function of temperature (a) and modelled Rh (b), and the relationship between air and soil temperature (c). In (b), the LT equation is shown using both air and soil temperature (green and orange crosses respectively), and the Carey equation uses soil temperature (purple crosses).

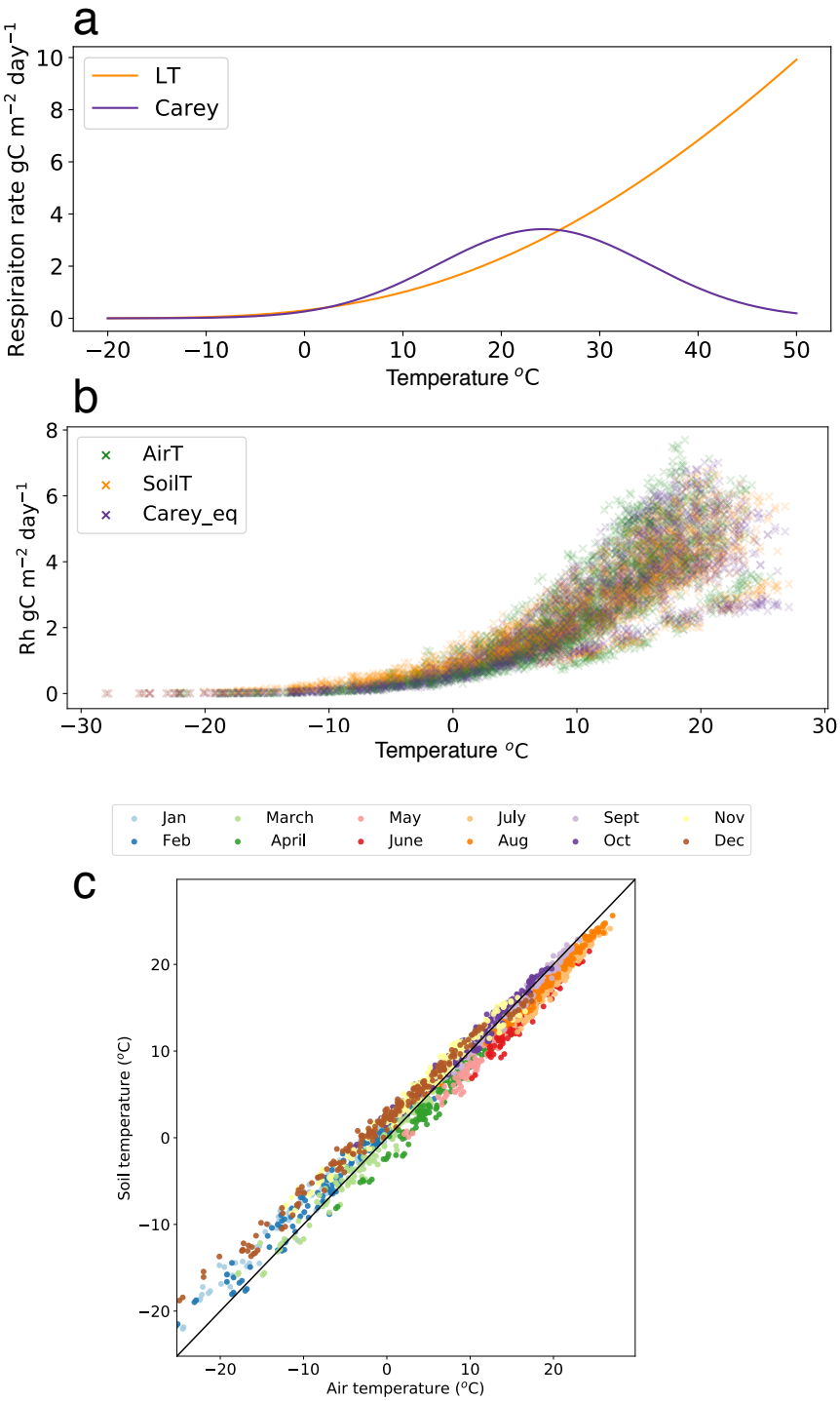
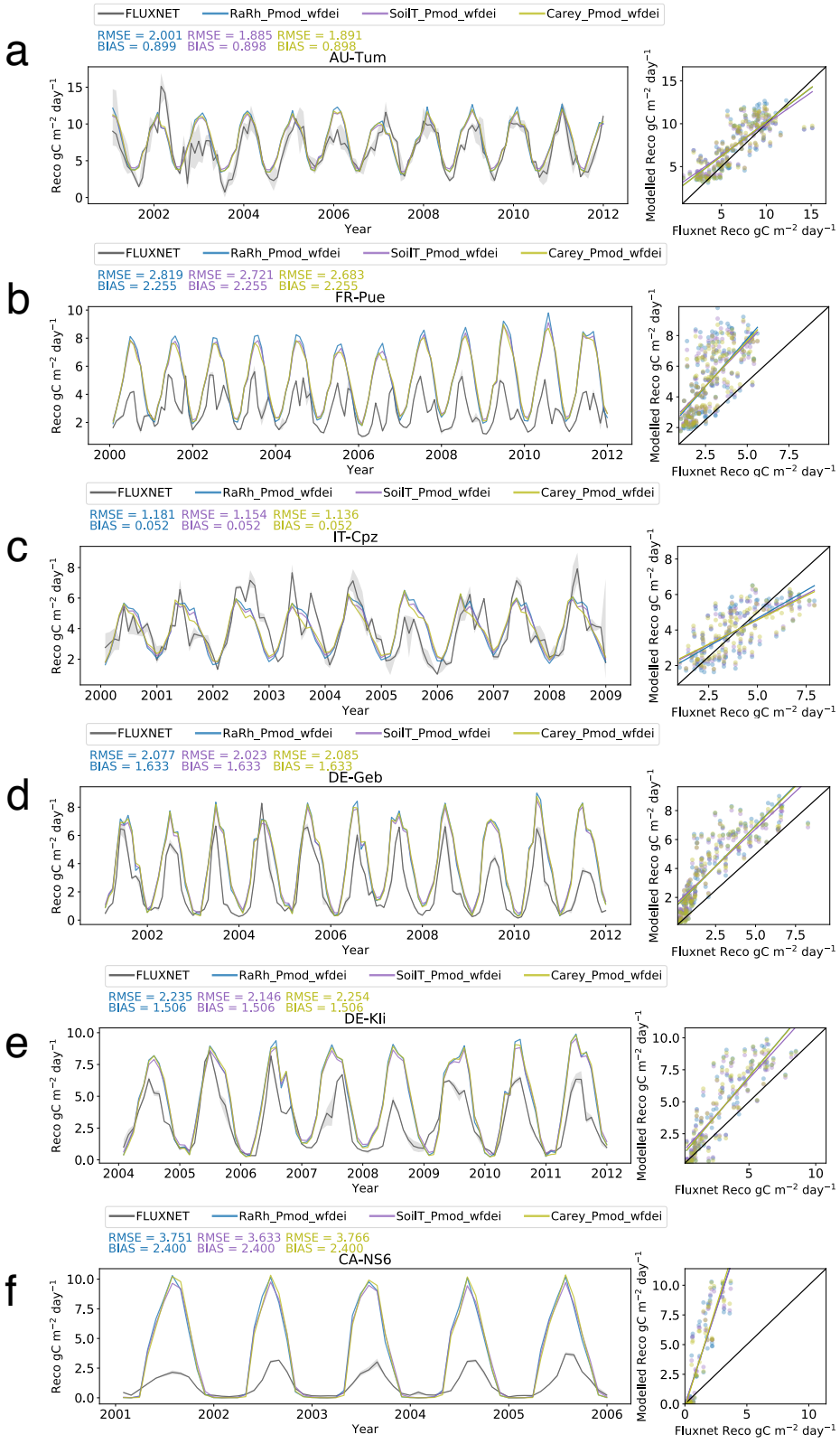
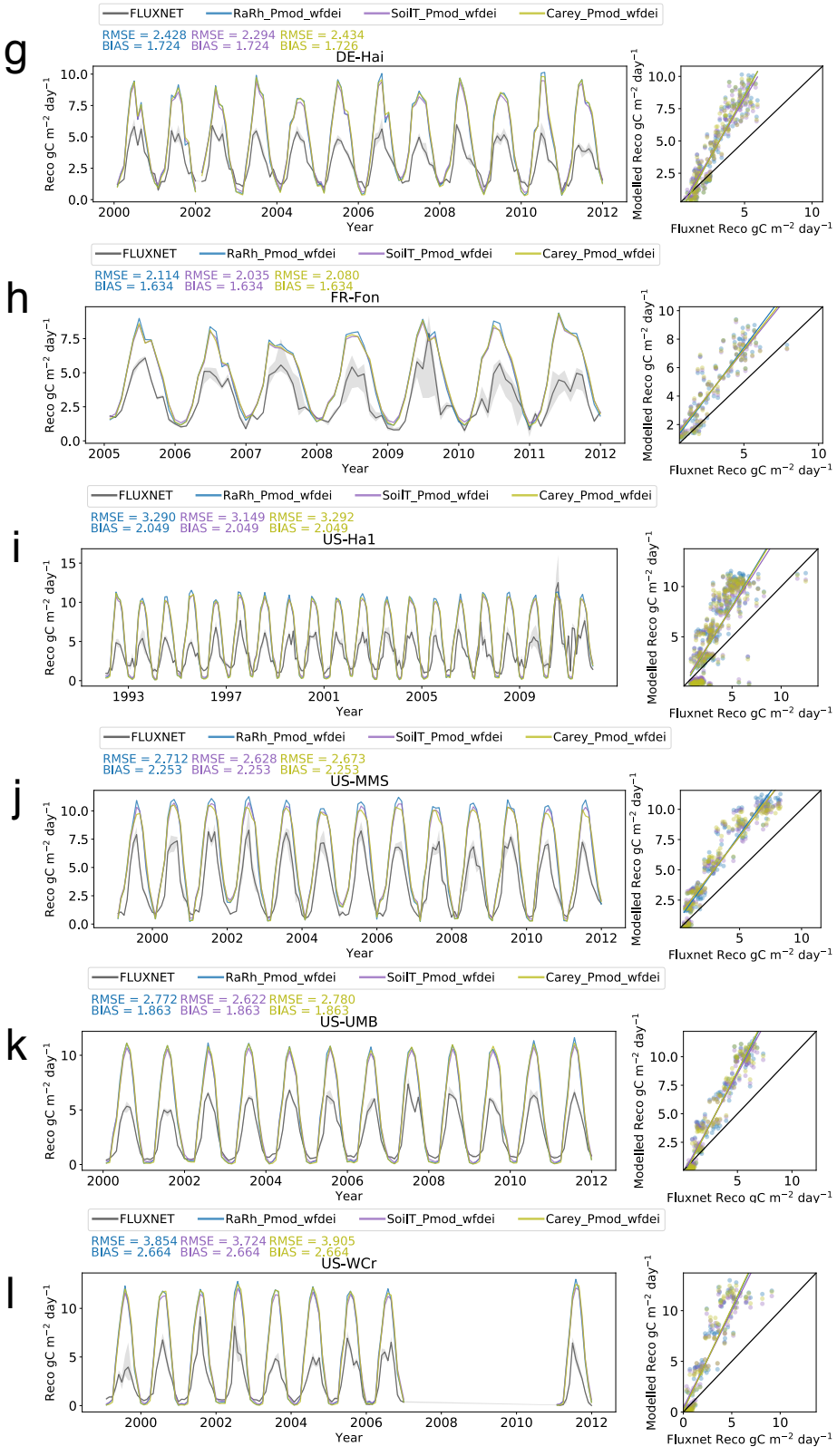


Figure 3.13: Reco seasonal cycle (left-hand side of panel) and monthly mean (right-hand side of panel) at the 17 Fluxnet sites (gC m^{-2} day $^{-1}$). Panels are grouped by vegetation type: a-c - EBF, d, e - CRO, f - OSH, g-l - DBF, m-q - ENF (Table 3.4). Observations (grey lines) are shown with errors (grey shading) and model output is shown for Reco calculated using GPP with Pmod_wfdei for the LT model using air temperature (blue - RaRh_Pmod_wfdei), LT model using soil temperature (purple - SoilT_Pmod_wfdei) and Carey model using soil temperature (green - Carey_Pmod_wfdei), with RMSE and bias in the respective colour. On the right-hand panels the regression line is plotted for each simulation and a 1:1 line is shown. Note that each site has a different scale.




g
FLUXNET
RaRh_Pmod_wfdei
SoilT_Pmod_wfdei
Carey_Pmod_wfdei
RMSE = 2.428 RMSE = 2.294 RMSE = 2.434
BIAS = 1.724 BIAS = 1.724 BIAS = 1.726
DE-Hai
Reco gC m−2 day−1
Year
Modelled Reco gC m−2 day−1
Fluxnet Reco gC m−2 day−1
h
RMSE = 2.114 RMSE = 2.035 RMSE = 2.080
BIAS = 1.634 BIAS = 1.634 BIAS = 1.634
FR-Fon
i
RMSE = 3.290 RMSE = 3.149 RMSE = 3.292
BIAS = 2.049 BIAS = 2.049 BIAS = 2.049
US-Ha1
j
RMSE = 2.712 RMSE = 2.628 RMSE = 2.673
BIAS = 2.253 BIAS = 2.253 BIAS = 2.253
US-MMS
k
RMSE = 2.772 RMSE = 2.622 RMSE = 2.780
BIAS = 1.863 BIAS = 1.863 BIAS = 1.863
US-UMB
l
RMSE = 3.854 RMSE = 3.724 RMSE = 3.905
BIAS = 2.664 BIAS = 2.664 BIAS = 2.664
US-WCr

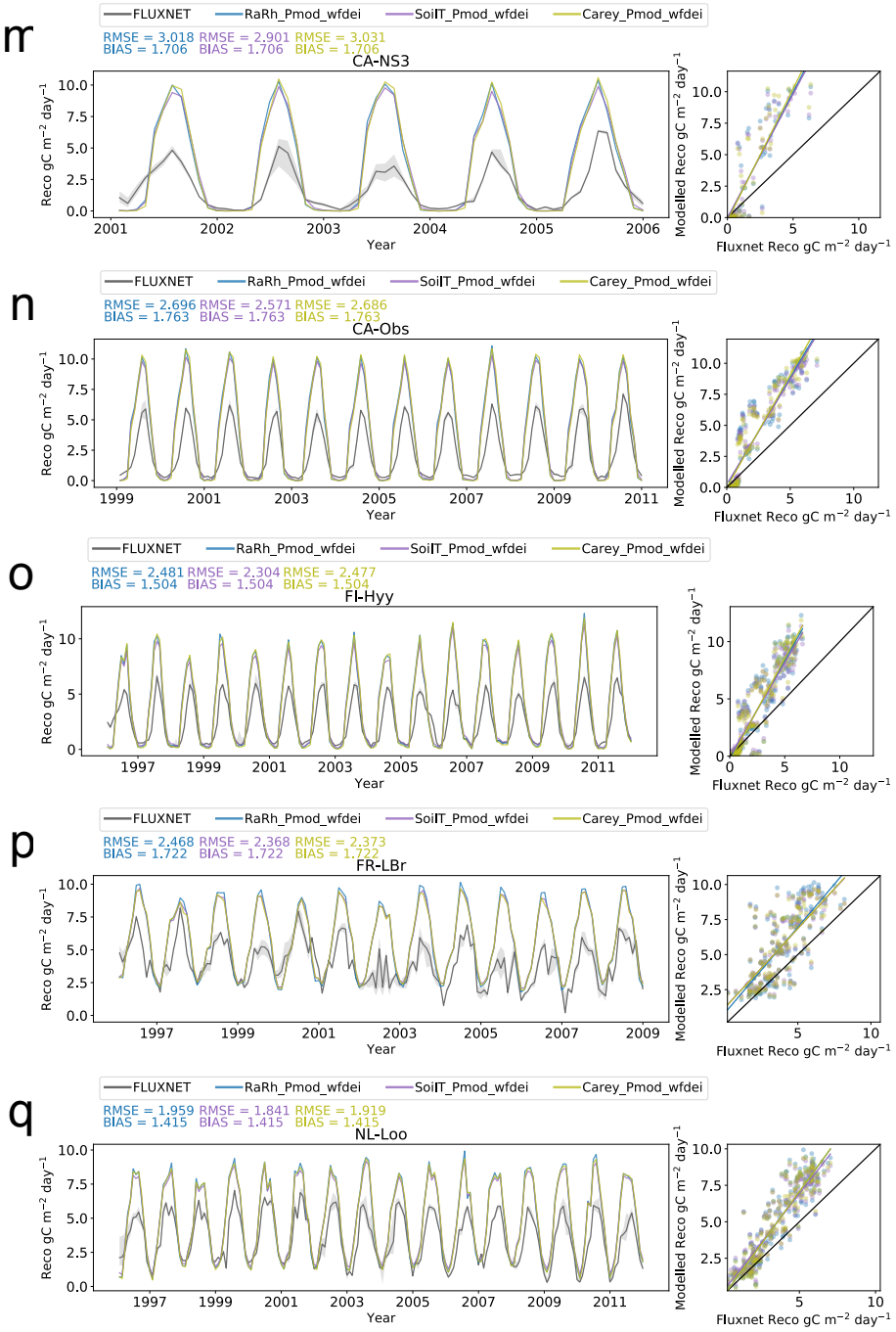
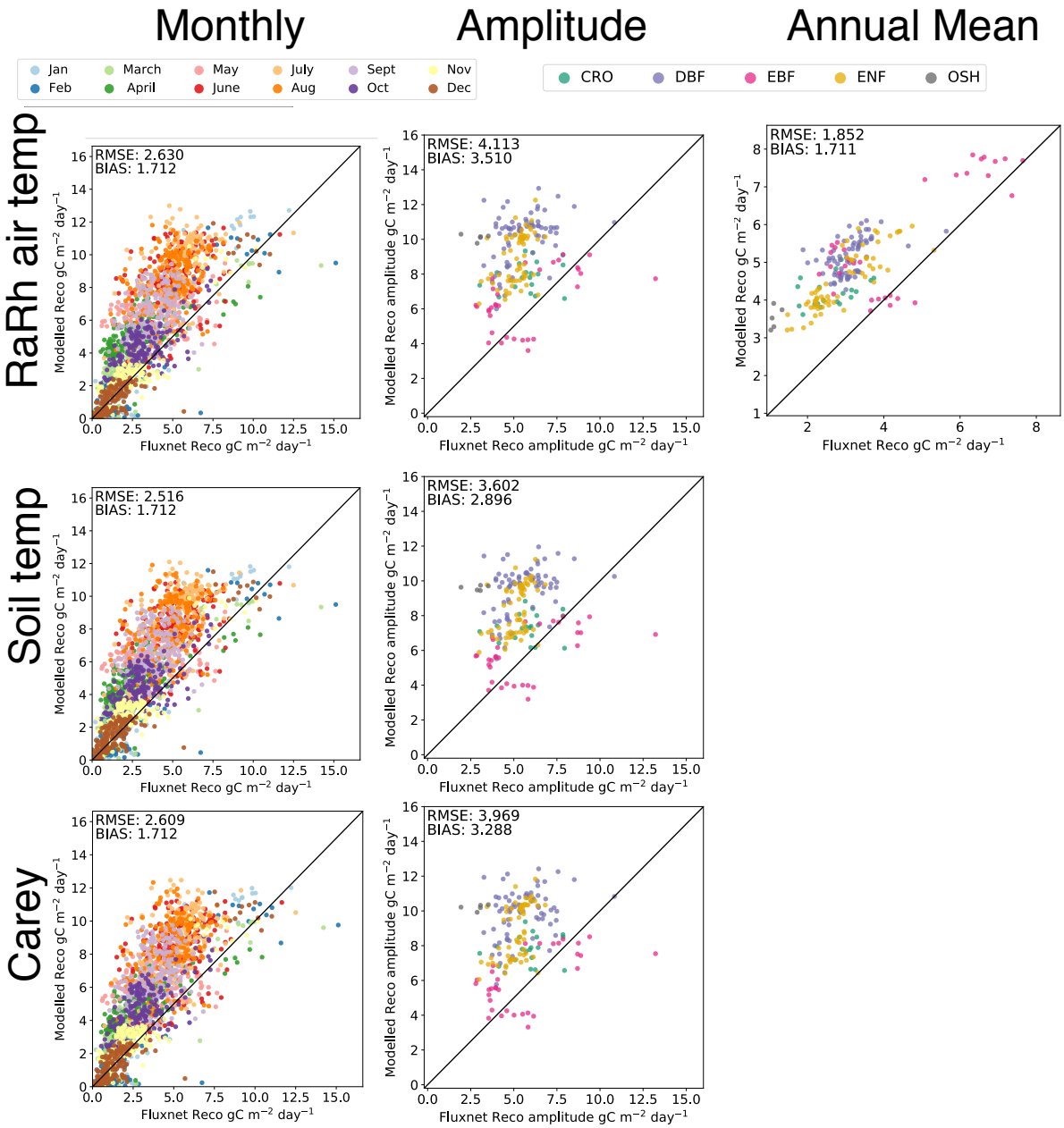

m
FLUXNET
RaRh_Pmod_wfdei
SoilT_Pmod_wfdei
Carey_Pmod_wfdei
RMSE = 3.018 RMSE = 2.901 RMSE = 3.031
BIAS = 1.706 BIAS = 1.706 BIAS = 1.706
CA-NS3
Reco gC m−2 day−1
Year
Modelled Reco gC m−2 day−1
Fluxnet Reco gC m−2 day−1
n
RMSE = 2.696 RMSE = 2.571 RMSE = 2.686
BIAS = 1.763 BIAS = 1.763 BIAS = 1.763
CA-Obs
o
RMSE = 2.481 RMSE = 2.304 RMSE = 2.477
BIAS = 1.504 BIAS = 1.504 BIAS = 1.504
FI-Hyy
p
RMSE = 2.468 RMSE = 2.368 RMSE = 2.373
BIAS = 1.722 BIAS = 1.722 BIAS = 1.722
FR-LBr
q
RMSE = 1.959 RMSE = 1.841 RMSE = 1.919
BIAS = 1.415 BIAS = 1.415 BIAS = 1.415
NL-Loo

Figure 3.14: Observed Vs modelled Reco fluxes for the 17 Fluxnet sites. Monthly Reco, the amplitude of Reco and annual mean Reco is shown for the estimates using 50:50 Ra:Rh with air temperature, 50:50 Ra:Rh with soil temperature, both with the Lloyd-Taylor equation, and for 50:50 Ra:Rh with soil temperature using the Carey equation. Monthly Reco is plotted by month and Reco amplitude and annual mean is plotted by vegetation type according to the IGBP class of the site (See Table 3.4 for more information). Annual mean Reco is the same for all estimates (Equation 3.4) and so this is just shown once. The RMSE and bias is shown in the top corner of each panel and a 1:1 line is plotted.



Box-and-whisker plots are shown in Figures 3.8b, 3.9b and 3.10b for all versions of the P-model and respiration equations. The estimates are ordered by median, and the grouping of results by P-model version highlights that the most significant difference between Reco estimates is the underlying GPP estimate. In general, the original and high resolution P-model estimates give an Reco estimate with a median closest to zero, while the WFDEI version tends to have the largest median. However, this increased skill in modelling Reco comes at the cost of a worse GPP representation, which is the key focus of this thesis. Thus, despite a slight improvement in Reco estimates, I still conclude that the WFDEI version is most appropriate for modelling the amplitude and annual flux of GPP.

None of the Reco models presented in this chapter are suitable for modelling Reco. All estimates are more biased than the GPP estimates, and also have skewed residuals for both monthly Reco and Reco amplitude. Although annual Reco has no skew, it has a positive bias which is at least twice that of the GPP estimates (Figures 3.5, 3.14). Varying the equation used, temperature driving data or partitioning between Ra and Rh had little influence on the overall estimate of Reco. This suggests that either the equations used to model Reco are too simplistic, or that the underlying steady-state assumption is wrong. The latter is probably more important given the observed changes in the terrestrial biosphere, and the systematic bias in the Reco estimates.

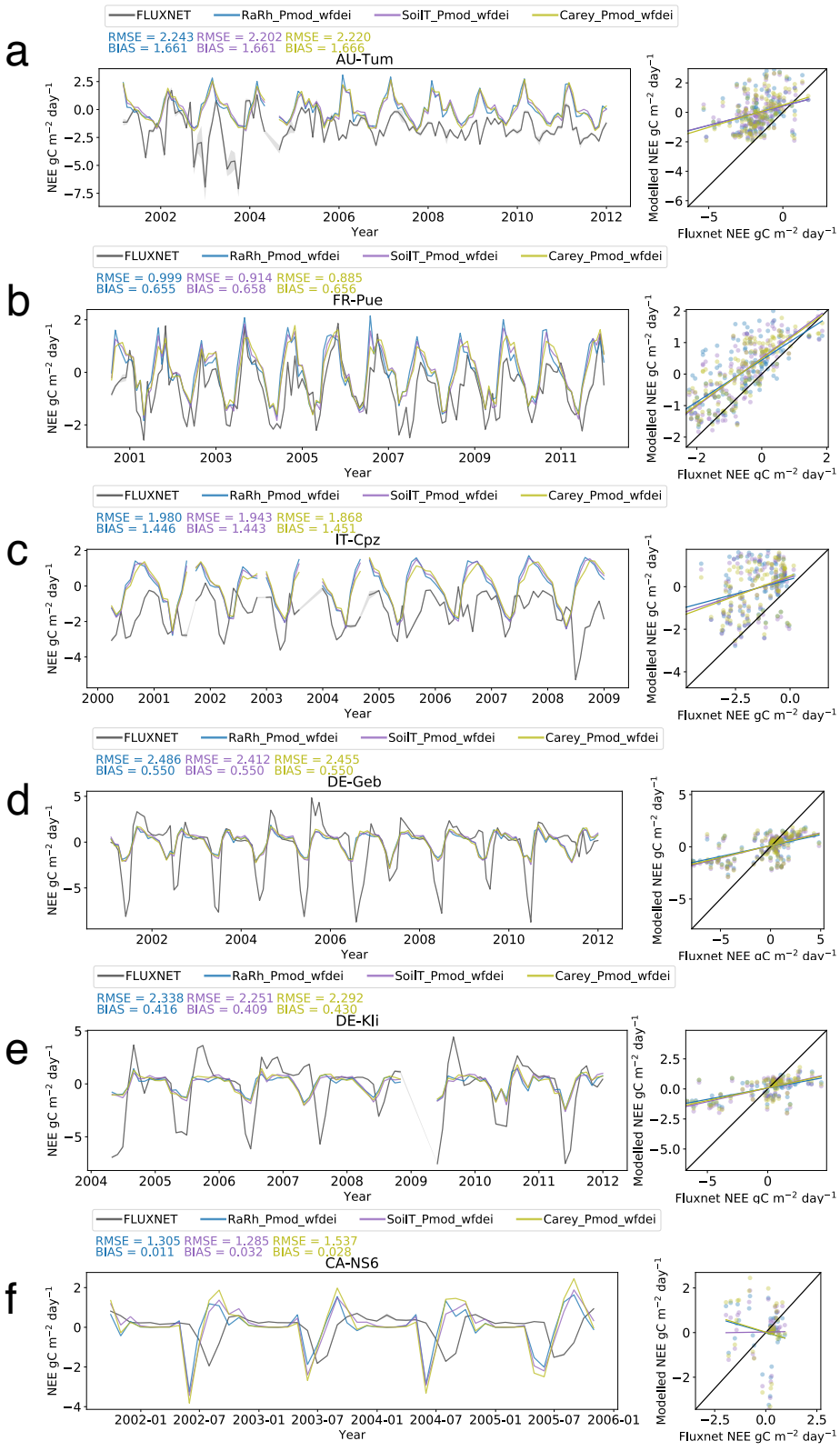
3.3.4 Net ecosystem exchange

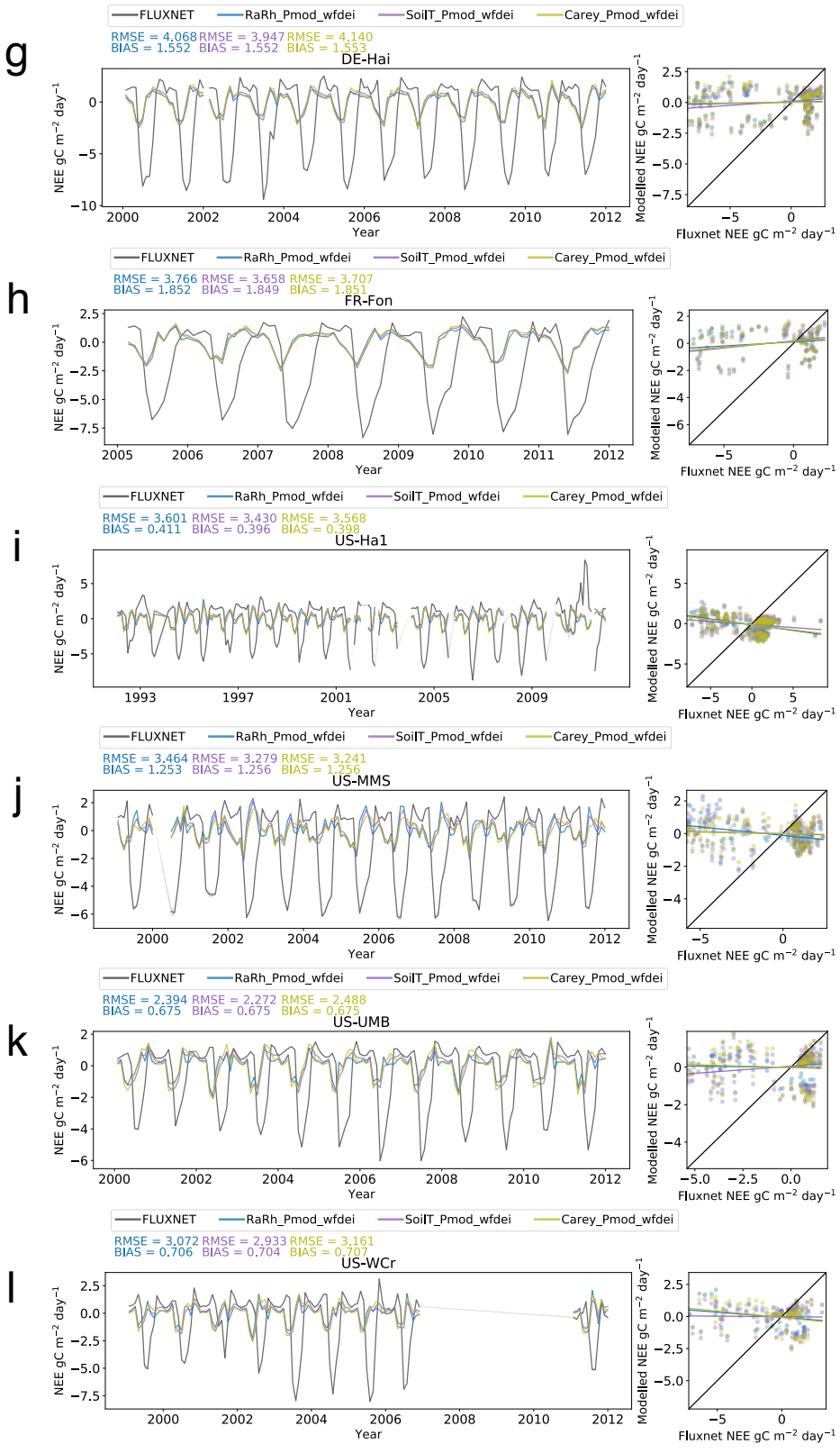
NEE was calculated for each of the model equation pairs and compared to observed NEE (Figure 3.15 - only P-model WFDEI with RaRh, RaRh_soilT and RaRh_Carey shown). No configuration of the model was able to capture the seasonal cycle of NEE well as the phasing was wrong and the magnitude was too small for most sites. The best site is FR-Pue where the model had good skill at capturing the seasonal cycle of NEE, but this is due to cancelling out of GPP and Reco, as both fluxes are overestimated (Figure 3.4b, 3.13b). Monthly NEE has similar IQR and median for all model combinations (Figure 3.8c), while NEE amplitude has varying skill between model combinations (Figure 3.9c). The best combinations (with the median closest to zero) tend to include the WFDEI model because of its superior performance

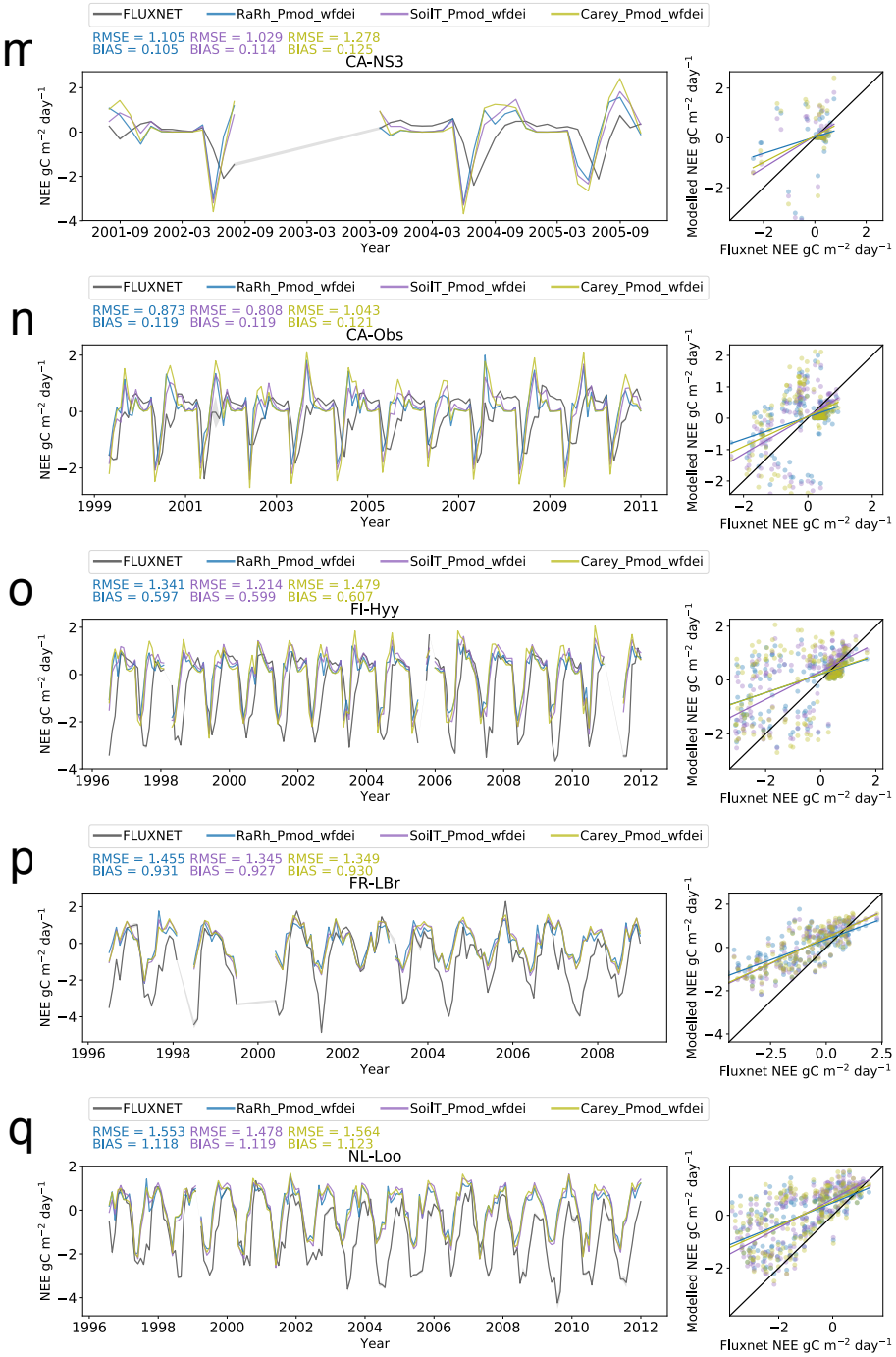
in modelling GPP amplitude, and the best Reco estimates are using no partitioning (LT), the 40:60 Ra:Rh partitioning, Carey Reco estimate and the soil temperature estimate. The 40:60 estimate may be the best partitioning scheme for these sites because this refers to the extreme case for wood Reco partitioning and most sites are forests. The opposite of this partitioning for the extreme case of foliage, with Ra:Rh of 64:36 performs worst in all the P-model variants. The two other best estimates both use soil temperature, suggesting that the slight decrease in peak temperature and increase in minimum temperature can improve Reco estimates.

Despite showing some skill in NEE estimates, the bias in monthly Reco and GPP, and in Reco amplitude prevents me from being confident in using the P-model with any Reco estimate to look at the NEE seasonal cycle over the northern hemisphere in the following chapter. Overestimated fluxes in GPP or Reco can cancel out to suggest good skill for NEE amplitude (Figure 3.4, 3.13), while the earlier analysis showed that all Reco estimates were biased (Figure 3.13).

Figure 3.15: NEE seasonal cycle (left-hand side of panels) and monthly mean (right-hand side of panels) at the 17 Fluxnet sites (gC m^{-2} day $^{-1}$). Panels are grouped by vegetation type: a-c - EBF, d, e - CRO, f - OSH, g-l - DBF, m-q - ENF (Table 3.4). Observations (grey lines) are shown with errors (grey shading) and model output is shown for NEE calculated using GPP from Pmod_wfdei and Reco using the LT model with air temperature (blue - RaRh_Pmod_wfdei), LT model with soil temperature (purple - SoilT_Pmod_wfdei) and Carey model with soil temperature (green - Carey_Pmod_wfdei), with RMSE and bias in the respective colour. On the right panel the regression line is plotted for each simulation and a 1:1 line is shown. Note that each site has a different scale.




g
FLUXNET
RaRh_Pmod_wfdei
SoilT_Pmod_wfdei
Carey_Pmod_wfdei
RMSE = 4.068 RMSE = 3.947 RMSE = 4.140
BIAS = 1.552 BIAS = 1.552 BIAS = 1.553
DE-Hai
NEE gC m⁻² day⁻¹
Year
Modelled NEE gC m⁻² day⁻¹
Fluxnet NEE gC m⁻² day⁻¹
h
RMSE = 3.766 RMSE = 3.658 RMSE = 3.707
BIAS = 1.852 BIAS = 1.849 BIAS = 1.851
FR-Fon
i
RMSE = 3.601 RMSE = 3.430 RMSE = 3.568
BIAS = 0.411 BIAS = 0.396 BIAS = 0.398
US-Ha1
j
RMSE = 3.464 RMSE = 3.279 RMSE = 3.241
BIAS = 1.253 BIAS = 1.256 BIAS = 1.256
US-MMS
k
RMSE = 2.394 RMSE = 2.272 RMSE = 2.488
BIAS = 0.675 BIAS = 0.675 BIAS = 0.675
US-UMB
l
RMSE = 3.072 RMSE = 2.933 RMSE = 3.161
BIAS = 0.706 BIAS = 0.704 BIAS = 0.707
US-WCr


m
FLUXNET
RaRh_Pmod_wfdei
SoilT_Pmod_wfdei
Carey_Pmod_wfdei
RMSE = 1.105 RMSE = 1.029 RMSE = 1.278
BIAS = 0.105 BIAS = 0.114 BIAS = 0.125
CA-NS3
NEE gC m⁻² day⁻¹
2001-09 2002-03 2002-09 2003-03 2003-09 2004-03 2004-09 2005-03 2005-09
Year
Modelled NEE gC m⁻² day⁻¹
Fluxnet NEE gC m⁻² day⁻¹
n
RMSE = 0.873 RMSE = 0.808 RMSE = 1.043
BIAS = 0.119 BIAS = 0.119 BIAS = 0.121
CA-Obs
1999 2001 2003 2005 2007 2009 2011
o
RMSE = 1.341 RMSE = 1.214 RMSE = 1.479
BIAS = 0.597 BIAS = 0.599 BIAS = 0.607
FI-Hyy
1996 1998 2000 2002 2004 2006 2008 2010 2012
p
RMSE = 1.455 RMSE = 1.345 RMSE = 1.349
BIAS = 0.931 BIAS = 0.927 BIAS = 0.930
FR-LBr
1996 1998 2000 2002 2004 2006 2008
q
RMSE = 1.553 RMSE = 1.478 RMSE = 1.564
BIAS = 1.118 BIAS = 1.119 BIAS = 1.123
NL-Loo
1996 1998 2000 2002 2004 2006 2008 2010 2012

3.4 Discussion

Modelled fluxes of GPP, Reco and NEE from the P-model and two models for ecosystem respiration were compared to 17 Fluxnet sites, predominately located in the high northern latitudes. The P-model was driven by PPFD from the SPLASH model and WFDEI reanalysis data, and using fAPAR3g at $1/2^o$ and $1/12^o$ resolution, while different estimates for Reco were generated by using a range of partitioning estimates for Ra:Rh on an annual basis, air and soil temperature to drive the Rh part of the model and two different equations to estimate Rh. The P-model with WFDEI PPFD was found to be suitable for estimating GPP amplitude and annual mean, but none of the Reco estimates were sufficiently skilful to be used in further analysis. Thus NEE can also not be estimated using the P-model and Reco combinations described in this chapter.

The skill of the P-model in representing GPP amplitude is comparable to that of other more complex ecosystem models. Compared to the bias in GPP amplitude of 0.07 PgC m^{-2} day^{-1} for the P-model (Figure 3.5), nine TRENDY DGVMs and the upscaled GPP-MTE product had a mean amplitude bias of -1.6±2.6 PgC m^{-2} day^{-1} and -0.8±1.7 PgC m^{-2} day^{-1}, respectively when evaluated against 16 Fluxnet sites (four overlapping with the sites used in this chapter) at high northern latitudes (Peng et al., 2014). A range of 24 enzyme-kinetics and LUE models, including the MODIS GPP product, were compared to 39 Fluxnet sites across North America and Canada (five overlapping sites) and also had a large negative bias in peak GPP across all models and sites (Schaefer et al., 2012). Further investigation of these models showed that they underestimated the increase in daily average GPP with radiation which resulted in the underestimated summer peak GPP. The models were driven by site-measured radiation, which is well correlated to the WFDEI PAR used to drive the P-model (Figure 3.1), suggesting that the P-model may be better able to capture the the relationship between peak GPP and peak PAR.

Annual mean GPP is well captured by the P-model despite the overestimation of GPP at the start of the growing season (Figure 3.5, 3.6). The positive bias in the WFDEI version comes

from sites with low GPP such as open shurbland and crops, for which GPP is overestimated. The poor representation of GPP in croplands is unsurprising as seasonal GPP is controlled by human management rather than climate, and so these sites are often not well represented by models (Schaefer et al., 2012; Turner et al., 2005).

The difficulty in modelling the start and end of the growing season is pervasive. The P-model was driven by monthly fAPAR, which may contribute to poorly represented seasonality. However, 14 TBMs driven at hourly to daily timesteps also overestimated GPP at the start and end of the growing season across a variety of biomes in North America and Canada, resulting in a positive bias in GPP particularly for deciduous biomes (Richardson et al., 2012). Similar results were also found for the TRENDY DGVMs, GPP-MTE (Peng et al., 2014) and the models used by Schaefer et al. (2012) which are all driven on an hourly to daily timestep and overestimated spring and autumn GPP too, highlighting the difficulty in capturing this part of the GPP seasonal cycle. Other possible reasons for this bias may result from the lack of incorporating soil moisture, resulting in an overestimation of GPP during dry conditions (Schaefer et al., 2012) or during cold periods when the soil is frozen (Murray-Tortarolo et al., 2013; Schaefer et al., 2012). Although recent analysis shows that the sites considered in this chapter may have little sensitivity to soil moisture (Stocker et al., 2018), the availability of soil moisture can reduce GPP in spring and autumn (Schaefer et al., 2012) so including this limitation may improve the seasonal representation of GPP. Furthermore, the current P-model set-up of restricting GPP when air temperatures below 0^oC may not be a sufficient limit, as GPP was zero for many different observation sites even when air temperature was above freezing (Figure 3.4). Nutrient dynamics are also missing from the current set-up, but play an important role in carbon uptake (Peng et al., 2014).

Previous studies using the JULES land surface model suggest that the climate is more important in determining GPP than the choice of fAPAR data (Slevin et al., 2015). Thus some of the model bias may result from the difference between the environmental conditions observed at Fluxnet sites, and the data used to drive the model. Although CRU temperature is representative of site-scale temperature, CRU-derived VPD was much smaller than the VPD observed at

the Fluxnet sites (Figure 3.1). Since partial regression analysis also showed that the P-model temperature and VPD response was in the wrong direction (Figure 3.7), these three factors may overall cancel out to provide the good fit during peak GPP. For example, when temperature is highest in the summer, the P-model may be underestimating the GPP response, but also underestimating the limit from VPD. This is not the case in the shoulder seasons when temperatures are lower, and so the overestimation of GPP is not offset by increased limitation from VPD.

Model performance could also be improved by replacing air temperature with land surface temperature, the temperature at the top of the canopy or bare soil, as this may better reflect the temperature experienced by vegetation. Land surface temperature has a much lager range than air temperature, but over forested regions is generally well coupled to air temperature (Mildrexler et al., 2018; Jin and Dickinson, 2010). However, leaves can be several degrees different to the air temperature (Dong et al., 2017) due to leaf thermoregulation (Michaletz et al., 2016) which can reduce the range of temperatures experienced by the vegetation. Including this effect may increase summer GPP for some biomes as the vegetation could be cooler than air temperature, thus reducing the negative effect of temperature on GPP.

The improvements in the GPP estimate would also improve the estimate of Reco, and may therefore reduce the bias and skew. The shape of the seasonal cycle of Reco was generally well captured by all model versions and so the poor performance may result from the poorly modelled monthly GPP. However another weakness was an overestimation of peak Reco, which may not be heavily influenced by improvements in GPP, as this was a feature that was well captured by the P-model. Instead, this could result from poor or over-simplified representation of Reco. Better representation of soil temperature, or the inclusion of parameters such as soil moisture or a base respiration rate could improve modelled estimates of Reco. Differences between soil and air temperature were small (Figure 3.12c) and may not fully reflect the surface soil temperature or temperature at different layers throughout the soil column (Har; Hachem et al., 2018). Using values for soil texture and available water in equation 3.11 that vary spatially and temporally could improve the estimation of thermal conductivity and therefore estimated soil temperature.

However, global soil texture is not well known and soil water content may only be important in very dry regions (Migliavacca et al., 2011). A recent study by Migliavacca et al. (2011) that used observed GPP from Fluxnet sites to test different models of Reco, found that their Reco estimates could be improved by including a base respiration rate and maximum leaf area, as this reflects ecosystem Reco potential. This could be calculated by estimating steady-state respiration for pre-industrial conditions, as in Keenan et al. (2016). A final improvement could be made by allowing Ra:Rh to vary, as observations suggest that this partitioning can change seasonally, with stand age and is sensitive to environmental conditions (Davidson et al., 2006b; Delucia et al., 2007).

The underlying assumption of a steady-state system may also be wrong, and this may be causing the systematic overestimation of Reco in the model estimates (Figures 3.14, 3.10b). Respiratory fluxes comprise of both slow and fast pools and not all the carbon that is assimilated by vegetation in a particular year will be respired that same year. A fraction of the carbon will be stored and will return to the atmosphere over the following years (Trumbore, 2006; Bon). As environmental conditions have changed over recent years, the seasonal flux of carbon has become unbalanced and annual GPP fluxes outweigh respiration. This has been observed as the net carbon sink, which modelling studies suggest is partly driven by increases in high latitude GPP (McGuire et al., 2009; Pan et al., 2011). Thus, allowing some of the assimilated carbon to be stored within the model for a number of years could remove some of this bias. However, this would induce further complications as the carbon turnover time (the amount of time that the carbon is stored within the system) is one of the most uncertain fluxes amongst models (Friend et al., 2014).

3.5 Conclusion

The results presented in this chapter support previous analysis showing that the P-model can capture annual GPP (Wang et al., 2017; Keenan et al., 2016), indicating that this is a robust feature of the model. This analysis went further and also showed that the P-model was skilful at capturing the amplitude of GPP but was unable to reproduce the seasonal cycle correctly

as GPP in spring and autumn was overestimated. Despite not including any additional information about PFTs, and having a minimal number of parameters, the model performed well across a range of different biomes. The skill of the P-model is comparable to more complex DGVMs that have been evaluated at a similar range of Fluxnet sites. Therefore, these results allow confidence in using the P-model to estimate the amplitude of GPP and annual GPP at the ecosystem scale, particularly across high northern latitudes which were well represented by the Fluxnet sites in this study. Future improvements in the P-model could be achieved by using land surface temperature instead of air temperature, including moisture limitations or using fAPAR data with higher temporal resolution. Unfortunately, none of the equations for Reco were sufficiently skilful to provide a good estimate of NEE, and so I will not be able to make an estimate of the seasonal cycle of CO_2 from the P-model. A number of improvements to the simple model of Reco are also suggested, but a better understanding of respiratory fluxes is required before a similarly simple and skilful model for Reco can be developed.

Chapter 4

Analysing changes in northern terrestrial productivity using the P-model

4.1 Introduction

The terrestrial biosphere takes up around a quarter of the anthropogenic CO_2 emitted to the atmosphere each year. This net sink of CO_2 is due to a larger annual uptake of carbon through gross primary production (GPP) than release through respiration and disturbances (Le Quere et al., 2018; Gurney and Eckels, 2011). Recent changes in environmental conditions have driven the increase in GPP, as the rate of GPP is sensitive to factors such as CO_2, temperature, light, atmospheric humidity and changes in land use. However, the role of each factor remains uncertain as GPP cannot be measured directly, and models disagree on the contribution to GPP changes from these drivers (Fisher et al., 2014; Houghton et al., 1998; Rogers et al., 2017; Zhao and Zeng, 2014). Previous studies suggest that models are missing or poorly representing key mechanisms that have increased GPP, as they are generally unable to capture the observed increase in the amplitude of the seasonal cycle of CO_2 at high northern latitudes which has been primarily driven by increases in carbon uptake (Graven et al., 2013; Thomas et al., 2016; Alexandrov, 2014), (Chapter 2). Specifically, since models are able to reproduce observed greening trends, it seems that they are able to capture increases in GPP from structural changes, but

missing or poorly representing mechanisms that can increase the physiological rate of carbon uptake; the ecosystem light-use efficiency (eLUE). Thus, in this chapter I use a next-generation terrestrial biosphere model, the P-model, which is driven by observed greening, to quantify the role of environmental drivers on the change in GPP and eLUE across high northern latitudes.

GPP can increase as a result of structural and/or physiological changes. Structural changes increase GPP through an increase in APAR (absorbed photosynthetically active radiation), which is a product of the PAR received by vegetation and the fraction that is absorbed by green vegetation (fAPAR). At the ecosystem scale, changes in fAPAR can result from an increase in the number of leaves per plant, an increase in the amount of vegetation in a particular area and changes in the type of vegetation (e.g. a transition from shrubs to trees). Satellite observations of vegetation greenness since the 1980's have shown a greening trend across northern latitudes (Zhu et al., 2016; Mao et al., 2016; Guay et al., 2014), of up to 15% (Murray-Tortarolo et al., 2013; Piao et al., 2006), (Chapter 2). Greening has primarily been driven by increases in temperature which has lengthened the growing season due to earlier snow melt, but also by increases in vegetation cover driven by CO_2, nitrogen deposition and changes in vegetation type (Zhou et al., 2001; Zhu et al., 2016; Mao et al., 2013). Models show good skill at reproducing the climate driven greening trend, but have poor skill at representing greening trends where warming is not the primary driver (Figure 2.5). Furthermore, terrestrial biosphere models tend to overestimate mean annual greenness because of assumptions made about different plant functional types (PFTs) or a lack of vegetation dynamics (Murray-Tortarolo et al., 2013).

Changes in APAR can also occur from variations in PAR. These tend to be regional as incoming radiation is effected by local conditions such as changes in aerosol emissions and cloudiness. The effect of changes in PAR on GPP are rarely singled out in model intercomparison studies but can have a large impacts on GPP trends, especially when considering changes in the quantity of radiation that is either direct or diffuse. Diffuse radiation is radiation that has been scattered by particles in the atmosphere (such as aerosols) and so the total PAR received at the earth surface is lower than if all the PAR was direct radiation. However, if the total PAR received by vegetation does not decrease too much, increases in diffuse PAR can increase GPP

because more vegetation receives light and less vegetation is light saturated (Mercado et al., 2009; Gu et al., 2002).

Physiological changes in vegetation alter the rate of CO_2 uptake per unit of vegetation, the ecosystem light-use efficiency (eLUE), and can be driven by a range of factors including CO_2 fertilisation and changes in climate and nutrient availability. GPP is often limited by one or more of these factors (Nemani et al., 2003). Recent environmental changes have reduced some of these limitations, which can also indirectly influence eLUE by changing carbon allocation and the type of vegetation in a particular area (Litton et al., 2007; Forkel et al., 2016; Barichivich et al., 2013). Changes in vegetation distribution can also occur directly from human influence through land management and the cultivation of croplands (Gray et al., 2014; Zeng et al., 2014). Over high northern latitudes, eLUE must have increased because the observed increase in ASC cannot be explained by structural changes alone (Chapter 2). For most terrestrial biosphere models, increases in eLUE are primarily driven by increases in CO_2 fertilisation (Chapter 2) but there is large variation in the overall magnitude of CO_2 fertilisation between different models (Friedlingstein et al., 2014; Zhao et al., 2016), and the contribution to changes in eLUE from other environmental changes (Chapter 2).

Factors effecting GPP interact dynamically such that the overall effect may be a change in productivity different to the addition of the individual factors, but these non-linear interactions are poorly understood. A recent meta-analysis considering the interaction between elevated CO_2 and temperature found large variations between measurement sites, and thus the current datasets are inconclusive on the size of this interaction (Baig et al., 2015). Nevertheless, it is important to understand how models are including these non-linear terms as this contributes to the total productivity. Ten TBMs were compared to observations from a PHACE (Prairie Heating and CO_2 Enrichment) experiment site which showed increases in NPP from CO_2 fertilisation, reductions in NPP from climate (through increases in temperature and decreases in moisture availability) and a larger increase in NPP from the combined effect of both drivers together (De Kauwe et al., 2017). However, model simulations of single-factor changes at this site were poor, and so the models were also unable to capture the non-linear interactions between

factors (De Kauwe et al., 2017). Although this multi-factor change is more realistic to real-world changes, it is not often analysed in models as full-factorial experiments can be expensive to run. In general, intercomparison projects (e.g. MsTMIP and TRENDY (Huntzinger et al., 2013; Sitch et al., 2015)) will run experiments following a semi-factorial approach whereby all variables are held constant at a particular time, and then one-by-one, each variable is turned on to vary over time. The individual effect of each factor is then calculated by subtracting each experiment from the subsequent run (e.g. (Chapter 2)). By analysing these semi-factorial experiments using multiple methods, it is possible to identify, but not explicitly quantify, non-linear interactions. The large effect of non-linear interactions has been highlighted for the TRENDY models using this approach, as the effect of CO_2 fertilisation on GPP was larger for simulations that included climate compared to those where only CO_2 was varying (Piao et al., 2013).

As models try to include a larger number of mechanisms to fully represent ecosystem functioning, uncertainty in model estimates increases and models can become so complex that it is often difficult to identify the source of particular behaviours (Fisher et al., 2014; Alexandrov, 2014; Prentice et al., 2014; Bonan and Doney, 2018). This has led to large uncertainties between models due to differences in model structure because the implementation of various mechanisms or the values for parameters differ between models (Lovenduski and Bonan, 2017; Rogers et al., 2017). Therefore, it is helpful to take a step back and evaluate our understanding of recent changes in productivity using a simple model in which all processes are fully traceable. The P-model, which is driven by empirical relationships and the best available data, lends itself to such an application. The complexities of modelling uncertain processes such as nutrient and moisture limitations are avoided by assuming that satellite fAPAR data will indirectly take these processes into account (Keenan et al., 2016; Wang et al., 2014). The main benefits of using the P-model over complex models are that it is quick to run, allowing for a variety of simulations to be explored, and that is driven by observed fAPAR, which allows the physiological changes in GPP to be explicitly quantified. Previous analysis also shows that it is skilful at representing mean annual GPP and GPP amplitude (Chapter 3) (Keenan et al., 2016; Wang et al., 2017). The main drawbacks of the P-model are that it can only be run over the satellite

observing period (1982-present) which means that it could not be directly used to analyse the changes in the amplitude of the seasonal cycle of CO2 (ASC) that the MsTMIP models have been used to analyse (Chapter 2), or be used to predict future GPP changes. Furthermore, the analysis in Chapter 3 casts some doubt on whether the temperature response of GPP in the P-model is correct, and this will need to be taken into account when analysing simulation outputs.

In this chapter, I use the P-model to analyse the drivers of trends in mean annual GPP and GPP amplitude across the high northern latitudes and I calculate eLUE to analyse physiological changes in vegetation. Full factorial experiments are run following the factor decomposition method by Stein and Alpert (1993) in order to quantify the contribution to modelled trends from CO_2, climate (temperature and VPD), fAPAR and PAR, and their non-linear interactions. The results are compared to the terrestrial biosphere models taking part in MsTMIP, which have already been extensively analysed (Ito et al., 2016) (Chapter 2). Although the factorial decomposition from the P-model is not directly comparable to the MsTMIP experiments, the results can be compared qualitatively.

4.2 Methods

4.2.1 The P-model

P-model GPP is calculated following the set up described in Chapter 3, with WFDEI shortwave radiation as the input for PPFD, and the model is run globally at a monthly timestep at 0.5^o x 0.5^o resolution from 1982-2010. Additional experiments are run to calculate the contribution to GPP changes from changes in each driver. The full factorial experiments are run such that drivers are either held constant at 1982 levels or allowed to vary over time in all possible combinations. The contribution to GPP change from each individual driver as well as the non-linear interactions between factors are then separated using the factor decomposition method devised by Stein and Alpert (1993). The contribution from a particular driver is calculated using one of the following equations:

$$f_1 = ef_1 - ef_0 \tag{4.1}$$

$$f_{12} = ef_{12} - (ef_1 + ef_2) + ef_0 \tag{4.2}$$

$$f_{123} = ef_{123} - (ef_{12} + ef_{13} + ef_{23}) + (ef_1 + ef_2 + ef_3) - ef_0 \tag{4.3}$$

$$f_0 = ef_x - (ef_{123} + ef_{134} + ef_{124} + ef_{234}) + (ef_{12} + ef_{13} + ef_{14} + ef_{23} + ef_{24} + ef_{34}) - (ef_1 + ef_2 + ef_3 + ef_4) + ef_0 \tag{4.4}$$

Equations 4.1, 4.2, 4.3, 4.4 show the general equations used for calculating the linear, 2-way non-linear, 3-way non-linear and 4-way non-linear factors respectively, and the full equations are given in Table 4.2. In the equations above, ef_i is a particular experiment, f_i is the contribution to the total flux from a particular factor and the subscripted numbers refer to the drivers that were allowed to vary in an experiment. The constant run is given as ef_0 and the 'all-on' run is ef_x. In this method, the sum of all the contributions (linear and non-linear) is equal to the experiment where all factors are varying. In order to consider all the individual and non-linear terms of the four drivers (CO_2, climate, fAPAR and PAR), 16 experiments are required as outlined in Table 4.1. The individual factors were then calculated using the equations in Table 4.2.

Table 4.1: Experiments run with global P-model. Constant (c) runs used the variables fixed at its value in 1982 and variable (V) runs used time-varying data from 1982-2010.

Experiment	**Climate (T, VPD)**	**CO_2**	**fAPAR**	**Radiation**
All Var (all_v)	V	V	V	V
Clim Var (Cl_v)	V	c	c	c
CO_2 Var (Co_v)	c	V	c	c
fAPAR Var (F_v)	c	c	V	c
Rad Var (R_v)	c	c	c	V
Clim CO_2 Var ($ClCo_v$)	V	V	c	c
Clim fAPAR Var (ClF_v)	V	c	V	c
Clim Rad Var (ClR_v)	V	c	c	V
CO_2 fAPAR Var (CoF_v)	c	V	V	c
CO_2 Rad Var (CoR_v)	c	V	c	V
fAPAR Rad Var (FR_v)	c	c	V	V
Clim Const (Cl_c)	c	V	V	V
CO_2 Const (Co_c)	V	c	V	V
fAPAR Const (F_c)	V	V	c	V
Rad Const (r_c)	V	V	V	c
All Const (all_c)	c	c	c	c

Table 4.2: Factor separation using experiments listed in Table 4.1 and following the method of Stein and Alpert (1993)

Name	Factor	Equation
All_const	All variables constant (control)	All const
Clim_var	Climate	Cl_v - all_c
CO_2_var	CO_2	Co_v - all_c
fapar_var	fAPAR	F_v - all_c
Rad_var	Radiation	R_v - all_c
Clim_CO_2_nonLin	Non-linear interaction of Climate and CO_2	$ClCo_v$ - (Cl_v + Co_v) + all_c
Clim_fAPAR_nonLin	Non-linear interaction of Climate and fAPAR	ClF_v - (Cl_v + F_v) + all_c
Clim_Rad_nonLin	Non-linear interaction of Climate and radiation	ClR_v - (Cl_v + R_v) + all_c
CO_2_fAPAR_nonLin	Non-linear interaction of CO_2 and fAPAR	CoF_v - (Co_v + F_v) + all_c
CO_2_Rad_nonLin	Non-linear interaction of CO_2 and radiation	CoR_v - (Co_v + R_v) + all_c
faAPR_Rad_nonLin	Non-linear interaction of fAPAR and radiation	FR_v - (F_v + R_v) + all_c
Clim_CO_2_fAPAR_nonLin	Non-linear interaction of Climate, CO_2 and fAPAR	R_c - ($ClCo_v$ + ClF_v + CoF_v) + (Cl_v + Co_v + F_v) - all_c
Clim_fAPAR_Rad_nonLin	Non-linear interaction of Climate, fAPAR and radiaiton	Co_c - (ClF_v + ClR_v + FR_v) + (Cl_v + F_v + R_v) - all_c
Clim_CO_2_Rad_nonLin	Non-linear interaction of Climate, CO_2 and radiation	F_c - ($ClCo_v$ + ClR_v + CoR_v) + (Cl_v + Co_v + R_v) - all_c
CO_2_Rad_fAPAR_nonLin	Non-linear interaction of CO_2, fAPAR and radiation	Cl_c - (CoF_v + CoR_v + FR_v) + (Co_v + F_v + R_v) - all_c
Clim_CO_2_Rad_fAPAR_nonLin	Non-linear interaction of Climate, CO_2, fAPAR and radiation	all_v - (R_c + F_c + Co_c + Cl_c) + (ClC_v + ClF_v + ClR_v + CoF_v + CoR_v + FR_v) - (Cl_v + Co_v + F_v + R_v) + all_c

4.2.2 Ecosystem Light-use efficiency

Ecosystem light-use efficiency (eLUE, gC MJ $^{-1}$) is calculated for the growing season per pixel as:

$$eLUE = \frac{\Sigma GPP}{\overline{APAR}}, \tag{4.5}$$

where ΣGPP is the annual growing season sum of GPP (gC m $^{-2}$ yr^{-1}), and $\overline{APAR}$ is the annual growing season mean for PAR x fAPAR (MJ m $^{-2}$ yr^{-1}). The growing season is defined per pixel as months where GPP is more than zero.

4.2.3 Analysis

The first part of the analysis will examine how realistic the P-model output is at global scales when compared to other more complex models and observations. For this stage, GPP and eLUE from the P-model is compared to the models from the MsTMIP project (Huntzinger et al., 2013) and the observation based estimate of GPP, GPP-FC (Jung et al., 2017). Only the 'All var' simulation is compared to these other estimates. The second stage is to understand the drivers of change in the P-model, and quantify the change in GPP and eLUE from each factor. This stage compares the factorial experiments of the P-model. Since I concluded in chapter 2 that changes in modelled ASC were underestimated by the MsTMIP models because they underestimated NPP and eLUE changes, a larger change in P-model GPP and/or eLUE is desired. Both analyses are for northern hemisphere land 30-90°N between 1982-2010.

The mean amplitude and mean annual GPP is analysed, where GPP amplitude is calculated for each pixel as the annual maximum monthly GPP minus the minimum (usually zero) GPP and mean annual GPP is the total GPP for each year. Mean growing season eLUE is calculated following equation 4.5. The trend in mean annual GPP, GPP amplitude and eLUE are also calculated for the P-model and MsTMIP models, but not for the observation based estimate since the GPP trend is not a robust feature of this product (Beer et al., 2010). Since the growing season is defined per pixel as months where GPP>0, the growing season length will be different for all models. Mean annual GPP trends in the factorial P-model experiments add

up to the 'All var' experiment, but this is not the case for GPP amplitude since the minimum and maximum month may be different in a particular pixel for different simulations and years. Therefore the percentage contribution to the overall trend in GPP for each P-model simulation is only shown for annual GPP.

4.2.4 MsTMIP models and GPP-FC

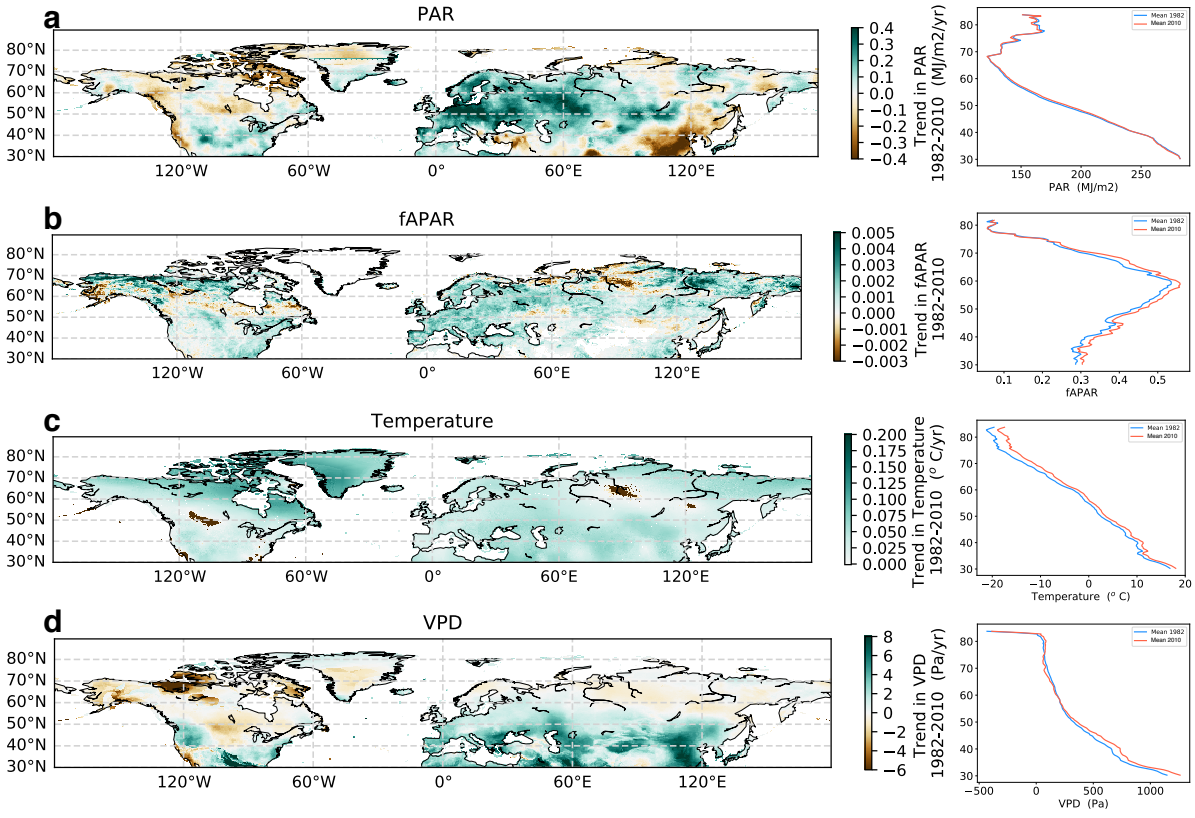
MsTMIP models

GPP and LAI from the 'all-on' simulation (i.e. all variables time-varying including nitrogen deposition for models with coupled carbon-nitrogen cycles) of the MsTMIP models was downloaded for 1982-2010 (Huntzinger et al., 2013) (Chapter 2). The output comes at a monthly timestep and 0.5^o x 0.5^o resolution, and six of the 13 models have a coupled carbon-nitrogen cycle (BIOME-BGC, CLM4, CLM4VIC, DLEM, ISAM and TEM6). LAI was transformed to fAPAR following Beer's law (as in Chapter 2) and eLUE was calculated following the method in section 4.2.2. The eLUE for MsTMIP models calculated in this chapter is slightly different to that in Chapter 2, as here I use GPP and CRU-NCEP shortwave radiation rather than NPP and WFDEI shortwave radiation, and consider only changes between 1982-2010 rather than between 1958-61 and 2009-10. I use CRU-NCEP shortwave radiation so that no additional uncertainty is introduced into the eLUE estimate from differences in PAR as this was the input used to drive the MsTMIP models.

GPP-FluxCom

The observation based estimate of GPP came from the FluxCom product (GPP-FC). Only the GPP generated using the Reichstein flux-partitioning method was used as Chapter 3 showed little difference between methods (Jung et al., 2017). In this product, relationships between GPP at Fluxnet sites and climate are established using three different machine learning techniques and these relationships are then used with global gridded climate data to provide an estimate of global GPP (Jung et al., 2017). The output from all three machine learning methods was averaged to give the estimated GPP. This GPP was also combined with the fAPAR3g dataset

Figure 4.1: Trend in environmental drivers of the P-model between 1982-2010. Left-hand panels show the mean annual trend for PAR (a), fAPAR (b), temperature (c) and VPD (d) across the region 30-90 ^{o}N and right-hand panels show the 1982 mean (blue) and 2010 mean (red line) in drivers averaged by latitude.



and WFDEI shortwave radiation derived PAR to give an observation based estimate of mean annual eLUE.

4.3 Results

4.3.1 Environmental change

Figure 4.1 shows the spatial distribution of the annual trend and change in four of the five driving datasets of the P-model: PAR, fAPAR, temperature and VPD, between 1982-2010. There has been an overall increase in VPD, temperature and fAPAR, but little change in PAR when averaged across all latitudes. Although the average trend in temperature shows an increase across all latitudes, there are a couple of regions where temperature trends show a slight

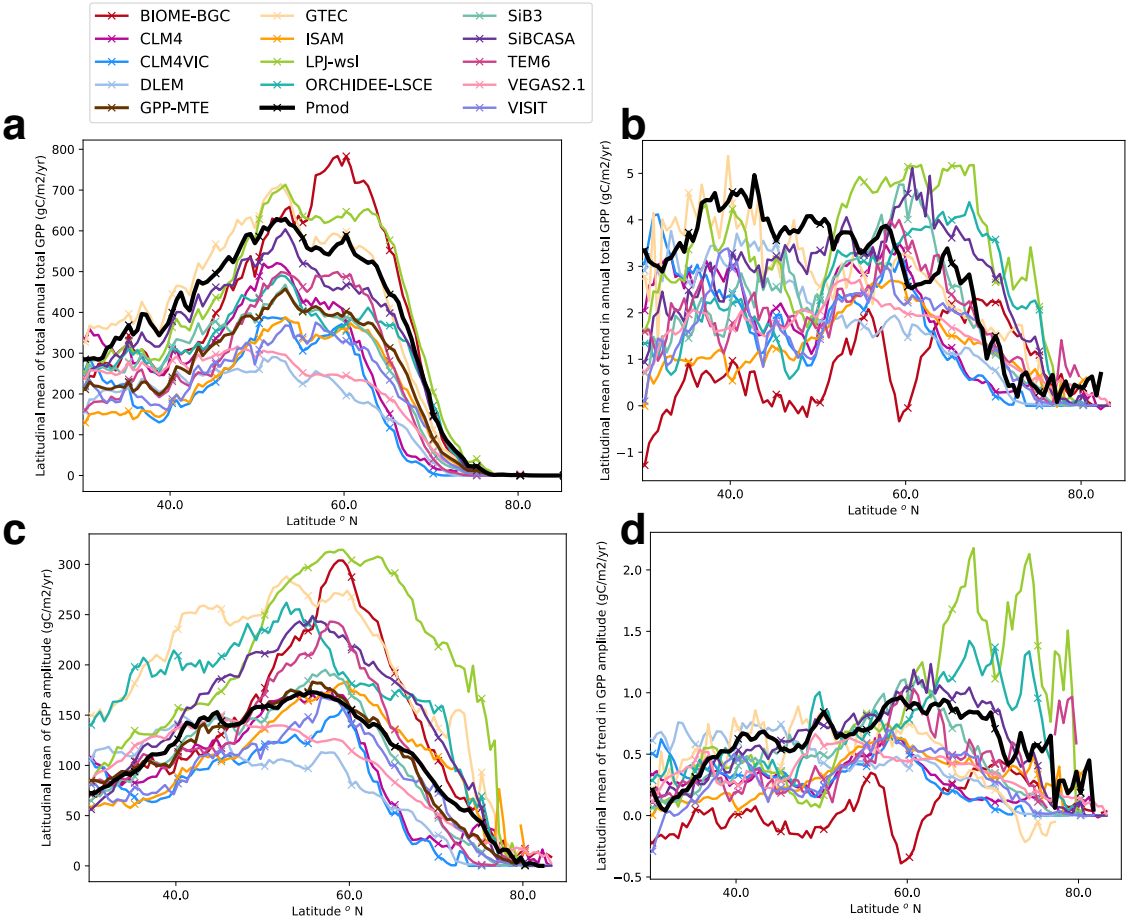
reduction due to the particular years used for this analysis (the brown areas in Figure 4.1c). The highest northern latitudes (60-80°N) have experienced the largest increases temperature and a decrease in VPD. Further south, between 30-50°N, both temperature and VPD have increased with very large increases in VPD in temperate regions. This latitudinal difference in VPD response to increased temperature may result from differences in available water. Temperatures have increased in the already dry southern regions which would increase VPD, while in northern regions, increasing temperatures may have increased the melting of snow and ice, reducing VPD here. The increase in fAPAR between 30-75°N is fairly uniform across latitudes, with peaks around 40°N, 55°N and 65°N, which could be due to increases in cropland in Europe (40°N) (Gray et al., 2014), and temperature driven increases in greenness (55°N and 65°N) (Zhu et al., 2016). The reductions in fAPAR that are shown at very high latitudes (75-90°N) may be due to poor quality satellite data (Jiang et al., 2017) as these areas are often cloudy, covered with snow or without daylight. The trend in PAR has more regional variability, with large increases around Europe and decreases around China due to decreases and increased emissions of aerosols, respectively (Wild, 2016). Not shown in Figure 4.1 is the increase in CO_2 as it has been almost linear between 1982-2010, increasing by 48.8ppm from 341.1 to 389.9 ppm, and the P-model is driven by this increase uniformly across latitudes.

4.3.2 GPP: P-model vs. other estimates

Mean annual GPP and GPP amplitude

The latitudinal shape of mean annual GPP and GPP amplitude in the P-model is similar to the MsTMIP models and GPP-FC (Figure 4.2a, c), although there is a large variation between estimates. The P-model has one of the highest estimates of annual GPP across all latitudes (Figure 4.2a) with an annual mean GPP between 1982-2010 for 30-90°N of 51.6PgCyr^{-1}. This is the third highest when compared to MsTMIP models (Table 4.3), and much higher than the observation based estimate from GPP-FC which has an annual mean GPP of 34.5PgCyr^{-1}. The higher estimates of GPP estimated by the P-model may not be unrealistic as a recent study using SIF data to optimise the ORCHIDEE model gave an estimate for annual mean GPP of 67.1PgCyr^{-1} over Boreal and temperate regions between 2007-11 (Macbean et al., 2018).

Figure 4.2: Annual GPP and GPP amplitude mean (a, c) and trend (b, d) over 1982-2010 for the P-model (black line), MsTMIP models (coloured lines) and GPP-FC (brown line - only for means).



The latitudinal mean GPP amplitude for the P-model is in the middle of the MsTMIP estimates, and has a very similar distribution to GPP-FC, with both estimates having an average GPP amplitude of 7.9PgCyr^{-1} (Figure 4.2c, Table 4.3). There is a large variation in the magnitude of mean GPP and GPP amplitude, particularly in boreal regions where estimates range from ∼200gC m^{-2}yr^{-1} to ∼600gC m^{-2}yr^{-1} for mean GPP and ∼75gC m^{-2}yr^{-1} to ∼300gC m^{-2}yr^{-1} for GPP amplitude. Previous studies have also found large differences in this region owing to structural differences between models (Chen et al., 2017). Similar to the other models and GPP-FC, mean GPP and GPP amplitude in the P-model increases from 30°N to a peak around 50-60°N, and then quickly drops off to zero around 80°N. The peaks in mean GPP and GPP amplitude occur in regions which are highly vegetated, have sufficient moisture and warmth, and have a strong dependency on the annual cycle of PAR and temperature ((Anav et al., 2015), Figure 4.1). The P-model is able to capture this latitudinal variability due to the underlying fAPAR data, but without the additional need for PFTs that are used by the other models.

Trends in mean annual GPP and GPP amplitude

The P-model has the second largest trend in mean annual GPP, with an increase of 0.21PgCyr^{-2} (12.9%), and the joint largest absolute increase in GPP amplitude at 0.038 PgCyr^{-2} (20.5%) (Table 4.3). This is a good result, as a larger GPP change may lead to a larger modelled change in ASC. Along with many of the MsTMIP models, the highest trends in annual mean GPP in the P-model are at lower latitudes between 30-50°N, with a sharp decline in trends north of 65°N, while some other models (LPJ-wsl, ORCHIDEE-LSCE, SiBCASA, TEM6 and SiB3) have a second peak at higher latitudes around 60-70°N (Figure 4.2b). The P-model has higher trends in GPP across temperate latitudes compared to most MsTMIP models, because this is where the models had poorer skill in representing greening trends (Figure 2.4). The trend in P-model amplitude is largest across 50-70°N, which is not the case for many MsTMIP models which have higher trends between 30-50°N or north of 60°N (Figure 4.3d). In Chapter 3, we saw that the P-model underestimated GPP amplitude for croplands and deciduous broadleaf forest, where GPP amplitude was largest. Therefore, even though the P-model already has

Table 4.3: Mean annual GPP and GPP amplitude, and their trends averaged over 30-90°N for 1982-2010 for the P-model MsTMIP models and GPP-FC in PgC yr^{-2} and % change from 1982.

Model	**GPP mean**	**GPP mean trend**		**GPP amplitude**	**GPP amplitude trend**	
	PgC yr^{-1}	PgC yr^{-2}	%	PgC yr^{-1}	PgC y^{-2}	%
Pmod	51.6	0.21	12.9	7.9	0.038	20.5
GPP-FluxCom	34.5	-	-	7.9	-	-
MsTMIP models						
BIOME-BGC	50.2	0.04	7.3	9.6	0.00067	3.7
CLM4	37.2	0.13	15.7	6.5	0.019	12.5
CLM4VIC	26.8	0.11	14.9	4.9	0.017	12.6
DLEM	24.6	0.12	21.0	5.4	0.027	19.2
GTEC	54.9	0.17	8.0	12.6	0.031	13.0
ISAM	27.6	0.08	10.6	6.6	0.018	7.9
LPJ-wsl	52.3	0.22	13.2	12.9	0.038	8.8
ORCHIDEE-LSCE	39.0	0.14	18.2	10.9	0.037	17.1
SiB3	36.8	0.15	20.1	7.7	0.033	17.5
SiBCASA	46.2	0.19	17.5	10.4	0.04	14.6
TEM6	34.7	0.13	14.7	8.3	0.024	9.3
VEGAS2.1	29.2	0.11	18.6	7.2	0.026	14.6
VISIT	28.7	0.11	12.5	6.2	0.019	8.4

large trends in GPP amplitude, trends in regions where these are the dominant plant type (40-60°N, Figure 3.2) may also be underestimated.

Contrasting spatial patterns are seen between the P-model and LPJ-wsl which is the model with the largest mean annual GPP trend and amplitude trend (Figure 4.2, 4.3). The key difference in LPJ-wsl is at high latitudes between 60°-80°N, where LPJ-wsl shows larger increases in mean GPP and GPP amplitude than the P-model. However, LPJ-wsl has been shown to over-predict the coverage of deciduous and needleleaf vegetation across Eurasian and Canadian boreal forests found in these regions, (Sitch et al., 2003) suggesting that smaller trends in these predominately shrubland regions may be more realistic.

There is a strong positive relationship between GPP amplitude trend and mean annual GPP for the P-model and MsTMIP models (Figure 4.4). This suggests that much of the increase in total GPP is driven by an increase in summer uptake, rather than an increase in shoulder

Figure 4.3: Change in GPP amplitude 1982-2010 (%) for the P-model and MsTMIP models.

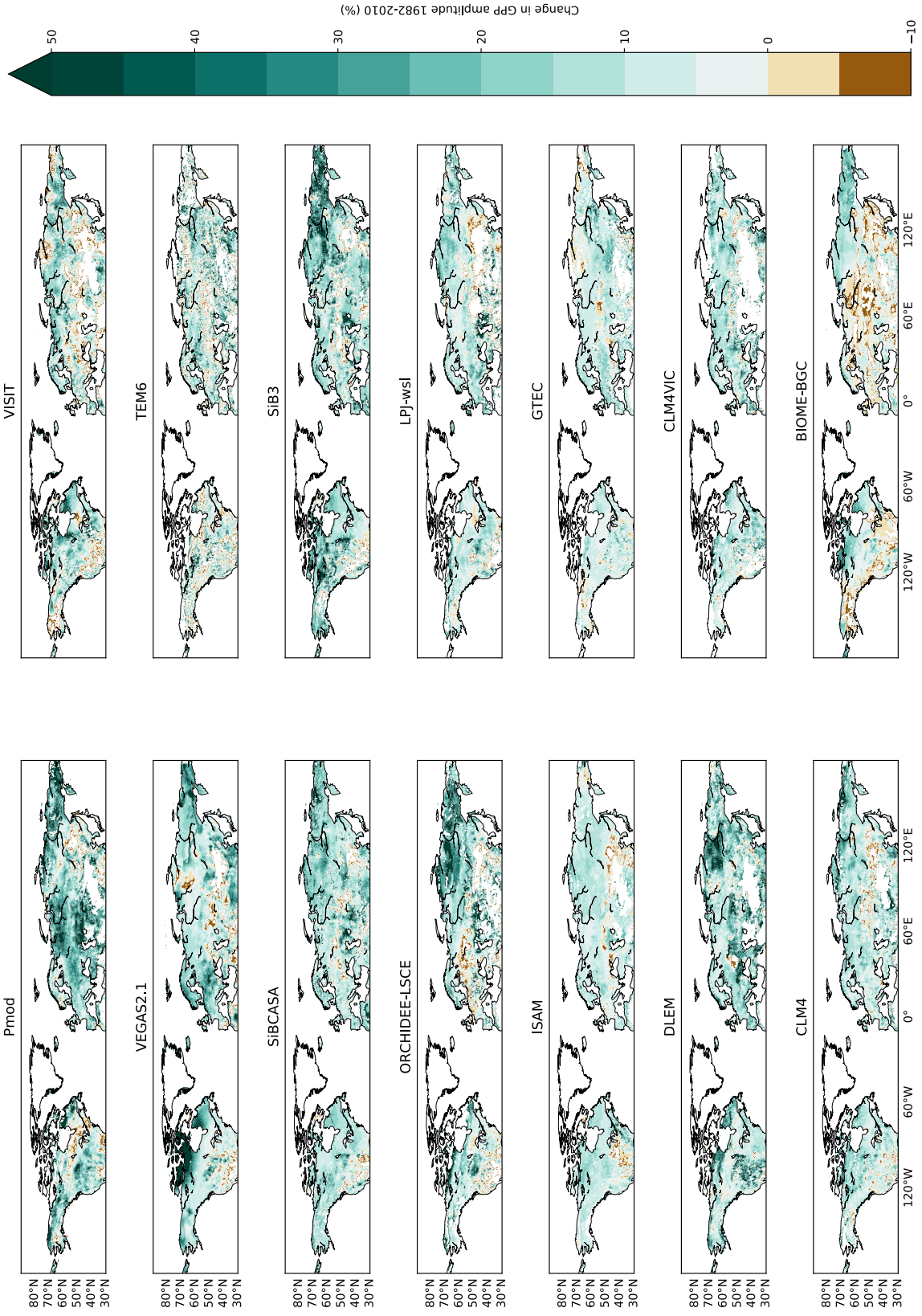
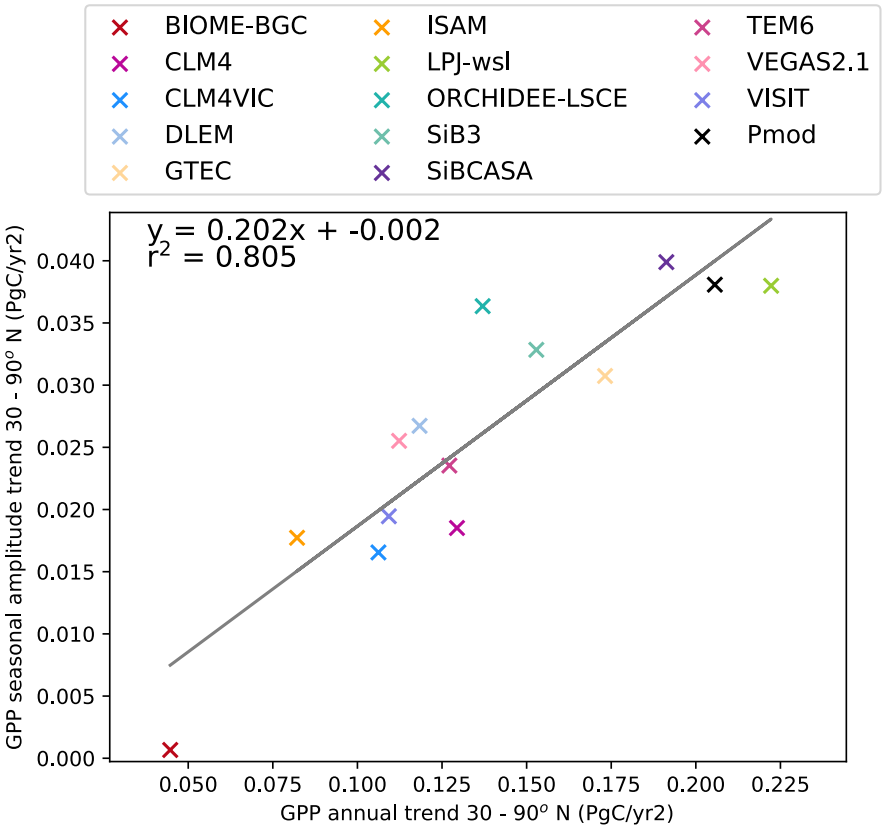


Figure 4.4: Trend in GPP amplitude vs trend in mean annual GPP for the P-model and MsTMIP models.



season GPP (Figure 4.4). I now further analyse the P-model to consider the role of different drivers on the overall change in mean GPP and GPP amplitude.

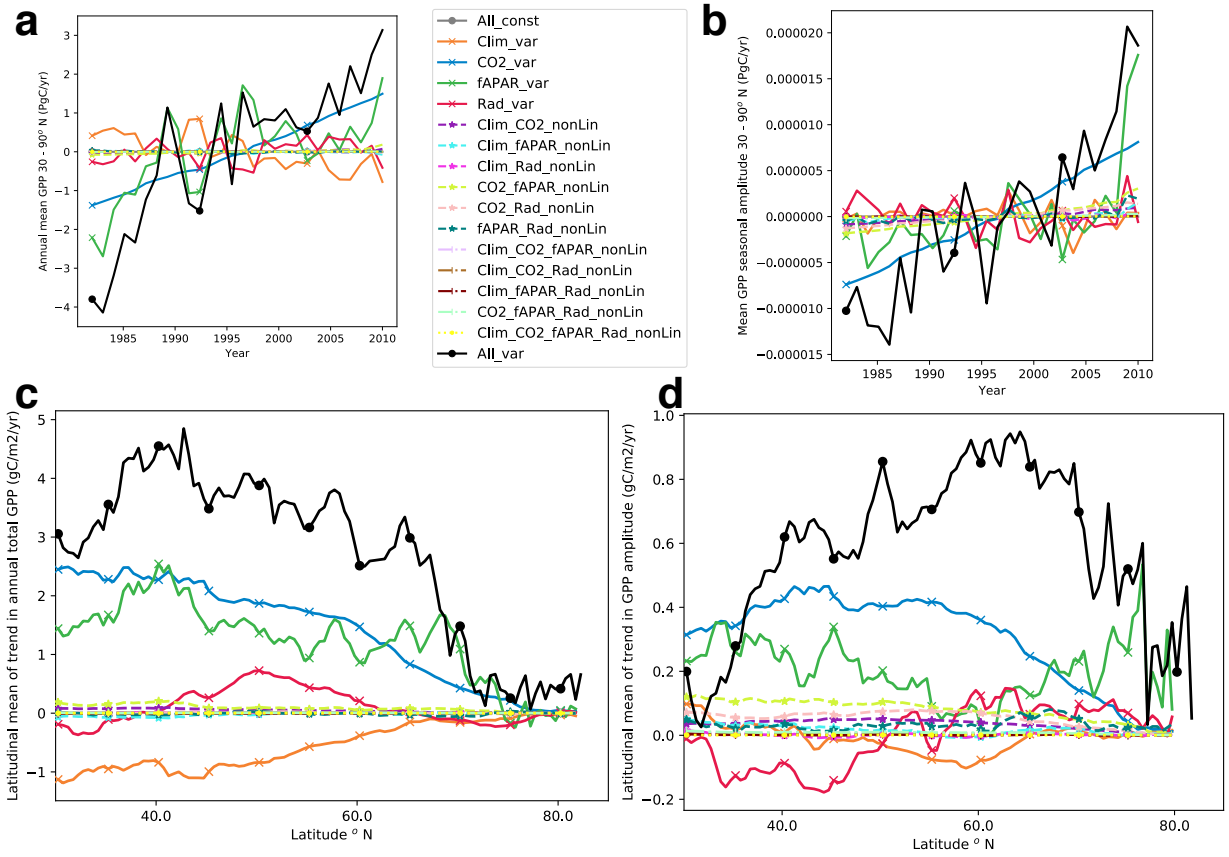
4.3.3 Drivers of GPP trends in the P-model

CO_2

The main driver of the GPP trend in the P-model is CO_2, accounting for 52% of the increase in mean annual GPP and a trend of 0.022 PgC yr^{-1} in GPP amplitude (Table 4.4). The CO_2-driven GPP trends have little regional variability due to the uniform increase in CO_2 across all latitudes, but the trend decreases with latitude as the amount of vegetation decreases (Figure 4.5). There is also little inter-annual variability in CO_2-driven GPP trends since the increase in atmospheric CO_2 has been almost linear over 1982-2010.

The increase in GPP from CO_2 alone is 0.057PgC $yr^{-1}ppm^{-1}$ or 0.12%ppm^{-1} (GPP increase

Figure 4.5: Time-series and trend in mean annual GPP and GPP amplitude for all the factorial experiments from the P-model. Experiment names in the legend refer to experiments calculated as in Table 4.2. Anomalies are shown for the time-series plots (a, b), calculated by subtracting the mean for each experiment. The trends are plotted by 0.5^o latitude band (c and d).



of 2.8PgC for the CO_2 increase of 48.8ppm), which is very close to the increase in NPP observed at four FACE (Free-Air CO_2 Enrichment) sites of 0.13%ppm^{-1} (Norby et al., 2005). The similarity between the modelled and observed increase should probably not be given too much weight however, as the measured change is for NPP rather than GPP, and recent studies indicate that these site-scale FACE experiments in temperate regions may not be representative of large-scale behaviours in other ecosystems (Hilker et al., 2008). Nevertheless, the consistency between the increase in productivity from the P-model and FACE observations is somewhat surprising given that the modelled increase in GPP only includes the direct effects of CO_2 on GPP and not any indirect effects on GPP changes from changes in vegetation driven by CO_2 fertilisation. However modelling studies suggest that this indirect effect of CO_2 fertilisation is small at high northern latitudes in comparison to the other drivers of greening (Zhu et al., 2016).

CO_2-driven annual mean GPP trends generally coincide with regions of increases in CO_2-driven GPP amplitude (Figure 4.5c, d), indicating that much of the increase in GPP comes from increases in peak summer GPP. These increases in GPP are likely driven by increases in water-use efficiency due to CO_2 fertilisation, as high summer temperatures reduce available water (Schwalm et al., 2010). This is seen particularly around 40-45°N which contains large regions of cropland and would therefore have a more pronounced seasonal cycle (Figure 3.2, (Falge et al., 2002)). A different pattern is seen at lower latitudes, 30-40°N, where GPP amplitude increases are small but mean GPP increases are similar to those at higher latitudes. Thus in these temperate, drier regions, increases in water-use efficiency due to CO_2 fertilisation during the shoulder seasons could be driving GPP increases, but this may still be insufficient to outweigh moisture stress or other limitations in these ecosystems during summer months (Penuelas et al., 2011).

fAPAR

Changes in fAPAR are the second most important driver to trends in mean annual GPP contributing 44% and accounting for a trend of 0.011 PgC yr^{-2} in GPP amplitude. The fAPAR driven trends have more regional and temporal variation than for CO_2, and this drives much

Table 4.4: Trend in mean annual GPP and GPP amplitude for each experiment run by the P-model averaged over 30-90°N for 1982-2010, and the % of contribution to mean GPP trend for each experiment.

Simulation	**Mean GPP trend** PgC yr^{-2}	**% contribution**	**Amplitude trend** PgC yr^{-2}
All_Var	0.21		0.038
Clim_var	-0.041	-20.50	-0.0009
CO_2_var	0.105	52.44	0.022
fAPAR_var	0.09	44.34	0.011
Rad_var	0.011	5.60	-0.001
Clim_CO_2_nonLin	0.003	1.64	0.003
Clim_fAPAR_nonLin	-0.002	-0.76	0.0001
Clim_Rad_nonLin	0.000	0.23	0.0001
CO_2_fAPAR_nonLin	0.006	3.22	0.006
CO_2_Rad_nonLin	0.000	0.16	0.004
fAPAR_Rad_nonLin	-0.001	-0.30	0.002
Clim_CO_2_Rad_nonLin	0.000	0.11	0.0004
Clim_fAPAR_Rad_nonLin	0.000	-0.12	0.0001
CO_2_fAPAR_Rad_nonLin	0.000	0.12	0.0005
Clim_CO_2_fAPAR_nonLin	0.000	0.01	0.000

of the inter-annual variability in total P-model GPP (Figure 4.5a). The largest increases in fAPAR driven mean GPP are around 40°N, where European forests have shown large greening trends (Figure 4.1b), while the largest changes in amplitude are at high latitudes around 70°N. Increases in GPP amplitude generally coincide with larger mean GPP trends particularly at the high latitudes where warming has lengthened the growing season and increased peak greenness (Buitenwerf et al., 2015). This agrees with previous studies showing that the lengthening growing season drives an increase in mean annual GPP (Piao et al., 2007), and that this is often accompanied by increases in GPP amplitude (Buitenwerf et al., 2015). However, this is not always the case and further south around 60°N, the large increase in mean annual GPP does not translate to an increase in GPP amplitude. This may be partly due to a cancelling out of greening and browning trends in fAPAR when averaged across the latitude (Figure 4.1b). Browning trends have been well documented in North America, and are thought to result from increased disturbances in the warmer and drier climate (Beck and Goetz, 2011; Verbyla, 2011). Since GPP is linearly related to fAPAR in the P-model, the mismatches between increases in fAPAR-driven trends in GPP amplitude and annual GPP may also result from competing effects of environmental drivers and stresses on fAPAR throughout the growing season such that overall, fAPAR driven annual GPP may increase despite a decrease in fAPAR-driven GPP

amplitude.

The P-model does not model its own vegetation, and so fAPAR-driven changes in GPP result from changes in vegetation from all the environmental drivers of CO_2, climate and PAR, as well as those that are not explicitly modelled such as nutrient availability and the effects of diffuse light. Studies using TRENDY models and MsTMIP models find that climate is the most important driver of fAPAR trends at high latitudes, and that CO_2 and other factors start to become more important south of 60°N (Zhu et al., 2016), (Chapter 2). This behaviour can be seen in the non-linear P-model simulations for CO_2 and fAPAR (lime green line), and CO_2, fAPAR and climate (pink line), which have a noticeable influence in GPP amplitude trends at these lower northern latitudes (Figure 4.5d). The importance of these non-linear interactions mirrors behaviour that has been observed at temperate grassland sites in the US (Reyes-Fox et al., 2014).

Climate

Climate contributes a negative trend to GPP, offsetting 20% of the increase in mean annual GPP, and with an overall negative trend in GPP amplitude of -0.0009 PgC yr^{-2}. The climate effect only contributes to decreasing mean GPP up to around 70°N, after which it has almost no effect on the trend in mean GPP (Figure 4.5c). The overall negative response of GPP to changes in climate are driven by the negative response of GPP to temperature, as well as the negative response to VPD (Chapter 3). The small trend at the highest latitudes might be due to the competing effects of VPD and temperature that were seen in Figure 4.1c and d, where VPD has decreased and increases in temperature have been particularly strong. These increases in temperature may be melting snow and ice, therefore reducing VPD. However, at lower latitudes, VPD has increased along with temperature which would increase water stress and thus both factors act to reduce GPP.

Comparing this P-model simulation to the TRENDY models, where only temperature was varied (rather than temperature and VPD together), we can see that the increase in VPD may

have played an important role in the reduction of GPP at temperate latitudes in the P-model (Piao et al., 2013). Only one of the TRENDY models showed a small decrease in mean annual GPP, while all other models showed increases in GPP, highlighting the potential role of water stress in these drier regions.In Boreal regions, GPP increased with temperature for all TRENDY models but this was largely driven by an increase in growing season length and vegetation greening (Piao et al., 2013). The role of a changing climate on NPP in CMIP5 models has the same latitudinal split, as Boreal regions tend to show increases in NPP with climate, while temperate regions have decreases or only a small increase (Peng et al., 2015). Similar results were found for the MsTMIP models, presented in Chapter 2, where NPP trends in the climate-only runs were generally positive and climate was also the main driver of greening trends in these models. Since the climatic effects on structural changes in vegetation are not included in this P-model simulation, the decreases in climate-driven GPP in the P-model suggests that vegetation may be becoming less efficient at taking up carbon at higher temperatures.

Negative trends in climate driven mean GPP are not generally matched by negative trends in GPP amplitude. Thus, the decrease in climate-driven mean annual GPP must be occurring at the beginning and end of the growing season. The main exception to this is around 50-70°N where both mean GPP and GPP amplitude have negative trends. These are also regions where trends in temperature are high but there has been little change in VPD (Figure 4.1), suggesting that peak summer GPP in these regions is being reduced due to heat stress.

PAR

The contribution to GPP trends from PAR are more regional and almost cancel out over the northern high latitudes. Overall, changes in PAR contribute only 5% to mean GPP and -0.001 Pg C yr^{-1} to GPP amplitude, but they play a significant role in mean annual GPP increase around 45-60°N (Figure 4.5c) and decreasing GPP amplitude in temperate regions (30-45°N) (Figure 4.5d). European 'brightening' has increased PAR levels in these regions (Figure 4.1a) which has led to a decrease in GPP amplitude as excess radiation is having a negative impact on GPP during the summer months, but the overall result is an increase in mean annual GPP

as GPP also increases during spring and autumn when light levels are not saturating. The opposite effect is seen at lower latitudes, 30-35°N, where decreases in PAR due to increased aerosol forcing is reducing mean annual GPP but having little effect on GPP amplitude.

Non-linear effects

Non-linear effects on GPP trends between two or more drivers can also be large, and this analysis highlights the importance of using fully-factorial experiments. The influence is largest for GPP amplitude, accounting for a third of the summed change from all factors. The trends are all positive and mostly from the non-linear interaction between CO_2 and the other drivers (Figure 4.5d). The largest effects are between CO_2 and fAPAR (lime-green line) and CO_2 and PAR (pink line) which are driven by the positive effects of CO_2 on GPP and the linear relationship between APAR (fAPAR x PAR) and GPP in the P-model (Equation 3.2). The increase in GPP amplitude from the non-linear interaction between CO_2 and climate will be driven by an increase in water-use efficiency that accompanies CO_2 fertilisation, alleviating moisture stress that might arise from increased temperature and VPD.

4.3.4 Ecosystem light-use efficiency: P-model vs. other estimates

In the P-model eLUE and eLUE trends are fairly uniform over the northern high latitudes while there is more regional variability in MsTMIP models, reflecting their dependence on PFTs (Figure 4.6). The differences in the latitudinal variation of mean eLUE between the MsTMIP models, GPP-FC and the P-model is responsible for much of the difference in mean GPP between these estimates. This is similar to previous findings when differences between modelled NPP were considered (Ruimy et al., 1999). The mean annual eLUE is 1.2 gC MJ^{-1}, lower than most MsTMIP model estimates which range from 0.29-3.46gC MJ^{-1}, but higher than the GPP-FC based estimate of 0.6 gC MJ^{-1}. The small GPP-FC based estimate is unsurprising since eLUE for the P-model and GPP-FC were calculated using the same data for APAR, but mean annual GPP was much higher in the P-model. The P-model eLUE is broadly consistent with values derived from Fluxnet sites, which ranged from 0.4 - 1.25 gC MJ^{-1} over the same region, but has different regional patterns. The highest eLUE values are found at high

Figure 4.6: Mean annual eLUE for the P-model, MsTMIP models and GPP-FC over 1982-2010.

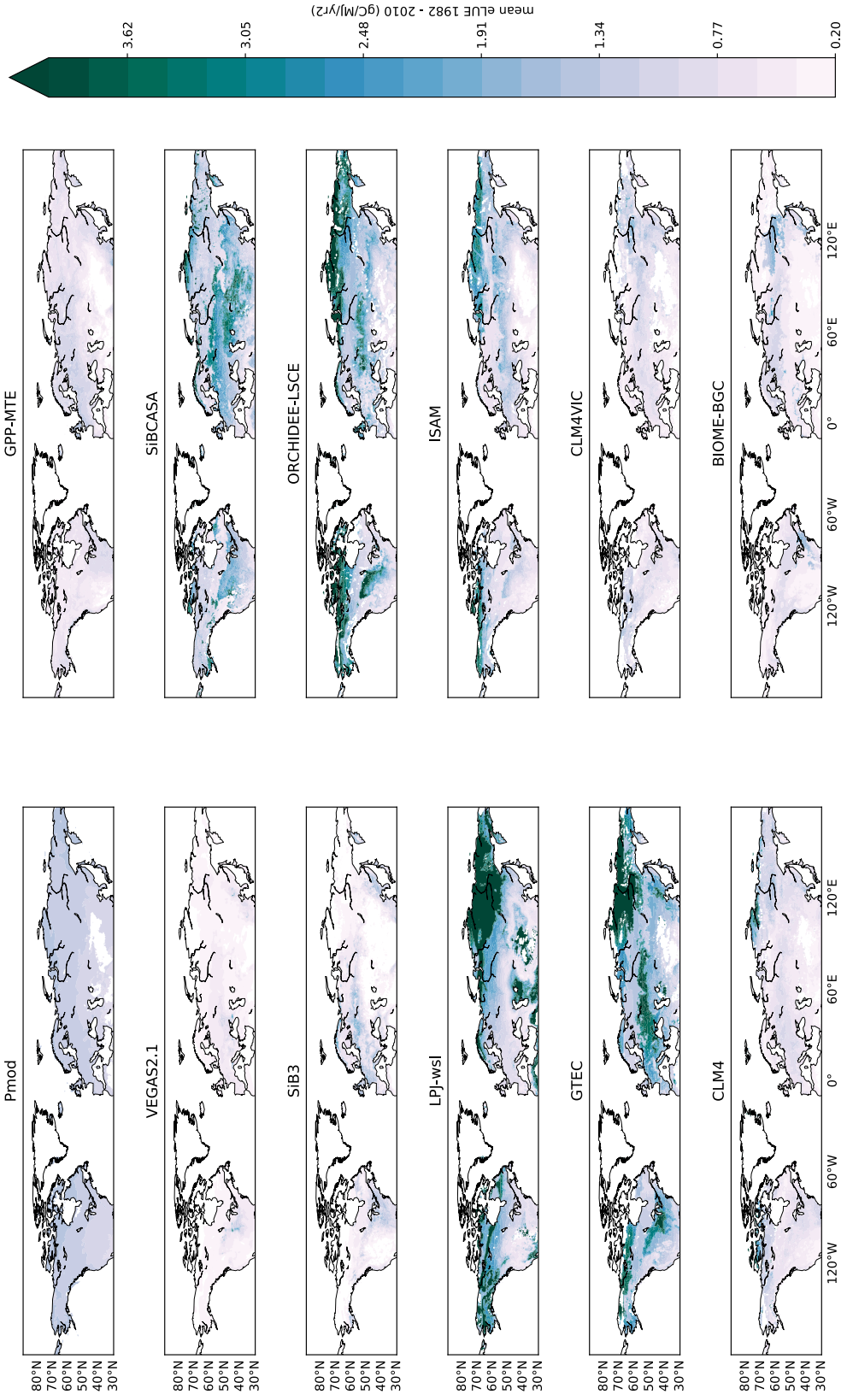


Table 4.5: Mean annual eLUE and change for the P-model, GPP-FC and MsTMIP models which provided LAI outputs.

Model	**Mean eLUE**	**eLUE trend**	
	gC $MJ^{-1}yr^{-1}$	gC $MJ^{-1}yr^{-2}$	% change
Pmod	1.23	1.54E-03	3.92
GPP-MTE	0.67	-	-
MsTMIP models			
BIOME-BGC	0.59	7.00E-04	5.44
CLM4	0.86	-1.65E-03	0.93
CLM4VIC	0.78	-3.16E-03	-0.81
GTEC	2.19	4.84E-04	4.03
ISAM	1.23	3.81E-03	9.83
LPJ-wsl	2.93	-2.70E-03	1.95
ORCHIDEE-LSCE	2.12	-2.76E-03	1.61
SiBCASA	1.69	-3.38E-03	1.53
VEGAS2.1	0.33	9.15E-04	10.99
VISIT	7.63	8.52E-03	2.53

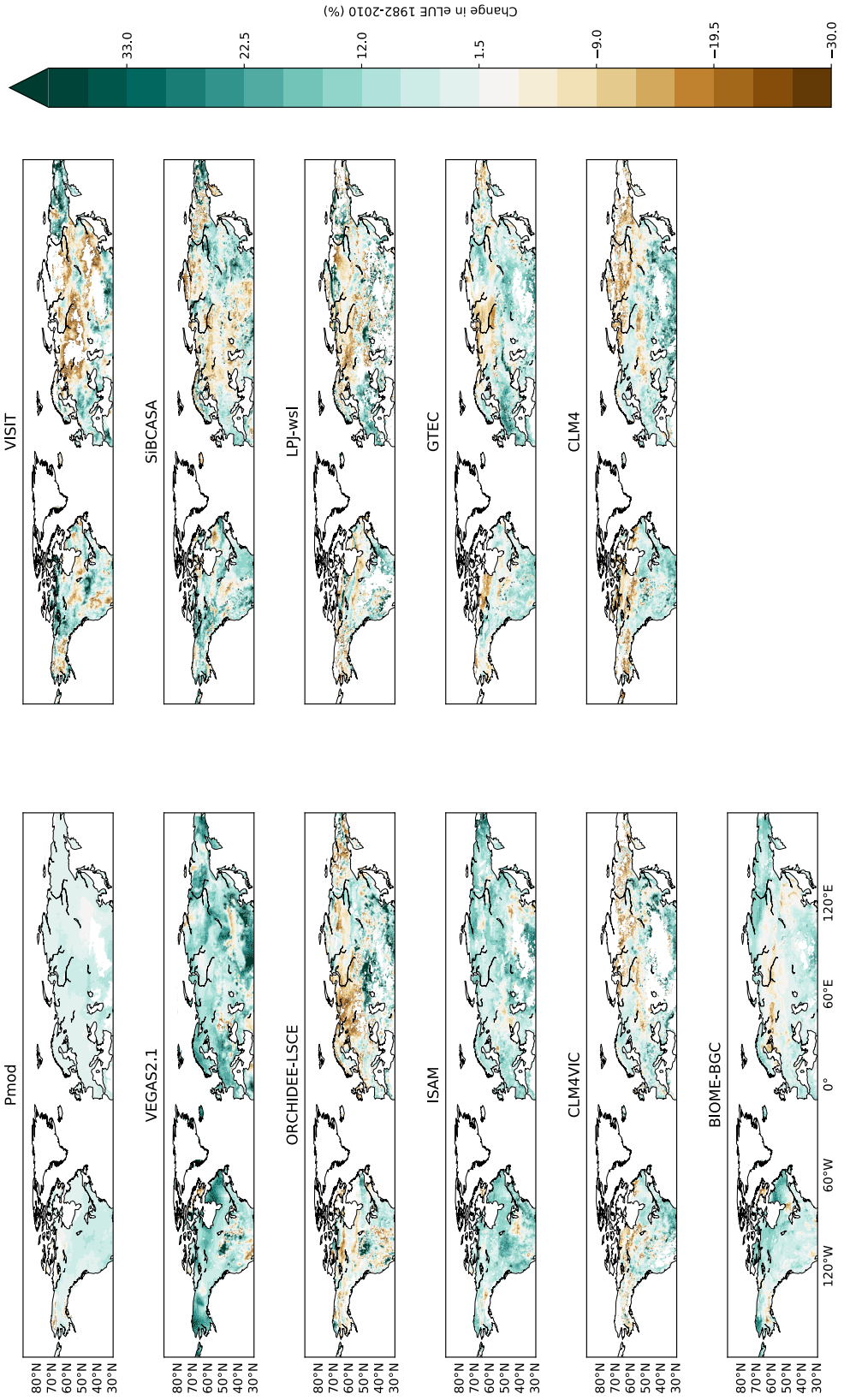
latitudes in the P-model, but this is where lower observed eLUE values were found (Garbulsky et al., 2010). However, the observation based estimates of eLUE were calculated using only a few sites for each biome and thus may not be representative of the whole ecosystem.

The trend in P-model eLUE is the third largest at 0.0015 gC MJ^{-1} yr^{-2}, compared to -0.0034 - 0.0085 gC MJ^{-1} yr^{-2} for the MsTMIP models (Table 4.5). The five models with negative trends in eLUE (SiBCASA, CLM4VIC, ORCHIDEE, LPJ-wsl and CLM4) show large regions of decreasing eLUE over boreal regions which are not compensated by the increasing eLUE trends elsewhere (Figure 4.7). When calculating eLUE from NPP (Chapter 2), negative trends in eLUE were only found for two of these models, CLM4 and CLM4VIC, indicating that the trend in eLUE may not be linear over time, and that eLUE calculated by different measures of productivity (NPP or GPP) are not directly comparable.

4.3.5 Drivers of eLUE trends in the P-model

In the P-model, the trend in eLUE is driven by CO_2 and modulated by climate, which also drives the inter-annual and spatial variability (Figure 4.8). Climate only simulations also decreased NPP-derived eLUE in the MsTMIP models (Chapter 2), but CO_2 did not always increase eLUE enough to outweigh this as is the case for the P-model. The competing effects of climate and

Figure 4.7: Trends in eLUE 1982-2010 for the P-model and all MsTMIP models which provided LAI outputs.



CO_2 in the P-model are particularly strong, and without the negative influence of climate, eLUE trends would be 50% larger. The non-linear interaction between CO_2 and climate drives a small but persistent increase in eLUE across all latitudes. As with GPP, the contribution to eLUE trends from CO_2 decreases with latitude, but this is not the case for climate, which has larger regional variations and defines the overall pattern of eLUE trends (Figure 4.8b). The trend in eLUE is positive across all latitudes except around 75°N, where climate driven eLUE reductions are larger than the positive effects from CO_2. The region of decline, in Northern Alaska, has experienced reductions in GPP due to a warmer and drier climate (Beck and Goetz, 2011; Verbyla, 2011). While this effect is primarily exhibited in structural changes as browning trends (Figures 4.1, 4.5), the negative trends in eLUE indicate that the changing climate has also reduced GPP through physiological changes.

4.3.6 Contribution to GPP trends from eLUE and APAR

To further investigate the role that structural and physiological changes in vegetation have on GPP trends, the contribution to the trend in mean annual GPP from APAR and eLUE was estimated. The APAR contribution was calculated by holding eLUE constant at its value in 1982, and allowing APAR to vary over time. The difference between the total GPP trend and this trend from varying APAR was then taken as the contribution from eLUE, noting that this will also include the contribution from non-linear interactions between eLUE and APAR. For the P-model, this is the same as calculating the contribution to GPP trends from the simulations where only CO_2 and climate were varying (CO_2_only, Clim_only and Clim_CO_2_nonlin, Table 4.2), but calculating the contribution to GPP trends from eLUE in this way allows the P-model to be compared to the MsTMIP models.

Figure 4.9 shows that except for models where eLUE contributed negatively to the trend in mean annual GPP, models with a larger contribution to GPP trends from APAR tended to have a larger increase in mean annual GPP. For the P-model, 66% of of the trend in GPP came from APAR, which is in the middle of the MsTMIP estimates that range from -5% to 137%. This equates to an 8.5% increase in GPP from APAR and a 4.4% increase in GPP from eLUE,

Figure 4.8: Time-series and trend in mean eLUE for factorial experiments from the P-model that considered changes in eLUE only. Experiment names in the legend refer to experiments calculated as in Table 4.2. Anomalies are shown for the time-series (a), calculated by subtracting the mean for each experiment. The trends are plotted by 0.5^o latitude band (b).

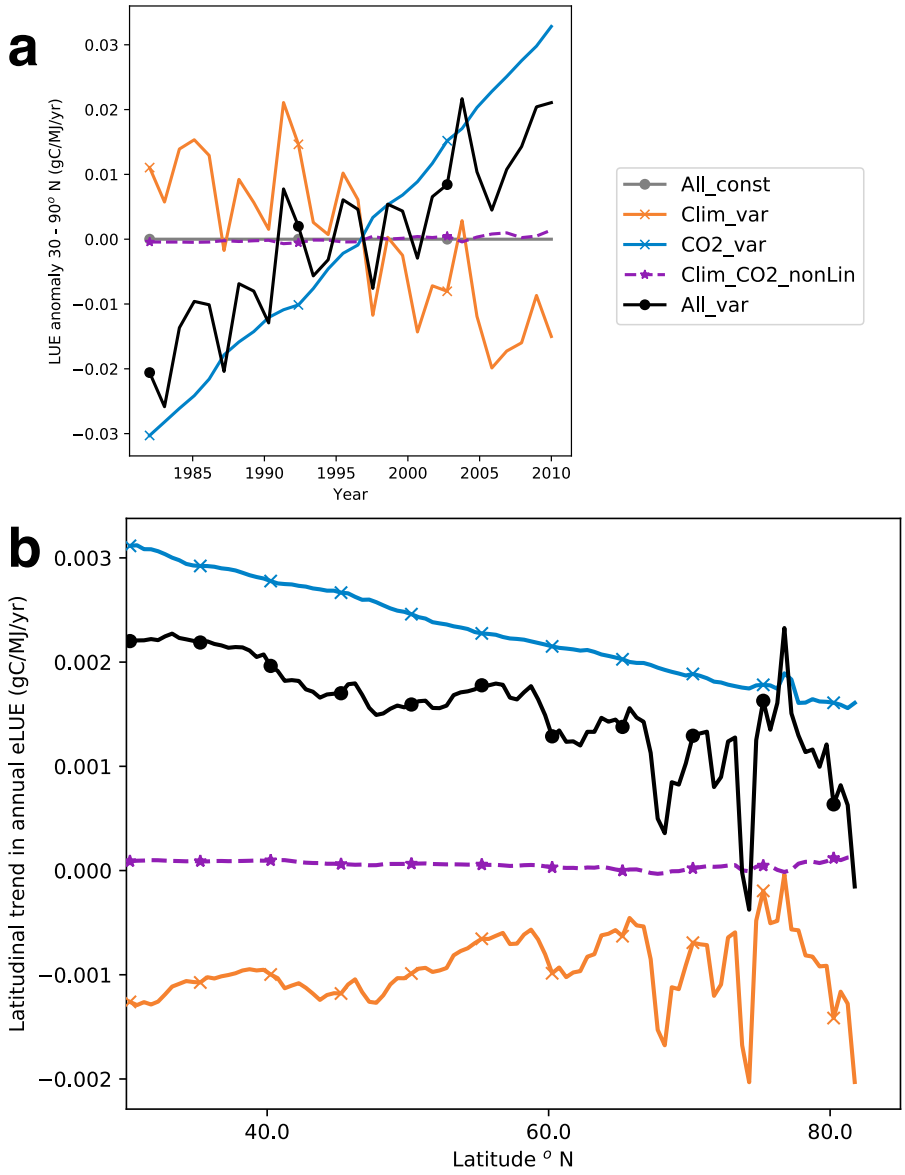
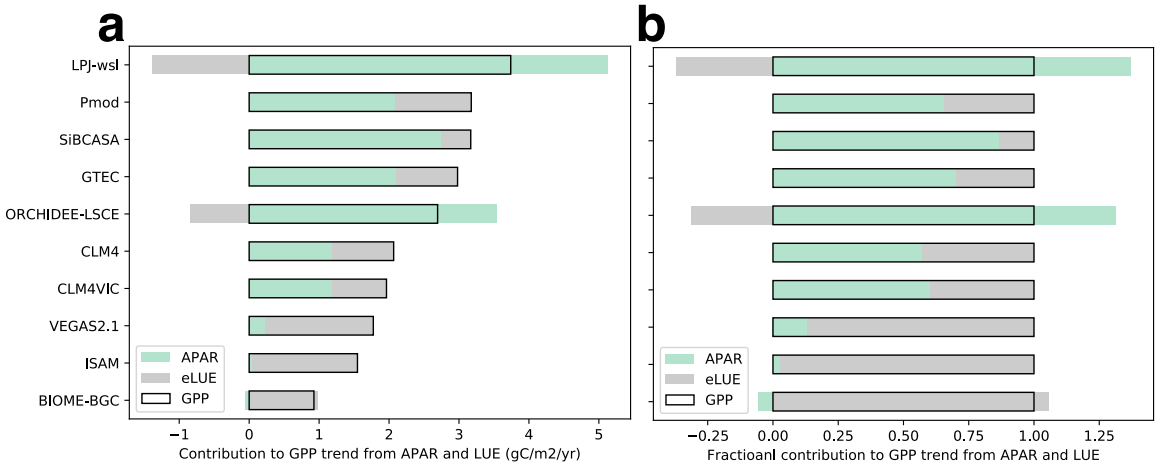


Figure 4.9: Bar plots of the contribution to GPP trends from changes in APAR (green) and eLUE + non-linear effects (grey) for the P-model and all MsTMIP models shown in Figure 4.7. The black outline shows the total GPP trend for each model and both the absolute (a) and relative (b) contributions to GPP trends are shown. Bars are ordered by GPP trends. VISIT is not included as it had unusual eLUE (Table 4.5.



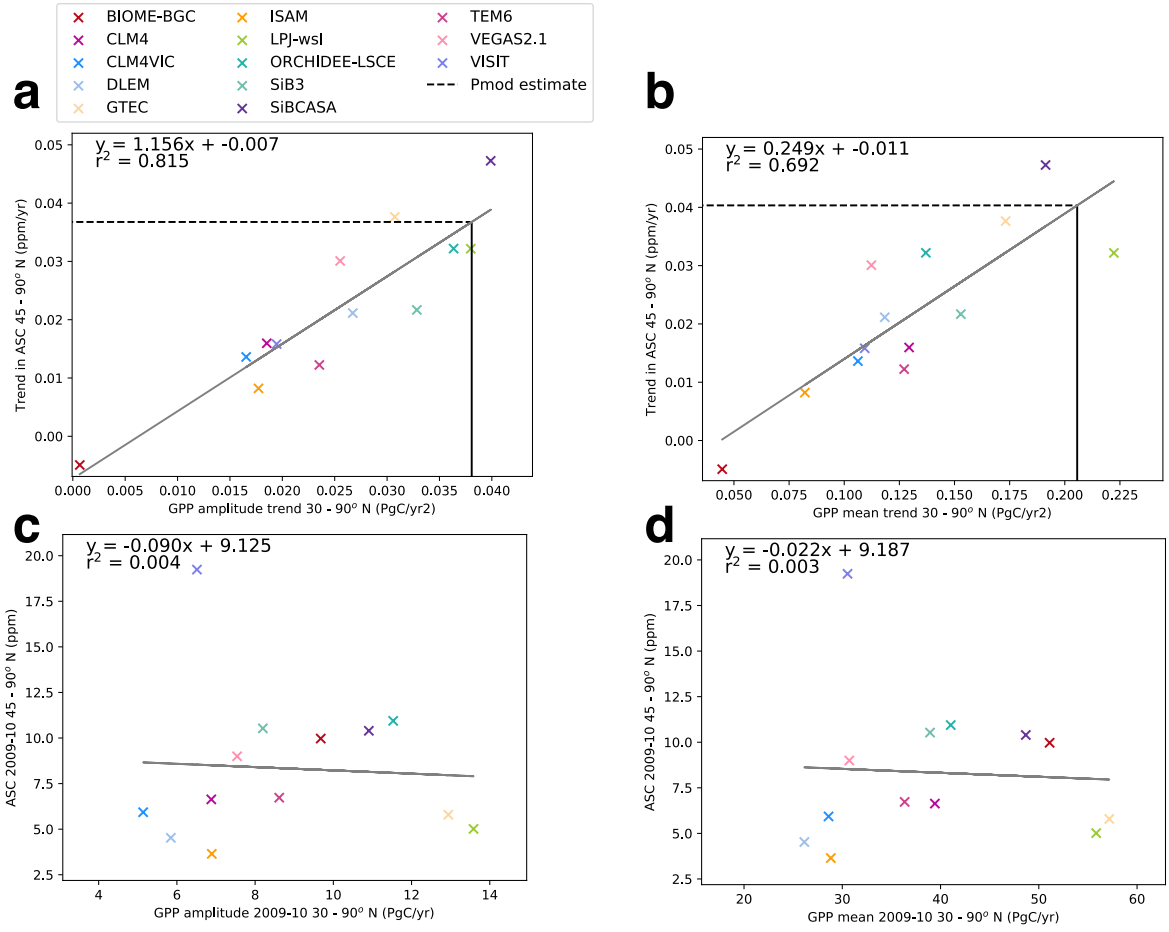
summing to the 12.9% increase in GPP (Table 4.3). Thus most of the increase in GPP in the P-model came from structural rather than physiological changes in vegetation. On average, GTEC has a similar GPP trend and fractional contribution from APAR and eLUE despite having different spatial distributions of eLUE trends. This is because the overall eLUE trend in GTEC, along with the other MsTMIP models, is a balance of positive and negative trends, while there is a smaller but more uniform increase in eLUE for the P-model (Figure 4.7). Models with larger contributions from eLUE include three models with a coupled carbon-nitrogen cycle, CLM4, CLM4VIC and ISAM (although ISAM is predominately driven by CO_2 and nitrogen plays a very small role (Chapter 2)), indicating that including a coupled nitrogen cycle in the P-model could alter the balance of structural and physiological vegetation changes. The dynamic vegetation model VEGAS2.1 also only attributes a small fraction of GPP trends to APAR, but since a large portion of trends in productivity are driven by land-use change (Zeng et al., 2014) (Chapter 2), I would expect most of the eLUE fraction to come from non-linearities through changes in vegetation distribution. BIOME-BGC has unreliable behaviour (Chapter 2) and is thus not considered. Two models, LPJ-wsl and ORCHIDEE-LSCE have a negative contribution to trends in GPP from eLUE and therefore the GPP trends in these models are being driven by the wrong mechanisms.

4.3.7 Seasonal amplitude of CO_2

It was not possible to estimate ASC changes using the P-model as none of the simple models for respiration were sufficiently robust (Chapter 3) to provide an estimate of NEE that could be transported and compared to atmospheric CO_2 concentrations. However, since changes in ASC are primarily driven by increases in carbon uptake (Graven et al., 2013; Randerson et al., 1997; Forkel et al., 2015) (Chapter 2), if I assume that trends in ASC are linear over the last 50 years, I can use the relationship between modelled GPP amplitude trends and ASC to estimate the change in ASC in the P-model. The annual trend in ASC was calculated for the MsTMIP models between 1958-61 and 2009-10 and the trend in mean annual GPP and GPP amplitude was calculated between 1982-2010. P-model GPP does not have strikingly different characteristics to the MsTMIP models, and so it is not unreasonable to assume that it would respond in a similar way if given the same respiratory fluxes as the MsTMIP models.

GPP amplitude trends and mean annual GPP trends in MsTMIP models are well correlated to their trend in ASC (r^2 = 0.82 and 0.69 respectively, Figure 4.10 a, b), however the same strong correlation was not found between mean GPP amplitude and ASC for 2009-10 (Figure 4.10c, d). This is in contrast to the findings from Chapter 2 where mean NPP amplitude was well correlated to ASC, but is perhaps unsurprising since the atmospheric CO_2 concentration is a balance between photosynthetic and respiratory fluxes and GPP has no information about the respiratory flux. NPP on the other hand is calculated from GPP and autotrophic respiration, and thus has some respiratory response included. The strong correlation between the GPP amplitude trends and ASC trend conforms with the underlying hypothesis that changes in ASC are being driven by changes in carbon uptake (Graven et al., 2013; Randerson et al., 1997; Forkel et al., 2015) (Chapter 2). Using this relationship, I estimate that the trend in ASC that might be predicted by the P-model is 0.037 ppm yr^{-1} (Figure 4.10), which would equate to an increase in ASC of 1.8 ppm over the 50 years between two two aircraft campaigns, less than half the observed increase of 5.0±0.8 ppm (Graven et al., 2013). This underestimation of ASC change is contrary to my expectations of the P-model, as I hoped that the freedom from PFTs and using only a couple of fixed parameters would allow eLUE and consequently GPP to

Figure 4.10: The relationship between ASC and GPP modelled by the MsTMIP models (ASC values taken from Chapter 2). Trends in annual GPP and GPP amplitude are compared to trends in ASC (a, b), and mean annual GPP and GPP amplitude for 2009-10 are compared to ASC in 2009-10 (c, d). The solid black line shows the P-model GPP trends and the dotted line is the estimated ASC trend based on the best-fit line (grey line) for the relationship between GPP and ASC trends from the MsTMIP models. The equations and r^2 values are shown in the top left corner of each panel. The observed trend in ASC is 0.1ppm/year (not shown) (Graven et al., 2013).



increase more than other models predict. Thus this suggests that the current models may be systematically wrong either in their representation of GPP or respiration, or in the mechanisms that allow these fluxes to change. However, it must also be kept in mind that when using this 'emergent-constraint' approach to estimate P-model ASC, it is unsurprising that the P-model estimate is smaller than the observed ASC change, since all the MsTMIP models underestimate the change in ASC.

4.4 Discussion

The P-model is skilful at capturing the latitudinal distribution of mean annual GPP and GPP amplitude across high northern latitudes compared to the observation based estimate of GPP-FC and more complex models within MsTMIP (Figure 4.2). The similarity of these fluxes between the P-model, GPP-FC and MsTMIP models is remarkable considering the simplicity of the P-model in comparison to these other estimates, and therefore shows that this model is able to capture many of the key relationships between GPP and the environment. Thus, this simple model can be used to analyse large-scale changes in productivity but has the added benefits that it is fast to run, driven almost entirely by observational data and is less constrained by fixed parameters than most other models.

P-model trends in mean annual GPP and GPP amplitude are amongst the largest and driven by increases in CO_2 and vegetation greening, while changes in climate generally contribute negatively and radiation changes have a regional influence that cancel out over the high northern latitudes (Figure 4.5, Tables 4.3, 4.4). Although CO_2 fertilisation was the most important single driver of changes in GPP, when this was combined with climate driven changes to calculate eLUE , changes in APAR, driven primarily by fAPAR changes, became the most important driver of GPP changes. The factorial experiments highlight that non-linearities between these drivers can be large; for GPP amplitude trends non-linear interactions between CO_2 and PAR or fAPAR in some regions were as important as changes in PAR or fAPAR alone.

The role of CO_2 fertilisation in the P-model is on the highest end of the estimates of CO_2 driven increases in GPP found by other models, even when non-linear effects between CO_2 and climate are included in the estimate. For TRENDY models, the direct CO_2 driven increases in GPP across Boreal and temperate regions is ∼0.002 - 0.052 PgC $yr^{-1}ppm^{-1}$ and ∼0.012 - 0.056 PgC $yr^{-1}ppm^{-1}$, respectively (Piao et al., 2013), compared to 0.057PgC $yr^{-1}ppm^{-1}$ across 30-90° for the P-model. One reason for the high CO_2 driven estimate in the P-model could be its lack of a coupled carbon-nitrogen cycle. TRENDY models which included coupled nitrogen cycles were generally in the lower end of the range, and so the estimate provided by the P-model would likely be reduced with the inclusion of nutrient limitations. However, including such limitations in models remains challenging since the underlying mechanisms are poorly constrained (Zaehle et al., 2014). Due to the importance of nitrogen limitations in controlling the CO2 fertilisation effect, many modelling groups were keen to include this feature for the next stage of CMIP, CMIP6 (Ilyina and Friedlingstein, 2016). Thus, future model output is likely to show a smaller CO_2 fertilisation effect, as nitrogen will become an increasingly limiting factor over time. However, the rush to include C-N interactions may overly limit the CO_2 fertilisation effect if carbon-nitrogen interactions are not correctly included. For example, a recent study by Terrer et al. (2016) showed that the type of mycorrhiza in the soil plays an important role in determining the long-term effect of CO_2 fertilisation, but mycorrhiza type is unlikely to be included in the CMIP6 models.

Climate reduced eLUE and GPP in temperate regions, mostly as a result of decreased GPP in spring or autumn (Figure 4.5c, d), which is different to results found by other modelling experiments where climate tends to drive increases in GPP (Forkel et al., 2016; Piao et al., 2013) (Chapter 2). The different climate response in the P-model comes from the co-ordination hypothesis which predicts a decrease in GPP with temperature (Chapter 3). The negative temperature response in the P-model may be wrong or overestimated since the analysis in Chapter 3 suggests that at the 17 Fluxnet stations used in the model validation, GPP should increase with temperature rather than decrease. However the climate response in other terrestrial biosphere models may also be flawed, as the response is likely based on observations of the temperature response of photosynthesis in light saturated conditions, which show an initial

increase in GPP with temperature (Farquhar et al., 1980). A further difference between the GPP-climate response for the P-model and the response shown by other modelling studies is that the climate effects on GPP in other studies are accompanied by increases in vegetation greenness. The unique set-up of these factorial experiments for the P-model isolates the climate effect without greening changes, and suggests that changes in climate alone can act to reduce GPP.

According to the relationship between GPP amplitude trends and ASC derived using MsTMIP models, the P-model would underestimate increases in ASC compared to aircraft measurements (Figure 4.10). Although the correlation between GPP amplitude trends and ASC trends was very strong for MsTMIP models, the extent to which the P-model would fit into this correlation could be questioned as the pattern of P-model trends for GPP amplitude is different to the MsTMIP models. This may reflect the lack of limitations in the P-model (e.g. from nutrient availability) as well as the lack of PFTs in the P-model. The main change in P-model GPP amplitude is in boreal regions, which is not the case for MsTMIP models. This different distribution of GPP amplitude trends could play an important role in defining the overall change in ASC, as optimised fits to the aircraft observations of CO_2 suggest over half of the change in ASC has come from boreal regions (Graven et al., 2013). However this is unlikely to be sufficient to explain the underestimation of ASC by 3.2ppm estimated by the P-model, and thus there must be a systematic error in all models and some key deficiencies in the P-model which result in this low estimate of changes in GPP amplitude and ASC. Since the P-model was driven by observed changes in fAPAR and PAR, it is the changes in P-model eLUE that must be too small.

In Chapter 2, I raised several issues with the implementation of mechanisms that could increase modelled NPP trends, including CO_2 fertilisation, changes in carbon allocation, acclimation of respiration, the incorporation of nutrient dynamics in models and the role of land use change. Of relevance to the P-model are CO_2 fertilisation and land use change, and so these will be discussed in relation to the trends in mean annual GPP and GPP amplitude found in this chapter, as well as the role of PAR which was also considered separately in the factorial simulations. Weaknesses in the GPP estimate from the P-model that were highlighted in Chapter 3 are also

now discussed in relation to the large-scale estimate of GPP.

The strength of the CO_2 fertilisation effect is still widely debated. Some studies suggest that models often overestimate the impact of CO_2 fertilisation on GPP, especially when they do not consider the effects of nutrient limitations, and that conservative estimates are more realistic (Wenzel et al., 2016; Smith et al., 2016; De Kauwe et al., 2016). However, it is difficult to see how CO_2 fertilisation is overestimated as the increases in GPP and eLUE from the P-model and other TBMs are not sufficient to explain the increase in ASC over the last 50 years (Figure 4.10, (Graven et al., 2013) (Chapter 2)). Furthermore, estimates of global GPP trends using carbonyl sulfide as a proxy have estimated that GPP has increased by 30% over the last century, which is larger than most models estimate (Campbell et al., 2017).

If CO_2 fertilisation is too large in models, then another driver must be underestimated in order to make up for the expected change in GPP over recent years. For the P-model, an obvious candidate would be the response of GPP to temperature. If the assumption that GPP decreases with temperature is wrong, then GPP would be higher across most of the high northern latitudes since temperatures have increased over this region over the last 30 years. A warming experiment in the Alaskan tundra suggests that a warming climate could have a positive effect on GPP trends at these high latitudes (Natali et al., 2011). However, the negative effect on eLUE from climate at these latitudes is already small in the P-model (Figure 4.5) and the reduction in GPP with temperature is small (See Figure x Chapter 3). In ecosystems further south which are more sensitive to moisture, the role of climate may be more seasonal, as a grassland warming experiment showed that warming increased annual GPP but reduced GPP amplitude (Ryan et al., 2017). Thus, it is possible that the prescribed temperature response is correct for some regions/vegetation types. Assuming that the temperature response is correct, the assumption that the CO_2 fertilisation response is too large may also indicate that the non-linear interactions between drivers is larger than models suggest. Non-linear effects between warming and CO_2 could be particularly large in drier ecosystems as plant water-use efficiency can increase with CO_2 fertilisation which can enhance GPP in regions where warming is driving an earlier start to the growing season and compensate for reductions in available

water (Reyes-Fox et al., 2014; Wang et al., 2012; Swann et al., 2016). However, the magnitude of non-linear interactions between CO_2 and temperature changes are still uncertain due to a lack of experimental data across different ecosystems, and thus further observations are required in order to improve our understanding of these interactions (Baig et al., 2015; Wang et al., 2012).

On the other hand, it is also possible that the trend in GPP driven by CO_2 fertilisation is underestimated by the P-model. Although the P-model showed large increases in GPP driven by CO_2 fertilisation (Figure 4.5c, d, Table 4.4), these were largely offset by climate-driven reductions in GPP when considering the APAR and eLUE components of the GPP trend (Figures 4.8b, 4.9) and resulted in eLUE driving only 34% of the trend in GPP. However, this increase in GPP from eLUE may be underestimated as an analysis of four FACE sites showed that under elevated CO_2 in ecosystems with high peak LAI, almost 100% of the increase in NPP came from increases in eLUE, while in ecosystems with lower peak LAI, eLUE changes drove 10-40% of the NPP changes (Norby et al., 2005). This suggests that in regions with high peak LAI, almost all of the 23% increase in NPP from elevated CO_2 at these sites was driven by increases in eLUE. However in the P-model, the increase in GPP from CO_2 fertilisation alone would only be 6.8% (52.44% of the 12.9% increase in GPP Tables 4.3, 4.4). Many regions in the high northern latitudes have peak LAI above the threshold that was considered high in the analysis by Norby et al. (2005), and so this suggests that the contribution to GPP trends from CO_2 fertilisation-driven increases in eLUE may be underestimated.

In the current implementation of the P-model, the response of GPP to increasing CO_2 declines as CO_2 increases (Keenan et al., 2016), but the rate of this decrease is poorly constrained (Rogers et al., 2017). If the P-model overestimates this acclimation to increasing CO_2, then CO_2-driven trends in GPP could be larger than currently predicted. GPP trends driven by CO_2 were fairly homogeneous in the P-model as all latitudes were driven by the same CO_2 concentration (Figure 4.1e). Assuming that the trend remained homogeneous across latitudes, the already large trends in GPP amplitude in boreal regions would also increase. This could be particularly important to modelled ASC changes since the boreal region is the source of over half of the ASC trends (Graven et al., 2013). Additionally because the boreal regions had

significant contributions to GPP amplitude form non-linear trends between CO_2 and the other drivers, GPP amplitude could increase more than might be expected.

By using satellite observed fAPAR to drive the P-model, errors and uncertainties from this driving data propagate into the GPP estimate. The fAPAR3g dataset that was used to drive the P-model requires an underlying landcover map in order to interpret the input data correctly. Zhu et al. (2013) used a constant landcover map averaged over the last decade, and therefore changes in vegetation distribution, which could lead to increases in GPP through structural changes i.e. changes in fAPAR, are not included in the current P-model estimate for GPP. Greening trends from fAPAR3g are smaller than the MsTMIP models with dynamic vegetation, LPJ-wsl and VEGAS2.1, and so the constant land cover may be artificially reducing GPP trends (Chapter 2). A variation of the LPJ model, LPJ-mL, found that dynamic vegetation changes were responsible for a large part of the trend in GPP at high northern latitudes (Forkel et al., 2016). The choice of fAPAR dataset is also important as datasets do not agree on global greening trends and there can be significant uncertainties between datasets at high latitudes of as much as 20% in each pixel (Jiang et al., 2017). The LAI3g dataset which has been developed alongside fAPAR3g, has one of the largest trends in greening when compared to other satellite products for LAI, and fewer regions of browning across high northern latitudes (Jiang et al., 2017). The regions of uncertainty often coincide with ecosystems where the P-model performed poorly at the site-scale, underestimating peak GPP in deciduous boradleaf forests and croplands (Chapter 3). The final year of the fAPAR3g dataset (2010) also has a particularly large greening trend (Figure 2.5) which is stronger than some other satellite products show (Guay et al., 2014). This could result in a larger trend in greening as well as a larger trend in GPP estimated by the P-model. With all of this in mind, it would therefore be useful to generate estimates of GPP using different fAPAR datasets to drive the P-model and analyse the effect of differences in the choice of driving data.

The influence of changes in PAR is likely to be under-represented by the P-model, since it does not separate incoming light into direct and diffuse radiation. Aerosols and clouds increase the fraction of radiation that is diffuse and, if the reduction in total PAR is not too large, this can

increase GPP as more vegetation is exposed to light and light levels are generally not saturating (Mercado et al., 2009). The indirect effect of diffuse radiation will be accounted for by increases in the fAPAR-driven GPP, but direct physiological effects i.e. due to reduced light saturation (Gu et al., 2002) will not be included in any GPP estimate from the P-model. Using the JULES land surface model, Mercado et al. (2009) found that the contribution to GPP from diffuse radiation reduced over Europe between 1980-1999, but remained steady across the East coast of North America and Asia. When both direct and diffuse radiation were considered, there was a net increase in GPP of up to 80gC m^{-1} yr^{-1} in some regions. In northern temperate regions, diffuse PAR has increased due to increased aerosol emissions. Currently this is represented in the PAR data as a reduction in overall PAR (Figure 4.1b, Figure 4.5c, d), but the increase in diffuse radiation could be sufficiently large to outweigh this decrease and drive increases in GPP (Wild, 2016; Gu et al., 2002). Including the effects of diffuse radiation would therefore be a useful next step in the development of the P-model.

4.5 Conclusion

A simple next-generation biosphere model, the P-model, is able to reproduce patterns of mean annual GPP and GPP amplitude that are similar to the more complex TBMs from the MsTMIP ensemble, and the observation-based estimate GPP-FC. I have identified that trends in GPP in the P-model are driven by structural changes in vegetation while physiological changes play a secondary role, driven by CO_2 fertilisation and moderated by changes in climate. There is a large range in the contribution to GPP trends from structural and physiological changes for MsTMIP models, although models which include a coupled carbon-nitrogen cycle or dynamic vegetation attribute a smaller fraction of GPP trends to structural changes. This suggests that including some of these more dynamic processes alters ecosystem functioning in models such that the balance between structural and physiological drivers can change. Although the P-model was able to capture site-level GPP from Fluxnet stations with good skill (Chapter 3), the trend in mean annual GPP and GPP amplitude may not be sufficient to explain the increase in ASC over the last 50 years observed by aircraft campaigns. This analysis once again highlights the powerful constraint that aircraft data can provide (Graven et al., 2013) (Chapter

2), as these observations represent ecosystem changes at larger scales then can be observed using ground data or site stations alone. The aircraft data used in this analysis only considers changes in the seasonal amplitude of CO_2, but as more aircraft data becomes available through projects such as ATom (Atmospheric Tomography Mission) (Czech, 2018), aircraft data based benchmarks could be provided for a larger variety of carbon-cycle features.

The use of fully-factorial experiments in this analysis also highlighted that even in a simple model, non-linear interactions between drivers can be important. Thus, comparisons between modelling studies where experiments were run in different orders and contributions from each driver were calculated using the common differencing approach, may be attributing these non-linear effects to different factors. Although computationally more expensive, the running of additional experiments in order to quantify the non-linear effects provides a useful insight into complex models and can enhance our understanding of real-world ecosystems which respond to simultaneous changes in multiple drivers.

Since this analysis indicates that the P-model is unable to capture the observed trend in ASC, the mechanisms driving the increase in ASC remain uncertain. However, as the P-model is driven by observed structural changes in vegetation through the use of satellite data for trends in greening and incoming light, this analysis also indicates the possibility of larger changes in eLUE over the last 50 years than models currently allow. These could be achieved through stronger CO_2 fertilisation or larger non-linear interactions between CO_2 and climate. Further investigation is needed to fully understand the mechanisms driving the changes in eLUE, as the functioning of the terrestrial biosphere is likely to continue to change in response to future environmental changes.

Chapter 5

Conclusion

5.1 Summary of key findings

Productivity in the high latitudes of northern hemisphere has increased over the last few decades, driven by anthropogenic environmental changes. The aim of this thesis was to explore key mechanisms responsible for this increase using observations, existing terrestrial biosphere models (TBMs) from the MsTMIP experiments and a new model for photosynthesis, the P-model. Despite its simplicity, the P-model has similar patterns of mean annual GPP and GPP amplitude compared to TBMs from the MsTMIP project and an observation based estimate for GPP from the FluxCom project. P-model GPP trends are amongst the largest, driven primarily by CO_2 fertilisation and also by vegetation greening. Similar results were found for NPP in the MsTMIP models, although there was a large variation in the magnitude of CO_2 fertilisation between models. I found a strong correlation between trends in the amplitude of the seasonal cycle of CO_2 (ASC) at high northern latitudes and the trends in GPP and NPP amplitude for the MsTMIP models, reaffirming previous studies which suggest that the observed increase in ASC over the last 50 years has been primarily driven by increases in productivity. Since the MsTMIP models underestimated ASC trends, this suggests that they are underestimating changes in productivity. I therefore extended the use of the ecosystem light-use efficiency (eLUE) metric, which allowed me to separate modelled productivity trends into structural and physiological changes. I found that modelled trends in ecosystem light-use efficiency (eLUE) are probably underestimated because models underestimated ASC trends

despite capturing the greening of vegetation observed over recent years, i.e. the structural changes. Using the emergent relationship between GPP amplitude trends and ASC trends, I found that the P-model might also underestimate the increase in ASC, despite being driven by observed greening trends. Thus, eLUE trends, larger than current models allow are driving increases in productivity across high northern latitudes.

Although trends in productivity cannot be directly measured, trends in ASC between 45-90°N are well correlated to trends in productivity 30-90°N and can thus be used to analyse changes in productivity across these ecosystems. Optimised regional fits to the observations of ASC trends show that the largest contribution to increases in ASC came from arctic and northern boreal regions ($\sim$60-90°N) (Graven et al., 2013). Increasing temperatures across these regions have lengthened the growing season, and MsTMIP models are able to capture the resulting increase in vegetation greening. Although models have poorer skill in temperate ecosystems, the large influence of the high latitude greening trends means that they are generally able to capture the overall greening trend compared to observations from fAPAR3g when averaged across 30-90°N.

Since MsTMIP models have good skill at capturing greening trends, one might expect that they are also skilful at capturing ASC changes. However this is not the case, and all MsTMIP models underestimate the trend in ASC between 45-90°N, estimating changes of -0.5 to 2.4 ppm compared to the observed change of 5.0$\pm$0.8 ppm for 1958-61 to 2009-11 (Graven et al., 2013). The poor skill at representing greening trends in temperate ecosystems is not the primary cause of this underestimation, as the P-model was driven by observed greening trends from fAPAR3g and I estimated that it would only give an increase in ASC of 1.8ppm. Since changes in productivity are driven by physiological as well as structural changes, my analysis of the P-model and the MsTMIP models suggests that current models are underestimating physiological changes in vegetation that could lead to increases in productivity. Trends in productivity in the P-model are primarily driven by structural changes, and eLUE only accounts for 1/3 of the trend in GPP. However it is clear from this analysis that eLUE-driven GPP trends could be much larger.

Trends in eLUE ranged from -7.8 to 6.9% (when calculating eLUE using NPP) for 1958-61 to 2009-10 and -0.81 to 11% (eLUE calculated using GPP) for 1982-2010 for the MsTMIP models, while the P-model had an increase in eLUE of 3.9% for 1982-2010. Factorial experiments with the MsTMIP models and the P-model showed that CO_2 fertilisation was the main driver of trends in eLUE driven productivity, although the strength of this effect varied between models. MsTMIP models had decreases in climate-driven eLUE which generally resulted in decreased in climate-driven ASC, suggesting that the modelled increases in climate-driven NPP are primarily due to vegetation greening. Using the P-model, I was able to isolate the climate-driven physiological changes in GPP from the structural changes in GPP, and found that climate change reduced the positive effect of elevated CO_2 on eLUE by 50%. CO_2 fertilisation in the P-model was large enough to outweigh this decrease in eLUE, but this was not the case for some MsTMIP models, and so some models had overall decreases in eLUE when all variables were considered together.

Vegetation may be responding to environmental changes in a more dynamic way than any model currently allows. The MsTMIP models may not have the flexibility to respond to the observed environmental changes as they contain many fixed parameters, often varying according to a fixed distribution of modelled plant functional type (PFTs), and these models generally do not allow vegetation to acclimate to environmental changes. Although some MsTMIP models had dynamically varying vegetation (LPJ-wsl and VEGAS2.1), or included terms that allowed autotrophic respiration to acclimate to higher temperatures (LPJ-wsl and VISIT), these differences are not sufficient to make the modelled increases in productivity distinct from the models which do not include these terms.

Although the P-model is not restricted by PFTs, it still underestimates productivity changes. This suggests that other drivers, such as CO_2 fertilisation could be much larger than currently estimated, and its representation in the P-model may need to be re-evaluated. Other suggested improvements to the P-model are given in Section 5.2 below. Furthermore, I found that non-linear interactions between different drivers, particularly their interaction with CO_2, can make an important contribution to productivity trends. These are not often explicitly resolved in

model intercomparison studies but since vegetation is responding to multiple environmental changes simultaneously, further understanding the mechanisms driving these non-linear interactions may also improve our representation of dynamic vegetation responses to environmental changes.

Combining atmospheric CO_2 measurements and observed greening trends provides a powerful constraint on TBMs. In this thesis, I benchmarked TBMs against atmospheric CO_2 measurements of ASC trends from aircraft campaigns for the first time. This constraint allowed me to identify that the underestimation of ASC trends was a common weakness across all current TBMs, and that this resulted from poor representation of land processes rather than modelled climate. Analysing models with the metric of eLUE in the context of observed greening trends allowed me to go further than previous studies and conclude that it is the representation of physiological changes that requires improvement in models. Together, the benchmark of aircraft ASC trends and the metric of eLUE has given me insights into the mechanisms driving productivity changes in models. This can be particularity useful for analysing complex models to understand a little more about the processes taking place within the 'black-box'.

5.2 Future Work

Global GPP trends remain poorly known, but many Fluxnet sites have now been recording data for long enough for trends in GPP to emerge. Comparing the GPP trends from the P-model against these long-term sites could thus provide further insights into how well the P-model is able to capture GPP trends and the mechanisms driving these trends. This would also help inform the improvements that could be made to the P-model which are discussed below.

Several developments could be made to the P-model which may improve its estimation of GPP and GPP trends. The choice of driving data, particularly the choice of fAPAR data, may alter both the mean GPP estimate and the trend in GPP, as greening trends at very high northern latitudes are highly uncertain and any errors in fAPAR3g will propagate through to

the P-model GPP estimate. Furthermore, I found that monthly fAPAR was not suitable for analysing monthly GPP estimates from the P-model, which could influence trends in total GPP. To analyse this uncertainty in the P-model, I would estimate GPP using a variety of different fAPAR data products over different timescales and compare outputs. This would alter the structural competent of GPP estimates, but the eLUE trends would remain the same.

P-model GPP trends driven by changes in eLUE may be larger than currently estimated. Since the ethos of the P-model is to be the simplest representation of GPP possible, the first steps to improving eLUE are to consider processes that are currently modelled. Firstly, instead of using air temperature to drive the P-model, land surface temperature could be used as this may better reflect the temperature experienced by the vegetation. Further including a term which accounts for leaf thermoregulation could also be considered, as this would take into account the fact that leaves can be cooler or warmer than the air temperature and thus would also better reflect the temperature at which photosynthesis is taking place. Further analysis is also required to fully understand the relationship between GPP and temperature, as the current model does not represent this well. A change in the representation of CO_2 fertilisation and the interaction of CO_2 with other drivers could also increase modelled eLUE trends, although this would additionally require analysis of current observations to develop a new function for such a change. A simple additional process to include would be the effect of diffuse light on vegetation. Although this is already included within the fAPAR data, explicitly accounting for the physiological changes in GPP that may occur due to changes in diffuse light may increase GPP estimates. A term for the effect of diffuse light on GPP could be simply included by using the two-stream approach to estimate the direct and diffuse components of radiation (Sellers, 1985).

The estimates of ecosystem respiration (Reco) from the simple models used in Chapter 3 were not skilful enough to use for global estimates of Reco and NEE. One reason for the poor estimate is that the underlying assumption of a net-neutral biosphere is not appropriate for modelling ecosystem fluxes given their current change. Including terms to allow longer-term storage of carbon within the model may therefore be necessary. Alternatively, scaling an observation

based estimate of Reco (e.g. from the FluxCom project), or an estimate from other models to the P-model GPP could be used to calculate NEE instead. This would allow the P-model to be used to calculate changes in ASC, and it would be interesting to see how closely this matches the ASC change that was estimated using the relationship between GPP amplitude trends and ASC trends from the MsTMIP models.

Further developments in model benchmarks may also help to guide model improvements. For example, the estimate of GPP using solar induced florescence (SIF) measurements looks like a promising way to more directly measure GPP from satellites. This could be useful in furthering our understanding of the mechanisms controlling mean annual GPP and GPP amplitude, but these observations have not yet been made for long enough to consider trends. A more direct estimate of global GPP could also improve global estimates of eLUE, as GPP is currently the largest unknown in the calculation of this metric. The metric of eLUE would also benefit from having a site-scale comparison. Currently, fAPAR is not a standard measurement at Fluxnet sites, but including this may help improve our understanding of eLUE at these well documented sites and thus our understanding of eLUE at global scales.

Questions still remain about the mechanisms driving the changes in productivity of northern terrestrial ecosystems. The increase in ASC over recent decades remains largely unexplained as current models are unable to match the observed trend. I have identified that increases in eLUE larger than current models allow are required to improve the estimate of modelled productivity change. Increases in eLUE could be achieved by CO_2 fertilisation, climate change, changes in diffuse radiation and dynamic changes in vegetation, but their current representation in the MsTMIP models and the P-model does not produce GPP trends that are sufficiently large to explain the ASC trends. The future evolution of the terrestrial biosphere as a net carbon sink will depend on whether trends in productivity continue to increase faster than respiration. Thus it is vital that we continue to strive to understand the mechanisms controlling changes in the terrestrial biosphere as the rate of environmental change isn't slowing.

Appendix A

Permissions

Figure A.1: Permissions for Thomas et al. (2016). Figures used in Chapter 2.

5/2/2018 RightsLink Printable License

JOHN WILEY AND SONS LICENSE TERMS AND CONDITIONS

May 02, 2018

This Agreement between Miss. Rebecca Thomas ("You") and John Wiley and Sons ("John Wiley and Sons") consists of your license details and the terms and conditions provided by John Wiley and Sons and Copyright Clearance Center.

License Number	4340670501487
License date	May 02, 2018
Licensed Content Publisher	John Wiley and Sons
Licensed Content Publication	Geophysical Research Letters
Licensed Content Title	Increased light-use efficiency in northern terrestrial ecosystems indicated by CO2 and greening observations
Licensed Content Author	Rebecca T. Thomas, Iain Colin Prentice, Heather Graven, et al
Licensed Content Date	Nov 4, 2016
Licensed Content Volume	43
Licensed Content Issue	21
Licensed Content Pages	11
Type of use	Dissertation/Thesis
Requestor type	Author of this Wiley article
Format	Print and electronic
Portion	Full article
Will you be translating?	No
Title of your thesis / dissertation	Changes in productivity across northern terrestrial ecosystems
Expected completion date	May 2018
Expected size (number of pages)	200
Requestor Location	Miss. Rebecca Thomas Flat 16, 35 Furnival Street London, EC4A 1JQ United Kingdom Attn: Miss. Rebecca Thomas
Publisher Tax ID	EU826007151
Total	0.00 GBP
Terms and Conditions	

TERMS AND CONDITIONS

This copyrighted material is owned by or exclusively licensed to John Wiley & Sons, Inc. or one of its group companies (each a"Wiley

Company") or handled on behalf of a society with which a Wiley Company has exclusive publishing rights in relation to a particular work (collectively "WILEY"). By clicking "accept" in connection with completing this licensing transaction, you agree that the following terms and conditions apply to this transaction (along with the billing and payment terms and conditions established by the Copyright Clearance Center Inc., ("CCC's Billing and Payment terms and conditions"), at the time that you opened your RightsLink account (these are available at any time at http://myaccount.copyright.com).

Terms and Conditions

- The materials you have requested permission to reproduce or reuse (the "Wiley Materials") are protected by copyright.

- You are hereby granted a personal, non-exclusive, non-sub licensable (on a stand-alone basis), non-transferable, worldwide, limited license to reproduce the Wiley Materials for the purpose specified in the licensing process. This license, **and any CONTENT (PDF or image file) purchased as part of your order,** is for a one-time use only and limited to any maximum distribution number specified in the license. The first instance of republication or reuse granted by this license must be completed within two years of the date of the grant of this license (although copies prepared before the end date may be distributed thereafter). The Wiley Materials shall not be used in any other manner or for any other purpose, beyond what is granted in the license. Permission is granted subject to an appropriate acknowledgement given to the author, title of the material/book/journal and the publisher. You shall also duplicate the copyright notice that appears in the Wiley publication in your use of the Wiley Material. Permission is also granted on the understanding that nowhere in the text is a previously published source acknowledged for all or part of this Wiley Material. Any third party content is expressly excluded from this permission.

- With respect to the Wiley Materials, all rights are reserved. Except as expressly granted by the terms of the license, no part of the Wiley Materials may be copied, modified, adapted (except for minor reformatting required by the new Publication), translated, reproduced, transferred or distributed, in any form or by any means, and no derivative works may be made based on the Wiley Materials without the prior permission of the respective copyright owner.**For**

STM Signatory Publishers clearing permission under the terms of the STM Permissions Guidelines only, the terms of the license are extended to include subsequent editions and for editions in other languages, provided such editions are for the work as a whole in situ and does not involve the separate exploitation of the permitted figures or extracts, You may not alter, remove or suppress in any manner any copyright, trademark or other notices displayed by the Wiley Materials. You may not license, rent, sell, loan, lease, pledge, offer as security, transfer or assign the Wiley Materials on a stand-alone basis, or any of the rights granted to you hereunder to any other person.

- The Wiley Materials and all of the intellectual property rights therein shall at all times remain the exclusive property of John Wiley & Sons Inc, the Wiley Companies, or their respective licensors, and your interest therein is only that of having possession of and the right to reproduce the Wiley Materials pursuant to Section 2 herein during the continuance of this Agreement. You agree that you own no right, title or interest in or to the Wiley Materials or any of the intellectual property rights therein. You shall have no rights hereunder other than the license as provided for above in Section 2. No right, license or interest to any trademark, trade name, service mark or other branding ("Marks") of WILEY or its licensors is granted hereunder, and you agree that you shall not assert any such right, license or interest with respect thereto

- NEITHER WILEY NOR ITS LICENSORS MAKES ANY WARRANTY OR REPRESENTATION OF ANY KIND TO YOU OR ANY THIRD PARTY, EXPRESS, IMPLIED OR STATUTORY, WITH RESPECT TO THE MATERIALS OR THE ACCURACY OF ANY INFORMATION CONTAINED IN THE MATERIALS, INCLUDING, WITHOUT LIMITATION, ANY IMPLIED WARRANTY OF MERCHANTABILITY, ACCURACY, SATISFACTORY QUALITY, FITNESS FOR A PARTICULAR PURPOSE, USABILITY, INTEGRATION OR NON-INFRINGEMENT AND ALL SUCH WARRANTIES ARE HEREBY EXCLUDED BY WILEY AND ITS LICENSORS AND WAIVED BY YOU.

- WILEY shall have the right to terminate this Agreement immediately upon breach of this Agreement by you.

- You shall indemnify, defend and hold harmless WILEY, its Licensors and their respective directors, officers, agents and employees, from and against any actual or threatened claims, demands, causes of action or proceedings arising from any breach of this Agreement by you.

- IN NO EVENT SHALL WILEY OR ITS LICENSORS BE LIABLE TO YOU OR ANY OTHER PARTY OR ANY OTHER PERSON OR ENTITY FOR ANY SPECIAL, CONSEQUENTIAL, INCIDENTAL, INDIRECT, EXEMPLARY OR PUNITIVE DAMAGES, HOWEVER CAUSED, ARISING OUT OF OR IN CONNECTION WITH THE DOWNLOADING, PROVISIONING, VIEWING OR USE OF THE MATERIALS REGARDLESS OF THE FORM OF ACTION, WHETHER FOR BREACH OF CONTRACT, BREACH OF WARRANTY, TORT, NEGLIGENCE, INFRINGEMENT OR OTHERWISE (INCLUDING, WITHOUT LIMITATION, DAMAGES BASED ON LOSS OF PROFITS, DATA, FILES, USE, BUSINESS OPPORTUNITY OR CLAIMS OF THIRD PARTIES), AND WHETHER OR NOT THE PARTY HAS BEEN ADVISED OF THE POSSIBILITY OF SUCH DAMAGES. THIS LIMITATION SHALL APPLY NOTWITHSTANDING ANY FAILURE OF ESSENTIAL PURPOSE OF ANY LIMITED REMEDY PROVIDED HEREIN.

- Should any provision of this Agreement be held by a court of competent jurisdiction to be illegal, invalid, or unenforceable, that provision shall be deemed amended to achieve as nearly as possible the same economic effect as the original provision, and the legality, validity and enforceability of the remaining provisions of this Agreement shall not be affected or impaired thereby.

- The failure of either party to enforce any term or condition of this Agreement shall not constitute a waiver of either party's right to enforce each and every term and condition of this Agreement. No breach under this agreement shall be deemed waived or excused by either party unless such waiver or consent is in writing signed by the party granting such waiver or consent. The waiver by or consent of a party to a breach of any provision of this Agreement shall not operate or be construed as a waiver of or consent to any other or subsequent breach by such other party.

- This Agreement may not be assigned (including by operation of law or otherwise) by you without WILEY's prior written consent.

- Any fee required for this permission shall be non-refundable after thirty (30) days from receipt by the CCC.

- These terms and conditions together with CCC's Billing and Payment terms and conditions (which are incorporated herein) form the entire agreement between you and WILEY concerning this licensing transaction and (in the absence of fraud) supersedes all prior agreements and representations of the parties, oral or written. This Agreement may not be amended except in writing signed by both parties. This Agreement shall be binding upon and inure to the benefit of the parties' successors, legal representatives, and authorized assigns.

- In the event of any conflict between your obligations established by these terms and conditions and those established by CCC's Billing and Payment terms and conditions, these terms and conditions shall prevail.

- WILEY expressly reserves all rights not specifically granted in the combination of (i) the license details provided by you and accepted in the course of this licensing transaction, (ii) these terms and conditions and (iii) CCC's Billing and Payment terms and conditions.

- This Agreement will be void if the Type of Use, Format, Circulation, or Requestor Type was misrepresented during the licensing process.

- This Agreement shall be governed by and construed in accordance with the laws of the State of New York, USA, without regards to such state's conflict of law rules. Any legal action, suit or proceeding arising out of or relating to these Terms and Conditions or the breach thereof shall be instituted in a court of competent jurisdiction in New York County in the State of New York in the United States of America and each party hereby consents and submits to the personal jurisdiction of such court, waives any objection to venue in such court and consents to service of process by registered or certified mail, return receipt requested, at the last known address of such party.

WILEY OPEN ACCESS TERMS AND CONDITIONS

Wiley Publishes Open Access Articles in fully Open Access Journals and in Subscription journals offering Online Open. Although most of the fully Open Access journals publish open access articles under the terms of the Creative Commons Attribution (CC BY) License only, the subscription journals and a few of the Open Access Journals offer a choice of Creative Commons Licenses. The license type is clearly identified on the article.

The Creative Commons Attribution License

The Creative Commons Attribution License (CC-BY) allows users to copy, distribute and transmit an article, adapt the article and make commercial use of the article. The CC-BY license permits commercial and non-

Creative Commons Attribution Non-Commercial License

The Creative Commons Attribution Non-Commercial (CC-BY-NC)License permits use, distribution and reproduction in any medium, provided the original work is properly cited and is not used for commercial purposes.(see below)

Creative Commons Attribution-Non-Commercial-NoDerivs License

The Creative Commons Attribution Non-Commercial-NoDerivs License (CC-BY-NC-ND) permits use, distribution and reproduction in any medium, provided the original work is properly cited, is not used for commercial purposes and no modifications or adaptations are made. (see below)

Use by commercial "for-profit" organizations

Use of Wiley Open Access articles for commercial, promotional, or marketing purposes requires further explicit permission from Wiley and will be subject to a fee.

Further details can be found on Wiley Online Library http://olabout.wiley.com/WileyCDA/Section/id-410895.html

Other Terms and Conditions:

v1.10 Last updated September 2015

Questions? customercare@copyright.com or +1-855-239-3415 (toll free in the US) or +1-978-646-2777.

5/2/2018 RightsLink Printable License

https://s100.copyright.com/AppDispatchServlet 7/7

Bibliography

Abtew, W. and Melesse, A. M. *Evaporation and Evapotranspiration: Measurements and Estimations*, chapter Vapor Pressure Calculation Methods, pages 53–54. Springer, New York, 2013.

Ai, Jinlong; Jia, Gensuo; Epstein, Howard E.; Wang, Hesong; Zhang, Anzhi, and Hu, Yonghong. Modis-based estimates of global terrestrial ecosystem respiration. *Journal of Geophysical Research: Biogeosciences*, 123(2):326–352, 2018.

Ainsworth, E. A. and Long, S. P. What have we learned from 15 years of free-air co_2 enrichment (face) a meta-analytic review of the responses of photosynthesis, canopy. *New Phytologist*, 165(2):351–371, 2005.

Alexandrov, G. A. Explaining the seasonal cycle of the globally averaged co_2 with a carbon-cycle model. *Earth System Dynamics*, 5(2):345–354, 2014.

Anav, A.; Friedlingstein, P.; Kidston, M.; Bopp, L.; Ciais, P.; Cox, P.; Jones, C.; Jung, M.; Myneni, R., and Zhu, Z. Evaluating the land and ocean components of the global carbon cycle in the cmip5 earth system models. *Journal of Climate*, 26(18):6801–6843, 2013.

Anav, A.; Friedlingstein, P.; Beer, C.; Ciais, P.; Harper, A.; Jones, C.; Murray-Tortarolo, G.; Papale, D.; Parazoo, N. C.; Peylin, P.; Piao, S. L.; Sitch, S.; Viovy, N.; Wiltshire, A., and Zhao, M. S. Spatiotemporal patterns of terrestrial gross primary production: A review. *Reviews of Geophysics*, 53(3):785–818, 2015.

Andres, R. J.; Gregg, J. S.; Losey, L.; Marland, G., and Boden, T. A. Monthly, global emissions of carbon dioxide from fossil fuel consumption. *Tellus Series B-Chemical and Physical Meteorology*, 63(3):309–327, 2011.

Arneth, A.; Sitch, S.; Pongratz, J.; Stocker, B. D.; Ciais, P.; Poulter, B.; Bayer, A. D.; Bondeau, A.; Calle, L.; Chini, L. P.; Gasser, T.; Fader, M.; Friedlingstein, P.; Kato, E.; Li, W.; Lindeskog, M.; Nabel, J. E. M. S.; Pugh, T. A. M.; Robertson, E.; Viovy, N.; Yue, C., and Zaehle, S. Historical carbon dioxide emissions caused by land-use changes are possibly larger than assumed. *Nature Geoscience*, 10(2):79, 2017.

Arora, V. K.; Boer, G. J.; Friedlingstein, P.; Eby, M.; Jones, C. D.; Christian, J. R.; Bonan, G.; Bopp, L.; Brovkin, V.; Cadule, P.; Hajima, T.; Ilyina, T.; Lindsay, K.; Tjiputra, J. F., and Wu, T. Carbon-concentration and carbon-climate feedbacks in cmip5 earth system models. *Journal of Climate*, 26(15):5289–5314, 2013.

Baig, S.; Medlyn, B. E.; Mercado, L. M., and Zaehle, S. Does the growth response of woody plants to elevated co_2 increase with temperature? a model-oriented meta-analysis. *Global Change Biology*, 21(12):4303–4319, 2015.

Baker, I. T.; Prihodko, L.; Denning, A. S.; Goulden, M.; Miller, S., and Da Rocha, H. R. Seasonal drought stress in the amazon: Reconciling models and observations. *Journal of Geophysical Research-Biogeosciences*, 113, 2008.

Baldocchi, D. Breathing of the terrestrial biosphere: lessons learned from a global network of carbon dioxide flux measurement systems. *Australian Journal of Botany*, 56(1):1–26, 2008.

Baldocchi, D.; Chu, H. S., and Reichstein, M. Inter-annual variability of net and gross ecosystem carbon fluxes: A review. *Agricultural and Forest Meteorology*, 249:520–533, 2018.

Ballantyne, A. P.; Alden, C. B.; Miller, J. B.; Tans, P. P., and White, J. W. C. Increase in

observed net carbon dioxide uptake by land and oceans during the past 50 years. *Nature*, 488(7409):70–+, 2012.

Barichivich, J.; Briffa, K. R.; Myneni, R. B.; Osborn, T. J.; Melvin, T. M.; Ciais, P.; Piao, S. L., and Tucker, C. Large-scale variations in the vegetation growing season and annual cycle of atmospheric co_2 at high northern latitudes from 1950 to 2011. *Global Change Biology*, 19 (10):3167–3183, 2013.

Barr, A. G.; Richardson, A. D.; Hollinger, D. Y.; Papale, D.; Arain, M. A.; Black, T. A.; Bohrer, G.; Dragoni, D.; Fischer, M. L.; Gu, L.; Law, B. E.; Margolis, H. A.; Mccaughey, J. H.; Munger, J. W.; Oechel, W., and Schaeffer, K. Use of change-point detection for friction-velocity threshold evaluation in eddy-covariance studies. *Agricultural and Forest Meteorology*, 171:31–45, 2013.

Beck, Pieter S A and Goetz, Scott J. Satellite observations of high northern latitude vegetation productivity changes between 1982 and 2008: Ecological variability and regional differences. 2011.

Beer, Christian; Reichstein, Markus; Tomelleri, Enrico; Ciais, Philippe; Jung, Martin; Carvalhais, Nuno; Roedenbeck, Christian; Arain, M. Altaf; Baldocchi, Dennis; Bonan, Gordon B.; Bondeau, Alberte; Cescatti, Alessandro; Lasslop, Gitta; Lindroth, Anders; Lomas, Mark; Luyssaert, Sebastiaan; Margolis, Hank; Oleson, Keith W.; Roupsard, Olivier; Veenendaal, Elmar; Viovy, Nicolas; Williams, Christopher; Woodward, F. Ian, and Papale, Dario. Terrestrial gross carbon dioxide uptake: Global distribution and covariation with climate. *Science*, 329(5993):834–838, 2010.

Bernacchi, C. J.; Singsaas, E. L.; Pimentel, C.; Portis, A. R., and Long, S. P. Improved temperature response functions for models of rubisco-limited photosynthesis. *Plant Cell and Environment*, 24(2):253–259, 2001.

Bonan, G. B. Forests and climate change: Forcings, feedbacks, and the climate benefits of forests. *Science*, 320(5882):1444–1449, 2008.

Bonan, G. B. and Doney, S. C. Climate, ecosystems, and planetary futures: The challenge to predict life in earth system models. *Science*, 2018.

Bond-Lamberty, B. and Thomson, A. Temperature-associated increases in the global soil respiration record. *Nature*, 464(7288):579–U132, 2010.

Bond-Lamberty, B.; Epron, D.; Harden, J.; Harmon, M. E.; Hoffman, F.; Kumar, J.; McGuire, A. D., and Vargas, R. Estimating heterotrophic respiration at large scales: challenges, approaches, and next steps. *Ecosphere*, 7(6):13, 2016.

BondLamberty, B; Wang, C, and Gower, S. T. A global relationship between the heterotrophic and autotrophic components of soil respiration? *Global Change Biology*, 10(10):1756–1766, 2004.

Bradford, M. A. and Crowther, T. W. Carbon use efficiency and storage in terrestrial ecosystems. *New Phytologist*, 199(1):7–9, 2013.

Buitenwerf, Robert; Rose, Laura, and Higgins, Steven I. Three decades of multi-dimensional change in global leaf phenology. *Nature Climate Change*, 5(4):364–368, 2015.

Campbell, J. E.; Berry, J. A.; Seibt, U.; Smith, S. J.; Montzka, S. A.; Launois, T.; Belviso, S.; Bopp, L., and Laine, M. Large historical growth in global terrestrial gross primary production. *Nature*, 544(7648):84–87, 2017.

Carey, J. C.; Tang, J. W.; Templer, P. H.; Kroeger, K. D.; Crowther, T. W.; Burton, A. J.; Dukes, J. S.; Emmett, B.; Frey, S. D.; Heskel, M. A.; Jiang, L.; Machmuller, M. B.; Mohan, J.; Panetta, A. M.; Reich, P. B.; Reinsch, S.; Wang, X.; Allison, S. D.; Bamminger, C.; Bridgham, S.; Collins, S. L.; De Dato, G.; Eddy, W. C.; Enquist, B. J.; Estiarte, M.; Harte, J.; Henderson, A.; Johnson, B. R.; Larsen, K. S.; Luo, Y.; Marhan, S.; Melillo, J. M.; Peuelas, J.; Pfeifer-Meister, L.; Poll, C.; Rastetter, E.; Reinmann, A. B.; Reynolds, L. L.; Schmidt, I. K.; Shaver, G. R.; Strong, A. L.; Suseela, V., and Tietema, A. Temperature response of soil respiration largely unaltered with experimental warming. *Proceedings of the National Academy of Sciences of the United States of America*, 113(48):13797–13802, 2016.

F. S.Chapin, Iii; Woodwell, G. M.; Randerson, J. T.; Rastetter, E. B.; Lovett, G. M.; Baldocchi, D. D.; Clark, D. A.; Harmon, M. E.; Schimel, D. S.; Valentini, R.; Wirth, C.; Aber, J. D.; Cole, J. J.; Goulden, M. L.; Harden, J. W.; Heimann, M.; Howarth, R. W.; Matson, P. A.; McGuire, A. D.; Melillo, J. M.; Mooney, H. A.; Neff, J. C.; Houghton, R. A.; Pace, M. L.;

Ryan, M. G.; Running, S. W.; Sala, O. E.; Schlesinger, W. H., and Schulze, E. D. Reconciling carbon-cycle concepts, terminology, and methods. *Ecosystems*, 9(7):1041–1050, 2006.

Chen, M.; Rafique, R.; Asrar, G. R.; Bond-Lamberty, B.; Ciais, P.; Zhao, F.; Reyer, C. P. O.; Ostberg, S.; Chang, J. F.; Ito, A.; Yang, J.; Zeng, N.; Kalnay, E.; West, T.; Leng, G. Y.; Francois, L.; Munhoven, G.; Henrot, A.; Tian, H. Q.; Pan, S. F.; Nishina, K.; Viovy, N.; Morfopoulos, C.; Betts, R.; Schaphoff, S.; Steinkamp, J., and Hickler, T. Regional contribution to variability and trends of global gross primary productivity. *Environmental Research Letters*, 12(10), 2017.

Chen, Y. Z.; Xia, J. Y.; Sun, Z. G.; Li, J. L.; Luo, Y. Q.; Gang, C. C., and Wang, Z. Q. The role of residence time in diagnostic models of global carbon storage capacity: model decomposition based on a traceable scheme. *Scientific Reports*, 5, 2015.

Ciais, P.; Sabine, C.; Bala, G.; Bopp, L.; Brovkin, V.; Canadell, J.; Chhabra, A.; Defries, R.; Galloway, J.; Heimann, M.; Jones, C.; Le QueRe, C.; Myneni, R.B.; Piao, S. L., and Thornton, P. E. Carbon and other biogeochemical cycles. *Climate Change 2013: The Physical Science Basis. Contribution of Working Group I to the Fifth Assessment Report of the Intergovernmental Panel on Climate Change*, 2013. URL `http://www.ipcc.ch/pdf/assessment-report/ar5/wg1/WG1AR5_Chapter06_FINAL.pdf`.

Collatz, G. J.; Ball, J. T.; Grivet, C., and Berry, J. A. Physiological and environmental-regulation of stomatal conductance, photosynthesis and transpiration - a model that includes a laminar boundary-layer. *Agricultural and Forest Meteorology*, 54(2-4):107–136, 1991.

Cowan, I. R. and Farquhar, G. D. Stomatal function in relation to leaf metabolism and environment. *Symposia of the Society for Experimental Biology*, (31):471–505, 1977.

Cox, Peter M.; Pearson, David; Booth, Ben B.; Friedlingstein, Pierre; Huntingford, Chris; Jones, Chris D., and Luke, Catherine M. Sensitivity of tropical carbon to climate change constrained by carbon dioxide variability. *Nature*, 494(7437):341–344, 2013.

Czech, E. Atom: The atmospheric tomography mission, 2018.

Dai, A. G. and Zhao, T. B. Uncertainties in historical changes and future projections of drought. part i: estimates of historical drought changes. *Climatic Change*, 144(3):519–533, 2017.

Dalmonech, D. and Zaehle, S. Towards a more objective evaluation of modelled land-carbon trends using atmospheric co_2 and satellite-based vegetation activity observations. *Biogeosciences*, 10(6):4189–4210, 2013.

Damour, G.; Simonneau, T.; Cochard, H., and Urban, L. An overview of models of stomatal conductance at the leaf level. *Plant Cell and Environment*, 33(9):1419–1438, 2010.

Dargaville, R. J.; Heimann, M.; McGuire, A. D.; Prentice, I. C.; Kicklighter, D. W.; Joos, F.; Clein, J. S.; Esser, G.; Foley, J.; Kaplan, J.; Meier, R. A.; Melillo, J. M.; Moore, B.; Ramankutty, N.; Reichenau, T.; Schloss, A.; Sitch, S.; Tian, H.; Williams, L. J., and Wittenberg, U. Evaluation of terrestrial carbon cycle models with atmospheric co_2 measurements: Results from transient simulations considering increasing co_2, climate, and land-use effects. *Global Biogeochemical Cycles*, 16(4), 2002.

Davidson, E. A.; Janssens, I. A., and Luo, Y. Q. On the variability of respiration in terrestrial ecosystems: moving beyond q(10). *Global Change Biology*, 12(2):154–164, 2006a.

Davidson, E. A.; Richardson, A. D.; Savage, K. E., and Hollinger, D. Y. A distinct seasonal pattern of the ratio of soil respiration to total ecosystem respiration in a spruce-dominated forest. *Global Change Biology*, 12(2):230–239, 2006b.

Davis, T.W.; Prentice, I. C.; Stocker, B.; Thomas, R. T.; Whitley, R. J.; Wang, H.; Evans, B.; Gallego-Sala, A.V.; Skyes, M.T., and Cramer, W. Simple process-led algorithms for simulating habitats (splash v.1.0): Robust indices of radiation, evapotranspiration and plant-available moisture. *Geoscientific Model Develpment*, 10(2), 2016.

De Kauwe, M. G.; Medlyn, B. E.; Walker, A. P.; Zaehle, S.; Asao, S.; Guenet, B.; Harper, A. B.; Hickler, T.; Jain, A. K.; Luo, Y. Q.; Lu, X. J.; Luus, K.; Parton, W. J.; Shu, S. J.; Wang, Y. P.; Werner, C.; Xia, J. Y.; Pendall, E.; Morgan, J. A.; Ryan, E. M.; Carrillo, Y.; Dijkstra, F. A.; Zelikova, T. J., and Norby, R. J. Challenging terrestrial biosphere models with data from the long-term multifactor prairie heating and co_2 enrichment experiment. *Global Change Biology*, 23(9):3623–3645, 2017.

De Kauwe, Martin G.; Keenan, Trevor F.; Medlyn, Belinda E.; Prentice, I. Colin, and Terrer,

Cesar. Satellite based estimates underestimate the effect of co_2 fertilization on net primary productivity. *Nature Climate Change*, 6:892–893, 2016.

Delucia, E. H.; Drake, J. E.; Thomas, R. B., and Gonzalez-Meler, M. Forest carbon use efficiency: is respiration a constant fraction of gross primary production? *Global Change Biology*, 13(6):1157–1167, 2007.

Dewar, Roderick C. The correlation between plant growth and intercepted radiation: An interpretation in terms of optimal plant nitrogen content. *Annals of Botany*, 78(1):125–136, 1996.

Dlugokencky, E. and Tans, P. Noaa/esrl, 2018. URL `www.esrl.noaa.gov/gmd/ccgg/trends/`.

Dong, N.; Prentice, I. C.; Harrison, S. P.; Song, Q. H., and Zhang, Y. P. Biophysical homoeostasis of leaf temperature: A neglected process for vegetation and land-surface modelling. *Global Ecology and Biogeography*, 26(9):998–1007, 2017.

Eastman, J. Ronald; Sangermano, Florencia; Machado, Elia A.; Rogan, John, and Anyamba, Assaf. Global trends in seasonality of normalized difference vegetation index (ndvi), 1982-2011. *Remote Sensing*, 5(10):4799–4818, 2013.

Elmendorf, Sarah C.; Henry, Gregory H. R.; Hollister, Robert D.; Bjork, Robert G.; Boulanger-Lapointe, Noemie; Cooper, Elisabeth J.; Cornelissen, Johannes H. C.; Day, Thomas A.; Dorrepaal, Ellen; Elumeeva, Tatiana G.; Gill, Mike; Gould, William A.; Harte, John; Hik, David S.; Hofgaard, Annika; Johnson, David R.; Johnstone, Jill F.; Jonsdottir, Ingibjorg Svala; Jorgenson, Janet C.; Klanderud, Kari; Klein, Julia A.; Koh, Saewan; Kudo, Gaku; Lara, Mark; Levesque, Esther; Magnusson, Borgthor; May, Jeremy L.; Mercado-Diaz, Joel A.; Michelsen, Anders; Molau, Ulf; Myers-Smith, Isla H.; Oberbauer, Steven F.; Onipchenko, Vladimir G.; Rixen, Christian; Schmidt, Niels Martin; Shaver, Gaius R.; Spasojevic, Marko J.; Porhallsdottir, Pora Ellen; Tolvanen, Anne; Troxler, Tiffany; Tweedie, Craig E.; Villareal, Sandra; Wahren, Carl-Henrik; Walker, Xanthe; Webber, Patrick J.; Welker, Jeffrey M., and Wipf, Sonja. Plot-scale evidence of tundra vegetation change and links to recent summer warming. *Nature Climate Change*, 2(6):453–457, 2012.

Entin, Jared K.; Robock, Alan; Vinnikov, Konstantin Y.; Hollinger, Steven E.; Liu, Suxia, and Namkhai, A. Temporal and spatial scales of observed soil moisture variations in the extratropics. *Journal of Geophysical Research: Atmospheres*, 105(D9):11865–11877, 2000.

Evans, John. Photosynthesis and nitrogen relationships in leaves of c3 plants. 1989.

Eyring, V.; Bony, S.; Meehl, G. A.; Senior, C. A.; Stevens, B.; Stouffer, R. J., and Taylor, K. E. Overview of the coupled model intercomparison project phase 6 (cmip6) experimental design and organization. *Geoscientific Model Development*, 9(5):1937–1958, 2016.

Falge, E.; Baldocchi, D.; Tenhunen, J.; Aubinet, M.; Bakwin, P.; Berbigier, P.; Bernhofer, C.; Burba, G.; Clement, R.; Davis, K. J.; Elbers, J. A.; Goldstein, A. H.; Grelle, A.; Granier, A.; Guomundsson, J.; Hollinger, D.; Kowalski, A. S.; Katul, G.; Law, B. E.; Malhi, Y.; Meyers, T.; Monson, R. K.; Munger, J. W.; Oechel, W.; Paw, K. T.; Pilegaard, K.; Rannik, U.; Rebmann, C.; Suyker, A.; Valentini, R.; Wilson, K., and Wofsy, S. Seasonality of ecosystem respiration and gross primary production as derived from fluxnet measurements. *Agricultural and Forest Meteorology*, 113(1-4):53–74, 2002.

Farquhar, G. D.; Caemmerer, S. V., and Berry, J. A. A biochemical-model of photosynthetic co_2 assimilation in leaves of c-3 species. *Planta*, 149(1):78–90, 1980.

Fernandez-Martinez, M.; Vicca, S.; Janssens, I. A.; Ciais, P.; Obersteiner, M.; Bartrons, M.; Sardans, J.; Verger, A.; Canadell, J. G.; Chevallier, F.; Wang, X.; Bernhofer, C.; Curtis, P. S.; Gianelle, D.; Gruwald, T.; Heinesch, B.; Ibrom, A.; Knohl, A.; Laurila, T.; Law, B. E.; Limousin, J. M.; Longdoz, B.; Loustau, D.; Mammarella, I.; Matteucci, G.; Monson, R. K.; Montagnani, L.; Moors, E. J.; Munger, J. W.; Papale, D.; Piao, S. L., and Penuelas, J. Atmospheric deposition, co_2, and change in the land carbon sink. *Scientific Reports*, 7(1): 9632, 2017.

Field, C. B.; Jackson, R. B., and Mooney, H. A. Stomatal responses to increased co_2 - implications from the plant to the global-scale. *Plant Cell and Environment*, 18(10):1214–1225, 1995.

Fisher, J. B.; Huntzinger, D. N.; Schwalm, C. R., and Sitch, S. Modeling the terrestrial biosphere. *Annual Review of Environment and Resources, Vol 39*, 39(1):91–123, 2014.

Fluxnet, . Fluxnet: About data. 2018, February 2017 2017. URL `http://fluxnet.fluxdata.org/data/fluxnet2015-dataset/fullset-data-product/`.

Forkel, M.; Migliavacca, M.; Thonicke, K.; Reichstein, M.; Schaphoff, S.; Weber, U., and Carvalhais, N. Codominant water control on global interannual variability and trends in land surface phenology and greenness. *Global Change Biology*, 21(9):3414–3435, 2015.

Forkel, M.; Carvalhais, N.; Rodenbeck, C.; Keeling, R.; Heimann, M.; Thonicke, K.; Zaehle, S., and Reichstein, M. Enhanced seasonal co_2 exchange caused by amplified plant productivity in northern ecosystems. *Science*, 351(6274):696–699, 2016.

Frank, D. C.; Poulter, B.; Saurer, M.; Esper, J.; Huntingford, C.; Helle, G.; Treydte, K.; Zimmermann, N. E.; Schleser, G. H.; Ahlstrom, A.; Ciais, P.; Friedlingstein, P.; Levis, S.; Lomas, M.; Sitch, S.; Viovy, N.; Andreu-Hayles, L.; Bednarz, Z.; Berninger, F.; Boettger, T.; D'alessandro, C. M.; Daux, V.; Filot, M.; Grabner, M.; Gutierrez, E.; Haupt, M.; Hilasvuori, E.; Jungner, H.; Kalela-Brundin, M.; Krapiec, M.; Leuenberger, M.; Loader, N. J.; Marah, H.; Masson-Delmotte, V.; Pazdur, A.; Pawelczyk, S.; Pierre, M.; Planells, O.; Pukiene, R.; Reynolds-Henne, C. E.; Rinne, K. T.; Saracino, A.; Sonninen, E.; Stievenard, M.; Switsur, V. R.; Szczepanek, M.; Szychowska-Krapiec, E.; Todaro, L.; Waterhouse, J. S., and Weigl, M. Water-use efficiency and transpiration across european forests during the anthropocene. *Nature Climate Change*, 5(6):579–583, 2015.

Franks, P. J.; Adams, M. A.; Amthor, J. S.; Barbour, M. M.; Berry, J. A.; Ellsworth, D. S.; Farquhar, G. D.; Ghannoum, O.; Lloyd, J.; Mcdowell, N.; Norby, R. J.; Tissue, D. T., and Von Caemmerer, S. Sensitivity of plants to changing atmospheric co_2 concentration: from the geological past to the next century. *New Phytologist*, 197(4):1077–1094, 2013.

Friedlingstein, P.; Cox, P.; Betts, R.; Bopp, L.; Von Bloh, W.; Brovkin, V.; Cadule, P.; Doney, S.; Eby, M.; Fung, I.; Bala, G.; John, J.; Jones, C.; Joos, F.; Kato, T.; Kawamiya, M.; Knorr, W.; Lindsay, K.; Matthews, H. D.; Raddatz, T.; Rayner, P.; Reick, C.; Roeckner, E.; Schnitzler, K. G.; Schnur, R.; Strassmann, K.; Weaver, A. J.; Yoshikawa, C., and Zeng, N. Climate-carbon cycle feedback analysis: Results from the (cmip)-m-4 model intercomparison. *Journal of Climate*, 19(14):3337–3353, 2006.

Friedlingstein, P.; Meinshausen, M.; Arora, V. K.; Jones, C. D.; Anav, A.; Liddicoat, S. K., and Knutti, R. Uncertainties in cmip5 climate projections due to carbon cycle feedbacks. *Journal of Climate*, 27(2):511–526, 2014.

Friend, A. D.; Lucht, W.; Rademacher, T. T.; Keribin, R.; Betts, R.; Cadule, P.; Ciais, P.; Clark, D. B.; Dankers, R.; Falloon, P. D.; Ito, A.; Kahana, R.; Kleidon, A.; Lomas, M. R.; Nishina, K.; Ostberg, S.; Pavlick, R.; Peylin, P.; Schaphoff, S.; Vuichard, N.; Warszawski, L.; Wiltshire, A., and Woodward, F. I. Carbon residence time dominates uncertainty in terrestrial vegetation responses to future climate and atmospheric co_2. *Proceedings of the National Academy of Sciences of the United States of America*, 111(9):3280–3285, 2014.

Frouin, R. and Pinker, R. T. Estimating photosynthetically active radiation (par) at the earths surface from satellite-observations. *Remote Sensing of Environment*, 51(1):98–107, 1995.

Garbulsky, M. F.; Penuelas, J.; Papale, D.; Ardo, J.; Goulden, M. L.; Kiely, G.; Richardson, A. D.; Rotenberg, E.; Veenendaal, E. M., and Filella, I. Patterns and controls of the variability of radiation use efficiency and primary productivity across terrestrial ecosystems. *Global Ecology and Biogeography*, 19(2):253–267, 2010.

Gobron, N. and Verstraete, M. M. Lai: Leaf area index. Technical report, GTOS Secretariat, NRL, Food and Agriculture Organization of the United Nations (FAO), 2009.

Graven, H. D.; Keeling, R. F.; Piper, S. C.; Patra, P. K.; Stephens, B. B.; Wofsy, S. C.; Welp, L. R.; Sweeney, C.; Tans, P. P.; Kelley, J. J.; Daube, B. C.; Kort, E. A.; Santoni, G. W., and Bent, J. D. Enhanced seasonal exchange of co_2 by northern ecosystems since 1960. *Science*, 341(6150):1085–1089, 2013.

Gray, Josh M.; Frolking, Steve; Kort, Eric A.; Ray, Deepak K.; Kucharik, Christopher J.; Ramankutty, Navin, and Friedl, Mark A. Direct human influence on atmospheric co_2 seasonality from increased cropland productivity. *Nature*, 515(7527):398–401, 2014.

Greve, P.; Roderick, M. L., and Seneviratne, S. I. Simulated changes in aridity from the last glacial maximum to 4xco(2). *Environmental Research Letters*, 12(11), 2017.

Gu, Lianhong; Baldocchi, Dennis; Verma, Shashi B.; Black, T. A.; Vesala, Timo; Falge, Eva M.,

and Dowty, Pete R. Advantages of diffuse radiation for terrestrial ecosystem productivity. *Journal of Geophysical Research: Atmospheres*, 107(D6), 2002.

Guanter, L.; Frankenberg, C.; Dudhia, A.; Lewis, P. E.; Gomez-Dans, J.; Kuze, A.; Suto, H., and Grainger, R. G. Retrieval and global assessment of terrestrial chlorophyll fluorescence from gosat space measurements. *Remote Sensing of Environment*, 121:236–251, 2012.

Guay, K. C.; Beck, P. S. A.; Berner, L. T.; Goetz, S. J.; Baccini, A., and Buermann, W. Vegetation productivity patterns at high northern latitudes: a multi-sensor satellite data assessment. *Global Change Biology*, 20(10):3147–3158, 2014.

Gurney, K. R. and Eckels, W. J. Regional trends in terrestrial carbon exchange and their seasonal signatures. *Tellus Series B-Chemical and Physical Meteorology*, 63(3):328–339, 2011.

Gurney, K. R.; Law, R. M.; Denning, A. S.; Rayner, P. J.; Pak, B. C.; Baker, D.; Bousquet, P.; Bruhwiler, L.; Chen, Y. H.; Ciais, P.; Fung, I. Y.; Heimann, M.; John, J.; Maki, T.; Maksyutov, S.; Peylin, P.; Prather, M., and Taguchi, S. Transcom 3 inversion intercomparison: Model mean results for the estimation of seasonal carbon sources and sinks. *Global Biogeochemical Cycles*, 18(1), 2004.

Hachem, S.; Duguay, C. R., and Allard, M. Comparison of modis-derived land surface temperatures with ground surface and air temperature measurements in continuous permafrost terrain. *The Cryosphere*, 6(1):51–69, 2018.

Harris, I.; Jones, P. D.; Osborn, T. J., and Lister, D. H. Updated high-resolution grids of monthly climatic observations - the cru ts3.10 dataset. *International Journal of Climatology*, 34(3):623–642, 2014.

Harsch, Melanie A.; Hulme, Philip E.; Mcglone, Matt S., and Duncan, Richard P. Are treelines advancing? a global meta-analysis of treeline response to climate warming. *Ecology Letters*, 12(10):1040–1049, 2009.

Hashimoto, S.; Carvalhais, N.; Ito, A.; Migliavacca, M.; Nishina, K., and Reichstein, M. Global spatiotemporal distribution of soil respiration modeled using a global database. *Biogeosciences*, 12(13):4121–4132, 2015.

Haxeltine, A. and Prentice, I. C. A general model for the light-use efficiency of primary production. *Functional Ecology*, 10(5):551–561, 1996.

Hayes, D. J.; McGuire, A. D.; Kicklighter, D. W.; Gurney, K. R.; Burnside, T. J., and Melillo, J. M. Is the northern high-latitude land-based co_2 sink weakening? *Global Biogeochemical Cycles*, 25, 2011.

Heimann, M. and Korner, S. The global atmospheric tracer model tm3: Model description and users manual, release 3.8a. Technical report, Max-Planck-Institute for Biogeochemistry, 2003.

Heskel, M. A.; Atkin, O. K.; Turnbull, M. H., and Griffin, K. L. Bringing the kok effect to light: A review on the integration of daytime respiration and net ecosystem exchange. *Ecosphere*, 4(8), 2013.

Hilker, T.; Coops, N. C.; Wulder, M. A.; Black, T. A., and Guy, R. D. The use of remote sensing in light use efficiency based models of gross primary production: A review of current status and future requirements. *Science of the Total Environment*, 404(2-3):411–423, 2008.

Houghton, R. A. Biotic changes consistent with the increased seasonal amplitude of atmospheric co_2 concentrations. *Journal of Geophysical Research-Atmospheres*, 92(D4):4223–4230, 1987.

Houghton, R. A.; Davidson, E. A., and Woodwell, G. M. Missing sinks, feedbacks, and understanding the role of terrestrial ecosystems in the global carbon balance. *Global Biogeochemical Cycles*, 12(1):25–34, 1998.

Huntzinger, D. N.; Schwalm, C.; Michalak, A. M.; Schaefer, K.; King, A. W.; Wei, Y.; Jacobson, A.; Liu, S.; Cook, R. B.; Post, W. M.; Berthier, G.; Hayes, D.; Huang, M.; Ito, A.; Lei, H.; Lu, C.; Mao, J.; Peng, C. H.; Peng, S.; Poulter, B.; Riccuito, D.; Shi, X.; Tian, H.; Wang, W.; Zeng, N.; Zhao, F., and Zhu, Q. The north american carbon program multi-scale synthesis and terrestrial model intercomparison project - part 1: Overview and experimental design. *Geoscientific Model Development*, 6(6):2121–2133, 2013.

Huntzinger, D. N.; Michalak, A. M.; Schwalm, C.; Ciais, P.; King, A. W.; Fang, Y.; Schaefer, K.; Wei, Y.; Cook, R. B.; Fisher, J. B.; Hayes, D.; Huang, M.; Ito, A.; Jain, A. K.; Lei, H.;

Lu, C.; Maignan, F.; Mao, J.; Parazoo, N.; Peng, S.; Poulter, B.; Ricciuto, D.; Shi, X.; Tian, H.; Wang, W.; Zeng, N., and Zhao, F. Uncertainty in the response of terrestrial carbon sink to environmental drivers undermines carbon-climate feedback predictions. *Scientific Reports*, 7:8, 2017.

Huntzinger, D.N.; Schwalm, C.R.; Wei, Y.; Cook, R.B.; Michalak, A.M.; Schaefer, K.; Jacobson, A.R.;; Arain, M.A.; Ciais, P.; Fisher, J.B.; Hayes, D.J.; Huang, M.; Huang, S.; Ito, A.; Jain, A.K.; Lei, H.; Lu, C.; Maignan, F.; Mao, J.; Parazoo, N.; Peng, C.; Peng, S.; Poulter, B.; Ricciuto, D.M.; Tian, H.; Shi, Xiaoying; Wang, W.; Zeng, N.; Zhao, F., and Zhu, Q. Nacp mstmip: Global 0.5-deg terrestrial biosphere model outputs (version 1) in standard format., 2014.

Ilyina, T. and Friedlingstein, P. Wcrp grand challenge: Carbon feedbacks in the climate system, 2016.

Ito, A. and Oikawa, T. A simulation model of the carbon cycle in land ecosystems (sim-cycle): a description based on dry-matter production theory and plot-scale validation. *Ecological Modelling*, 151(2-3):143–176, 2002.

Ito, A.; Inatomi, M.; Huntzinger, D. N.; Schwalm, C.; Michalak, A. M.; Cook, R.; King, A. W.; Mao, J. F.; Wei, Y. X.; Mac Post, W.; Wang, W. L.; Arain, M. A.; Huang, S.; Hayes, D. J.; Ricciuto, D. M.; Shi, X. Y.; Huang, M. Y.; Lei, H. M.; Tian, H. Q.; Lu, C. Q.; Yang, J.; Tao, B.; Jain, A.; Poulter, B.; Peng, S. S.; Ciais, P.; Fisher, J. B.; Parazoo, N.; Schaefer, K.; Peng, C. H.; Zeng, N., and Zhao, F. Decadal trends in the seasonal-cycle amplitude of terrestrial co_2 exchange resulting from the ensemble of terrestrial biosphere models. *Tellus Series B-Chemical and Physical Meteorology*, 68, 2016.

Ito, Akihiko and Inatomi, Motoko. Water-use efficiency of the terrestrial biosphere: A model analysis focusing on interactions between the global carbon and water cycles. *Journal of Hydrometeorology*, 13(2):681–694, 2012.

Jain, A. K. and Yang, X. J. Modeling the effects of two different land cover change data sets on the carbon stocks of plants and soils in concert with co_2 and climate change. *Global Biogeochemical Cycles*, 19(2), 2005.

Jiang, C. Y.; Ryu, Y.; Fang, H. L.; Myneni, R.; Claverie, M., and Zhu, Z. C. Inconsistencies of interannual variability and trends in long-term satellite leaf area index products. *Global Change Biology*, 23(10):4133–4146, 2017.

Jin, M. L. and Dickinson, R. E. Land surface skin temperature climatology: benefitting from the strengths of satellite observations. *Environmental Research Letters*, 5(4), 2010.

Jung, M.; Reichstein, M.; Schwalm, C. R.; Huntingford, C.; Sitch, S.; Ahlstrom, A.; Arneth, A.; Camps-Valls, G.; Ciais, P.; Friedlingstein, P.; Gans, F.; Ichii, K.; Ain, A. K. J.; Kato, E.; Papale, D.; Poulter, B.; Raduly, B.; Rodenbeck, C.; Tramontana, G.; Viovy, N.; Wang, Y. P.; Weber, U.; Zaehle, S., and Zeng, N. Compensatory water effects link yearly global land co_2 sink changes to temperature. *Nature*, 541(7638):516–520, 2017.

Jung, Martin; Reichstein, Markus; Margolis, Hank A.; Cescatti, Alessandro; Richardson, Andrew D.; Arain, M. Altaf; Arneth, Almut; Bernhofer, Christian; Bonal, Damien; Chen, Jiquan; Gianelle, Damiano; Gobron, Nadine; Kiely, Gerald; Kutsch, Werner; Lasslop, Gitta; Law, Beverly E.; Lindroth, Anders; Merbold, Lutz; Montagnani, Leonardo; Moors, Eddy J.; Papale, Dario; Sottocornola, Matteo; Vaccari, Francesco, and Williams, Christopher. Global patterns of land-atmosphere fluxes of carbon dioxide, latent heat, and sensible heat derived from eddy covariance, satellite, and meteorological observations. *Journal of Geophysical Research-Biogeosciences*, 116, 2011.

Kattge, J. and Knorr, W. Temperature acclimation in a biochemical model of photosynthesis: a reanalysis of data from 36 species. *Plant Cell and Environment*, 30(9):1176–1190, 2007.

Keeling, C. D.; Harris, T. B., and Wilkins, E. M. Concentration of atmospheric carbon dioxide at 500 and 700 millibars. *Journal of Geophysical Research*, 73(4511).

Keeling, C. D.; Chin, J. F. S., and Whorf, T. P. Increased activity of northern vegetation inferred from atmospheric co_2 measurements. *Nature*, 382(6587):146–149, 1996a.

Keeling, C. D.; Piper, S. C.; Bacastow, R. B.; Wahlen, M.; Whorf, T. P.; Heimann, M., and Meijer, H. A. Exchanges of atmospheric co_2 and $13co_2$ with the terrestrial biosphere and oceans from 1978 to 2000. *Global aspects, SIO Reference Series*, 2001. URL `http://scrippsCO2.ucsd.edu/data/atmospheric_CO2/mlo`.

Keeling, R. F. and Manning, A. C. *Studies of Recent Changes in Atmospheric O_2 Content*, pages 385–404. Elsevier, Oxford, 2014.

Keeling, R. F.; Piper, S. C., and Heimann, M. Global and hemispheric co_2 sinks deduced from changes in atmospheric o-2 concentration. *Nature*, 381(6579):218–221, 1996b.

Keenan, T. F.; Hollinger, D. Y.; Bohrer, G.; Dragoni, D.; Munger, J. W.; Schmid, H. P., and Richardson, A. D. Increase in forest water-use efficiency as atmospheric carbon dioxide concentrations rise. *Nature*, 499(7458):324–327, 2013.

Keenan, T. F.; Prentice, I. C.; Canadell, J. G.; Williams, C. A.; Wang, H.; Raupach, M., and Collatz, G. J. Recent pause in the growth rate of atmospheric co_2 due to enhanced terrestrial carbon uptake. *Nature Communications*, 7, 2016.

Kelley, D.I.; Prentice, I. Colin; Harrison, S.P.; Wang, H.; Simard, M.; Fisher, J.B., and Willis, K.O. A comprehensive benchmarking system for evaluating global vegetation models. *Biogeosciences*, 10(5):3313–3340, 2013.

Keppel-Aleks, G.; Wennberg, P. O.; Washenfelder, R. A.; Wunch, D.; Schneider, T.; Toon, G. C.; Andres, R. J.; Blavier, J. F.; Connor, B.; Davis, K. J.; Desai, A. R.; Messerschmidt, J.; Notholt, J.; Roehl, C. M.; Sherlock, V.; Stephens, B. B.; Vay, S. A., and Wofsy, S. C. The imprint of surface fluxes and transport on variations in total column carbon dioxide. *Biogeosciences*, 9(3):875–891, 2012.

Knauer, J.; Zaehle, S.; Reichstein, M.; Medlyn, B. E.; Forkel, M.; Hagemann, S., and Werner, C. The response of ecosystem water-use efficiency to rising atmospheric co_2 concentrations: sensitivity and large-scale biogeochemical implications. *New Phytologist*, 213(4):1654–1666, 2017.

Knauer, J.; Zaehle, S.; Medlyn, B. E.; Reichstein, M.; Williams, C. A.; Migliavacca, M.; De Kauwe, M. G.; Werner, C.; Keitel, C.; Kolari, P.; Limousin, J. M., and Linderson, M. L. Towards physiologically meaningful water-use efficiency estimates from eddy covariance data. *Global Change Biology*, 24(2):694–710, 2018.

Knorr, W. and Heimann, M. Impact of drought stress and other factors on seasonal land

biosphere co_2 exchange studied through an atmospheric tracer transport model. *Tellus Series B-Chemical and Physical Meteorology*, 47(4):471–489, 1995.

Knorr, Wolfgang. Annual and interannual co_2 exchanges of the terrestrial biosphere: process-based simulations and uncertainties. *Global Ecology and Biogeography*, 9(3):225–252, 2000.

Krinner, G.; Viovy, N.; De Noblet-Ducoudre, N.; Ogee, J.; Polcher, J.; Friedlingstein, P.; Ciais, P.; Sitch, S., and Prentice, I. C. A dynamic global vegetation model for studies of the coupled atmosphere-biosphere system. *Global Biogeochemical Cycles*, 19(1), 2005.

Lasslop, G.; Reichstein, M.; Papale, D.; Richardson, A. D.; Arneth, A.; Barr, A.; Stoy, P., and Wohlfahrt, G. Separation of net ecosystem exchange into assimilation and respiration using a light response curve approach: critical issues and global evaluation. *Global Change Biology*, 16(1):187–208, 2010.

Le Quere, C.; Moriarty, R.; Andrew, R. M.; Peters, G. P.; Ciais, P.; Friedlingstein, P.; Jones, S. D.; Sitch, S.; Tans, P.; Arneth, A.; Boden, T. A.; Bopp, L.; Bozec, Y.; Canadell, J. G.; Chini, L. P.; Chevallier, F.; Cosca, C. E.; Harris, I.; Hoppema, M.; Houghton, R. A.; House, J. I.; Jain, A. K.; Johannessen, T.; Kato, E.; Keeling, R. F.; Kitidis, V.; Goldewijk, K. Klein; Koven, C.; Landa, C. S.; Landschuetzer, P.; Lenton, A.; Lima, I. D.; Marland, G.; Mathis, J. T.; Metzl, N.; Nojiri, Y.; Olsen, A.; Ono, T.; Peng, S.; Peters, W.; Pfeil, B.; Poulter, B.; Raupach, M. R.; Regnier, P.; Roedenbeck, C.; Saito, S.; Salisbury, J. E.; Schuster, U.; Schwinger, J.; Seferian, R.; Segschneider, J.; Steinhoff, T.; Stocker, B. D.; Sutton, A. J.; Takahashi, T.; Tilbrook, B.; Van Der Werf, G. R.; Viovy, N.; Wang, Y. P.; Wanninkhof, R.; Wiltshire, A., and Zeng, N. Global carbon budget 2014. *Earth System Science Data*, 7(1): 47–85, 2015.

Le Quere, C.; Andrew, R. M.; Friedlingstein, P.; Sitch, S.; Pongratz, J.; Manning, A. C.; Korsbakken, J. I.; Peters, G. P.; Canadell, J. G.; Jackson, R. B.; Boden, T. A.; Tans, P. P.; Andrews, O. D.; Arora, V. K.; Bakker, D. C. E.; Barbero, L.; Becker, M.; Betts, R. A.; Bopp, L.; Chevallier, F.; Chini, L. P.; Ciais, P.; Cosca, C. E.; Cross, J.; Currie, K.; Gasser, T.; Harris, I.; Hauck, J.; Haverd, V.; Houghton, R. A.; Hunt, C. W.; Hurtt, G.; Ilyina, T.; Jain, A. K.; Kato, E.; Kautz, M.; Keeling, R. F.; Goldewijk, K. K.; Kortzinger, A.; Landschutzer, P.; Lefevre, N.; Lenton, A.; Lienert, S.; Lima, I.; Lombardozzi, D.; Metzl, N.;

Millero, F.; Monteiro, P. M. S.; Munro, D. R.; Nabel, Jems; Nakaoka, S.; Nojiri, Y.; Padin, X. A.; Peregon, A.; Pfeil, B.; Pierrot, D.; Poulter, B.; Rehder, G.; Reimer, J.; Rodenbeck, C.; Schwinger, J.; Seferian, R.; Skjelvan, I.; Stocker, B. D.; Tian, H. Q.; Tilbrook, B.; Tubiello, F. N.; Van Der Laan-Luijkx, I. T.; Van Der Werf, G. R.; Van Heuven, S.; Viovy, N.; Vuichard, N.; Walker, A. P.; Watson, A. J.; Wiltshire, A. J.; Zaehle, S., and Zhu, D. Global carbon budget 2017. *Earth System Science Data*, 10(1):405–448, 2018.

Leakey, A. D. B.; Ainsworth, E. A.; Bernacchi, C. J.; Rogers, A.; Long, S. P., and Ort, D. R. Elevated co_2 effects on plant carbon, nitrogen, and water relations: six important lessons from face. *Journal of Experimental Botany*, 60(10):2859–2876, 2009.

Li, Hongyi; Huang, Maoyi; Wigmosta, Mark S.; Ke, Yinghai; Coleman, Andre M.; Leung, L. Ruby; Wang, Aihui, and Ricciuto, Daniel M. Evaluating runoff simulations from the community land model 4.0 using observations from flux towers and a mountainous watershed. *Journal of Geophysical Research-Atmospheres*, 116, 2011.

Litton, C. M.; Raich, J. W., and Ryan, M. G. Carbon allocation in forest ecosystems. *Global Change Biology*, 13(10):2089–2109, 2007.

Lloyd, J. and Taylor, J. A. On the temperature-dependence of soil respiration. *Functional Ecology*, 8(3):315–323, 1994.

Long, S. P.; Ainsworth, E. A.; Rogers, A., and Ort, D. R. Rising atmospheric carbon dioxide: Plants face the future. *Annual Review of Plant Biology*, 55:591–628, 2004.

Lovenduski, N. S. and Bonan, G. B. Reducing uncertainty in projections of terrestrial carbon uptake. *Environmental Research Letters*, 12(4):7, 2017.

Lu, M.; Zhou, X. H.; Yang, Q.; Li, H.; Luo, Y. Q.; Fang, C. M.; Chen, J. K.; Yang, X., and Li, B. Responses of ecosystem carbon cycle to experimental warming: a meta-analysis. *Ecology*, 94(3):726–738, 2013.

Luo, Y. Q. Terrestrial carbon-cycle feedback to climate warming. *Annual Review of Ecology Evolution and Systematics*, 38:683–712, 2007.

Luyssaert, S.; Inglima, I.; Jung, M.; Richardson, A. D.; Reichstein, M.; Papale, D.; Piao, S. L.; Schulzes, E. D.; Wingate, L.; Matteucci, G.; Aragao, L.; Aubinet, M.; Beers, C.; Bernhofer, C.; Black, K. G.; Bonal, D.; Bonnefond, J. M.; Chambers, J.; Ciais, P.; Cook, B.; Davis, K. J.; Dolman, A. J.; Gielen, B.; Goulden, M.; Grace, J.; Granier, A.; Grelle, A.; Griffis, T.; Grunwald, T.; Guidolotti, G.; Hanson, P. J.; Harding, R.; Hollinger, D. Y.; Hutyra, L. R.; Kolar, P.; Kruijt, B.; Kutsch, W.; Lagergren, F.; Laurila, T.; Law, B. E.; Le Maire, G.; Lindroth, A.; Loustau, D.; Malhi, Y.; Mateus, J.; Migliavacca, M.; Misson, L.; Montagnani, L.; Moncrieff, J.; Moors, E.; Munger, J. W.; Nikinmaa, E.; Ollinger, S. V.; Pita, G.; Rebmann, C.; Roupsard, O.; Saigusa, N.; Sanz, M. J.; Seufert, G.; Sierra, C.; Smith, M. L.; Tang, J.; Valentini, R.; Vesala, T., and Janssens, I. A. Co_2 balance of boreal, temperate, and tropical forests derived from a global database. *Global Change Biology*, 13 (12):2509–2537, 2007.

Macbean, N.; Maignan, F.; Bacour, C.; Lewis, P.; Peylin, P.; Guanter, L.; Kohler, P.; Gomez-Dans, J., and Disney, M. Strong constraint on modelled global carbon uptake using solar-induced chlorophyll fluorescence data. *Scientific Reports*, 8, 2018.

Maire, V.; Martre, P.; Kattge, J.; Gastal, F.; Esser, G.; Fontaine, S., and Soussana, J. F. The coordination of leaf photosynthesis links c and n fluxes in c-3 plant species. *Plos One*, 7(6), 2012.

Mankin, J. S.; Smerdon, J. E.; Cook, B. I.; Williams, A. P., and Seager, R. The curious case of projected twenty-first-century drying but greening in the american west. *Journal of Climate*, 30(21):8689–8710, 2017.

Mao, J. F.; Shi, X. Y.; Thornton, P. E.; Hoffman, F. M.; Zhu, Z. C., and Myneni, R. B. Global latitudinal-asymmetric vegetation growth trends and their driving mechanisms: 1982-2009. *Remote Sensing*, 5(3):1484–1497, 2013.

Mao, J. F.; Ribes, A.; Yan, B. Y.; Shi, X. Y.; Thornton, P. E.; Seferian, R.; Ciais, P.; Myneni, R. B.; Douville, H.; Piao, S. L.; Zhu, Z. C.; Dickinson, R. E.; Dai, Y. J.; Ricciuto, D. M.; Jin, M. Z.; Hoffman, F. M.; Wang, B.; Huang, M. T., and Lian, X. Human-induced greening of the northern extratropical land surface. *Nature Climate Change*, 6(10):959–963, 2016.

Mao, Jiafu; Thornton, Peter E.; Shi, Xiaoying; Zhao, Maosheng, and Post, Wilfred M. Remote sensing evaluation of clm4 gpp for the period 2000-09. *Journal of Climate*, 25(15):5327–5342, 2012.

Mccarthy, Heather R.; Oren, Ram; Finzi, Adrien C., and Johnsen, Kurt H. Canopy leaf area constrains co_2 -induced enhancement of productivity and partitioning among aboveground carbon pools. *Proceedings of the National Academy of Sciences of the United States of America*, 103(51):19356–19361, 2006.

McGuire, A. D.; Sitch, S.; Clein, J. S.; Dargaville, R.; Esser, G.; Foley, J.; Heimann, M.; Joos, F.; Kaplan, J.; Kicklighter, D. W.; Meier, R. A.; Melillo, J. M.; Moore, B.; Prentice, I. C.; Ramankutty, N.; Reichenau, T.; Schloss, A.; Tian, H.; Williams, L. J., and Wittenberg, U. Carbon balance of the terrestrial biosphere in the twentieth century: Analyses of co_2, climate and land use effects with four process-based ecosystem models. *Global Biogeochemical Cycles*, 15(1):183–206, 2001.

McGuire, A. David; Anderson, Leif G.; Christensen, Torben R.; Dallimore, Scott; Guo, Laodong; Hayes, Daniel J.; Heimann, Martin; Lorenson, Thomas D.; Macdonald, Robie W., and Roulet, Nigel. Sensitivity of the carbon cycle in the arctic to climate change. *Ecological Monographs*, 79(4):523–555, 2009.

Medlyn, B. E. Physiological basis of the light use efficiency model. *Tree Physiology*, 18(3): 167–176, 1998.

Medlyn, Belinda E.; Duursma, Remko A.; Eamus, Derek; Ellsworth, David S.; Prentice, I. Colin; Barton, Craig V. M.; Crous, Kristine Y.; De Angelis, Paolo; Freeman, Michael, and Wingate, Lisa. Reconciling the optimal and empirical approaches to modelling stomatal conductance. *Global Change Biology*, 17(6):2134–2144, 2011.

Melillo, Jerry M.; Butler, Sarah; Johnson, Jennifer; Mohan, Jacqueline; Steudler, Paul; Lux, Heidi; Burrows, Elizabeth; Bowles, Francis; Smith, Rose; Scott, Lindsay; Vario, Chelsea; Hill, Troy; Burton, Andrew; Zhou, Yu-Mei, and Tang, Jim. Soil warming, carbon-nitrogen interactions, and forest carbon budgets. *Proceedings of the National Academy of Sciences of the United States of America*, 108(23):9508–9512, 2011.

Mercado, Lina M.; Bellouin, Nicolas; Sitch, Stephen; Boucher, Olivier; Huntingford, Chris; Wild, Martin, and Cox, Peter M. Impact of changes in diffuse radiation on the global land carbon sink. *Nature*, 458(7241):1014–U87, 2009.

Michaletz, S. T.; Weiser, M. D.; Mcdowell, N. G.; Zhou, J. Z.; Kaspari, M.; Helliker, B. R., and Enquist, B. J. The energetic and carbon economic origins of leaf thermoregulation. *Nature Plants*, 2(9), 2016.

Migliavacca, M.; Reichstein, M.; Richardson, A. D.; Colombo, R.; Sutton, M. A.; Lasslop, G.; Tomelleri, E.; Wohlfahrt, G.; Carvalhais, N.; Cescatti, A.; Mahecha, M. D.; Montagnani, L.; Papale, D.; Zaehle, S.; Arain, A.; Arneth, A.; Black, T. A.; Carrara, A.; Dore, S.; Gianelle, D.; Helfter, C.; Hollinger, D.; Kutsch, W. L.; Lafleur, P. M.; Nouvellon, Y.; Rebmann, C.; Da Rocha, H. R.; Rodeghiero, M.; Roupsard, O.; Sebastia, M. T.; Seufert, G.; Soussana, J. F., and Van Der Molen, M. K. Semiempirical modeling of abiotic and biotic factors controlling ecosystem respiration across eddy covariance sites. *Global Change Biology*, 17(1): 390–409, 2011.

Mildrexler, David J.; Zhao, Maosheng, and Running, Steven W. A global comparison between station air temperatures and modis land surface temperatures reveals the cooling role of forests. *Journal of Geophysical Research: Biogeosciences*, 116(G3), 2018.

Miller, P. A. and Smith, B. Modelling tundra vegetation response to recent arctic warming. *Ambio*, 41:281–291, 2012.

Monson, R. K.; Lipson, D. L.; Burns, S. P.; Turnipseed, A. A.; Delany, A. C.; Williams, M. W., and Schmidt, S. K. Winter forest soil respiration controlled by climate and microbial community composition. *Nature*, 439(7077):711–714, 2006.

Montane, F.; Fox, A. M.; Arellano, A. F.; Macbean, N.; Alexander, M. R.; Dye, A.; Bishop, D. A.; Trouet, V.; Babst, F.; Hessl, A. E.; Pederson, N.; Blanken, P. D.; Bohrer, G.; Gough, C. M.; Litvak, M. E.; Novick, K. A.; Phillips, R. P.; Wood, J. D., and Moore, D. J. P. Evaluating the effect of alternative carbon allocation schemes in a land surface model (clm4.5) on carbon fluxes, pools, and turnover in temperate forests. *Geoscientific Model Development*, 10(9):3499–3517, 2017.

Monteith, J. L. Solar-radiation and productivity in tropical ecosystems. *Journal of Applied Ecology*, 9(3):747–766, 1972.

Murray-Tortarolo, Guillermo; Anav, Alessandro; Friedlingstein, Pierre; Sitch, Stephen; Piao, Shilong; Zhu, Zaichun; Poulter, Benjamin; Zaehle, Soenke; Ahlstrom, Anders; Lomas, Mark; Levis, Sam; Viovy, Nicholas, and Zeng, Ning. Evaluation of land surface models in reproducing satellite-derived lai over the high-latitude northern hemisphere. part i: Uncoupled dgvms. *Remote Sensing*, 5(10):4819–4838, 2013.

Myneni, R. B.; Keeling, C. D.; Tucker, C. J.; Asrar, G., and Nemani, R. R. Increased plant growth in the northern high latitudes from 1981 to 1991. *Nature*, 386(6626):698–702, 1997.

Natali, S. M.; Schuur, E. A. G.; Trucco, C.; Pries, C. E. H.; Crummer, K. G., and Lopez, A. F. B. Effects of experimental warming of air, soil and permafrost on carbon balance in alaskan tundra. *Global Change Biology*, 17(3):1394–1407, 2011.

Nemani, R. R.; Keeling, C. D.; Hashimoto, H.; Jolly, W. M.; Piper, S. C.; Tucker, C. J.; Myneni, R. B., and Running, S. W. Climate-driven increases in global terrestrial net primary production from 1982 to 1999. *Science*, 300(5625):1560–1563, 2003.

NOAA, . Esrl global monitoring division - global greenhouse gas reference network. 2016-07-05 2016. URL `https://www.esrl.noaa.gov/gmd/ccgg/trends/`.

Nobrega, S. and Grogan, P. Deeper snow enhances winter respiration from both plant-associated and bulk soil carbon pools in birch hummock tundra. *Ecosystems*, 10(3):419–431, 2007.

Norby, R. J. and Zak, D. R. Ecological lessons from free-air co_2 enrichment (face) experiments. *Annual Review of Ecology, Evolution, and Systematics, Vol 42*, 42:181–203, 2011.

Norby, R. J.; Sholtis, J. D.; Gunderson, C. A., and Jawdy, S. S. Leaf dynamics of a deciduous forest canopy: no response to elevated co_2. *Oecologia*, 136(4):574–584, 2003.

Norby, R. J.; Delucia, E. H.; Gielen, B.; Calfapietra, C.; Giardina, C. P.; King, J. S.; Ledford, J.; Mccarthy, H. R.; Moore, D. J. P.; Ceulemans, R.; De Angelis, P.; Finzi, A. C.; Karnosky, D. F.; Kubiske, M. E.; Lukac, M.; Pregitzer, K. S.; Scarascia-Mugnozza, G. E.; Schlesinger, W. H., and Oren, R. Forest response to elevated co_2 is conserved across a broad range

of productivity. *Proceedings of the National Academy of Sciences of the United States of America*, 102(50):18052–18056, 2005.

Notaro, M.; Liu, Z. Y.; Gallimore, R.; Vavrus, S. J.; Kutzbach, J. E.; Prentice, I. C., and Jacob, R. L. Simulated and observed preindustrial to modern vegetation and climate changes. *Journal of Climate*, 18(17):3650–3671, 2005.

Osakabe, Y.; Osakabe, K.; Shinozaki, K., and Tran, L. S. P. Response of plants to water stress. *Front Plant Sci*, 5:86, 2014.

Pan, Yude; Birdsey, Richard A.; Fang, Jingyun; Houghton, Richard; Kauppi, Pekka E.; Kurz, Werner A.; Phillips, Oliver L.; Shvidenko, Anatoly; Lewis, Simon L.; Canadell, Josep G.; Ciais, Philippe; Jackson, Robert B.; Pacala, Stephen W.; McGuire, A. David; Piao, Shilong; Rautiainen, Aapo; Sitch, Stephen, and Hayes, Daniel. A large and persistent carbon sink in the world's forests. *Science*, 333(6045):988–993, 2011.

Parazoo, N. C.; Bowman, K.; Fisher, J. B.; Frankenberg, C.; Jones, D. B. A.; Cescatti, A.; Perez-Priego, O.; Wohlfahrt, G., and Montagnani, L. Terrestrial gross primary production inferred from satellite fluorescence and vegetation models. *Global Change Biology*, 20(10): 3103–3121, 2014.

Patra, P. K.; Niwa, Y.; Schuck, T. J.; Brenninkmeijer, C. A. M.; Machida, T.; Matsueda, H., and Sawa, Y. Carbon balance of south asia constrained by passenger aircraft co_2 measurements. *Atmospheric Chemistry and Physics*, 11(9):4163–4175, 2011.

Peng, J.; Dan, L., and Huang, M. Sensitivity of global and regional terrestrial carbon storage to the direct co_2 effect and climate change based on the cmip5 model intercomparison. *Plos One*, 9(4), 2014.

Peng, S. S.; Ciais, P.; Chevallier, F.; Peylin, P.; Cadule, P.; Sitch, S.; Piao, S. L.; Ahlstrom, A.; Huntingford, C.; Levy, P.; Li, X. R.; Liu, Y. W.; Lomas, M.; Poulter, B.; Viovy, N.; Wang, T.; Wang, X. H.; Zaehle, S.; Zeng, N.; Zhao, F., and Zhao, H. F. Benchmarking the seasonal cycle of co_2 fluxes simulated by terrestrial ecosystem models. *Global Biogeochemical Cycles*, 29(1):46–64, 2015.

Penuelas, J.; Canadell, J. G., and Ogaya, R. Increased water-use efficiency during the 20th century did not translate into enhanced tree growth. *Global Ecology and Biogeography*, 20 (4):597–608, 2011.

Peterhansel, C.; Horst, I.; Niessen, M.; Blume, C.; Kebeish, R.; Krkcoglu, S., and Kreuzaler, F. Photorespiration. *Arabidopsis Book*, 8, 2010.

Peylin, P.; Law, R. M.; Gurney, K. R.; Chevallier, F.; Jacobson, A. R.; Maki, T.; Niwa, Y.; Patra, P. K.; Peters, W.; Rayner, P. J.; Rdenbeck, C.; Laan-Luijkx, I. T. Van Der, and Zhang, X. Global atmospheric carbon budget: results from an ensemble of atmospheric co_2 inversions. *Biogeosciences*, 10(10):6699–6720, 2013.

Peylin, P.; Bacour, C.; Macbean, N.; Leonard, S.; Rayner, P.; Kuppel, S.; Koffi, E.; Kane, A.; Maignan, F.; Chevallier, F.; Ciais, P., and Prunet, P. A new stepwise carbon cycle data assimilation system using multiple data streams to constrain the simulated land surface carbon cycle. *Geoscientific Model Development*, 9(9):3321–3346, 2016.

Piao, S. L.; Friedlingstein, P.; Ciais, P.; Viovy, N., and Demarty, J. Growing season extension and its impact on terrestrial carbon cycle in the northern hemisphere over the past 2 decades. *Global Biogeochemical Cycles*, 21(3), 2007.

Piao, S. L.; Sitch, S.; Ciais, P.; Friedlingstein, P.; Peylin, P.; Wang, X. H.; Ahlstrom, A.; Anav, A.; Canadell, J. G.; Cong, N.; Huntingford, C.; Jung, M.; Levis, S.; Levy, P. E.; Li, J. S.; Lin, X.; Lomas, M. R.; Lu, M.; Luo, Y. Q.; Ma, Y. C.; Myneni, R. B.; Poulter, B.; Sun, Z. Z.; Wang, T.; Viovy, N.; Zaehle, S., and Zeng, N. Evaluation of terrestrial carbon cycle models for their response to climate variability and to co_2 trends. *Global Change Biology*, 19 (7):2117–2132, 2013.

Piao, S. L.; Nan, H. J.; Huntingford, C.; Ciais, P.; Friedlingstein, P.; Sitch, S.; Peng, S. S.; Ahlstrom, A.; Canadell, J. G.; Cong, N.; Levis, S.; Levy, P. E.; Liu, L. L.; Lomas, M. R.; Mao, J. F.; Myneni, R. B.; Peylin, P.; Poulter, B.; Shi, X. Y.; Yin, G. D.; Viovy, N.; Wang, T.; Wang, X. H.; Zaehle, S.; Zeng, N.; Zeng, Z. Z., and Chen, A. P. Evidence for a weakening relationship between interannual temperature variability and northern vegetation activity. *Nature Communications*, 5, 2014.

Piao, S. L.; Liu, Z.; Wang, T.; Peng, S. S.; Ciais, P.; Huang, M. T.; Ahlstrom, A.; Burkhart, J. F.; Chevallier, F.; Janssens, I. A.; Jeong, S. J.; Lin, X.; Mao, J. F.; Miller, J.; Mohammat, A.; Myneni, R. B.; Penuelas, J.; Shi, X. Y.; Stohl, A.; Yao, Y. T.; Zhu, Z. C., and Tans, P. P. Weakening temperature control on the interannual variations of spring carbon uptake across northern lands. *Nature Climate Change*, 7(5):359–363, 2017.

Piao, S. L.; Liu, Z.; Wang, Y. L.; Ciais, P.; Yao, Y. T.; Peng, S.; Chevallier, F.; Friedlingstein, P.; Janssens, I. A.; Penuelas, J.; Sitch, S., and Wang, T. On the causes of trends in the seasonal amplitude of atmospheric co_2. *Global Change Biology*, 24(2):608–616, 2018.

Piao, Shilong; Friedlingstein, Pierre; Ciais, Philippe; Zhou, Liming, and Chen, Anping. Effect of climate and co_2 changes on the greening of the northern hemisphere over the past two decades. *Geophysical Research Letters*, 33(23), 2006.

Piao, Shilong; Ciais, Philippe; Friedlingstein, Pierre; Peylin, Philippe; Reichstein, Markus; Luyssaert, Sebastiaan; Margolis, Hank; Fang, Jingyun; Barr, Alan; Chen, Anping; Grelle, Achim; Hollinger, David Y.; Laurila, Tuomas; Lindroth, Anders; Richardson, Andrew D., and Vesala, Timo. Net carbon dioxide losses of northern ecosystems in response to autumn warming. *Nature*, 451(7174):49–U3, 2008.

Pielke, R. A.; Pitman, A.; Niyogi, D.; Mahmood, R.; Mcalpine, C.; Hossain, F.; Goldewijk, K. K.; Nair, U.; Betts, R.; Fall, S.; Reichstein, M.; Kabat, P., and De Noblet, N. Land use/land cover changes and climate: modeling analysis and observational evidence. *Wiley Interdisciplinary Reviews-Climate Change*, 2(6):828–850, 2011.

Poorter, Hendrik; Niklas, Karl J.; Reich, Peter B.; Oleksyn, Jacek; Poot, Pieter, and Mommer, Liesje. Biomass allocation to leaves, stems and roots: meta-analyses of interspecific variation and environmental control. *New Phytologist*, 193(1):30–50, 2012.

Prentice, I. C. and Thomas, R. T. Development and validation of a global gpp/npp model using meris and sentinel-3 data (terra-p). 2017. URL `https://Terra-P.vito.be/sites/Terra-P.vito.be/files/Terra-P_atbdv1_i2.00.pdf`.

Prentice, I. C.; Dong, N.; Gleason, S. M.; Maire, V., and Wright, I. J. Balancing the costs of

carbon gain and water transport: testing a new theoretical framework for plant functional ecology. *Ecology Letters*, 17(1):82–91, 2014.

Prentice, I. C.; Liang, X.; Medlyn, B. E., and Wang, Y. P. Reliable, robust and realistic: the three r's of next-generation land-surface modelling. *Atmospheric Chemistry and Physics*, 15 (10):5987–6005, 2015.

Randerson, J. T.; Thompson, M. V.; Conway, T. J.; Fung, I. Y., and Field, C. B. The contribution of terrestrial sources and sinks to trends in the seasonal cycle of atmospheric carbon dioxide. *Global Biogeochemical Cycles*, 11(4):535–560, 1997.

Rayner, P. J.; Stavert, A.; Scholze, M.; Ahlstrom, A.; Allison, C. E., and Law, R. M. Recent changes in the global and regional carbon cycle: analysis of first-order diagnostics. *Biogeosciences*, 12(3):835–844, 2015.

Reich, P. B.; Sendall, K. M.; Stefanski, A.; Wei, X. R.; Rich, R. L., and Montgomery, R. A. Boreal and temperate trees show strong acclimation of respiration to warming. *Nature*, 531 (7596):633–636, 2016.

Reichstein, M.; Falge, E.; Baldocchi, D.; Papale, D.; Aubinet, M.; Berbigier, P.; Bernhofer, C.; Buchmann, N.; Gilmanov, T.; Granier, A.; Grunwald, T.; Havrankova, K.; Ilvesniemi, H.; Janous, D.; Knohl, A.; Laurila, T.; Lohila, A.; Loustau, D.; Matteucci, G.; Meyers, T.; Miglietta, F.; Ourcival, J. M.; Pumpanen, J.; Rambal, S.; Rotenberg, E.; Sanz, M.; Tenhunen, J.; Seufert, G.; Vaccari, F.; Vesala, T.; Yakir, D., and Valentini, R. On the separation of net ecosystem exchange into assimilation and ecosystem respiration: review and improved algorithm. *Global Change Biology*, 11(9):1424–1439, 2005.

Reichstein, M.; Bahn, M.; Mahecha, M. D.; Kattge, J., and Baldocchi, D. D. Linking plant and ecosystem functional biogeography. *Proceedings of the National Academy of Sciences of the United States of America*, 111(38):13697–13702, 2014.

Reyes-Fox, Melissa; Steltzer, Heidi; Trlica, M. J.; Mcmaster, Gregory S.; Andales, Allan A.; Lecain, Dan R., and Morgan, Jack A. Elevated co_2 further lengthens growing season under warming conditions. *Nature*, 510(7504):259, 2014.

Ricciuto, Daniel M.; King, Anthony W.; Dragoni, D., and Post, Wilfred M. Parameter and prediction uncertainty in an optimized terrestrial carbon cycle model: Effects of constraining variables and data record length. *Journal of Geophysical Research-Biogeosciences*, 116, 2011.

Richardson, A. D.; Anderson, R. S.; Arain, M. A.; Barr, A. G.; Bohrer, G.; Chen, G. S.; Chen, J. M.; Ciais, P.; Davis, K. J.; Desai, A. R.; Dietze, M. C.; Dragoni, D.; Garrity, S. R.; Gough, C. M.; Grant, R.; Hollinger, D. Y.; Margolis, H. A.; Mccaughey, H.; Migliavacca, M.; Monson, R. K.; Munger, J. W.; Poulter, B.; Raczka, B. M.; Ricciuto, D. M.; Sahoo, A. K.; Schaefer, K.; Tian, H. Q.; Vargas, R.; Verbeeck, H.; Xiao, J. F., and Xue, Y. K. Terrestrial biosphere models need better representation of vegetation phenology: results from the north american carbon program site synthesis. *Global Change Biology*, 18(2):566–584, 2012.

Roedenbeck, C.; Houweling, S.; Gloor, M., and Heimann, M. Time-dependent atmospheric co_2 inversions based on interannually varying tracer transport. *Tellus Series B Chemical and Physical Meteorology*, 55B(2):488–497, 2003.

Rogers, Alistair; Medlyn, Belinda E.; Dukes, Jeffrey S.; Bonan, Gordon; Caemmerer, Susanne Von; Dietze, Michael C.; Kattge, Jens; Leakey, Andrew D. B.; Mercado, Lina M.; Niinemets, lo; Prentice, I. Colin; Serbin, Shawn P.; Sitch, Stephen; Way, Danielle A., and Zaehle, Snke. A roadmap for improving the representation of photosynthesis in earth system models. *New Phytologist*, 213(1):22–42, 2017.

Ruimy, A.; Kergoat, L.; Bondeau, A., and Participants Potsdam, N. P. P. Model Intercomparison. Comparing global models of terrestrial net primary productivity (npp): analysis of differences in light absorption and light-use efficiency. *Global Change Biology*, 5:56–64, 1999.

Running, S. W.; Nemani, R. R.; Heinsch, F. A.; Zhao, M. S.; Reeves, M., and Hashimoto, H. A continuous satellite-derived measure of global terrestrial primary production. *Bioscience*, 54(6):547–560, 2004.

Ryan, E. M.; Ogle, K.; Peltier, D.; Walker, A. P.; De Kauwe, M. G.; Medlyn, B. E.; Williams, D. G.; Parton, W.; Asao, S.; Guenet, B.; Harper, A. B.; Lu, X. J.; Luus, K. A.; Zaehle, S.; Shu, S. J.; Werner, C.; Xia, J. Y., and Pendall, E. Gross primary production responses to

warming, elevated co_2, and irrigation: quantifying the drivers of ecosystem physiology in a semiarid grassland. *Global Change Biology*, 23(8):3092–3106, 2017.

Ryan, M. G. and Law, B. E. Interpreting, measuring, and modeling soil respiration. *Biogeochemistry*, 73(1):3–27, 2005.

Saurer, M.; Spahni, R.; Frank, D. C.; Joos, F.; Leuenberger, M.; Loader, N. J.; Mccarroll, D.; Gagen, M.; Poulter, B.; Siegwolf, R. T. W.; Andreu-Hayles, L.; Boettger, T.; Linan, I. D.; Fairchild, I. J.; Friedrich, M.; Gutierrez, E.; Haupt, M.; Hilasvuori, E.; Heinrich, I.; Helle, G.; Grudd, H.; Jalkanen, R.; Levanic, T.; Linderholm, H. W.; Robertson, I.; Sonninen, E.; Treydte, K.; Waterhouse, J. S.; Woodley, E. J.; Wynn, P. M., and Young, G. H. F. Spatial variability and temporal trends in water-use efficiency of european forests. *Global Change Biology*, 20(12):3700–3712, 2014.

Sawa, Y.; Machida, T., and Matsueda, H. Aircraft observation of the seasonal variation in the transport of co_2 in the upper atmosphere. *Journal of Geophysical Research-Atmospheres*, 117, 2012.

Schaefer, K.; Schwalm, C. R.; Williams, C.; Arain, M. A.; Barr, A.; Chen, J. M.; Davis, K. J.; Dimitrov, D.; Hilton, T. W.; Hollinger, D. Y.; Humphreys, E.; Poulter, B.; Raczka, B. M.; Richardson, A. D.; Sahoo, A.; Thornton, P.; Vargas, R.; Verbeeck, H.; Anderson, R.; Baker, I.; Black, T. A.; Bolstad, P.; Chen, J. Q.; Curtis, P. S.; Desai, A. R.; Dietze, M.; Dragoni, D.; Gough, C.; Grant, R. F.; Gu, L. H.; Jain, A.; Kucharik, C.; Law, B.; Liu, S. G.; Lokipitiya, E.; Margolis, H. A.; Matamala, R.; Mccaughey, J. H.; Monson, R.; Munger, J. W.; Oechel, W.; Peng, C. H.; Price, D. T.; Ricciuto, D.; Riley, W. J.; Roulet, N.; Tian, H. Q.; Tonitto, C.; Torn, M.; Weng, E. S., and Zhou, X. L. A model-data comparison of gross primary productivity: Results from the north american carbon program site synthesis. *Journal of Geophysical Research-Biogeosciences*, 117:15, 2012.

Schaefer, Kevin; Collatz, G. James; Tans, Pieter; Denning, A. Scott; Baker, Ian; Berry, Joe; Prihodko, Lara; Suits, Neil, and Philpott, Andrew. Combined simple biosphere/carnegie-ames-stanford approach terrestrial carbon cycle model. *Journal of Geophysical Research-Biogeosciences*, 113(G3), 2008.

Schimel, D.; Stephens, B. B., and Fisher, J. B. Effect of increasing co_2 on the terrestrial carbon cycle. *Proceedings of the National Academy of Sciences of the United States of America*, 112 (2):436–441, 2015.

Schwalm, C. R.; Williams, C. A.; Schaefer, K.; Arneth, A.; Bonal, D.; Buchmann, N.; Chen, J. Q.; Law, B. E.; Lindroth, A.; Luyssaert, S.; Reichstein, M., and Richardson, A. D. Assimilation exceeds respiration sensitivity to drought: A fluxnet synthesis. *Global Change Biology*, 16(2):657–670, 2010.

Schwalm, Christopher R.; Huntzinger, Deborah N.; Fisher, Joshua B.; Michalak, Anna M.; Bowman, Kevin; Ciais, Philippe; Cook, Robert; El-Masri, Bassil; Hayes, Daniel; Huang, Maoyi; Ito, Akihiko; Jain, Atul; King, Anthony W.; Lei, Huimin; Liu, Junjie; Lu, Chaoqun; Mao, Jiafu; Peng, Shushi; Poulter, Benjamin; Ricciuto, Daniel; Schaefer, Kevin; Shi, Xiaoying; Tao, Bo; Tian, Hanqin; Wang, Weile; Wei, Yaxing; Yang, Jia, and Zeng, Ning. Toward "optimal" integration of terrestrial biosphere models. *Geophysical Research Letters*, 42(11): 4418–4428, 2015.

Sellers, P. J. Canopy reflectance, photosynthesis and transpiration. *International Journal of Remote Sensing*, 6(8):1335–1372, 1985.

Shi, Xiaoying; Mao, Jiafu; Thornton, Peter E.; Hoffman, Forrest M., and Post, Wilfred M. The impact of climate, co_2, nitrogen deposition and land use change on simulated contemporary global river flow. *Geophysical Research Letters*, 38, 2011.

Sitch, S.; Smith, B.; Prentice, I. C.; Arneth, A.; Bondeau, A.; Cramer, W.; Kaplan, J. O.; Levis, S.; Lucht, W.; Sykes, M. T.; Thonicke, K., and Venevsky, S. Evaluation of ecosystem dynamics, plant geography and terrestrial carbon cycling in the lpj dynamic global vegetation model. *Global Change Biology*, 9(2):161–185, 2003.

Sitch, S.; Friedlingstein, P.; Gruber, N.; Jones, S. D.; Murray-Tortarolo, G.; Ahlstrom, A.; Doney, S. C.; Graven, H.; Heinze, C.; Huntingford, C.; Levis, S.; Levy, P. E.; Lomas, M.; Poulter, B.; Viovy, N.; Zaehle, S.; Zeng, N.; Arneth, A.; Bonan, G.; Bopp, L.; Canadell, J. G.; Chevallier, F.; Ciais, P.; Ellis, R.; Gloor, M.; Peylin, P.; Piao, S. L.; Le Quere, C.;

Smith, B.; Zhu, Z., and Myneni, R. Recent trends and drivers of regional sources and sinks of carbon dioxide. *Biogeosciences*, 12(3):653–679, 2015.

Skillman, J. B. Quantum yield variation across the three pathways of photosynthesis: not yet out of the dark. *Journal of Experimental Botany*, 59(7):1647–1661, 2008.

Slayback, D. A.; Pinzon, J. E.; Los, S. O., and Tucker, C. J. Northern hemisphere photosynthetic trends 1982-99. *Global Change Biology*, 9(1):1–15, 2003.

Slevin, D.; Tett, S. F. B., and Williams, M. Multi-site evaluation of the jules land surface model using global and local data. *Geoscientific Model Development*, 8(2):295–316, 2015.

Smith, K.; Biederman, J. A.; Scott, R. L.; Moore, D. J. P.; He, M.; Kimball, J. S.; Yan, D.; Hudson, A.; Barnes, M. L.; Macbean, N.; Fox, A. M., and Litvak, M. E. Chlorophyll fluorescence better captures seasonal and interannual gross primary productivity dynamics across dryland ecosystems of southwestern north america. *Geophysical Research Letters*, 45 (2):748–757, 2018.

Smith, W. Kolby; Reed, Sasha C.; Cleveland, Cory C.; Ballantyne, Ashley P.; Anderegg, William R. L.; Wieder, William R.; Liu, Yi Y., and Running, Steven W. Large divergence of satellite and earth system model estimates of global terrestrial co_2 fertilization. *Nature Climate Change*, 6(3):306–310, 2016.

Stein, U. and Alpert, P. Factor separation in numerical simulations. *Journal of the Atmospheric Sciences*, 50(14):2107–2115, 1993.

Stephens, B. B.; Gurney, K. R.; Tans, P. P.; Sweeney, C.; Peters, W.; Bruhwiler, L.; Ciais, P.; Ramonet, M.; Bousquet, P.; Nakazawa, T.; Aoki, S.; Machida, T.; Inoue, G.; Vinnichenko, N.; Lloyd, J.; Jordan, A.; Heimann, M.; Shibistova, O.; Langenfelds, R. L.; Steele, L. P.; Francey, R. J., and Denning, A. S. Weak northern and strong tropical land carbon uptake from vertical profiles of atmospheric co(2). *Science*, 316(5832):1732–1735, 2007.

Still, C. J.; Berry, J. A.; Collatz, G. J., and Defries, R. S. Global distribution of c-3 and c-4 vegetation: Carbon cycle implications. *Global Biogeochemical Cycles*, 17(1), 2003.

Stocker, Benjamin; Zscheischler, Jakob;; Keenan, Trevor;; Prentice, Iain;, and Peuelas, Josep. Quantifying soil moisture impacts on light use efficiency across biomes. *New Phytologist*, 218: 1430–1449, 2018.

Suseela, Vidya; Conant, Richard T.; Wallenstein, Matthew D., and Dukes, Jeffrey S. Effects of soil moisture on the temperature sensitivity of heterotrophic respiration vary seasonally in an oldfield climate change experiment. 2011.

Suyker, Andrew E. and Verma, Shashi B. Yearround observations of the net ecosystem exchange of carbon dioxide in a native tallgrass prairie. *Global Change Biology*, 7(3):279–289, 2001.

Swann, Abigail L. S.; Hoffman, Forrest M.; Koven, Charles D., and Randerson, James T. Plant responses to increasing co_2 reduce estimates of climate impacts on drought severity. 2016.

Sweeney, C.; Karion, A.; Wolter, S.; Newberger, T.; Guenther, D.; Higgs, J. A.; Andrews, A. E.; Lang, P. M.; Neff, D.; Dlugokencky, E.; Miller, J. B.; Montzka, S. A.; Miller, B. R.; Masarie, K. A.; Biraud, S. C.; Novelli, P. C.; Crotwell, M.; Crotwell, A. M.; Thoning, K., and Tans, P. P. Seasonal climatology of co_2 across north america from aircraft measurements in the noaa/esrl global greenhouse gas reference network. *Journal of Geophysical Research-Atmospheres*, 120(10):5155–5190, 2015.

Taylor, K. E.; Stouffer, R. J., and Meehl, G. A. An overview of cmip5 and the experiment design. *Bulletin of the American Meteorological Society*, 93(4):485–498, 2012.

Terrer, C.; Vicca, S.; Hungate, B. A.; Phillips, R. P., and Prentice, I. C. Mycorrhizal association as a primary control of the co_2 fertilization effect. *Science*, 353(6294):72–74, 2016.

Terrer, C.; Vicca, S.; Stocker, B. D.; Hungate, B. A.; Phillips, R. P.; Reich, P. B.; Finzi, A. C., and Prentice, I. C. Ecosystem responses to elevated co_2 governed by plant-soil interactions and the cost of nitrogen acquisition. *New Phytologist*, 217(2):507–522, 2018.

Thomas, R. T.; Prentice, L. C.; Graven, H.; Ciais, P.; Fisher, J. B.; Hayes, D. J.; Huang, M. Y.; Huntzinger, D. N.; Ito, A.; Jain, A.; Mao, J. F.; Michalak, A. M.; Peng, S. S.; Poulter, B.; Ricciuto, D. M.; Shi, X. Y.; Schwalm, C.; Tian, H. Q., and Zeng, N. Increased light-use efficiency in northern terrestrial ecosystems indicated by co_2 and greening observations. *Geophysical Research Letters*, 43(21):11339–11349, 2016.

Thornton, P. E.; Law, B. E.; Gholz, H. L.; Clark, K. L.; Falge, E.; Ellsworth, D. S.; Golstein, A. H.; Monson, R. K.; Hollinger, D.; Falk, M.; Chen, J., and Sparks, J. P. Modeling and measuring the effects of disturbance history and climate on carbon and water budgets in evergreen needleleaf forests. *Agricultural and Forest Meteorology*, 113(1-4):185–222, 2002.

Tian, H.; Melillo, J. M.; Kicklighter, D. W.; McGuire, A. D., and Helfrich, J. The sensitivity of terrestrial carbon storage to historical climate variability and atmospheric co_2 in the united states. *Tellus Series B-Chemical and Physical Meteorology*, 51(2):414–452, 1999.

Tian, Hanqin; Xu, Xiaofeng; Lu, Chaoqun; Liu, Mingliang; Ren, Wei; Chen, Guangsheng; Melillo, Jerry, and Liu, Jiyuan. Net exchanges of co_2, ch4, and n2o between china's terrestrial ecosystems and the atmosphere and their contributions to global climate warming. *Journal of Geophysical Research-Biogeosciences*, 116, 2011.

Tian, Hanqin; Chen, Guangsheng; Zhang, Chi; Liu, Mingliang; Sun, Ge; Chappelka, Arthur; Ren, Wei; Xu, Xiaofeng; Lu, Chaoqun; Pan, Shufen; Chen, Hua; Hui, Dafeng; Mcnulty, Steven; Lockaby, Graeme, and Vance, Eric. Century-scale responses of ecosystem carbon storage and flux to multiple environmental changes in the southern united states. *Ecosystems*, 15(4):674–694, 2012.

Trumbore, S. Carbon respired by terrestrial ecosystems - recent progress and challenges. *Global Change Biology*, 12(2):141–153, 2006.

Turner, D. P.; Ritts, W. D.; Cohen, W. B.; Maeirsperger, T. K.; Gower, S. T.; Kirschbaum, A. A.; Running, S. W.; Zhao, M. S.; Wofsy, S. C.; Dunn, A. L.; Law, B. E.; Campbell, J. L.; Oechel, W. C.; Kwon, H. J.; Meyers, T. P.; Small, E. E.; Kurc, S. A., and Gamon, J. A. Site-level evaluation of satellite-based global terrestrial gross primary production and net primary production monitoring. *Global Change Biology*, 11(4):666–684, 2005.

Verbyla, David. Browning boreal forests of western north america. *Environmental Research Letters*, 6(4):041003, 2011.

Wang, D.; Heckathorn, S. A.; Wang, X. Z., and Philpott, S. M. A meta-analysis of plant physiological and growth responses to temperature and elevated co_2. *Oecologia*, 169(1):1–13, 2012.

Wang, H.; Prentice, I. C., and Davis, T. W. Biophsyical constraints on gross primary production by the terrestrial biosphere. *Biogeosciences*, 11(20):5987–6001, 2014.

Wang, H.; Prentice, I. C.; Keenan, T. F.; Davis, T. W.; Wright, I. J.; Cornwell, W. K.; Evans, B. J., and Peng, C. H. Towards a universal model for carbon dioxide uptake by plants. *Nature Plants*, 3(9):734–741, 2017.

Way, Danielle A. and Oren, Ram. Differential responses to changes in growth temperature between trees from different functional groups and biomes: a review and synthesis of data. *Tree Physiology*, 30(6):669–688, 2010.

Weedon, G. P.; Gomes, S.; Viterbo, P.; Shuttleworth, W. J.; Blyth, E.; Oesterle, H.; Adam, J. C.; Bellouin, N.; Boucher, O., and Best, M. Creation of the watch forcing data and its use to assess global and regional reference crop evaporation over land during the twentieth century. *Journal of Hydrometeorology*, 12(5):823–848, 2011.

Weedon, G. P.; Balsamo, G.; Bellouin, N.; Gomes, S.; Best, M. J., and Viterbo, P. The wfdei meteorological forcing data set: Watch forcing data methodology applied to era-interim reanalysis data. *Water Resources Research*, 50(9):7505–7514, 2014.

Wehr, R.; Munger, J. W.; Mcmanus, J. B.; Nelson, D. D.; Zahniser, M. S.; Davidson, E. A.; Wofsy, S. C., and Saleska, S. R. Seasonality of temperate forest photosynthesis and daytime respiration. *Nature*, 534(7609):680–683, 2016.

Wei, Y.; Liu, S.; Huntzinger, D. N.; Michalak, A. M.; Viovy, N.; Post, W. M.; Schwalm, C. R.; Schaefer, K.; Jacobson, A. R.; Lu, C.; Tian, H.; Ricciuto, D. M.; Cook, R. B.; Mao, J., and Shi, X. The north american carbon program multi-scale synthesis and terrestrial model intercomparison project - part 2: Environmental driver data. *Geoscientific Model Development*, 7(6):2875–2893, 2014.

Welp, L. R.; Keeling, R. F.; Meijer, H. A. J.; Bollenbacher, A. F.; Piper, S. C.; Yoshimura, K.; Francey, R. J.; Allison, C. E., and Wahlen, M. Interannual variability in the oxygen isotopes of atmospheric co_2 driven by el nino. *Nature*, 477(7366):579–582, 2011.

Welp, L. R.; Patra, P. K.; Rodenbeck, C.; Nemani, R.; Bi, J.; Piper, S. C., and Keeling, R. F. Increasing summer net co_2 uptake in high northern ecosystems inferred from atmospheric

inversions and comparisons to remote-sensing ndvi. *Atmospheric Chemistry and Physics*, 16 (14):9047–9066, 2016.

Wenzel, S.; Cox, P. M.; Eyring, V., and Friedlingstein, P. Projected land photosynthesis constrained by changes in the seasonal cycle of atmospheric co_2. *Nature*, 538(7626):499–501, 2016.

Wieder, William R.; Cleveland, Cory C.; Smith, W. Kolby, and Todd-Brown, Katherine. Future productivity and carbon storage limited by terrestrial nutrient availability. *Nature Geoscience*, 8(6):441–U35, 2015.

Wild, M. Decadal changes in radiative fluxes at land and ocean surfaces and their relevance for global warming. *Wiley Interdisciplinary Reviews-Climate Change*, 7(1):91–107, 2016.

Wofsy, S. C.; Team, Hippo Sci; Cooperating Modellers, Team, and Satellite, Team. Hiaper pole-to-pole observations (hippo): fine-grained, global-scale measurements of climatically important atmospheric gases and aerosols. *Philosophical Transactions of the Royal Society a-Mathematical Physical and Engineering Sciences*, 369(1943):2073–2086, 2011.

Wright, I. J.; Reich, P. B., and Westoby, M. Least-cost input mixtures of water and nitrogen for photosynthesis. *American Naturalist*, 161(1):98–111, 2003.

Wright, I. J.; Reich, P. B.; Westoby, M.; Ackerly, D. D.; Baruch, Z.; Bongers, F.; Cavender-Bares, J.; Chapin, T.; Cornelissen, J. H. C.; Diemer, M.; Flexas, J.; Garnier, E.; Groom, P. K.; Gulias, J.; Hikosaka, K.; Lamont, B. B.; Lee, T.; Lee, W.; Lusk, C.; Midgley, J. J.; Navas, M. L.; Niinemets, U.; Oleksyn, J.; Osada, N.; Poorter, H.; Poot, P.; Prior, L.; Pyankov, V. I.; Roumet, C.; Thomas, S. C.; Tjoelker, M. G.; Veneklaas, E. J., and Villar, R. The worldwide leaf economics spectrum. *Nature*, 428(6985):821–827, 2004.

Wullschleger, S. D.; Epstein, H. E.; Box, E. O.; Euskirchen, E. S.; Goswami, S.; Iversen, C. M.; Kattge, J.; Norby, R. J.; Van Bodegom, P. M., and Xu, X. *Plant functional types in Earth system models: past experiences and future directions for application of dynamic vegetation models in high-latitude ecosystems*, volume 114, pages 1–16. 2014.

Xu, L.; Myneni, R. B.; F. S.Chapin, Iii; Callaghan, T. V.; Pinzon, J. E.; Tucker, C. J.; Zhu, Z.; Bi, J.; Ciais, P.; Tommervik, H.; Euskirchen, E. S.; Forbes, B. C.; Piao, S. L.; Anderson,

B. T.; Ganguly, S.; Nemani, R. R.; Goetz, S. J.; Beck, P. S. A.; Bunn, A. G.; Cao, C., and Stroeve, J. C. Temperature and vegetation seasonality diminishment over northern lands. *Nature Climate Change*, 3(6):581–586, 2013.

Xu, M. and Shang, H. Contribution of soil respiration to the global carbon equation. *Journal of Plant Physiology*, 203:16–28, 2016.

Yuan, W. P.; Cai, W. W.; Xia, J. Z.; Chen, J. Q.; Liu, S. G.; Dong, W. J.; Merbold, L.; Law, B.; Arain, A.; Beringer, J.; Bernhofer, C.; Black, A.; Blanken, P. D.; Cescatti, A.; Chen, Y.; Francois, L.; Gianelle, D.; Janssens, I. A.; Jung, M.; Kato, T.; Kiely, G.; Liu, D.; Marcolla, B.; Montagnani, L.; Raschi, A.; Roupsard, O.; Varlagin, A., and Wohlfahrt, G. Global comparison of light use efficiency models for simulating terrestrial vegetation gross primary production based on the la thuile database. *Agricultural and Forest Meteorology*, 192:108–120, 2014.

Yuan, Y. G.; Ge, L. T.; Yang, H. S., and Ren, W. Z. A meta-analysis of experimental warming effects on woody plant growth and photosynthesis in forests. *Journal of Forestry Research*, 29(3):727–733, 2018.

Zaehle, S. and Dalmonech, D. Carbon-nitrogen interactions on land at global scales: current understanding in modelling climate biosphere feedbacks. *Current Opinion in Environmental Sustainability*, 3(5):311–320, 2011.

Zaehle, S.; Medlyn, B. E.; De Kauwe, M. G.; Walker, A. P.; Dietze, M. C.; Hickler, T.; Luo, Y. Q.; Wang, Y. P.; El-Masri, B.; Thornton, P.; Jain, A.; Wang, S. S.; Warlind, D.; Weng, E. S.; Parton, W.; Iversen, C. M.; Gallet-Budynek, A.; Mccarthy, H.; Finzi, A. C.; Hanson, P. J.; Prentice, I. C.; Oren, R., and Norby, R. J. Evaluation of 11 terrestrial carbon-nitrogen cycle models against observations from two temperate free-air co_2 enrichment studies. *New Phytologist*, 202(3):803–822, 2014.

Zeng, N.; Mariotti, A., and Wetzel, P. Terrestrial mechanisms of interannual co(2) variability. *Global Biogeochemical Cycles*, 19(1), 2005.

Zeng, Ning; Zhao, Fang; Collatz, George J.; Kalnay, Eugenia; Salawitch, Ross J.; West, Tris-

tram O., and Guanter, Luis. Agricultural green revolution as a driver of increasing atmospheric co_2 seasonal amplitude. *Nature*, 515(7527):394–397, 2014.

Zhang, Q.; Wang, Y. P.; Matear, R. J.; Pitman, A. J., and Dai, Y. J. Nitrogen and phosphorous limitations significantly reduce future allowable co_2 emissions. *Geophysical Research Letters*, 41(2):632–637, 2014.

Zhang, T.; Barry, R. G.; Knowles, K.; Ling, F., and Armstrong, R. L. Distribution of seasonally and perennially frozen ground in the northern hemisphere. *Permafrost*, pages 1289–1294, 2003.

Zhao, F. and Zeng, N. Continued increase in atmospheric co_2 seasonal amplitude in the 21st century projected by the cmip5 earth system models. *Earth System Dynamics*, 5(2):423–439, 2014.

Zhao, F.; Zeng, N.; Akihiko, I.; Asrar, G.; Friedlingstein, P.; Jain, A.; Kalnay, E.; Kato, E.; Koven, C. D.; Poulter, B.; Rafique, R.; Sitch, S.; Shu, S.; Stocker, B.; Viovy, N.; Wiltshire, A., and Zaehle, S. Role of co_2, climate and land use in regulating the seasonal amplitude increase of carbon fluxes in terrestrial ecosystems: a multimodel analysis. *Biogeosciences Discuss.*, 2016:1–32, 2016.

Zhou, L. M.; Tucker, C. J.; Kaufmann, R. K.; Slayback, D.; Shabanov, N. V., and Myneni, R. B. Variations in northern vegetation activity inferred from satellite data of vegetation index during 1981 to 1999. *Journal of Geophysical Research-Atmospheres*, 106(D17):20069–20083, 2001.

Zhu, Z. C.; Bi, J.; Pan, Y. Z.; Ganguly, S.; Anav, A.; Xu, L.; Samanta, A.; Piao, S. L.; Nemani, R. R., and Myneni, R. B. Global data sets of vegetation leaf area index (lai)3g and fraction of photosynthetically active radiation (fpar)3g derived from global inventory modeling and mapping studies (gimms) normalized difference vegetation index (ndvi3g) for the period 1981 to 2011. *Remote Sensing*, 5(2):927–948, 2013.

Zhu, Z. C.; Piao, S. L.; Myneni, R. B.; Huang, M. T.; Zeng, Z. Z.; Canadell, J. G.; Ciais, P.; Sitch, S.; Friedlingstein, P.; Arneth, A.; Cao, C. X.; Cheng, L.; Kato, E.; Koven, C.; Li, Y.; Lian, X.; Liu, Y. W.; Liu, R. G.; Mao, J. F.; Pan, Y. Z.; Peng, S. S.; Penuelas, J.; Poulter,

B.; Pugh, T. A. M.; Stocker, B. D.; Viovy, N.; Wang, X. H.; Wang, Y. P.; Xiao, Z. Q.; Yang, H.; Zaehle, S., and Zeng, N. Greening of the earth and its drivers. *Nature Climate Change*, 6(8):791–+, 2016.

Zimov, S. A.; Davidov, S. P.; Zimova, G. M.; Davidova, A. I.; Chapin, F. S.; Chapin, M. C., and Reynolds, J. F. Contribution of disturbance to increasing seasonal amplitude of atmospheric co_2. *Science*, 284(5422):1973–1976, 1999.

Zscheischler, Jakob; Michalak, Anna M.; Schwalm, Christopher; Mahecha, Miguel D.; Huntzinger, Deborah N.; Reichstein, Markus; Berthier, Gwenaelle; Ciais, Philippe; Cook, Robert B.; El-Masri, Bassil; Huang, Maoyi; Ito, Akihiko; Jain, Atul; King, Anthony; Lei, Huimin; Lu, Chaoqun; Mao, Jiafu; Peng, Shushi; Poulter, Benjamin; Ricciuto, Daniel; Shi, Xiaoying; Tao, Bo; Tian, Hanqin; Viovy, Nicolas; Wang, Weile; Wei, Yaxing; Yang, Jia, and Zeng, Ning. Impact of large-scale climate extremes on biospheric carbon fluxes: An intercomparison based on mstmip data. *Global Biogeochemical Cycles*, 28(6):585–600, 2014.